*J. Fluid Mech.* (1970), *vol.* 42, *part* 3, *pp.* 433–446
*Printed in Great Britain*



# A free-streamline model of the two-dimensional sail

By J. P. DUGAN
University of Toronto

(Received 27 October 1969 and in revised form 12 January 1970)

The two-dimensional sail is considered in a free-streamline model to complement the oft-considered airfoil model which is limited to small angles of attack. The shape of the sail, the lift and drag coefficients, and the moment are obtained for various angles of attack and states of tension.

## 1. Introduction

The sailboat is an intriguing device long used by man in his livelihood and recreation. The sail, as the motive power for the boat, has been the object of much interest. Although there have been several attempts by fluid mechanicians over the years to model the sail analytically, most efforts to quantitatively evaluate its efficiency have been experimental (cf. Shenstone 1968). Probably the most interesting experiment, by which to obtain the efficiency of the sail set at different trim, is to measure the speed of one's own boat. Evidently, the efficiency of the sail is increased if the boat moves faster. There seems to be little doubt that this is the best way to design a sail (Marchaj 1964; Letcher 1965). However, to model a sail analytically presents a challenge that, in the end, could increase our knowledge of its workings.

The first model of a sail seems to be that of Cisotti (1932). This is a free-streamline model in which the flow separates at the edges of the sail, forming an infinite quiescent wake. Since Cisotti did not exhibit any results, his model is used here to determine the shape and the lift and drag coefficients of an idealized sail. This model is essentially different from the more recent aerodynamic models chosen by Voelz (1950) and Thwaites (1961). In these papers, the sail is replaced by a linear distribution of vortices just as is done in airfoil theory, with the exception of the change in the boundary condition. Voelz (1950) obtained the sail shape and the first eigenvalue of the linear integral equation for the strength of the vortex sheet. The solution for values of the parameter that are less than this eigenvalue is shown to be the usual concave shape expected of a sail. Somewhat surprisingly, however, the solution for values of the parameter greater than the eigenvalue showed an inflexion of the sail profile. Thwaites (1961), apparently unaware of the earlier work, covered some of the same ground and he showed the existence of higher eigenvalues, each one determining the onset of a higher mode of the sail shape. These papers also exhibit lift coefficients. Chambers (1966) confirmed the earlier numerical estimates of the eigenvalues by a variational procedure and Nielsen (1963), choosing to formulate the problem

in terms of airfoil camber and a differential equation for the aerodynamic loading of the sail instead of in an integral equation, obtained equivalent results. Nielsen (1963) also performed experiments on a flexible sail in a wind tunnel and, although the results shown are sketchy, a comment on the possible importance of the porosity of the sail fabric apparently stimulated an analysis of the effects of porosity by Barakat (1968).

The airfoil theory predicts some interesting characteristics of sails. Probably the most important is the existence of inflexion points in the profile when the tension is not too great. That theory is, however, limited to very small angles of attack (ones smaller than those usually found on boats) and it predicts zero drag. The model used here eliminates these difficulties, but it does still treat only two-dimensional sails, and it does have physical limitations of its own. For example, the free-streamline theory in the simple form used here predicts a wake of infinite length. One does find a long wake in practice as every sailor knows when he is 'covered', but it does not extend to infinity. Also, as used in practice, the sail is seldom fully 'stalled', that is, only partial separation occurs. Finally, this model still leaves out all effects of viscosity and turbulence.

This formulation, then, based on Cisotti's model, uses the conformal mapping technique of Levi-Civita (1907) as modified by Villat (1911) and as discussed by Birkhoff & Zarantonello (1957). Thus, the particulars are somewhat different from those of Cisotti. The resulting non-linear, singular integral equation has been solved for asymptotically small deflexion of the sail for the special case of a symmetric sail (Dugan 1966). Here, it is solved asymptotically for small deflexion, and solved numerically to obtain the sail and free streamline profiles and the drag, lift and moment experienced by the sail.

## 2. Formulation

The representation of incompressible, two-dimensional potential motion can be formulated in the complex notation,

$$\left.\begin{aligned} Z &= X+iY = L^{-1}(x+i\psi), \\ W &= \Phi+i\Psi = U^{-1}L^{-1}(\phi+i\psi), \\ \zeta &= U^{-1}(u-iv) = U^{-1}\frac{dw}{dz} = \frac{dW}{dZ}, \end{aligned}\right\} \tag{1}$$

where $U$ is the uniform fluid velocity at infinity, $L$ is the length of the sail, small-lettered variables are dimensional, and capital lettered ones non-dimensional. The co-ordinate system and appropriate variables are shown in figure 1. The boundary conditions are that the velocity is uniform at infinity, the pressure is continuous across the free streamlines, and the pressure difference across the sail is balanced by the tension along the sail. The first and second boundary conditions give

$$\tfrac{1}{2}\rho U^2|\zeta|^2+P = \tfrac{1}{2}\rho U^2+P_0 = \text{const.}, \tag{2}$$

where $P_0$ is the pressure in the quiescent wake. This gives the condition,

$$|\zeta|^2 = 1 \quad \text{on} \quad AJ_1 \quad \text{and} \quad BJ_2, \tag{3}$$

the free streamlines. A force balance on a differential element of the sail as shown in figure 2 gives

$$(P - P_0)\, dl \cos(d\beta) = T \sin(d\beta), \tag{4}$$

where $dl$ is the differential arc length and $d\beta$ is the differential angle of deflexion of the element. The tension $T$ is assumed to be constant and the sail to be inextensible. Since $d\beta$ is small, (2) and (4) give

$$T\frac{d\beta}{dl} = \tfrac{1}{2}\rho U^2(1 - |\zeta|^2), \tag{5}$$

as the boundary condition on the sail.

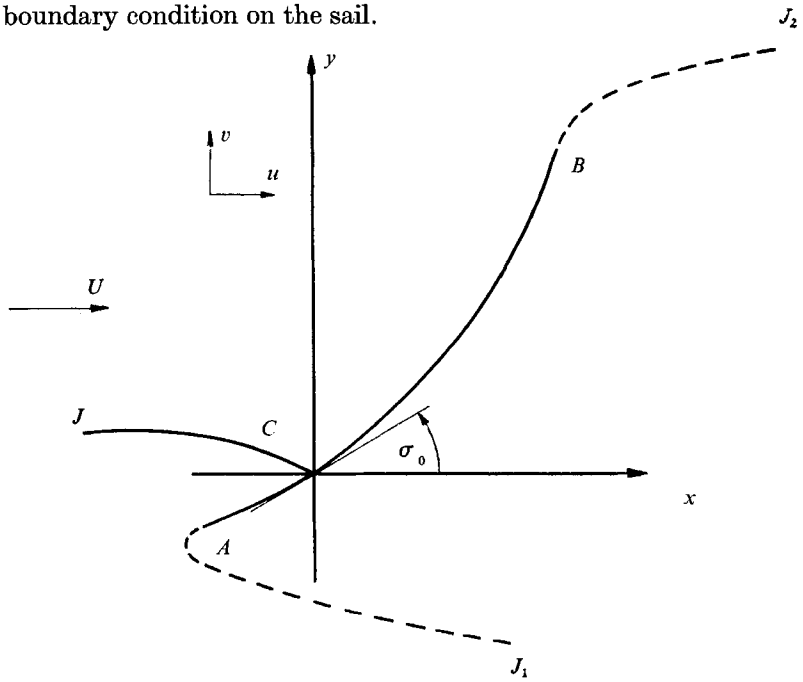


FIGURE 1. The physical $z$-plane.

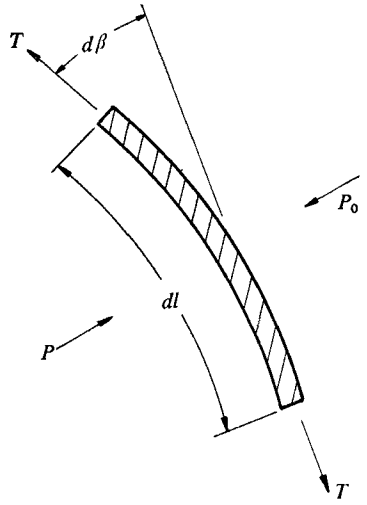


FIGURE 2. Force balance on an element of the sail.

If one could directly obtain the mapping of the $W$-plane into the $Z$-plane the problem would be simple indeed. However, this is not practically possible so it is convenient to utilize the technique of Levi-Civita (1907) as modified by Villat (1911). This method consists of mapping the $W$-plane into an auxiliary $t$-plane and finding an analytic function $\Omega$, called the Levi-Civita function, that maps the $t$-plane into the $\zeta$-plane where it is possible to apply the boundary conditions. The $t$-plane contains the flow field in the interior of a semi-circle, the circumference

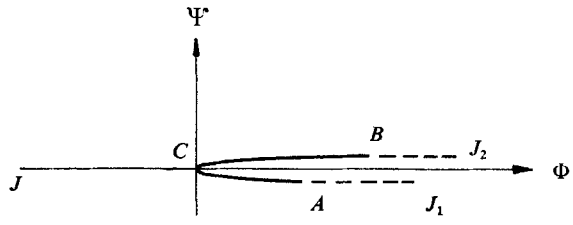


$W$-plane

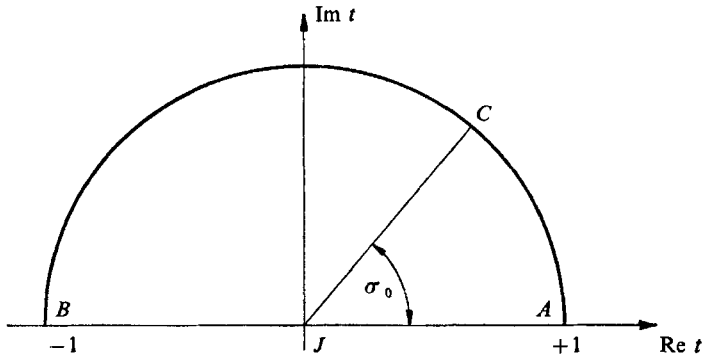


$t$-plane

FIGURE 3. Auxiliary complex planes.

of which corresponds to the sail and the diameter of which corresponds to the free streamlines. A functional relation involving the Levi-Civita function is assumed between the $\zeta$- and $t$-planes. This functional relation, once $\Omega$ is computed, completes the connexion between the $W$- and $\zeta$-planes.

The $W$-plane is mapped into the $t$-plane by the transformation,

$$W = M[\cos\sigma_0 - \tfrac{1}{2}(t + t^{-1})]^2, \tag{6}$$

as shown in figure 3. $M$ is an unknown constant introduced in the normalization of the semi-circle and reflects the fact that the separation points $A$ and $B$ cannot be explicitly located in the $W$-plane. An integral relation for $M$ will be derived

later. The functional relation between the $t$- and $\zeta$-planes is assumed to be of the form,

$$\zeta(t) = \frac{t - e^{i\sigma_0}}{1 - t\,e^{i\sigma_0}} e^{i(\pi - \sigma_0)} e^{-i\Omega(t)}. \tag{7}$$

The Levi-Civita function $\Omega$ is a complex quantity in general, and it may be written

$$\Omega = \theta + i\tau. \tag{8}$$

This particular form for the relation between the $\zeta$- and $t$-planes is chosen because it immediately allows $\Omega$ to be single-valued and continuous in $t$ and it allows automatic satisfaction of one of the boundary conditions. The choice is really fixed by the solution of the corresponding flat plate problem.

Thus, since the free streamlines correspond to the interval $(-1, 1)$ of the real line in the $t$-plane, the requirement,

$$t = \alpha, \quad -1 \leqslant \alpha \leqslant 1,$$

gives

$$|\zeta| = \left|\frac{\alpha - e^{i\sigma_0}}{1 - \alpha\, e^{i\sigma_0}}\right| \; \left| e^{i(\pi - \sigma_0)} e^{\tau} e^{-i\theta} \right| = e^{\tau}. \tag{9}$$

With (3), this gives

$$\tau = 0 \quad \text{on} \quad -1 \leqslant \operatorname{Re} t \leqslant 1. \tag{10}$$

Therefore, requiring $\Omega$ to be real on the real line will satisfy this boundary condition automatically. Also, the sail corresponds to

$$t = e^{i\sigma} \quad (0 \leqslant \sigma \leqslant \pi),$$

so that

$$\arg \zeta = \begin{cases} -\sigma_0 - \theta + \pi & \text{on} \quad 0 \leqslant \sigma < \sigma_0, \\ -\sigma_0 - \theta & \text{on} \quad \sigma_0 < \sigma \leqslant \pi. \end{cases} \tag{11}$$

Due to the form of (7), then, the fluid velocity has a jump in its argument of $\pi$ radians at the stagnation point $\sigma_0$, as it should from physical reasoning. This allows $\Omega$ to be single-valued and continuous everywhere in the interior of the $t$-plane.

It remains to use these expressions to obtain $\Omega$. A simple construction (Birkhoff & Zarantonello 1957, p. 134, or Dugan 1966, p. 11) shows that

$$\sigma_0 + \theta = \beta,$$

or

$$d\theta = d\beta,$$

so that (5) can be written as

$$\frac{d\theta}{d\sigma} = \frac{\rho U^2}{2T}(1 - |\zeta|^2)\frac{dl}{d\sigma}. \tag{12}$$

Geometric arguments give

$$dl = L|dZ|,$$

and this, with (1), yields

$$\frac{dl}{d\sigma} = L|\zeta^{-1}| \left|\frac{dW}{dt}\right| \left|\frac{dt}{d\sigma}\right|,$$

so that on $t = e^{i\sigma}$, and with (6) and (7),

$$\frac{d\theta}{d\sigma} = 2MK \sin\sigma \{\sin\sigma \sin\sigma_0 \cosh\tau(\sigma) - (1 - \cos\sigma \cos\sigma_0)\sinh\tau(\sigma)\} \quad (0 \leqslant \sigma \leqslant \pi), \tag{13}$$

where

$$K = \frac{\rho U^2 L}{2T}.$$

Recapitulating, (13) is a relation between $\theta$ and $\tau$, the real and imaginary parts of the Levi-Civita function. It represents the boundary condition on the sail.

The Levi-Civita function may be extended to an analytic function in the unit circle $|t| \leqslant 1$, so that the series

$$\Omega(t) = \sum_{n=0}^{\infty} a_n t^n \tag{14}$$

exists. The $a_n$'s must all be real constants by (10) (the boundary condition on the free streamlines), so that, with (8),

$$\left.\begin{aligned} \theta(\sigma) &= \sum_{n=0}^{\infty} a_n \cos n\sigma, \\ \tau(\sigma) &= \sum_{n=0}^{\infty} a_n \sin n\sigma, \end{aligned}\right\} \quad \text{on} \quad t = e^{i\sigma} \quad (0 \leqslant \sigma \leqslant \pi). \tag{15}$$

Since both expressions contain the same constants, this constitutes a second relation between $\theta$ and $\tau$. This relationship may be written in the more convenient form

$$\tau(\sigma) = \int_0^{\pi} D(\sigma, \sigma') \frac{d\theta}{d\sigma'} d\sigma',$$

$$\text{where} \quad D(\sigma, \sigma') = -\frac{2}{\pi} \sum_{j=1}^{\infty} \frac{\sin j\sigma \sin j\sigma'}{j} = -\frac{1}{\pi} \ln \left| \frac{\sin \frac{1}{2}(\sigma + \sigma')}{\sin \frac{1}{2}(\sigma - \sigma')} \right|. \tag{16}$$

(cf. Birkhoff & Zarantonello 1957, p. 136, or Dugan 1966, appendix IB). The substitution of (13) into the integral expression (16) gives

$$\tau(\sigma) = -\frac{2}{\pi} MK \int_0^{\pi} \ln \left| \frac{\sin \frac{1}{2}(\sigma + \sigma')}{\sin \frac{1}{2}(\sigma - \sigma')} \right| \sin \sigma' \{ \sin \sigma' \sin \sigma_0 \cosh \tau(\sigma') - (1 - \cos \sigma' \cos \sigma_0) \sinh \tau(\sigma') \} d\sigma' \quad (0 \leqslant \sigma \leqslant \pi). \tag{17}$$

This is a non-linear, singular integral equation for the imaginary part of the Levi-Civita function. Once $\tau(\sigma)$ is determined, $\Omega(t)$ can be constructed by obtaining the coefficients of the power series (14). However, there still remains in the integral equation the unknown constant $M$ that was introduced in the conformal mapping.

This constant can be determined from the side condition (that has not been used up to now) that the total length of the sail is $L$. Using the geometric argument before (13),

$$dl = L|dZ| = L|\zeta^{-1}| \left| \frac{dW}{dt} \right| \left| \frac{dt}{d\sigma} \right| d\sigma,$$

and, substituting from above,

$$dl = 2ML \sin \sigma [1 - \cos (\sigma + \sigma_0)] e^{-\tau(\sigma)} d\sigma,$$

so that, upon integration, the side condition on $M$ is

$$M = \left\{ 2 \int_0^{\pi} \sin \sigma [1 - \cos (\sigma + \sigma_0)] e^{-\tau(\sigma)} d\sigma \right\}^{-1}. \tag{18}$$

This relation, along with the integral equation (17) suffices to determine $\tau(\sigma)$.

The sail and free streamline profiles are obtained through (1)

$$dZ = \zeta^{-1}dW = \zeta^{-1}(t)\frac{dW}{dt}dt,$$

so that, substituting again from above,

$$dZ = -\frac{1-te^{i\sigma_0}}{t-e^{i\sigma_0}}e^{i(\sigma_0-\pi)}e^{i\Omega(t)}M[\cos\sigma_0-\tfrac{1}{2}(t+t^{-1})][1-t^{-2}]dt. \tag{19}$$

The parametric equations of the sail profile are obtained by substituting $t = e^{i\sigma}$ into this expression and integrating from the stagnation point $C$ to the ends of the sail, that is, from $t = e^{i\sigma_0}$ to $t = 1$ or $-1$. The equations are

$$\hat{Z} = 2M\int_{\sigma_0}^{\sigma}\sin\sigma'[1-\cos(\sigma'+\sigma_0)]\,e^{i(\sigma_0+\theta(\sigma'))}e^{-\tau(\sigma')}d\sigma', \tag{20}$$

where $\hat{Z} = \hat{X}+i\hat{Y}$ denotes the co-ordinates of the sail profile. The equations of the free streamline profiles are obtained by substituting $t = \alpha$ where $\alpha$ is real into (19), and integrating from the ends of the sail to infinity, that is, from $t = 1$ or $t = -1$ to $t = 0$. In this case, the equations are

$$Z-\hat{Z}_T = \tfrac{1}{2}M\int_{\pm1}^{\alpha}\alpha'^{-3}(1-\alpha'^2)\,[2\alpha'-(1+\alpha'^2)\cos\sigma_0 + i(1-\alpha'^2)\sin\sigma_0]e^{i(\sigma_0+\theta(\alpha'))}d\alpha', \tag{21}$$

where $\hat{Z}-\hat{Z}_T = (\hat{X}-\hat{X}_T)+i(\hat{Y}-\hat{Y}_T)$ denotes the co-ordinates of the profiles and $\hat{Z}_T = \hat{X}_T+i\hat{Y}_T$ denotes the co-ordinates of the ends of the sail.

Just as for the profiles, the forces acting on the sail can be obtained by quadratures. Thus, a simple derivation gives

$$d\mathbf{F} = -i(P-P_0)\,dz,$$

so that

$$\mathbf{F} = -\tfrac{1}{2}i\rho U^2L\int_0^{\pi}(1-|\zeta|^2)\,\zeta^{-1}(e^{i\sigma})\frac{dW}{dt}\frac{dt}{d\sigma}d\sigma$$

or,

$$\mathbf{F} = -2iM\rho U^2L\int_0^{\pi}\{\sin\sigma\sin\sigma_0\cosh\tau(\sigma) - (1-\cos\sigma\cos\sigma_0)\sinh\tau(\sigma)\}e^{i\sigma_0}e^{i\theta(\sigma)}\sin\sigma\,d\sigma. \tag{22}$$

It is easily shown that $F_y = 0$ for $\sigma_0 = \frac{1}{2}\pi$ and that with

$$\mathbf{F} = F_x+iF_y = \tfrac{1}{2}\rho U^2L(C_D+iC_L),$$

$$C_D = \frac{2\pi\sin^2\sigma_0}{4+\pi\sin\sigma_0}, \quad C_L = -\frac{2\pi\sin\sigma_0\cos\sigma_0}{4+\pi\sin\sigma_0}$$

in the limit of $K \to 0$ of (22). These are the results for the flat plate. The drag and lift could have been obtained through the elegant formulae of Levi-Civita (see Gurevich 1966, p. 98) instead of through the integral (22). Similarly, the moment is given by

$$\mathbf{M} = \mathrm{Re}\{-\tfrac{1}{2}\rho U^2\textstyle\int z\zeta^2\,dz\}, \tag{23}$$

or

$$\mathbf{M} = -\rho U^2L^2M\int_0^{\pi}[1-\cos(\sigma-\sigma_0)]\,e^{\tau(\sigma)}\sin\sigma \times\{\hat{X}(\sigma)\cos(\sigma_0+\theta(\sigma))+\hat{Y}(\sigma)\sin(\sigma_0+\theta(\sigma))\}d\sigma, \tag{24}$$

where $\hat{X}(\sigma)$ and $\hat{Y}(\sigma)$ are given by (20).

## 3. Solution of equations and results

The determination of the sail profile and the forces and moment acting on the sail rests upon the solution of (17) for $\tau(\sigma)$. The equation is solved below by an asymptotic technique for small deflexion of the sail and by a numerical technique for arbitrary deflexions.

The limit $K \to 0$ (this may be interpreted as $T \to \infty$) reduces the problem to the flat-plate problem considered by Rayleigh (1876). Equation (17) gives $\tau(\sigma) = 0$ so, by expressions (15), $\theta(\sigma) = 0$. Evidently, then, $\tau(\sigma)$ and $\theta(\sigma)$ are small for small deflexions of the sail ($K \ll 1$). In fact, the form of (17) implies that $MK$ is an appropriate perturbation parameter so that it is natural to assume a solution of the form,

$$\tau(\sigma) = \tau_0(\sigma) + MK\tau_1(\sigma) + (MK)^2\tau_2(\sigma) + \ldots, \tag{25}$$

for $MK \ll 1$. Actually, (17) also implies that $\tau(\sigma) \leqslant 0$, so (18) yields

$$M \leqslant (4 + \pi \sin\sigma_0)^{-1} \leqslant \tfrac{1}{4}, \tag{26}$$

verifying that $MK \ll 1$ if $K \ll 1$. Substituting the expansion (25) into (17), expanding the hyperbolic functions, and equating coefficients of equal powers in $MK$ gives the sequence of equations,

$$\left.\begin{aligned}
&\tau_0(\sigma) = 0,\\
&\tau_1(\sigma) = -4\pi^{-1}\sin\sigma_0 \int_0^\pi D(\sigma,\sigma')\sin\sigma'\,d\sigma',\\
&\tau_2(\sigma) = 4\pi^{-1}\int_0^\pi D(\sigma,\sigma')(1-\cos\sigma_0\cos\sigma')\tau_1(\sigma')\,d\sigma',\\
&\tau_3(\sigma) = -4\pi^{-1}\int_0^\pi D(\sigma,\sigma^1)\{2^{-1}\tau_1^2(\sigma')\sin\sigma_0\sin\sigma' - (1-\cos\sigma_0\cos\sigma')\tau_2(\sigma')\}\,d\sigma',\\
&\quad\vdots
\end{aligned}\right\} \tag{27}$$

where $D(\sigma,\sigma')$ is the former of the two kernel functions (16). Evaluation of these integrals gives

$$\left.\begin{aligned}
\tau_1(\sigma) &= 16\pi^{-1}\sin\sigma_0 \sum_{n=1}^{\infty} \frac{\sin(2n-1)\sigma}{(2n-1)^2[(2n-1)^2-4]},\\
\tau_2(\sigma) &= -256\pi^{-2}\sin\sigma_0 \sum_{j,n=1}^{\infty} \{(2j-1)[(2j-1)^2-4]\}^{-1}\\
&\quad\times\left\{\frac{\sin(2n-1)\sigma}{[(2n-1)^2-4(j-1)^2][(2n-1)^2-4j^2]} - \frac{\cos\sigma_0\cos 2n\sigma}{[4n^2-(2j-3)^2][4n^2-(2j+1)^2]}\right\}.\\
&\quad\vdots
\end{aligned}\right\} \tag{28}$$

The next correction $\tau_3(\sigma)$ has been computed, but it is quite messy and is not of sufficient interest to include here. The corresponding values of the constant $M$ can be obtained by substituting the expansion (25) and (28) into (18), so that

$$M = (4+\pi\sin\sigma_0)^{-1}\left\{1 - K\frac{16}{3\pi}\sin\sigma_0\frac{\pi+2\sin\sigma_0}{(4+\pi\sin\sigma_0)^2} + O(K^2)\right\}. \tag{29}$$

The resulting three-term approximate expression for $\tau(\sigma)$ appears to converge for values of $K$ up to unity; the two-term expansion for values up to about one-half. It is of more than passing interest to note that the first two terms above are identical to the first two terms of the Neumann series solution of the linearized form of (17). The non-linearity of (17) and, therefore, the non-linearity of the boundary condition on the sail becomes important when $K \gtrsim \frac{1}{2}$ since that is when the third and higher order terms in the expansion (25) become important. The Neumann series solution mentioned above converges strictly for $MK < 3^{-\frac{1}{2}}$, the first eigenvalue of the homogeneous linearized equation (see Courant & Hilbert 1953, p. 153; Tricomi 1957, p. 50). In the limit $\sigma_0 \to 0$ and $K \ll 1$, (29) gives $M = 4^{-1}$, so that the expansion converges for $K \lesssim 2{\cdot}310$. Considering that this is only an approximate estimate of the limit of $K$ in the linearized case of a completely different theory, it is remarkable that this value of $K$ is so close to Voelz's (1950) first eigenvalue, 2·299 in the present notation, which was corrected by Thwaites (1961) and Chambers (1966) to 2·316. This limiting value of $K$ has no bearing on the non-linear problem.

In the approximation above, the drag and lift coefficients (22) are given by

$$\mathbf{C} = \frac{2\pi \sin\sigma_0}{4+\pi\sin\sigma_0}(\sin\sigma_0 - i\cos\sigma_0)\left\{1+\frac{16}{3\pi}\frac{K}{4+\pi\sin\sigma_0} \times\left(1-\sin\sigma_0\frac{\pi+2\sin\sigma_0}{4+\pi\sin\sigma_0}\right)-O(K^2)\right\}. \quad (30)$$

The integral equation (17) with the side condition (18) also has been solved by successive approximations whereby, assuming an initial $M_0$ and $\tau_0(\sigma)$, corrections are found successively by the formulae

$$M_{n+1} = \left\{2\int_0^\pi \sin\sigma'[1-\cos(\sigma'+\sigma_0)]\,e^{\tau_n(\sigma')}d\sigma'\right\}^{-1}$$

and
$$\tau_{n+1}(\sigma) = 2M_{n+1}K\int_0^\pi D(\sigma,\sigma')\sin\sigma' \times\{\sin\sigma'\sin\sigma_0\cosh\tau_n(\sigma') - (1-\cos\sigma'\cos\sigma_0)\sinh\tau_n(\sigma')\}d\sigma', \quad (31)$$

where $D(\sigma,\sigma')$ is the second kernel function (16). The integrals are evaluated numerically by Simpson's rule, proper care being taken with the singularity. The details of this and the calculation of the remaining integrals do not seem worth repeating here, they are straight-forward and, in any case, they may be found in Dugan (1966). We note only that the solution of (31) above converges nicely ($|M_{n+1}-M_n| < 0{\cdot}0001$, $\max|\tau_{n+1}(\sigma)-\tau_n(\sigma)| < 0{\cdot}0001$) for $\sigma_0 \gtrsim 5°$, $K \lesssim 7$. Sample solutions for the sail profile are shown in figure 4 for several values of $K$ and the angle of attack and, the lift and drag coefficients are plotted in figures 5 and 6. Figure 7 is a plot of the lift/drag coefficient and figure 8 shows the moment acting on the sail. It should be noted that the parameter $\sigma_0$ is the angle of attack of the 'equivalent' flat-plate problem. Since the positions of the endpoints $\hat{Z}_T$ of the sail vary with $K$ as well as with $\sigma_0$, the real angle of attack (angle between a line joining the endpoints and the $x$-axis) can only be determined from the sail

profile. This is of minor importance but it does cause difficulty in an attempt to compare the resulting sail profiles with previously derived ones. In the figures, the angle of attack is the real angle of attack as defined above, not the angle of attack of the 'equivalent' flat-plate problem.

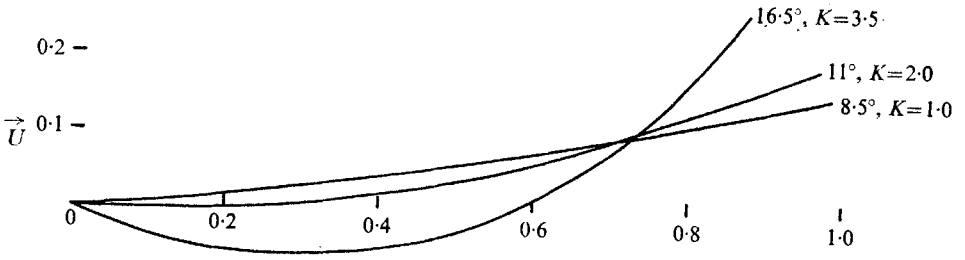


FIGURE 4. Sail profiles. In each case $\sigma_0 = 7{\cdot}5°$. Actual angle of attack = 8·5° for $K = 1$, 11° for $K = 2$, 16·5° for $K = 3{\cdot}5$.

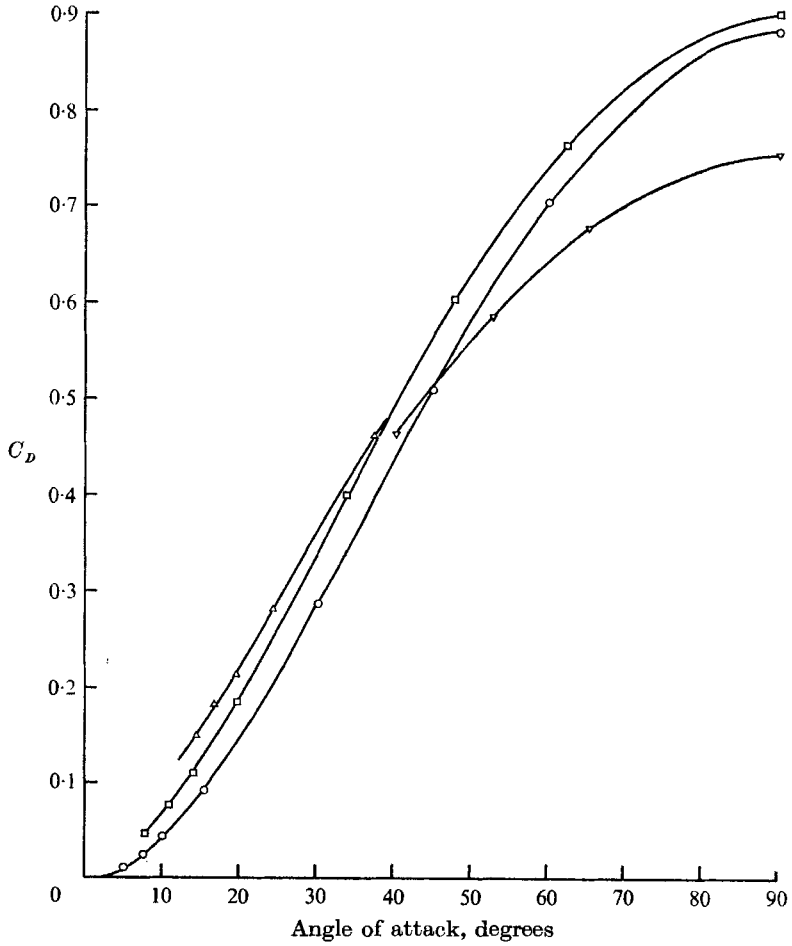


FIGURE 5. Plot of $C_D$ *versus* angle of attack for various $K$. ○, $K = 0{\cdot}1$; △, $K = 3{\cdot}5$; □, $K = 2$; ▽, $K = 5$.

The lift and drag coefficients as defined in § 2 are proportional to those usually defined in airfoil theory except that the area is not the cross-sectional area but is the length $L$ of the sail. The calculated drag coefficients are relatively independent of the parameter $K$, but the maximum lift coefficient increases markedly with increasing $K$, the maximum occurring at smaller angles of attack for larger values of $K$. This theory is invalid for zero angle of attack and this evidently

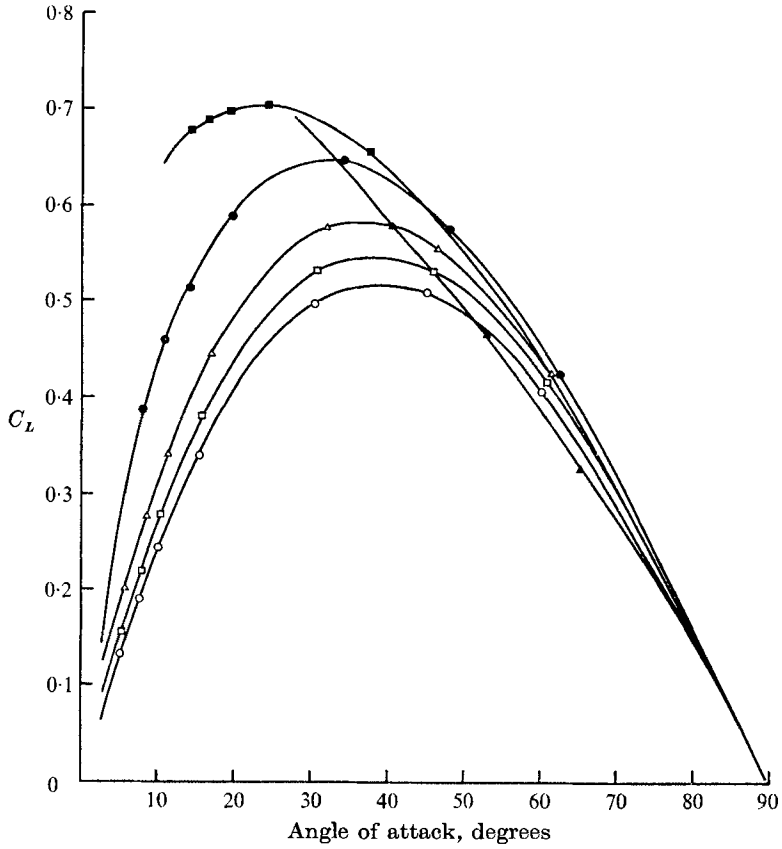


FIGURE 6. Plot of $C_L$ *versus* angle of attack for various $K$. ○, $K = 0{\cdot}1$; □, $K = 0{\cdot}5$; △, $K = 1$; ●, $K = 2$; ■, $K = 3{\cdot}5$; ▲, $K = 5$.

appears in the difficulty in obtaining convergent solutions of the integral equations in this neighbourhood. However, the iterative scheme does converge for small angles of attack if $K$ is small or moderate. The resulting lift coefficients which are plotted in figure 6 do not agree with those predicted by the airfoil analysis. The lift coefficient appears to increase linearly with the angle of attack for small angles but the limiting value is one-quarter the value predicted by Voelz (1950) and others. The disparity is embedded in the assumption that there is not separation in the airfoil theory while there is separation in the present case. However, since the experimental values of the lift coefficient obtained by Nielsen (1963) were one-half to one-third of those predicted by the airfoil theory, the

values predicted here in the limit of $\sigma_0 \to 0$ appear to be as valid as the previous ones. Figure 8 shows that the moment decreases with increasing values of $K$.

As mentioned above, this model breaks down when the angle of attack is too small. The tension in the sail has to be increased ($K$ decreased), the smaller the

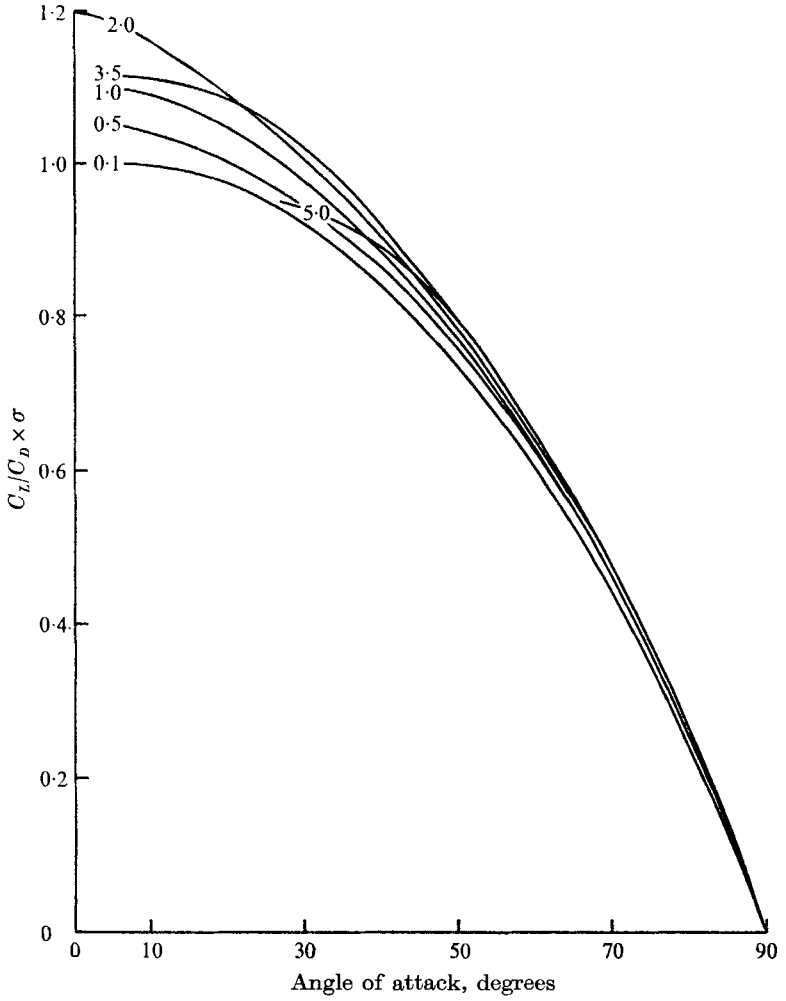


FIGURE 7. Plot of $C_L/C_D$ times angle of attack *versus* angle of attack.

angle of attack, in order to obtain a convergent solution of (17). This is as might be expected physically, presumably foretelling the onset of a higher mode as predicted by the airfoil model.

In conclusion, then, the free-streamline model can be used to describe the aerodynamics of a two-dimensional sail. This model complements rather than supercedes the airfoil model because of different ranges of validity in the angle of attack. In the small range where each can predict solutions, this model should

be a better representation of reality because the stream would begin to separate from the back of the sail.

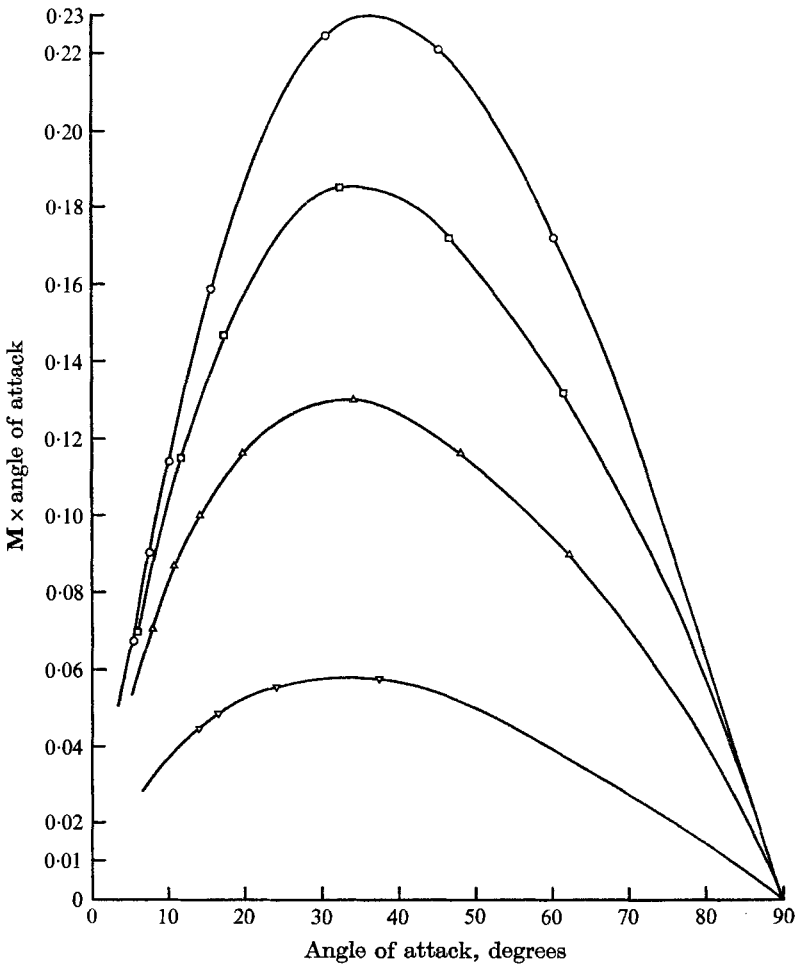


FIGURE 8. Plot of moment times angle of attack *versus* angle of attack. The moment = $\mathbf{M}.\rho U^2L^2$. ○, $K = 0{\cdot}1$; △, $K = 2$; □, $K = 1$; ▽, $K = 3{\cdot}5$.

It is a pleasure to thank W. E. Olmstead for his suggestion of this problem and his valuable guidance. A simpler version of the work made up an M.Sc. thesis submitted to Northwestern University, where the author was a NASA Fellow. Its final preparation was supported by NRC Grant A-7365.

## REFERENCES

BARAKAT, R. 1968 Incompressible flow around porous two-dimensional sail and wings. *J. Math. Phys.* **47**, 327–349.

BIRKHOFF, G. & ZARANTONELLO, E. H. 1957 *Jets, Wakes and Cavities.* New York: Academic.

CHAMBERS, L. G. 1966 A variational formulation of the Thwaites sail equation. *Quart. J. Mech. Appl. Math.* **19**, 221–231.

CISOTTI, V. 1932 Moto con scia di un profilo flessibile, Nota I and II. *Rendiconti della reale Accad. Nat. dei Lincei* **15**, 166–173, 253–257.

COURANT, R. & HILBERT, D. 1953 *Methods of Mathematical Physics*, vol. 1. New York: Interscience.

DUGAN, J. P. 1966 Two-dimensional potential flow around a flexible membrane. M.S. Thesis, Northwestern University.

GUREVICH, M. I. 1966 *The Theory of Jets in an Ideal Fluid*. New York: Pergamon.

LETCHER, J. S. 1965 Balance of helm and static directional stability of yachts sailing close-hauled. *J. Roy. Aero. Soc.* **69**, 241–248.

LEVI-CIVITA, T. 1907 Scie e leggi di resistenzia. *Rend. Circolo Math. Palermo*, **23**, 1–37.

MARCHAJ, C. A. 1964 *Sailing Theory and Practice*. New York: Dodd-Mead.

NIELSEN, J. N. 1963 Theory of flexible aerodynamic surfaces. *J. Appl. Mech.* **30**, 435–442.

RAYLEIGH, LORD 1876 On the resistance of fluids. *Phil. Mag.* (5) **2**, 430–441.

SHENSTONE, B. S. 1968 Unconventional flight. *Aeronaut. J.* **72**, 655–666.

THWAITES, B. 1961 The aerodynamic theory of sails, I. Two-dimensional sails. *Proc. Roy. Soc.* A **261**, 402–422.

TRICOMI, F. G. 1957 *Integral Equations*. New York: Interscience.

VILLAT, H. 1911 Sur la résistance des fluides. *Ann. Sci. Ec. Norm.* **28**, 203–240.

VOELZ, K. 1950 Profil und Auftrieb eines Segels. *ZAMM* **30**, 301–317.

*J. Fluid Mech.* (1970), *vol.* 42, *part* 3, *pp.* 447–464
*Printed in Great Britain*



# On the oscillations of harbours of arbitrary shape

By LI-SAN HWANG
Tetra Tech, Incorporated, Pasadena, California, U.S.A.
AND ERNEST O. TUCK
University of Adelaide, Adelaide, Australia

(Received 21 January 1969 and in revised form 23 January 1970)

A theory is developed for calculating oscillations of harbours of constant depth and arbitrary shape. This theory is based on the solution of a singular integral equation. Numerical results have been calculated for rectangular harbours so as to check the accuracy of the method. Examples for wave amplification factor and velocity field for both rectangular and actual complex-shaped harbours are given.

## 1. Introduction

The occurrence of resonance in harbours is fundamentally due to the fact that waves arriving at a widening or narrowing (or at a depth increase or decrease) are partially reflected. Consider, for example, a rectangular harbour open to the sea. Waves arriving within the harbour are reflected seaward by the rear boundary; these outgoing waves, upon reaching the harbour entrance again, are partially reflected by the sudden widening, with the net result that part of the wave energy which got in does not get back out. This trapping of energy by the harbour leads to resonance if the phases of the various incident and reflected waves happen to be such that reinforcement occurs. In this case, the amplitude of oscillation may grow, within the harbour, to values far greater than those incident. At some stage of growth, however, energy dissipation and radiation equals energy trapping and the oscillation amplitude reaches its maximum. The dissipation is of three main forms: wave breaking within the harbour when the oscillation exceeds the breaking limit, frictional effects at the bottom, and wave absorption on the bounding beaches. However, radiation seaward is generally more important than all of these.

The problems of developing a practical calculation procedure applicable to these processes, already difficult, are compounded by the facts that harbours are usually of complex shape and that incident waves are never periodic. Irregularity of shape causes complicated reflexions of the waves within the harbour so that even for periodic input the agitation may appear highly irregular. The response to random sea or swell or to a dispersive wave train generated by a localized disturbance is still more difficult to analyze. Furthermore, oscillations may be induced by other mechanisms such as fluctuations in atmospheric conditions, currents moving past the entrance which generate a series of alternating

vortices, and even ship transit in and out of the harbour. It is no wonder, then, that taken in its entirety the problem of harbour resonance is intimidating.

Yet, some form of solution must be found since the harbour resonance problem is of very great practical importance in coastal engineering. This is particularly so in connexion with ship mooring problems. It is well known that harbour oscillations of only a few inches may excite large motions in ship-mooring systems causing mooring lines to break, and ships to collide with adjacent structures. To minimize such events is the goal of harbour and breakwater design, and for that purpose one must be able to determine harbour response characteristics.

Analytical studies in this area are, for the most part, quite recent. McNown (1952) determined the resonant frequency of a circular harbour with a small opening under the assumption that the entrance remains as a node of a standing wave; a similar approach was applied by Kravtchenko & McNown (1955) to the rectangular harbour. Miles & Munk (1961) considered harbours of arbitrary shape and formulated an integral equation describing the agitation within the harbour by matching conditions inside and outside the harbour at the entrance. But they imposed the restrictions of narrow openings, and slim and rectangular harbours, in order to obtain analytical expressions for the resonant conditions and maximum amplification. Ippen & Goda (1963) applied Fourier transformation methods and obtained the solution of the rectangular harbour by matching the wave amplitude and velocity approximately at the entrance. The results were compared with a series of experiments. For long harbours, the agreement between theory and experiment was good except, of course, at the resonance point where viscous dissipation is important and the experiments become difficult. Biesel & Le Méhauté (1955, 1956) and Le Méhauté (1960, 1961) presented an interesting approach in the solution of a rectangular harbour under various types of entrance conditions through the use of the theory of complex numbers. Most recently, Leendertse (1967) has developed a numerical procedure to determine the response of basins to long waves, elevation at open boundaries being prescribed.

All of the foregoing studies suffer to some degree from various deficiencies; either they are applicable only to idealized shapes or matching conditions are required at the harbour entrance. The present study requires no prescribed entrance conditions, and permits solution for completely arbitrary shape. Furthermore, the present method is highly economical for practical use since the numerical scheme involved does not require long computing time (computation time for both the results of figures 4 and 9 is less than one minute on the CDC 6600).

## 2. Theoretical formulation

Assuming that the fluid is inviscid, incompressible, and irrotational, there exists a velocity potential $\Phi(x, y, z; t)$ which satisfies the Laplace equation

$$\nabla^2\Phi = 0 \tag{2.1}$$

throughout the fluid contained within the boundary surfaces as shown in figure 1. If the wave is assumed to be of small amplitude, the velocity term in the Bernoulli equation may be neglected. Thus, the governing dynamic boundary condition on the free surface becomes

$$\zeta = -\frac{1}{g}\frac{\partial \Phi}{\partial t} \quad \text{at} \quad z = 0, \tag{2.2}$$

where $\zeta$ is the wave elevation and $g$ is gravitational acceleration.

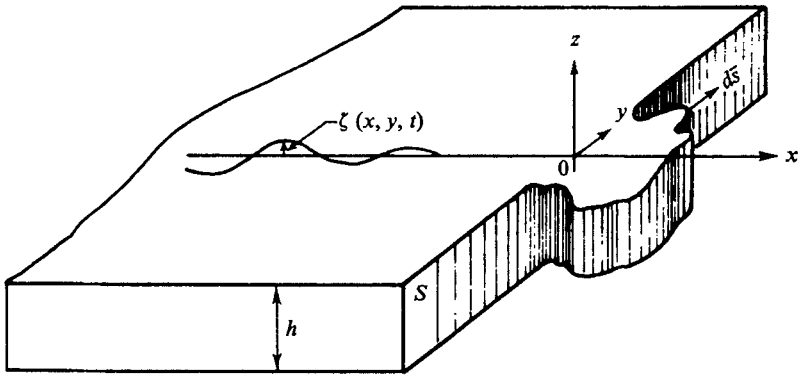


FIGURE 1. A schematic drawing of the harbour.

The linearized kinematic condition at the free surface, which follows from the fact that surface water particles stay on the surface, is expressed in the form

$$\partial \zeta / \partial t = \partial \Phi / \partial z \quad \text{at} \quad z = 0. \tag{2.3}$$

The condition on the fixed boundary surface is that the velocity normal to the surface equals zero; that is

$$\partial \Phi / \partial n = 0 \tag{2.4}$$

on the boundary $S$.

Since we are dealing with uniform water depth $h$, the condition at the bottom is simply

$$\partial \Phi / \partial z = 0 \quad \text{at} \quad z = -h. \tag{2.5}$$

Finally, the condition at infinity requires that

$$\Phi = \Phi_0 + \Phi_1, \tag{2.6}$$

$$\Phi_0 = \cos(kx \cos\beta) \exp[-i(\omega t - ky \sin\beta)], \tag{2.7}$$

and

$$\Phi_1 \text{ is an outgoing wave.} \tag{2.8}$$

The above equations complete the formulation of the problem of oscillation in a constant depth harbour of arbitrary shape.

Since the water depth is uniform, we may assume that the velocity potential is a product of functions of $x$ and $y$, $z$, and $t$, such as

$$\Phi(x, y, z; t) = (1/\omega i)\, \phi(x, y)\, Z(z)\, e^{-i\omega t}, \tag{2.9}$$

where $\omega$ is the angular frequency.

Substituting the above expression into the Laplace equation, separating the functions of $x$ and $y$, and $z$ and equating them to a constant, say $k^2$, we have

$$\frac{\partial^2\phi}{\partial x^2}+\frac{\partial^2\phi}{\partial y^2}+k^2\phi = 0 \tag{2.10}$$

and

$$\frac{\partial^2 Z}{\partial z^2}-k^2 Z = 0. \tag{2.11}$$

The solution of (2.11) together with the bottom boundary condition

$$\partial Z/\partial z = 0 \quad \text{at} \quad z = -h \tag{2.12}$$

and the kinematic surface boundary condition

$$\zeta = -\frac{1}{g}\frac{\partial\Phi}{\partial t}\bigg|_{z=0} = A\phi(x,y)\,e^{-i\omega t} \tag{2.13}$$

can be found in some text-books (e.g. Stoker 1963), and is simply

$$Z(z) = -Ag\cosh k(z+h)/\cosh kh, \tag{2.14}$$

where $A$ is the amplitude of a standing wave at infinity. The constant, $k$, is a wave-number, and is related to the angular frequency $\omega$ and the water depth $h$ through the kinematic boundary condition at the free surface. This relationship can be simply obtained by substituting (2.9), (2.13) and (2.14) into (2.3). One finds

$$\omega^2 = gk\tanh kh. \tag{2.15}$$

The problem now is to obtain the solution of (2.10) with the boundary condition

$$\partial\phi/\partial n = 0 \quad \text{on the solid boundary } S, \tag{2.16}$$

which is obtained from the substitution of (2.9) into (2.6), and with the prescribed condition at infinity. The condition at infinity can be determined as if the harbour were absent. This is due to the fact that the influence of radiated waves from the harbour tends to zero at infinity. Thus, for a straight-crested standing wave at infinity with the crest at an angle $\beta$ to the shoreline, we have

$$\phi_0 = \cos(kx\cos\beta)\exp[-iky\sin\beta] \quad (0<\beta<\pi), \tag{2.17}$$

which corresponds to the wave form

$$\zeta = A\cos(kx\cos\beta)\exp[-i(\omega t-ky\sin\beta)] \tag{2.18}$$

at infinity. If the wave front propagates directly toward the shore, $\beta$ is equal to zero, so that

$$\phi_0 = \cos kx. \tag{2.19}$$

## 3. Derivation of the integral equation

For a standing wave of unit amplitude at infinity, the solution of Weber's equation (2.10), together with the boundary conditions, (2.16) and (2.17), can be found through the introduction of a source function $Q(\xi,\eta)$ along the boundary $S$, where $\xi$ and $\eta$ refer to co-ordinates on the boundary.

Thus, the value of $\phi(x,y)$ at any point $(x,y)$, is equal to the sum of two parts; one is the influence from infinity $\phi_0(x,y)$ and the other is the contribution of the source distribution, that is, the scattered wave caused by the presence of the boundary. The latter will be given by

$$\int_S dS\, Q(\xi,\eta)\, G(x,y;\xi,\eta), \tag{3.1}$$

where $G(x,y;\xi,\eta)$ is the Green's function and $Q(\xi,\eta)$ is the unknown source distribution, which can be determined from the boundary conditions.

The Green's function has to be chosen so that it is the solution of Weber's equation, (2.10), satisfies the radiation condition at infinity, and has a singularity at the source point. Thus we choose the Green's function to be a Hankel function of the first kind rather than of the second kind to guarantee that the disturbance, due to the harbour, at infinity takes the form of an outgoing wave rather than an incoming wave.

$$G(x,y;\xi,\eta) = -\tfrac{1}{4}iH_0^{(1)}(kR), \tag{3.2}$$

where

$$R = [(x-\xi)^2+(y-\eta)^2]^{\frac{1}{2}}, \tag{3.3}$$

so that the value of $\phi(x,y)$ at any point $(x,y)$ is

$$\phi(x,y) = \phi_0(x,y) + \int_S dS\, Q(\xi,\eta)\, G(x,y;\xi,\eta). \tag{3.4}$$

The problem now is to determine the strength of the source distribution $Q(\xi,\eta)$. This can be accomplished by applying the boundary condition (2.16), which gives

$$\lim_{x,y\to\xi',\eta'} \left[\frac{\partial\phi_0(x,y)}{\partial n} + \frac{\partial}{\partial n}\int_S dS\, Q(\xi,\eta)\, G(x,y;\xi,\eta)\right] = 0. \tag{3.5}$$

Since the limit is singular inside the integral, it has to be treated with care. We evaluate the integral in (3.5) by use of contour integration. The path of the integral is along the boundary except around the point $(\xi',\eta')$ where the contour is deformed into a small circle with a radius $\epsilon$. Since the contribution around a large semicircle is zero, the integral in (3.5) may be evaluated as follows:

$$\begin{aligned}\lim_{x,y\to\xi',\eta'} \frac{\partial}{\partial n}\int_S dS\, Q(\xi,\eta)\, G(x,y;\xi,\eta) \\ = \text{⨍}_S dS\, Q(\xi,\eta)\, G_n(\xi',\eta';\xi,\eta) + \lim_{x,y\to\xi',\eta'}\int_\epsilon dS\, Q(\xi,\eta)\, G_n(x,y;\xi,\eta),\end{aligned} \tag{3.6}$$

where the sign $\text{⨍}_S$ refers to a principal value in the sense of Cauchy. Since the Hankel function can be approximated by

$$-\tfrac{1}{4}iH_0^{(1)}(kR) \to \frac{1}{2\pi}\ln(kR) \quad (R\to 0) \tag{3.7}$$

the second integral of the right-hand side of (3.6) may be integrated analytically. We have

$$\lim_{x,y\to\xi',\eta'} \frac{\partial}{\partial n}\int_\epsilon dS\, Q(\xi,\eta)\, G(x,y;\xi,\eta) = \lim_{R\to 0}\frac{1}{2\pi}Q(\xi',\eta')\int_{-\pi}^{\pi}\frac{\partial}{\partial R}\ln kR\, R\, d\theta = \tfrac{1}{2}Q(\xi',\eta'). \tag{3.8}$$

Thus the integral equation becomes

$$\tfrac{1}{2}Q(\xi',\eta')+\int\!\!\!\!\!\!-_S dS\,Q(\xi,\eta)\,G_n(kR) = -\frac{\partial}{\partial n}\phi_0(\xi',\eta'), \tag{3.9}$$

where

$$G_n(kR) = -\tfrac{1}{4}i\,\partial(H_0^{(1)}(kR))/\partial n. \tag{3.10}$$

The above equation cannot be solved analytically. A numerical method for evaluating the source distribution $Q(\xi,\eta)$ is derived in the following section.

## 4. Numerical solution

Let us divide the boundary $S$ into many segments with length $\Delta S_j$ along the boundary, where $j = 1, 2, 3, \ldots, N$. The lengths of these segments need not be uniform; however, they must be small enough so that within each segment, the source strength $Q(\xi,\eta)$ does not vary too much. Furthermore, let the midpoint of $\Delta S_i$ be $(\xi_i, \eta_i)$ and evaluate the integral at this midpoint of each segment. Within each segment the source strength does not vary much, so that we take $Q(\xi,\eta)$ to be constant and equal to $Q_j$ within $\Delta S_j$. Then (3.9) becomes

$$\tfrac{1}{2}Q_i+\sum_{j=1}^{N} Q_j\left[\int\!\!\!\!\!\!-_{\Delta S_j} dS\,G_n(\xi_i,\eta_i;\xi,\eta)\right] = -\frac{\partial\phi_0(\xi_i,\eta_i)}{\partial n}; \tag{4·1}$$

for simplicity, we may write the above equation in the following form

$$\sum_{j=1}^{N} B_{ij}Q_j = b_i, \tag{4.2}$$

where

$$\left.\begin{aligned} B_{ij} &= \tfrac{1}{2}\delta_{ij}+\int\!\!\!\!\!\!-_{\Delta S_j} dS\,G_n(\xi_i,\eta_i;\xi,\eta),\\ b_i &= -\frac{\partial\phi_0(\xi_i,\eta_i)}{\partial n}\end{aligned}\right\} \tag{4.3}$$

and $\delta_{ij}$ is the Kronecker delta.

Equation (4.2) is an algebraic equation which can be solved easily provided the constants $B_{ij}$ are known.

To evaluate $B_{ij}$, let us split $G(kR) = -\frac{1}{4}iH_0^{(1)}$ into two parts; one singular part and the regular part:

$$G(kR) = (1/2\pi)\log R + M(kR). \tag{4.4}$$

Substituting (4.4) into (4.2), we have

$$B_{ij} = \tfrac{1}{2}\delta_{ij}+\frac{1}{2\pi}\int\!\!\!\!\!\!-_{\Delta S_j} dS\frac{\partial}{\partial n}\log R+\int\!\!\!\!\!\!-_{\Delta S_j}\frac{\partial M}{\partial n}\,dS. \tag{4.5}$$

The first integral on the right-hand side of the equation can be calculated analytically and is

$$\frac{1}{2\pi}\int\!\!\!\!\!\!-_{\Delta S_j} dS\frac{\partial}{\partial n}\log R = \frac{\Delta\theta_{ij}}{2\pi}, \tag{4.6}$$

where $\Delta\theta_{ij}$ is the angle subtended at $(\xi_i,\eta_i)$ by the segment of $S$ between $(X_j, Y_j)$ and $(X_{j+1}, Y_{j+1})$.

Now we fix an index $i$ [that is, choose a point $(\xi_i, \eta_i)$] and then run over the whole set of $j = 1, 2, 3, \ldots, N$ and evaluate the angle $\Delta\theta_{ij}$ as follows:

For $i \neq j$
$$\Delta\theta_{ij} = \tan^{-1}\frac{Y_{j+1}-\eta_i}{X_{j+1}-\xi_i} - \tan^{-1}\frac{Y_j-\eta_i}{X_j-\xi_i}. \tag{4.7}$$

For $i = j$
$$\Delta\theta_{ij} = 0. \tag{4.8}$$

The last integral in (4.5) is not singular, thus the bar on the integral can be left out. It can be approximated directly to be

$$\int_{\Delta S_j} dS\, \partial M/\partial n = \Delta S_j\, \partial M/\partial n \tag{4.9}$$

and $\Delta S_j\, \partial M/\partial n$ can be evaluated as follows:

$$\begin{aligned}\Delta S_j M_n &= \Delta Y_j M_X - \Delta X_j M_Y \\ &= \Delta Y_j \frac{\partial M}{\partial R}\frac{X_j-\xi_i}{R} - \Delta X_j \frac{\partial M}{\partial R}\frac{Y_j-\eta_i}{R},\end{aligned} \tag{4.10}$$

where
$$\Delta X_j = X_{j+1}-X_j, \quad \Delta Y_j = Y_{j+1}-Y_j. \tag{4.11}$$

The value of $b_i$ in (4.2) can be obtained in a similar way, i.e.

$$\begin{aligned}-b_i &= \frac{\partial \phi_0(X_i Y_i)}{\partial n} \\ &= \frac{\partial \phi_0}{\partial x}\frac{\Delta Y}{[(\Delta X)^2+(\Delta Y)^2]^{\frac{1}{2}}} + \frac{\partial \phi_0}{\partial y}\frac{\Delta X}{[(\Delta X)^2+(\Delta Y)^2]^{\frac{1}{2}}}.\end{aligned} \tag{4.12}$$

Once the source strength $Q$ has been calculated, the value of $\phi(x, y)$ can be evaluated as follows:

$$\begin{aligned}\phi(x,y) &= \phi_0(x,y) + \int_S dS\, Q(\xi,\eta)\, G(kR) \\ &= \phi_0(x,y) + \int_S dS\, Q(\xi,\eta)\left[\frac{1}{2\pi}\log R + M(kR)\right] \\ &= \phi_0(x,y) + \sum_j Q_j \Delta S_j M_j + \sum_j Q_j A_j,\end{aligned} \tag{4.13}$$

where
$$\begin{aligned}A_j &= \frac{1}{2\pi}\int_{\Delta S_j} \log R\, dS \\ &= \mathrm{Re}\left\{\frac{1}{2\pi}\int_{\Delta S_j} \log z\, dz\, .\, e^{i\alpha}\right\} \\ &= \mathrm{Re}\left\{\frac{1}{2\pi} e^{-i\alpha}[z_2 \log z_2 - z_2 - z_1 \log z_1 + z_1]\right\}.\end{aligned}$$

The symbols $z_1$, $z_2$ and $\alpha$ are as indicated in figure 2, and are related to the original system as follows ($z_1$ and $z_2$ are complex numbers):

$$\left.\begin{aligned} e^{-i\alpha} &= \frac{X_{j+1}-X_j-i(Y_{j+1}-Y_j)}{\Delta S_j}, \\ \Delta S_j &= [(X_{j+1}-X_j)^2+(Y_{j+1}-Y_j)^2]^{\frac{1}{2}}, \\ z_2 &= (X_{j+1}-\xi_i)+i(Y_{j+1}-\eta_i) \\ \text{and} \quad z_1 &= (X_j-\xi_i)+i(Y_j-\eta_i).\end{aligned}\right\} \tag{4.14}$$

Once the value of $\phi(x, y)$ is known, the velocity potential can be calculated from (2.9).

$$\Phi(x, y, z; t) = -\frac{Ag}{\omega i}\phi(x, y)\frac{\cosh k(z+h)}{\cosh kh}e^{-i\omega t}, \tag{4.15}$$

where $\phi(x, y)$ is the value obtained from (4.13).

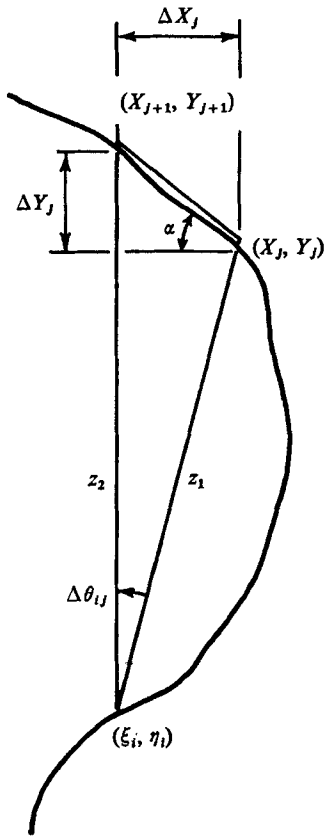


FIGURE 2. Co-ordinates used to evaluate the integral $\frac{1}{2\pi}\int_{\Delta S_j} dS \log R$.

The velocity components at any location $(x, y, z)$ can be calculated as

$$u = -\frac{\partial \Phi_r}{\partial x} = -\frac{Ag}{\omega}\left[\frac{\partial \phi_i}{\partial x}\cos\omega t - \frac{\partial \phi_r}{\partial x}\sin\omega t\right]\frac{\cosh k(z+h)}{\cosh kh}, \tag{4.16}$$

$$v = -\frac{\partial \Phi_r}{\partial y} = -\frac{Ag}{\omega}\left[\frac{\partial \phi_i}{\partial y}\cos\omega t - \frac{\partial \phi_r}{\partial y}\sin\omega t\right]\frac{\cosh k(z+h)}{\cosh kh}, \tag{4.17}$$

where the subscripts $i$ and $r$ refer to the imaginary and real parts of the complex values, respectively.

The amplification factor at any point $(x, y)$ is equal to the ratio of maximum wave height obtained at point $(x, y)$ to the wave height at infinity. The maximum

wave amplitude at infinity is $A$. However, the maximum wave amplitude at point $(x, y)$ is

$$\zeta_{\max} = \left| -\frac{1}{g}\frac{\partial \Phi}{\partial t}\bigg|_{z=0} \right| = A\,|\phi(x, y)|.$$

Thus the amplification factor at any point $(x, y)$ is simply

$$R = |\phi(x, y)|. \tag{4.18}$$

The actual choice of number and distribution of segments around the harbour is necessarily largely intuitive. The results presented in this paper were computed with about 60 segments, distributed fairly evenly around the harbour and extending to about two wavelengths along the straight outside edges. Essentially the same results (to an accuracy of better than one per cent inside the harbour) were obtained using 40 segments, either by truncating closer to the harbour entrance (say at one wavelength distance) or by reducing the overall density of segments. Generally speaking, a density of eight segments per wavelength was found to be satisfactory, with more points where the shoreline changes rapidly or at points of special interest.

## 5. Results and discussion

To check the accuracy of the numerical results obtained by the present theory, a rectangular harbour of dimension $12{\cdot}25 \times 2{\cdot}38$ inches was chosen first for numerical calculation. This particular harbour geometry has been studied both analytically and experimentally by Ippen & Goda (1963); therefore, a comparison of their results with the results obtained by the present theory can be made. Furthermore, this is a relatively long harbour, so that Ippen & Goda's approximations should be acceptable, and our results should agree with theirs.

Figure 3 shows the frequency response of the rectangular harbour. The experimental results are indicated by the small circles, while the theoretical results obtained by Ippen & Goda are the solid curve. The dotted line was calculated by the present theory. All results were calculated and measured at location $A$ as shown on the figure. Both theoretical curves are in agreement with the experimental data except around the fundamental mode.

The scattering of the experimental amplification factors, around the fundamental mode of resonance, has been indicated by Ippen & Goda to be due to inefficiency of the wave energy dissipators for incident waves of very low steepness. For low wave steepness, the transmission coefficient of wave filters increases, and their effectiveness for dissipation becomes small. Thus, the incident waves generated by the wave paddle were interfered with by the waves radiated from the wall.

The experimental results are lower than theory close to the fundamental periods. This is probably due to energy dissipation generated by eddies around the entrance and friction along the side wall and bottom, which has not been considered in either theory.

As shown in figure 3, in the immediate neighbourhood of the fundamental period, the results obtained by the present theory are slightly larger than those

reported by Ippen & Goda. These differences are probably due to the result of approximation used by Ippen & Goda.

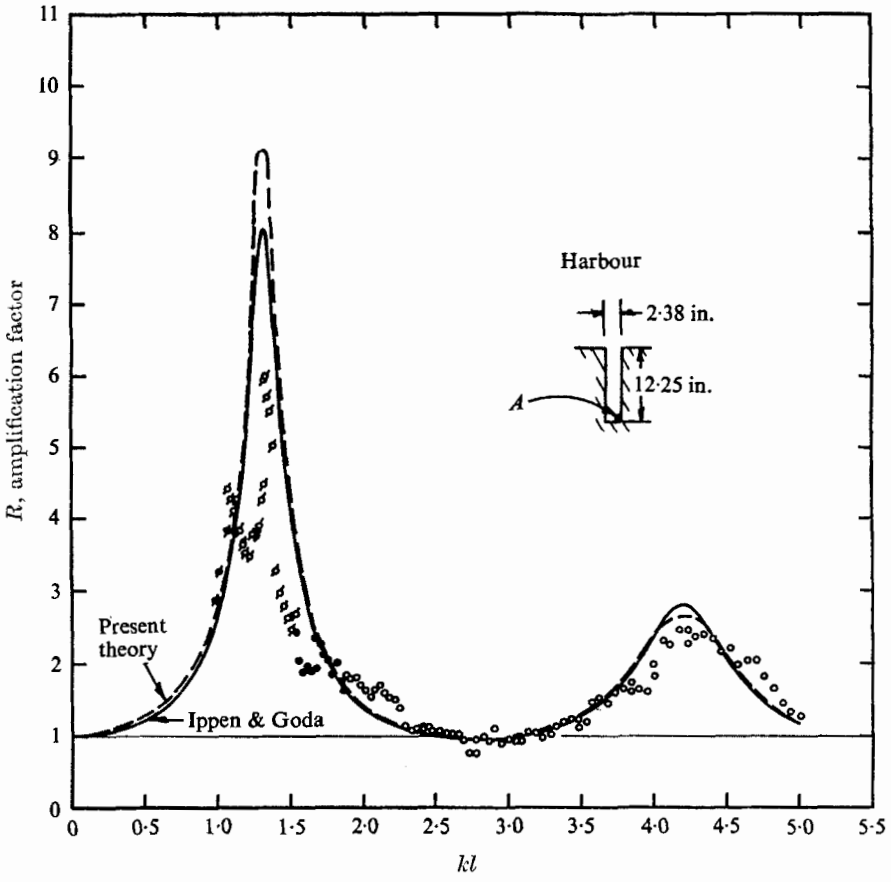


FIGURE 3. A comparison of theoretical and experimental results for frequency response of a fully open harbour.

Typical amplification fields of wave height for the rectangular harbour were calculated by use of (4.18). The results of these calculations are plotted in figures 4, 5 and 6. The units indicated on the figures represent the scale of the wave height relative to the incoming wave height. The results plotted in figures 4 and 5 are for $kl$ equal to 1·3 and 4. They are located near the fundamental and the first harmonic, respectively. Thus the maximum wave height inside the harbour is larger than the wave height outside the harbour. Furthermore, it is interesting to point out that the waves outside the harbour entrance do not decrease uniformly as the distance from the harbour increases. Instead, they exhibit a modulation phenomenon which results from the superposition of the radiated waves and the incident waves. The results plotted in figures 4 and 6 have the same wave-number, but a different incident angle. It is clear that the amplification factor in figure 6 is considerably less than that in figure 4. This is

expected because the effective wave-number decreases when the incident wave is at an angle, and the effective frequency of excitation is further away from the fundamental period of oscillation.

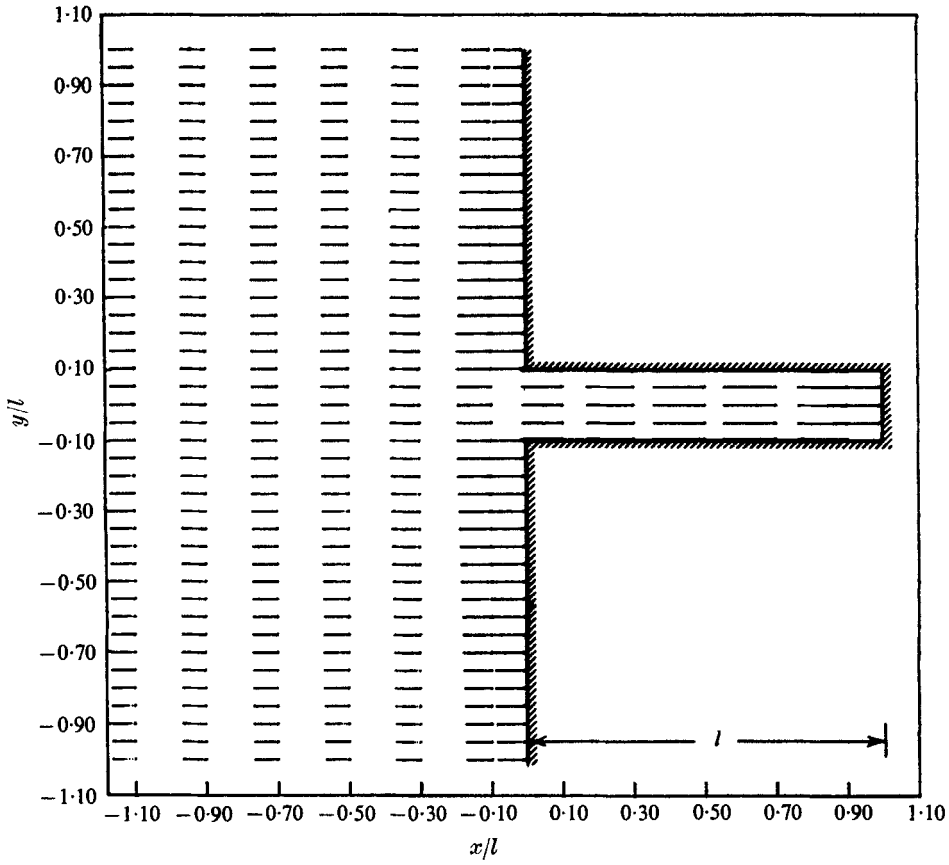


FIGURE 4. Amplification factor field of the wave height at $kl = 1{\cdot}3$, $\beta = 0°$. ——— 15 units.

Figures 7 and 8 show the amplification factor of the wave height for a bay with a complex shape. In the case where the wave-number is small (long waves), the water level inside the entire harbour oscillates almost uniformly; thus the amplification factor is more or less uniform inside the harbour as shown in figure 7.

In contrast, in figure 8, the incident wavelength $L$ is relatively short in comparison to harbour length $l$ ($L \approx 1{\cdot}5l$). The oscillations inside the harbour become rather complicated. Each basin inside the harbour may develop its own mode of oscillation, and at the same time may also affect the oscillation of a neighbouring basin. Such mutual interaction may be referred to as a 'coupling oscillation'. Thus, in determining oscillations of a harbour with multiple basins, one cannot treat each basin separately without considering these interaction phenomena. As can be seen in figure 7, there is hardly any nodal line at the entrance of the bay, while in figure 8, one may identify a nodal line near the entrance. The

presence and location of such a nodal line is not only a function of harbour geometry but also depends on the frequency of the incoming wave. A solution with an imposed condition at the entrance is, therefore, not the solution of the actual problem. Such a condition has often been assumed (McNown 1952;

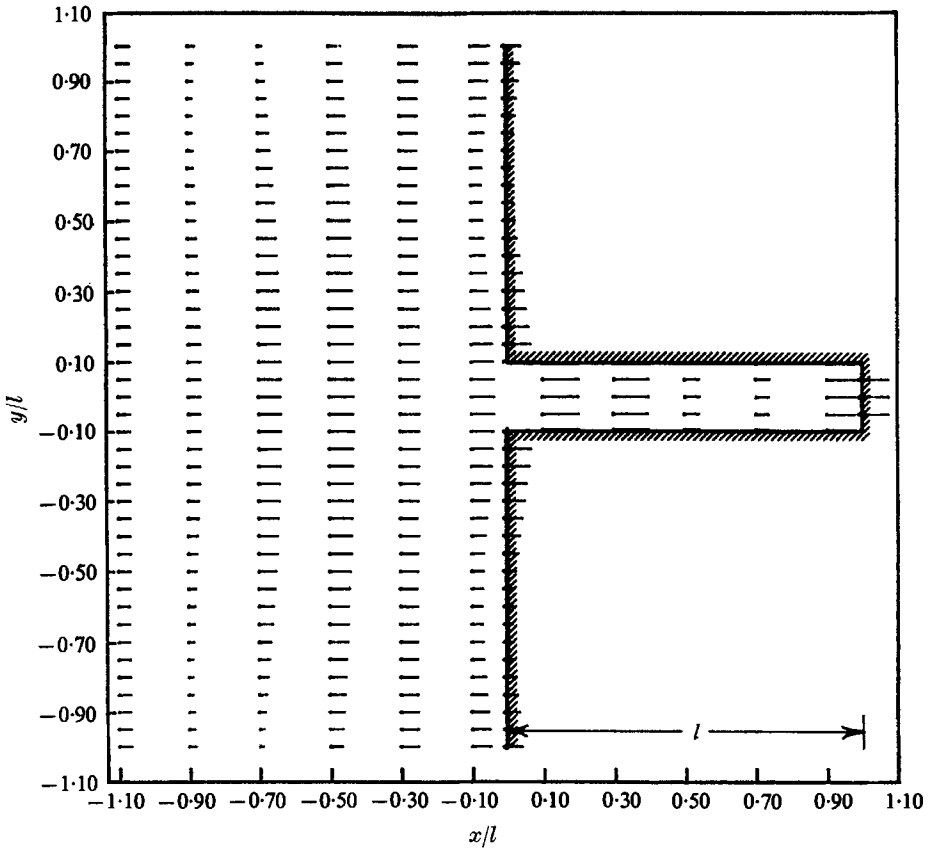


FIGURE 5. Amplification factor field of the wave height at $kl = 4$, $\beta = 0°$. ——— 6 units.

Wilson, Hendrickson & Kilmer 1965; Leendertse 1967; Loomis 1966). In particular, the use of the assumption of a nodal line at the entrance may introduce a large degree of inaccuracy, and may sometimes lead to wrong conclusions. With a complicated open harbour, it is, in any case, quite arbitrary what we might call the 'entrance'.

The velocity at any point can be calculated from (4·16) and (4.17). At the free surface, the velocity can be obtained simply by letting $z = 0$ so that

$$u = -\frac{\partial \Phi_r}{\partial x} = -\frac{Ag}{\omega}\left[\frac{\partial \phi_i}{\partial x}\cos\omega t - \frac{\partial \phi_r}{\partial x}\sin\omega t\right], \tag{5.1}$$

$$v = -\frac{\partial \Phi_r}{\partial y} = -\frac{Ag}{\omega}\left[\frac{\partial \phi_i}{\partial y}\cos\omega t - \frac{\partial \phi_r}{\partial y}\sin\omega t\right]; \tag{5.2}$$

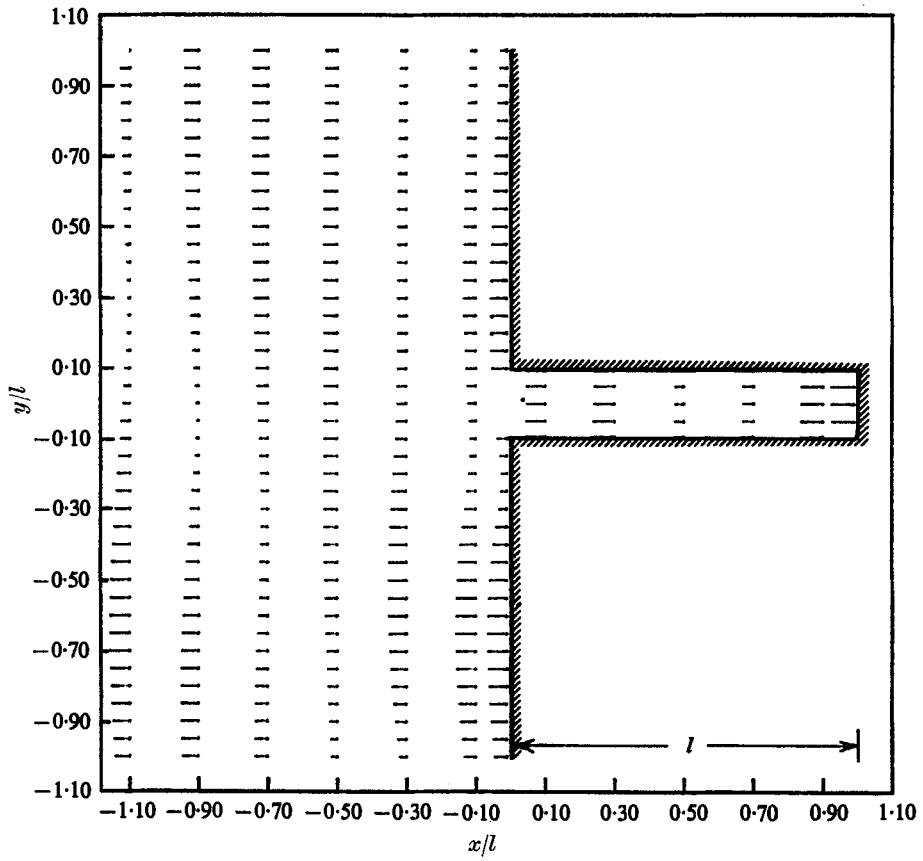


FIGURE 6. Amplification factor field of the wave height at $kl = 4$, $\beta = 45°$. ——— 6 units.

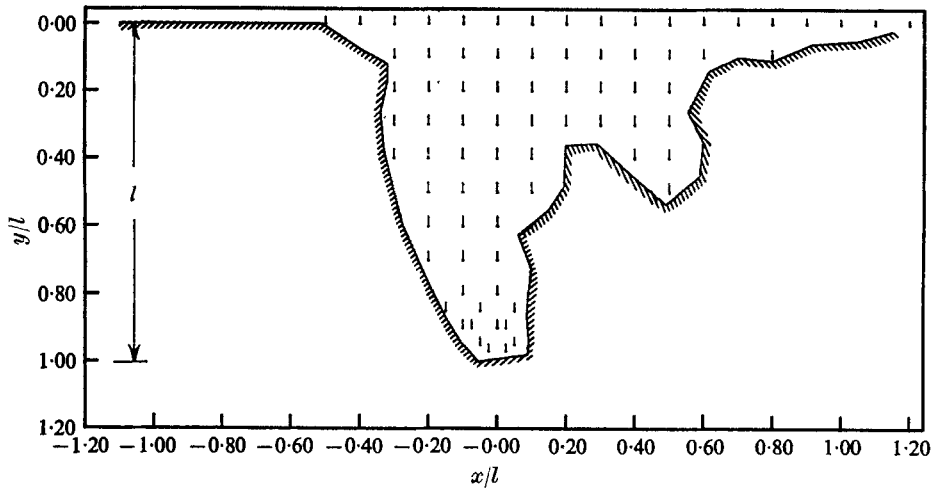


FIGURE 7. Amplification factor field of the wave height in an arbitrarily shaped bay at $kl = 1{\cdot}3$, $\beta = 0°$. ——— 12 units.

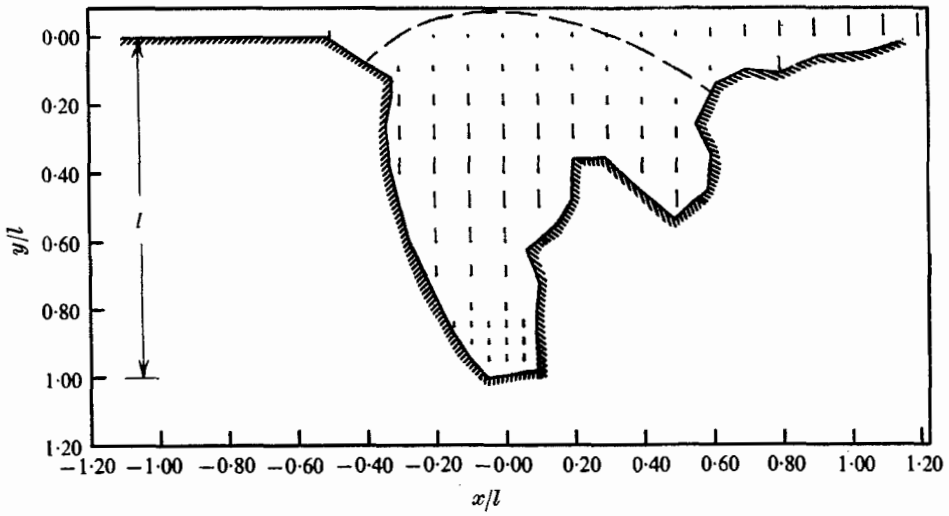


FIGURE 8. Amplification factor field of the wave height in an arbitrarily shaped bay at $kl = 4$, $\beta = 0°$. ——— 5 units.

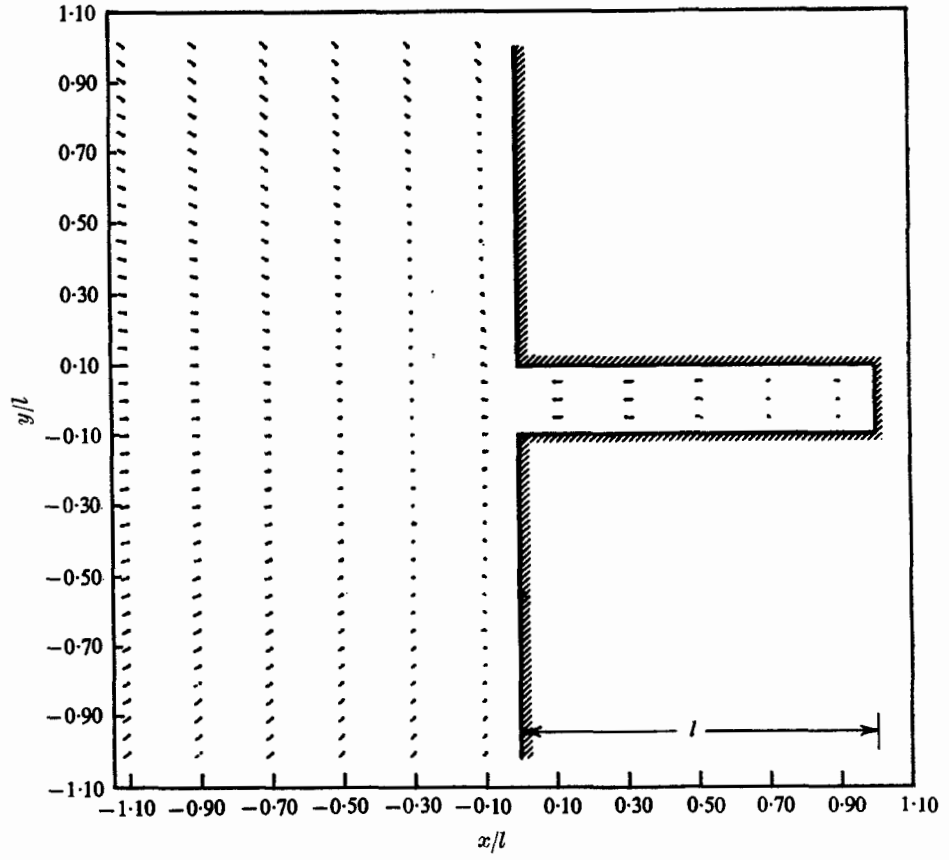


FIGURE 9. Velocity field in a rectangular harbour at $kl = 1{\cdot}3$, $\beta = 0°$. ——— 50 units.

from the above equations, it is clear that at a given point the magnitude and the direction of the velocity varies from time to time and the period of such variation equals the period of the incoming waves.

Figures 9 and 10 show the velocity field of the rectangular harbour corresponding to the phase $\omega t = \frac{1}{2}\pi$ with $kl = 1{\cdot}3$ and 4. The small line segments on

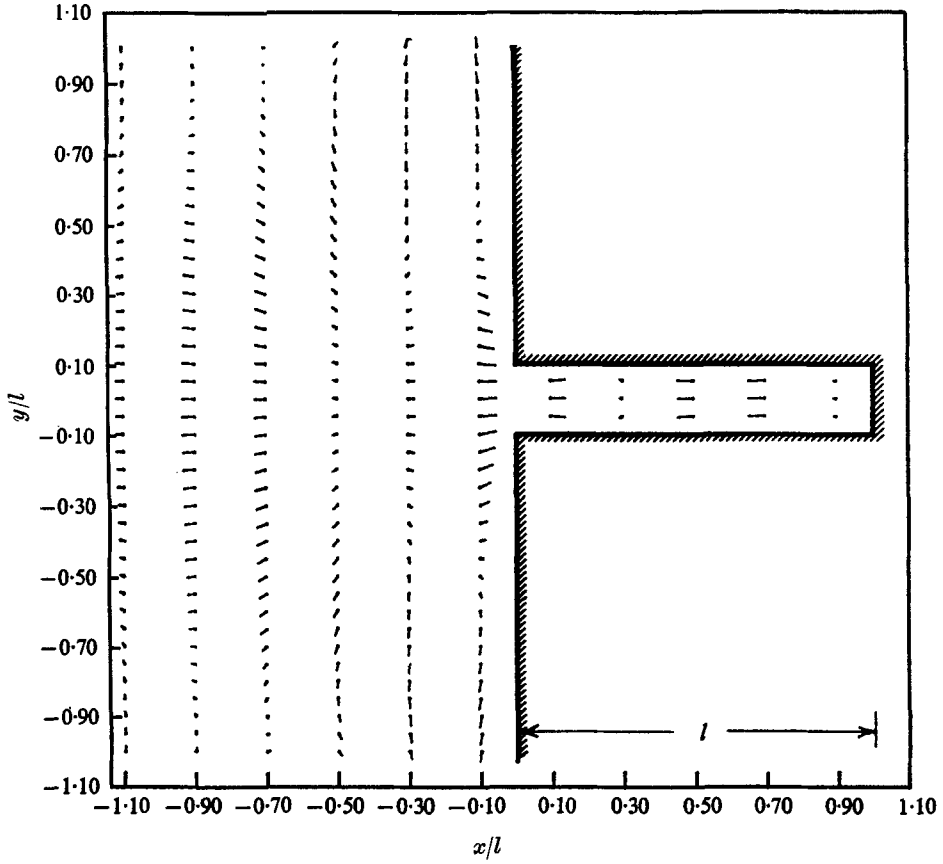


FIGURE 10. Velocity field in a rectangular harbour at $kl = 4$, $\beta = 0°$.
——— 16 units.

the figures indicate the magnitude and the direction of the velocity. The small black dots at the ends of the line segments indicate the locations where the velocity was calculated. The line pointing away from the black dot indicates the direction of the velocity. Figure 9 indicates that the velocity vectors around the harbour, at that instant, point toward the harbour entrance. This inflow of water in all directions around the entrance results in an increase of wave elevation inside the harbour. The magnification of the wave amplitude inside the harbour is associated with the proper match of the inflow of water with the outflow from the reflexions on the harbour boundary. If the characteristics of the harbour are such that the outflow and the inflow of water are properly matched with the incident wave, resonance is achieved. The wave-number or period for which the proper match can be achieved is a characteristic of the harbour.

Figure 11 shows the velocity field for $kl = 4$, but the incident wave is at an angle $\beta = 45$ degrees with the shoreline. The velocity outside the harbour is not symmetric with respect to the centreline. However, inside the harbour, the velocity pattern is still relatively uniform due to the relative narrowness of the harbour.

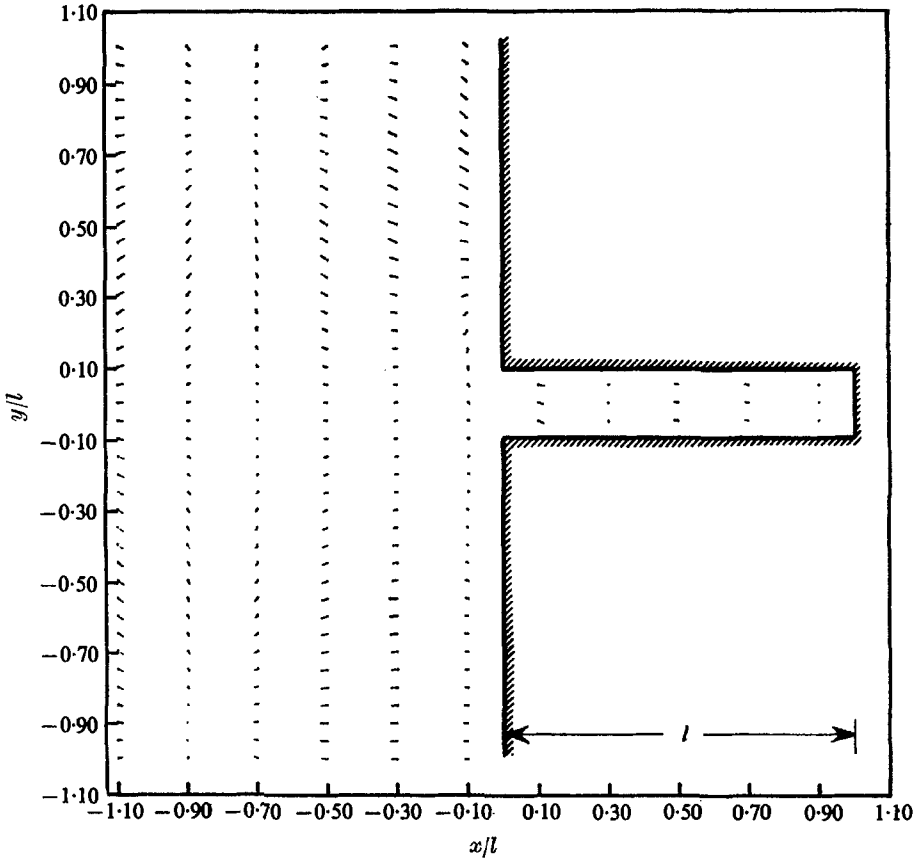


FIGURE 11. Velocity field in a rectangular harbour at $kl = 4$, $\beta = 45°$. ——— 30 units.

Figure 12 (plate 1) shows two reproduced photos of path-line patterns taken by Ippen & Goda. These two photos were taken at periods $T = 0{\cdot}6$ and $0{\cdot}5$ sec, as indicated in the figures. The velocity patterns shown on figures 9–11 exhibit some resemblance to the path-line patterns indicated in figure 12, although no quantitative agreement is to be expected since the harbour dimensions are different.

Figures 13 and 14 show the velocity field of an arbitrarily shaped bay. It is interesting to see that the velocity inside the harbour is not uniform. The existence of such complicated motions results from the phase lag of the reflected wave from the complex boundary. Such a complicated motion is more pronounced when the incident wave period becomes small, as can be seen from a comparison of figures 13 and 14.

This work was sponsored by the Atomic Energy Commission under contract AT(26-1)-289(M 002).

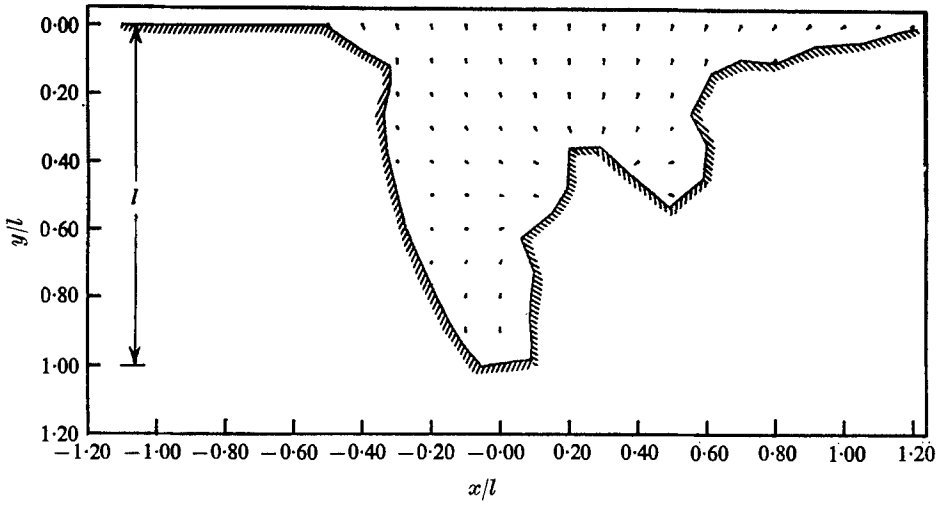


FIGURE 13. Velocity field in an arbitrarily shaped bay at $kl = 1{\cdot}3$, $\beta = 0°$. ——— 20 units.

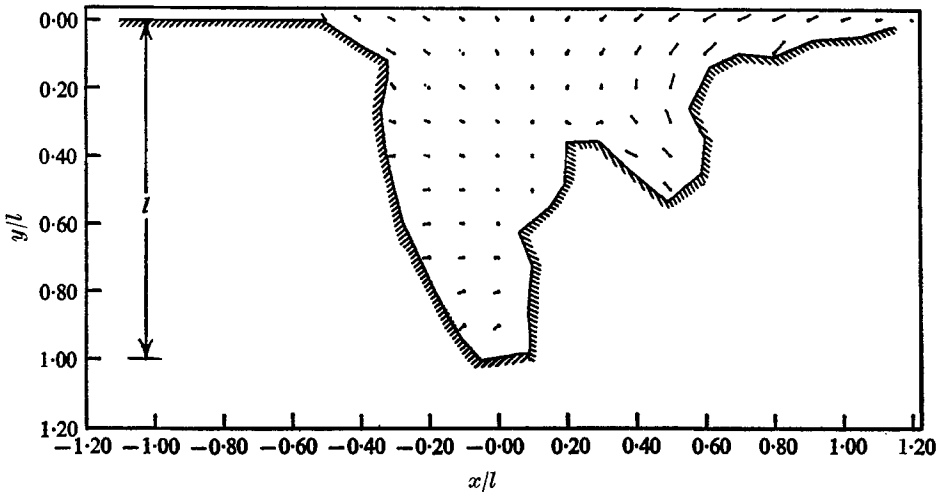


FIGURE 14. Velocity field in an arbitrarily shaped bay at $kl = 4$, $\beta = 0°$. ——— 15 units.

## REFERENCES

BIESEL, F. & LE MÉHAUTÉ, B. 1955 Etude theorique de la reflexion de la houle sur certains obstacles. *La Houille Blanche*, pp. 130–140.

BIESEL, F. & LE MÉHAUTÉ, B. 1956 Mouvements de resonance a deux dimensions dans une enceinte sous l'action d'ondes incidentes. *La Houille Blanche*, pp. 348–374.

IPPEN, A. T. & GODA, Y. 1963 Wave induced oscillations in harbours: The solution for a rectangular harbour connected to the open sea. *Hydro Lab., Mass. Inst. of Tech.*

KRAVTCHENKO, J. & MCNOWN, J. S. 1955 Seiche in rectangular ports. *Quart. Appl. Math.* **13**, 19–26.

LEENDERTSE, JAN J. 1967 Aspects of a computational model for long period water-wave propagation. *Rand Co. Report* no. RM-5294-PR.

LE MÉHAUTÉ, B. 1960 Periodical gravity wave on a discontinuity. *J. Hydraulics Div. ASCE*, pp. 11–41.

LE MÉHAUTÉ, B. 1961 Theory of wave agitation in a harbour. *J. Hydraulics Div. ASCE*, no. 2765.

LOOMIS, H. 1966 Some numerical hydrodynamics for Hilo harbour, Hawaii. *Institute of Geophysics, University of Hawaii.*

MCNOWN, J. S. 1952 Waves and Seiche in idealized ports. *Gravity Waves Symposium*, National Bureau of Standards, Circular 521.

MILES, J. & MUNK, W. 1961 Harbour paradox. *Journal of Waterways and Harbours Division, ASCE*, no. 2888.

STOKER, J. J. 1963 *Water Waves.* New York: Interscience.

WILSON, B. W., HENDRICKSON, J. A. & KILMER, R. E. 1965 Feasibility study for surge-action model of Monterey harbour, California. *U.S. Army Engineers, WES, Corps of Engineers.*

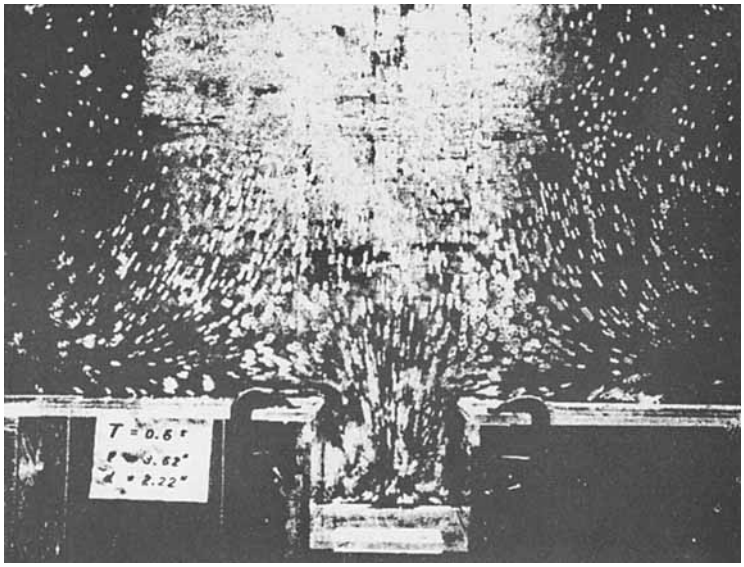


Resonance ($T$ = 0·6 sec).

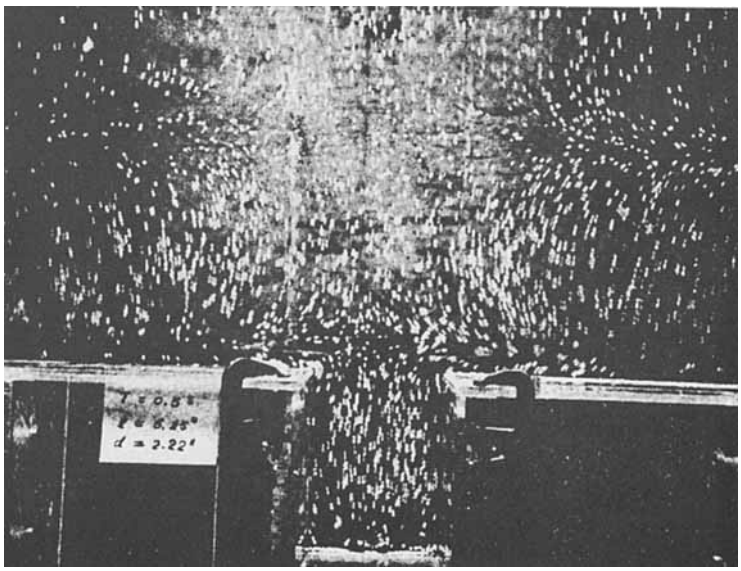


Anti-Resonance ($T$ = 0·5 sec).

FIGURE 12. Path-line pattern (reproduced from Ippen & Goda 1963).

*J. Fluid Mech.* (1970), *vol.* 42, *part* 3, *pp.* 465–470
*Printed in Great Britain*



# On the instability of natural convection flow on inclined plates

By J. R. LLOYD AND E. M. SPARROW
University of Minnesota, Minneapolis, Minnesota

(Received 7 October 1969)

Experiments are carried out to establish the relationship between the nature of the flow instability and the inclination angle of the plate. The angular dependence of the Rayleigh number characterizing the onset of instability is also determined. An electrochemical flow visualization technique is utilized to expose the patterns of fluid motion. It is found that for inclination angles of less than 14° (relative to the vertical), waves are the mode of instability. On the other hand, for inclination angles in excess of 17°, the instability is characterized by longitudinal vortices. The range between 14° and 17° is a zone of continuous transition, with the two modes of instability co-existing.

## Introduction

The onset of laminar-turbulent transition in natural convection flow on a vertical plate is characterized by wave-type disturbances (ideally, plane waves travelling in the streamwise direction). On the other hand, for plates inclined such that the surface normal has a component in the upward vertical direction, there is a range of angles of inclination for which the onset of transition is characterized by longitudinal vortices (Sparrow & Husar 1969). The inclination angle at which one type of instability gives way to the other has not been known heretofore.

The present investigation is aimed at establishing the relationship between the inclination angle and the nature of the instability and, additionally, at determining accurate quantitative information on the angular dependence of the Rayleigh number for instability. The realization of these objectives was facilitated by the use of a flow visualization technique which permits observation of the three-dimensional character of the flow field. As described later, the visualization is accomplished by an electrochemical reaction which results in local colour changes of the fluid. The working fluid in the experiments was water.

Prior experimental investigations of natural convection instability on inclined plates have been limited by an inability to observe the three-dimensional aspects of the flow (Lock, Gort & Pond 1967; Tritton 1963). Consequently, although values of the instability Rayleigh number are reported (the accuracy of which will be discussed later), the nature of the instability went undetected. Indeed, in Lock, Gort & Pond (1967), it was implied that instability on an inclined plate is of the same character as instability on a vertical plate. Natural convection heat transfer studies on inclined plates have been performed by several investigators (e.g. Schmidt 1932; Rich 1953; Kierkus 1968; Vliet 1969), but without

specific concern for the details of the transition process. Estimates of the instability Rayleigh number can be made from some of the available heat transfer information. Comparisons will be made between the instability Rayleigh numbers determined herein and those of the prior literature.

## Apparatus and measurement technique

The plate employed in these experiments was designed to present an isothermal surface to the flow. It was fabricated from heavy aluminium (coated with nickel to minimize corrosion), with fourteen longitudinal channels milled into the interior to facilitate the circulation of fluid from a constant temperature bath. The plate was 20 cm wide and 21·5 cm long. Plastic strips were fixed to the lateral edges to minimize end effects. The temperature of the heating fluid circulating through the plate was controlled to within $\pm$ 0·03 °C by the constant temperature bath.

The plate was placed at one end of a glass-walled tank whose dimensions were 58 cm in length, 30 cm in width, and 40 cm in depth. The tank contained water plus small amounts of additives as required by the electrochemical flow visualization technique. The leading edge of the plate was positioned about 6 cm off the bottom of the tank. The angle of the inclination of the isothermal surface relative to the vertical was measured with a protractor, the accuracy of the measurement being within one degree. Positive inclination angles denote the situation in which the outward normal to the isothermal surface has a component in the upward vertical direction, and negative angles correspond to the case in which the surface normal has a downward vertical component.

The flow visualization technique is an adaptation of that described by Baker (1966), and was also used in Sparrow & Husar (1969). A pH indicator, thymol blue, is added to the water in an amount approximately 0·01 percent by weight. The colour of the solution is yellow orange when the pH is below 8 and blue when the pH exceeds 8. By sequential addition of sodium hydroxide and hydrochloric acid, the pH is brought very near to the end-point so that the solution is yellow orange in colour. If a small d.c. voltage is applied between two electrodes situated in the solution, there is a transfer of electrons at the cathode, which increases the pH and results in a colour change in the fluid at the cathode. The thus-created blue dye is neutrally buoyant and faithfully follows the fluid motion. In these experiments, the isothermal plate served as the cathode. The voltages employed were between 6 and 16$\frac{1}{2}$ volts.

When the flow instability is characterized by longitudinal vortices, the visualization pattern is an array of more or less regularly spaced lines aligned with the streamwise direction and distributed across the width of the plate (see photographs presented in Sparrow & Husar 1969). Each line corresponds to the outflow leg of a longitudinal vortex. On the other hand, in the case of the plane wave type of instability, one sees lines transverse to the flow direction, more or less parallel to the leading edge.

The onset of instability is taken to coincide with the first appearance of either of the just-discussed types of lines. That is, the lowest point on the plate surface

at which the lines could be observed was regarded as the point at which instability first occurred. A single determination of a point of instability was made over a span of 10 min of careful observation. As discussed later, ten independent determinations were made at each angle of inclination.

The surface temperature of the plate was measured with calibrated copper constantan thermocouples inserted into holes drilled from the back side of the plate. Laboratory grade thermometers were employed to measure the bulk fluid temperature. The vertical distribution of the bulk temperature was monitored throughout each data run. No data were taken when the vertical gradient exceeded 0·045 °C/cm. The fluid was thoroughly mixed prior to the initiation of each run. The bulk fluid temperature was typically about 20 °C, while the wall to bulk temperature difference ranged from 15·5 °C to 27·5 °C.

## Results and discussion

### *Nature of the flow instability*

Experiments were performed for inclination angles ranging from $-10°$ to $+60°$. It was initially established that instability is characterized by longitudinal vortices for inclination angles exceeding 20°, while waves are the mode of instability for angles less than 10°.

The range of angles between 10° and 20° was painstakingly examined to observe the manner in which one type of instability gives way to the other. Starting at 20° and decreasing the angle of inclination, one first observes the intermittent presence of waves at about 17°, co-existing with the longitudinal vortices. With decreasing angle, the waves become stronger, while the vortices tend to weaken. At about 14°, the vortices can no longer be observed. This same behaviour is in evidence when one starts at 10° and increases the angle of inclination.

Thus, the range of inclination angle from 14° to 17° is a transition zone within which the character of the instability changes continuously from waves to longitudinal vortices. That is, the transition between the two types of instability is not abrupt.

### *Instability Rayleigh numbers*

The first occurrence of instability is reported here in terms of the Rayleigh number, defined as

$$Ra = g\beta(T_w - T_\infty)x^3/\alpha\nu, \tag{1}$$

where $x$ is the streamwise co-ordinate, measured from the leading edge, at which instability is first observed. $T_w$ and $T_\infty$ respectively represent the wall and fluid bulk temperatures, $g$ the acceleration of gravity, $\beta$ the thermal expansion coefficient, and $\alpha$ and $\nu$ the thermal diffusivity and kinematic viscosity respectively. The quantity $\beta/\alpha\nu$ is a fluid property grouping which is temperature dependent; it was evaluated at the average of $T_w$ and $T_\infty$.

At each fixed angle of inclination, ten completely independent determinations of the instability Rayleigh number were made, encompassing a period of several days. The mean and standard deviation of these determinations were evaluated.

The mean instability Rayleigh number for each inclination angle is plotted in figure 1, with the fully blackened circles corresponding to the vortex instability and partly blackened circles corresponding to wave instability. A dashed line has been faired through these data points to provide continuity. A listing of the mean Rayleigh numbers and the standard deviations is given in table 1.

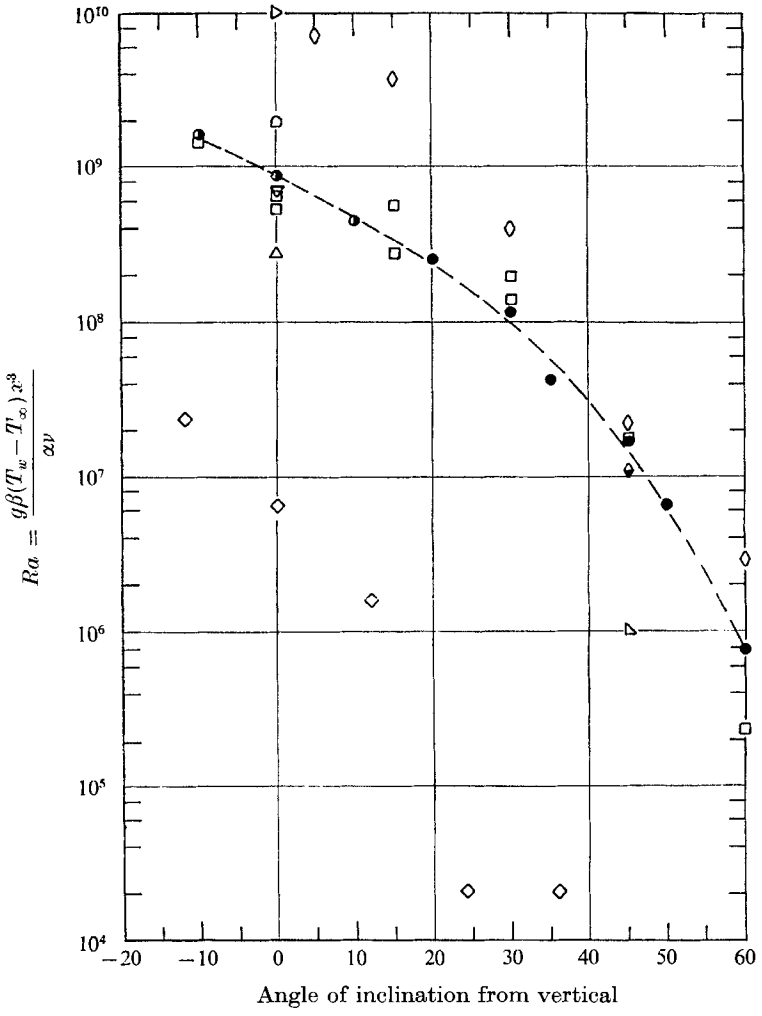


FIGURE 1. Instability Rayleigh numbers. Present investigation (water): ●, vortex instability; ◑, wave instability. □, Lock, Gort & Pond (air). ◇, Tritton (air). ◺, Kierkus (air). Uniform heat flux: ◇, Vliet (water); ◆, Vliet (air). △, Eckert & Soehngen (air). ▽, Hermann (air). ⌓, Saunders, (air). ▷, Szewczyk (water).

As evidenced by the figure, the instability Rayleigh number varies markedly with the angle of inclination. The effect of inclining the plate so that its normal has a component in the upward vertical direction (i.e. positive inclination angles) is to make the flow more susceptible to instability. On the other hand, a plate whose normal has a downward directed component is less susceptible to instability. In the range of angles between $-10°$ and $60°$, $Ra$ diminishes by more

than three orders of magnitude. For the vertical plate, the present experiments give a $Ra$ value of $8{\cdot}7 \times 10^8$, which, as discussed below, agrees very well with prior information.

In addition to the present results, figure 1 also contains data from several prior investigations, among which that of Lock and co-workers (1967) and of Tritton (1963) were concerned with instability and transition on an inclined plate. The Lock data were obtained either by observation of schlieren pictures

| Angle (degrees) | Mean $Ra$ | Standard deviation |
|---|---|---|
| −10 | $1{\cdot}6 \times 10^9$ | $0{\cdot}15 \times 10^9$ |
| 0 | $8{\cdot}7 \times 10^8$ | $1{\cdot}2 \times 10^8$ |
| 10 | $4{\cdot}5 \times 10^8$ | $1{\cdot}2 \times 10^8$ |
| 20 | $2{\cdot}5 \times 10^8$ | $0{\cdot}81 \times 10^8$ |
| 30 | $1{\cdot}2 \times 10^8$ | $0{\cdot}50 \times 10^8$ |
| 35 | $4{\cdot}2 \times 10^7$ | $1{\cdot}1 \times 10^7$ |
| 45 | $1{\cdot}7 \times 10^7$ | $0{\cdot}79 \times 10^7$ |
| 50 | $6{\cdot}8 \times 10^6$ | $2{\cdot}5 \times 10^6$ |
| 60 | $7{\cdot}7 \times 10^5$ | $4{\cdot}6 \times 10^5$ |

TABLE 1. Mean instability Rayleigh numbers and standard deviations

or by monitoring the output of thermocouples immersed in the fluid and distributed along the centreline of the plate. Since the schlieren apparatus necessarily averages along the direction of the light path, i.e. along the width of the plate, three-dimensional phenomena such as longitudinal vortices are obscured. In the absence of other information, it was presumed by those investigators that wave-type instability existed for all angles of inclination, a postulate which is invalidated by the present observations. Each of Lock's data points appearing in figure 1 corresponds to a single determination, and generally good agreement is seen to prevail with the results of the present study.

Tritton (1963) employed a fibre anemometer to detect transition. His experiments were performed in air, and observations were restricted to the midpoint of the plate width. As is seen from the figure, the Tritton data fall very much lower than those of all other investigators. This state of affairs may well be due to strong disturbances in the laboratory room (mentioned by Tritton himself) or to the presence of a solid wall situated parallel and above the test plate, thereby providing conditions for a channel-like flow. Also, the length of the fibre, 3·07 cm, introduces some uncertainty into the evaluation of the distance $x$ that appears in the Rayleigh number.

From inclined-plate heat transfer characteristics determined by Kierkus (1968) and Vliet (1969), values of the Rayleigh number for laminar-turbulent transition have been deduced and are shown in figure 1. Rayleigh numbers arrived at in this way need not necessarily correspond to the first appearance of instability. The Vliet data merit some discussion. They are the only data in figure 1 for the uniform surface heat flux boundary condition, all other being for uniform surface temperature. It has been demonstrated analytically by Gebhart (1969) that the instability of the flow can be influenced by the heat capacity of the

thin metallic foils commonly employed in experiments involving uniform heat flux.

For completeness, representative instability and transition data for the vertical plate have been brought together and are plotted in figure 1. The main body of the data fall in the Rayleigh number range from $2{\cdot}8 \times 10^8$ to $2 \times 10^9$.

Observations made during the course of the present investigation, as well as those of prior investigators (e.g. Lock *et al.* 1967; Tritton 1963; Vliet 1969) indicate that the instability Rayleigh number for a fixed angle of inclination contains a certain degree of randomness. It was in recognition of this fact that ten independent determinations were made at each inclination angle. The extent of the randomness is indicated by the listing of standard deviations in table 1. It is seen that the larger the angle of inclination, the more marked the randomness.

## Concluding remarks

The nature of the flow instability and reliable values of the instability Rayleigh number have now been experimentally established for natural convection on inclined isothermal surfaces. This body of information is, at least in principle, amenable to complementary analytical exploration. Thus far, it has been demonstrated (Gebhart 1969) that linear theory is capable of predicting the salient features of the instability for natural convection flow on a vertical plate. However, instability of the flow on inclined plates has yet to be subjected to analysis.

## REFERENCES


Baker, D. J. 1966 A technique for the precise measurement of small fluid velocities. *J. Fluid Mech.* **26**, 573.

Eckert, E. R. G. & Soehngen, E. 1951 Interferometric studies on the stability and transition to turbulence of a free convection boundary layer. *Gen. Disc. Heat Transfer, I. Mech. E., London*, p. 321.

Gebhart, B. 1969 Natural convection flow, instability, and transition. *J. Heat Transfer*, **91**, 293.

Hermann, R. 1954 Heat transfer by free convection from horizontal cylinders in diatomic gases. *NACA TM* 1366.

Kierkus, W. T. 1968 An analysis of laminar free convection flow and heat transfer about an inclined isothermal plate. *Int. J. Heat Mass Transfer*, **11**, 241.

Lock, G. S. H., Gort, C. & Pond, G. R. 1967 A study of instability in free convection from an inclined plate. *Appl. Sci. Res.* **18**, 171.

Rich, B. R. 1953 An investigation of heat transfer from an inclined flat plate in free convection. *Trans. ASME* **75**, 489.

Saunders, O. A. 1939 Natural convection in fluids. *Proc. Roy. Soc.* A **172**, 55.

Schmidt, E. 1932 Schlierenaufnahmen des Temperaturfeldes in der Nähe Wärmeabgebender Körper. *Forsch. Geb. Ingenieur.* **3**, 181.

Sparrow, E. M. & Husar, R. B. 1969 Longitudinal vortices in natural convection flow on inclined surfaces. *J. Fluid Mech.* **37**, 251.

Szewczyk, A. A. 1962 Stability and transition of the free-convection layer along a vertical flat plate. *Int. J. Heat Mass Transfer*, **5**, 903.

Tritton, D. J. 1963 Transition to turbulence in the free convection boundary layers on an inclined heated plate. *J. Fluid Mech.* **16**, 417.

Vliet, G. C. 1969 Natural convection local heat transfer on constant-heat-flux inclined surfaces. *J. Heat Transfer*, **91**, 511.

*J. Fluid Mech.* (1970), *vol.* 42, *part* 3, *pp.* 471–489
*Printed in Great Britain*



# Numerical solutions for steady flow past a circular cylinder at Reynolds numbers up to 100

By S. C. R. DENNIS AND GAU-ZU CHANG
Department of Applied Mathematics, University of Western Ontario, London, Canada

(Received 27 June 1969 and in revised form 3 February 1970)

Finite-difference solutions of the equations of motion for steady incompressible flow around a circular cylinder have been obtained for a range of Reynolds numbers from $R = 5$ to $R = 100$. The object is to extend the Reynolds number range for reliable data on the steady flow, particularly with regard to the growth of the wake. The wake length is found to increase approximately linearly with $R$ over the whole range from the value, just below $R = 7$, at which it first appears. Calculated values of the drag coefficient, the angle of separation, and the pressure and vorticity distributions over the cylinder surface are presented. The development of these properties with Reynolds number is consistent, but it does not seem possible to predict with any certainty their tendency as $R \to \infty$. The first attempt to obtain the present results was made by integrating the time-dependent equations, but the approach to steady flow was so slow at higher Reynolds numbers that the method was abandoned.

## 1. Introduction

Numerical solutions for two-dimensional flow past a circular cylinder can be divided into two broad classes. First, there are those obtained by integrating the equations of steady motion. Thom (1928) gave the first solution at $R = 10$, where $R$ is the Reynolds number based on the diameter of the cylinder. Subsequently Thom (1933) gave a solution at $R = 20$ and Kawaguti (1953*b*), Apelt (1961) have both obtained solutions at $R = 40$. The general features of all these solutions and their development with Reynolds number are in agreement with experimental observations. For example, they indicate an approximately linear growth with Reynolds number of the standing vortex pair behind the cylinder. This is in agreement with the experiments of Taneda (1956).

On the other hand, solutions given by Allen & Southwell (1955) over the range $R = 0$ to $10^3$ and by Dennis & Shimsoni (1965) for the range $R = 0{\cdot}01$ to $10^6$ are generally thought to be unreliable at the higher Reynolds numbers. The main reason is that both sets of results indicate that the length of the vortex wake starts to decrease for some value of the Reynolds number between 10 and 100. This effect is most likely to be the result of numerical inaccuracy. Recent calculations by Hameliec & Raal (1969) also indicate an ultimate decrease in wake length as $R$ increases. The only reliable solutions of the equations of steady motion beyond $R = 40$ appear to be the results of Takami & Keller (1969), in

which the Reynolds number range of calculations by Keller & Takami (1966, p. 115) has been extended to $R = 60$. These results again indicate linear dependence of wake length on Reynolds number up to $R = 60$. One of the main objectives of the present work has been to obtain some check on these results and to extend the Reynolds number range. It was found that reliable results could be obtained up to $R = 100$.

The second class of numerical solutions comes from integrating the time-dependent equations of motion. The first solutions for a circular cylinder were given by Payne (1958) for $R = 40$ and 100 and subsequently re-investigated by Ingham (1968), but Kawaguti & Jain (1966) appear to have been the first to have continued the integrations for sufficiently large times for a steady flow configuration to be reached. Steady solutions were obtained in this way for $R = 10$ up to 50, but solutions for $R = 60$ and 100 were discontinued after a large time and before a steady state was reached. The slow rate of approach to the final solution for larger values of the Reynolds number seems to be one of the main objections to obtaining steady solutions by integrating the time-dependent equations. Recent results of Son & Hanratty (1969) at $R = 40$, 200 and 500 seem to suggest that the wake in the cases $R = 200$, 500 had far from settled down when the integrations were stopped. The steady drag value at $R = 500$ was estimated by extrapolation.

Kawaguti & Jain had previously found it necessary to estimate steady drag values by extrapolation at higher Reynolds numbers. The same slow approach to the steady solution was noted when the present solutions were first attempted by time-dependent methods. Integrations at $R = 70$ and 100 were discontinued after a large time because of the extremely slow build up of the wake. It might also be noted th at solutions of the equations of steady motion may not be stable for these Reynolds numbers (see, for example, Van Dyke 1964, p. 150), and instability could tend to obviate an approach to the steady solution through the time-dependent problem. In any case, the general evidence seems to suggest that the. time-dependent method is not an efficient method of calculating steady solution s Its main use remains as a method of predicting flows which do not tend to a steady state as time increases. Solutions with this principal objective have been obtained by Hirota & Miyakoda (1965) and by Thoman & Szewczyk (1966).

One of the objects of obtaining numerical solutions for steady flow past a cylinder is to attempt to gain information on the nature of the theoretical steady flow limit as $R \to \infty$. This is still unknown, but various models have been suggested. A recent review by Roshko (1967) indicates concepts of considerably differing nature. The classical model is the discontinuous potential flow theory of Kirchhoff as propounded, for example, by Squire (1934) and Kawaguti (1953*a*). This model gives a finite drag on the cylinder as $R \to \infty$, with a wake of infinite length and zero velocity separated from an inviscid region by free streamlines. Batchelor (1956) has proposed a limiting solution with a closed wake of finite length, containing two regions with uniform vorticity, associated with zero drag on the body. Acrivos, Snowden, Grove & Petersen (1965) have suggested that the wake remains viscous in character as $R \to \infty$, and that its length grows linearly with the Reynolds number. This model is based mainly on the results of

experiments in which the wake was stabilized using a splitter plate, thereby allowing steady flow patterns to be obtained for Reynolds numbers up to 180. Further results in support of the model have been given by Acrivos, Leal, Snowden & Pan (1968).

In the present paper, the results of calculations for $R = 5$, 7, 10, 20, 40, 70 and 100 are given. They were obtained by solving finite-difference approximations to the equations of steady motion. Reasonable precautions have been taken to ensure that the solutions are accurate. The numerical procedures have been described fully by Dennis & Chang (1969*a*, 1969*b*) and will only be summarized. The results up to $R = 40$ are given in order to show the consistent development of the physical properties with Reynolds number. They are in excellent agreement with the results of Takami & Keller, and the numerical procedures are sufficiently different to provide a completely independent check. The development beyond $R = 40$ is also consistent with Takami & Keller's solutions and to some extent with the model of Acrivos *et al.*, in that the length of the wake continues to elongate in proportion to the Reynolds number and its breadth remains roughly of the order of the cylinder diameter.

## 2. Equations and method of approximation

The equations are given in dimensionless form, corresponding to a cylinder of radius $r = 1$ in a uniform stream of unit magnitude with its direction that of the positive axis of $x$. Modified polar co-ordinates $(\xi, \theta)$ are used, $\xi$ where $= \log r$. The equations governing steady motion are:

$$\frac{\partial^2 \zeta}{\partial \xi^2} + \frac{\partial^2 \zeta}{\partial \theta^2} = \frac{R}{2}\left(\frac{\partial \psi}{\partial \theta}\frac{\partial \zeta}{\partial \xi} - \frac{\partial \psi}{\partial \xi}\frac{\partial \zeta}{\partial \theta}\right), \tag{1}$$

$$\frac{\partial^2 \psi}{\partial \xi^2} + \frac{\partial^2 \psi}{\partial \theta^2} = e^{2\xi}\zeta. \tag{2}$$

Here, $\psi$ is the dimensionless stream function and $\zeta$ is the negative dimensionless vorticity. They are defined respectively by the equations $\psi = \psi'/Ua$ and $\zeta = -a\zeta'/U$, where $\psi'$ and $\zeta'$ are the dimensional stream function and vorticity for a cylinder of radius $a$ in a uniform stream $U$. The Reynolds number is defined in the usual way as $R = 2aU/\nu$. The flow is assumed to possess symmetry about the axis of $x$, and the boundary conditions necessary to obtain a solution in the region $\xi \geqslant 0$, $0 \leqslant \theta \leqslant \pi$ are

$$\psi = \frac{\partial \psi}{\partial \xi} = 0 \quad \text{for} \quad \xi = 0, \tag{3}$$

$$e^{-\xi}\frac{\partial \psi}{\partial \xi} \to \sin\theta, \quad e^{-\xi}\frac{\partial \psi}{\partial \theta} \to \cos\theta \quad \text{as} \quad \xi \to \infty, \tag{4}$$

$$\zeta \to 0 \quad \text{as} \quad \xi \to \infty, \tag{5}$$

$$\psi = \zeta = 0 \quad \text{for} \quad \theta = 0, \pi. \tag{6}$$

A numerical solution is obtained on the square grid shown in figure 1, which also shows the numbering system adopted for a set of points surrounding a

typical point 0. The line $\xi = \xi_m$ is taken as an outer boundary on which approximations to the conditions at infinity, equations (4) and (5), may be assumed to hold. The numerical method consists of replacing (1) by finite-difference approximations on this grid. It is convenient to write

$$\lambda(\xi, \theta) = -\tfrac{1}{4}R\frac{\partial \psi}{\partial \theta}, \quad \mu(\xi, \theta) = \tfrac{1}{4}R\frac{\partial \psi}{\partial \xi}. \tag{7}$$

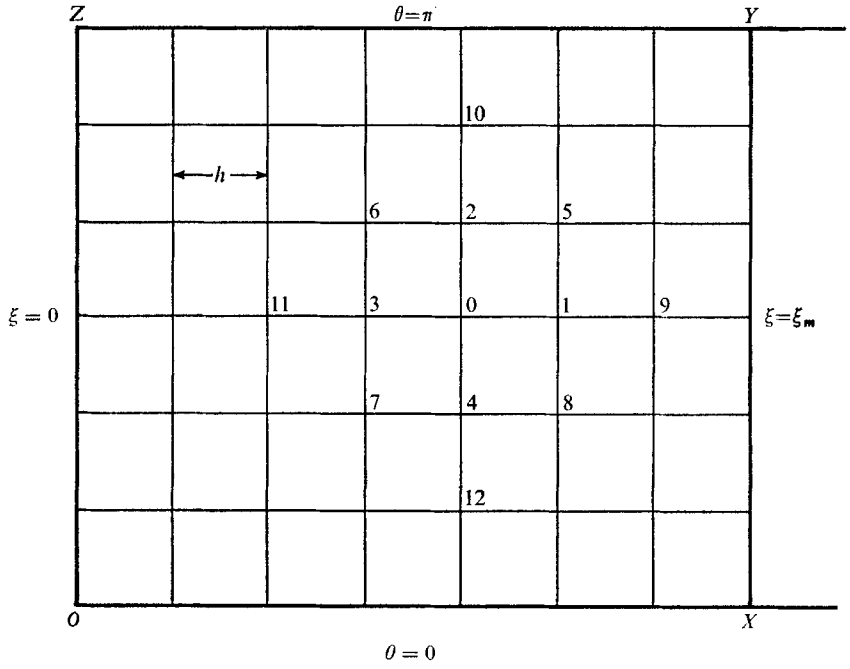


FIGURE 1. Domain of integration and grid structure.

The finite-difference equation obtained by replacing derivatives in (1) by the simplest possible approximations in central differences at 0 is

$$(1+h\lambda_0)\zeta_1+(1+h\mu_0)\zeta_2+(1-h\lambda_0)\zeta_3+(1-h\mu_0)\zeta_4-4\zeta_0 = 0. \tag{8}$$

Satisfaction of (8) at every internal grid point of the region $OXYZ$ of figure 1, subject to boundary conditions for $\zeta$ at every grid point of the boundary $OXYZ$, defines a numerical approximation to the solution of (1).

Boundary conditions on $OX$ and $YZ$ are given by (6), and we can take $\zeta = 0$ on $XY$ as a crude approximation to (5), assuming $\xi_m$ large enough. An improvement on this latter boundary condition is given by Dennis & Chang (1969*a*). The approximation $\zeta = 0$ is replaced by, effectively, a gradient condition for $\zeta$, on the assumption that the flow for $\xi \geqslant \xi_m$ is governed by Oseen's linearized equations. The details are almost the same as those already published by Dennis, Hudson & Smith (1968) and will be mentioned only briefly. The Oseen problem, which is valid for large $\xi$, is obtained by replacing the derivatives of $\psi$ in (1) by the expressions obtained from the boundary conditions (4). The equation which

results can then be solved formally and from the solution it is deduced, provided $\xi$ is large enough, that

$$\zeta(\xi, \theta) \sim G(\theta)\, \chi^{-\frac{1}{2}} \exp\{\chi(\cos\theta - 1)\}, \tag{9}$$

where $\chi = \frac{1}{4} R\, e^{\xi}$. Here, $G(\theta)$ is a function of $\theta$ alone and thus, if (9) is assumed to hold for $\xi \geqslant \xi_m$, we obtain the approximation

$$\zeta(\xi, \theta) = \zeta(\xi_m, \theta) \exp\{(\chi - \chi_m)(\cos\theta - 1) - \tfrac{1}{2}(\xi - \xi_m)\}, \tag{10}$$

where $\chi_m$ is the value of $\chi$ at $\xi = \xi_m$. In particular, if we put $\xi = \xi_m + h$ in (10), an expression for $\zeta(\xi_m + h, \theta)$ in terms of $\zeta(\xi_m, \theta)$ is obtained which can be used, in a similar manner to a gradient-type boundary condition, to eliminate $\zeta_1$ from (8) whenever the point 0 is situated on $\xi = \xi_m$.

The condition for $\zeta$ on $\xi = 0$ depends upon the solution of (2). It is in the method of solution of (2) and the calculation of boundary values of $\zeta$ on $\xi = 0$ that the present method differs from the usual finite-difference procedure. A solution of (2) is assumed in the form

$$\psi(\xi, \theta) = \sum_{n=1}^{\infty} f_n(\xi) \sin n\theta, \tag{11}$$

which automatically satisfies the conditions for $\psi$ in (6). Substitution in (2) gives

$$f_n'' - n^2 f_n = r_n(\xi) \quad (n = 1, 2, 3, \ldots). \tag{12}$$

Here, primes denote differentiation with regard to $\xi$ and

$$r_n(\xi) = \frac{2e^{2\xi}}{\pi} \int_0^{\pi} \zeta \sin n\theta \, d\theta. \tag{13}$$

From (3) it follows that

$$f_n(0) = f_n'(0) = 0, \tag{14}$$

and the equations (12) can be solved as a step-by-step integration, provided $r_n(\xi)$ is known for sufficient values of $n$ (say up to $n_0$) on all grid lines of constant $\xi$ from $\xi = 0$ to $\xi = \xi_m$. The number $n_0$ is the number of terms taken to approximate the infinite sum in (11). One further equation is necessary to complete the procedure. It can be deduced from the properties of the solutions of (12). In order that (4) shall be satisfied it is necessary that the condition

$$\int_0^{\infty} e^{-n\xi} r_n(\xi) \, d\xi = 2\delta_n \tag{15}$$

is satisfied, where $\delta_1 = 1$ and $\delta_n = 0$ $(n = 2, 3, \ldots)$. When the left side of (15) is expressed as a numerical quadrature formula over the grid lines of constant $\xi$, and with the upper limit approximated by $\xi_m$, it gives a formula for $r_n(0)$ in terms of grid values of $r_n(\xi)$ for $\xi \neq 0$. Thus, the condition (15) is used for calculating values of $r_n(0)$. From these values we can calculate $\zeta(0, \theta)$ from the result

$$\zeta(\xi, \theta) = e^{-2\xi} \sum_{n=1}^{\infty} r_n(\xi) \sin n\theta, \tag{16}$$

which follows from (13). In practice, the summation is again approximated by $n_0$ terms.

## 3. Calculation procedure

Suppose that a grid size $h$, a value for $\xi_m$, and a value for $n_0$ have been assigned for a given Reynolds number. A numerical solution is obtained by repeating the following cycle of steps until convergence is achieved. Suppose a starting approximation to $\psi$ is known and a boundary condition $\zeta(0,\theta)$ has been calculated from (16), using values of $r_n(0)$ determined to satisfy (15). Then:

(i) $\zeta(\xi,\theta)$ is determined by solving the equations (8) subject to the calculated boundary condition for $\zeta(0,\theta)$ and the other specified conditions on the remaining boundaries.

(ii) $r_n(\xi)$, $(n = 1, 2, \ldots, n_0)$ is calculated from (13) for all $\xi \neq 0$.

(iii) $r_n(0)$ is calculated to satisfy (15) and hence a new approximation to $\zeta(0,\theta)$ is found from (16).

(iv) The equations (12) are solved for $n = 1, 2, \ldots, n_0$ and a new approximation to $\psi(\xi,\theta)$ found from (11). This completes one cycle of the iteration.

Convergence of the procedure is decided by comparing some representative feature of two successive solutions. Many comparisons are possible. The one chosen was

$$|r_n^{(m+1)}(0) - r_n^{(m)}(0)| < \epsilon$$

for all $n \leqslant n_0$, where $\epsilon$ is a specified accuracy parameter and $m$, $m+1$ denote two successive iterates. This is a very representative convergence test because each $r_n(0)$, through (13) and then through (15), is calculated from a weighted sum involving every value of $\zeta$ (except those on $\xi = 0$) in the computational field. The test ensures, through (16), that the boundary vorticity has converged. One of the interesting features of the present method is that the vorticity on the cylinder is calculated by integration right throughout the field rather than from a few isolated values of $\psi$ near $\xi = 0$, as is the case in the usual finite-difference method of approximating (2). Moreover, equation (16) determines $\zeta(0,\theta)$ as a continuous function of $\theta$ more or less regardless of the grid size used in solving (1) provided, of course, that it is reasonably small. Features of the flow at the cylinder surface, such as the point of separation of the flow, can be determined accurately from (16).

The calculation procedure has been described in more detail by Dennis & Chang (1969*a*, 1969*b*) and only two points will be mentioned. The numerical evaluation of $r_n(\xi)$ from (13) is performed using the method of Filon (1928), since this gives uniformly accurate results, even if $n$ is large. Finally, at stage (iii) of the above calculation procedure, the new value of $\zeta(0,\theta)$ is not introduced directly as a new boundary condition on $OZ$. If a previous boundary condition $\zeta^{(m)}(0,\theta)$ gives rise, at stage (iii), to a calculated value $\zeta^*(0,\theta)$, the actual value introduced in the next iteration is

$$\zeta^{(m+1)}(0,\theta) = \kappa\zeta^*(0,\theta) + (1-\kappa)\zeta^{(m)}(0,\theta),$$

where $0 < \kappa \leqslant 1$. This is an empirical process of averaging which may prevent divergence of the iterations, by taking $\kappa$ small enough. It has been used in a number of the numerical studies cited in the introduction, often in a wider context than that used here, where it is applied only to the boundary of the cylinder.

Numerical solutions have been obtained for values of the parameters shown in table 1. The values of $\kappa$ could possibly be considerably larger; this point has not been fully investigated. For each Reynolds number, a numerical solution was obtained, using the above iterative method, in which the approximation to $\zeta(\xi, \theta)$ ultimately satisfied (8). Then, in order to check the accuracy and improve

| $R$ | $h$ | $\xi_m/\pi$ | $n_0$ | $\kappa$ |
|---|---|---|---|---|
| 5 | $\pi/40$ | 1 | 20 | 0·05 |
| 7 | $\pi/40$ | 1 | 20 | 0·05 |
| 10 | $\pi/40$ | 1 | 20 | 0·05 |
| 20 | $\pi/40$ | 1 | 30 | 0·05 |
| 40 | $\pi/40$ | 1 | 30 | 0·05 |
| 70 | $\pi/60$ | 7/6 | 40 | 0·03 |
| 100 | $\pi/60$ | 7/6 | 40 | 0·015 |

TABLE 1. Parameters used in the calculations

upon it, the difference correction method of Fox (1947) was used to obtain a higher approximation to (1). If $L_0$ denotes the left side of (8), a higher approximation to (1) which takes into account all central differences up to the fifth can be written

$$L_0 + K_0 = 0, \tag{17}$$

where

$$12K_0 = 4(1+h\lambda_0)\zeta_1 + 4(1+h\mu_0)\zeta_2 + 4(1-h\lambda_0)\zeta_3 + 4(1-h\mu_0)\zeta_4 - (1+2h\lambda_0)\zeta_9 - (1+2h\mu_0)\zeta_{10} - (1-2h\lambda_0)\zeta_{11} - (1-2h\mu_0)\zeta_{12} - 12\zeta_0. \tag{18}$$

When the grid size is small enough, the correction $K_0$, evaluated using the converged solution which satisfies $L_0 = 0$, should be reasonably small everywhere. This gives some check that the grid size has been chosen properly.

An improvement to the solution can be obtained by setting up a new iteration which includes the correction. If in the old iteration, without correction, an iterate $\zeta^{(m)}(\xi, \theta)$ is obtained by solving the difference equations $L_0^{(m)} = 0$, the new iteration consists of solving the equations

$$L_0^{(m)} + K_0^{(m-1)} = 0. \tag{19}$$

Here, the vector $K_0$ is calculated from the previous iterate $\zeta^{(m-1)}(\xi, \theta)$ and held fixed during the determination of the new iterate $\zeta^{(m)}(\xi, \theta)$. Provided the initial correction is small enough, the sequence of iterates converges to a limit which satisfies (17), in which $L_0$ and $K_0$ are mutually consistent.

There is no difficulty in calculating the correction $K_0$ at any point of the field. On grid lines adjacent to $\theta = 0$ and $\theta = \pi$, the formula (18) involves values of $\zeta$ which lie outside the field of computation $OXYZ$, but these can be expressed in terms of internal values of $\zeta$ from the relations

$$\zeta(\xi, -\theta) = -\zeta(\xi, \theta), \quad \zeta(\xi, \pi+\theta) = -\zeta(\xi, \pi-\theta),$$

which hold because the flow is symmetrical about the axis of $x$. External values of $\zeta$ also enter the calculation of $K_0$ at grid points on $XY$ and on the adjacent

grid line $\xi = \xi_m - h$. In view of the fact that the boundary condition on $\xi = \xi_m$ rests on the assumption that the flow for $\xi \geqslant \xi_m$ is Oseen flow, the necessary external values are calculated from (10). Finally, if the typical point 0 is on the grid line $\xi = h$, the value $\zeta_{11}$ is external to the field. In this case

$$\partial^2\zeta/\partial\xi^2 + \partial^2\zeta/\partial\theta^2 = 0 \quad \text{when} \quad \xi = 0$$

and hence, approximately,

$$\zeta_{11} = 4\zeta_3 - \zeta_0 - \zeta_6 - \zeta_7,$$

which enables $\zeta_{11}$ to be calculated from internal and boundary values of $\zeta$.

In the present results, the difference correction method yielded only a small change from the solutions computed to satisfy (8). For the lower Reynolds numbers the changes in the main physical properties, such as the total drag coefficient, were almost negligible while for $R = 70$ and 100 the properties changed by only a few per cent, certainly less than 5 %. This suggests that the final results are of good accuracy, and also that the grid sizes given in table 1 are satisfactory. The values of $\xi_m$ in table 1 which give the position of the outer boundary $XY$ were obtained as the result of experience, as also was the number of terms, $n_0$, used to approximate the infinite sums on the right sides of (11) and (16). The effect of varying both of these parameters was studied, and it was found that an increase in either parameter beyond the values indicated in the table had negligible effect on the computed solution. The whole question of the effect of the imposed boundary conditions on $\xi = \xi_m$ on the internal solution has been discussed in detail by Dennis & Chang (1969*a*).

## 4. Results

Streamlines of the motion for the range $R = 5$–100 are shown in figure 2. Separation has started at $R = 7$, and the length of the wake, $L$, from the rear of the cylinder to the end of the separated region, grows approximately linearly with $R$ over the whole range. The calculated length of the wake is compared with other theoretical calculations and with experimental measurements in figure 3. It is also given numerically in table 2. There is very good agreement with the recent calculations of Takami & Keller up to $R = 60$, and the same straight-line development is continued beyond this by the present results. Kawaguti & Jain's results, obtained by time-dependent methods, appear to be departing from the linear relationship after $R = 20$. Son & Hanratty do not give the steady wake length for Reynolds numbers greater than 40.

Despite good agreement of Kawaguti & Jain with Son & Hanratty for the wake length of about $L = 5$ at $R = 40$, both investigations have used the rather coarse grid size $\pi/30$ in the $\theta$ direction. This may lead to a spurious lengthening of the wake, for a similar effect was observed in an attempt, by present methods, to obtain the time-dependent flow at $R = 100$ with a square grid of size $\pi/40$. By the time $L$ had reached its steady limit it was almost 22, nearly 11 diameters of the cylinder. The vortex pair had also become distorted and fat, very much after the manner of Son & Hanratty's results for $R = 200$ and 500. A reduction

of the grid size to $\pi/60$ gave, in essence, the results of figure 2(*g*), although it was not possible to continue the integrations to the fully steady state. Although Son & Hanratty have used a rectangular grid, with considerably smaller grid sizes in the $\xi$ direction, the grid size in the $\theta$ direction is rather coarse. In the wake at large distances, the grid size in the $\theta$ direction dominates the accuracy at least as much as that in the $\xi$ direction. This is evident from the rapid exponential

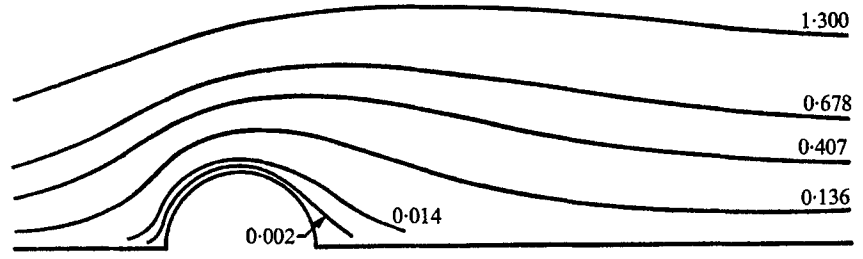


(*a*)

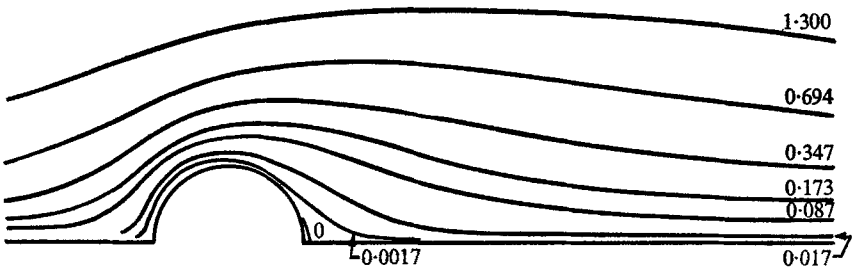


(*b*)

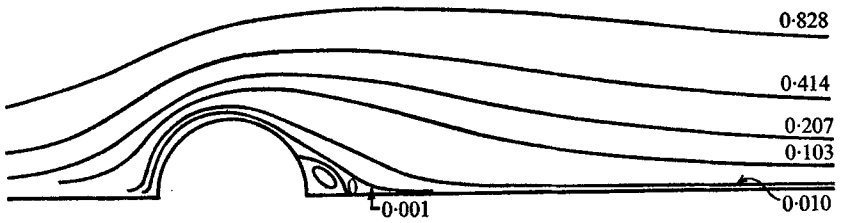


(*c*)

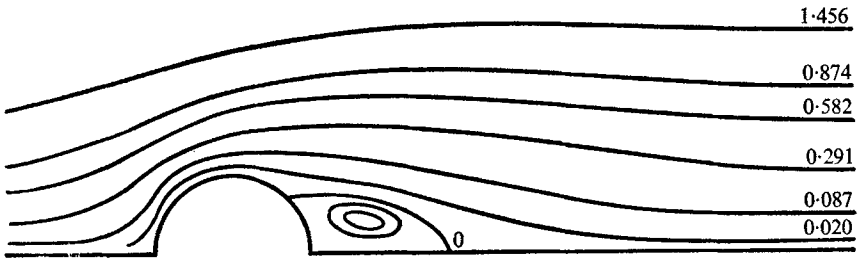


(*d*)

FIGURES 2(*a–d*). For legend see p. 480.

variation of $\zeta$ in the $\theta$ direction when $\xi$ is large, as indicated by the expression (9) obtained from Oseen theory. The variation depends, essentially, on how rapidly $\chi(1-\cos\theta)$ varies with $\theta$ for a given value of $\chi$. The grid size in the $\theta$ direction should be small enough to allow representation of the exponential variation adequately by finite differences for the largest value of $\chi$, $\chi = \chi_m$, in the domain of the numerical solution. This point has been considered more fully by Dennis & Chang (1969*a*).

The vorticity vanishes at the point of separation and it follows from (16) that the angle of separation, $\theta = \theta_s$, is a root of

$$\sum_{n=1}^{\infty} r_n(0) \sin n\theta = 0. \tag{20}$$

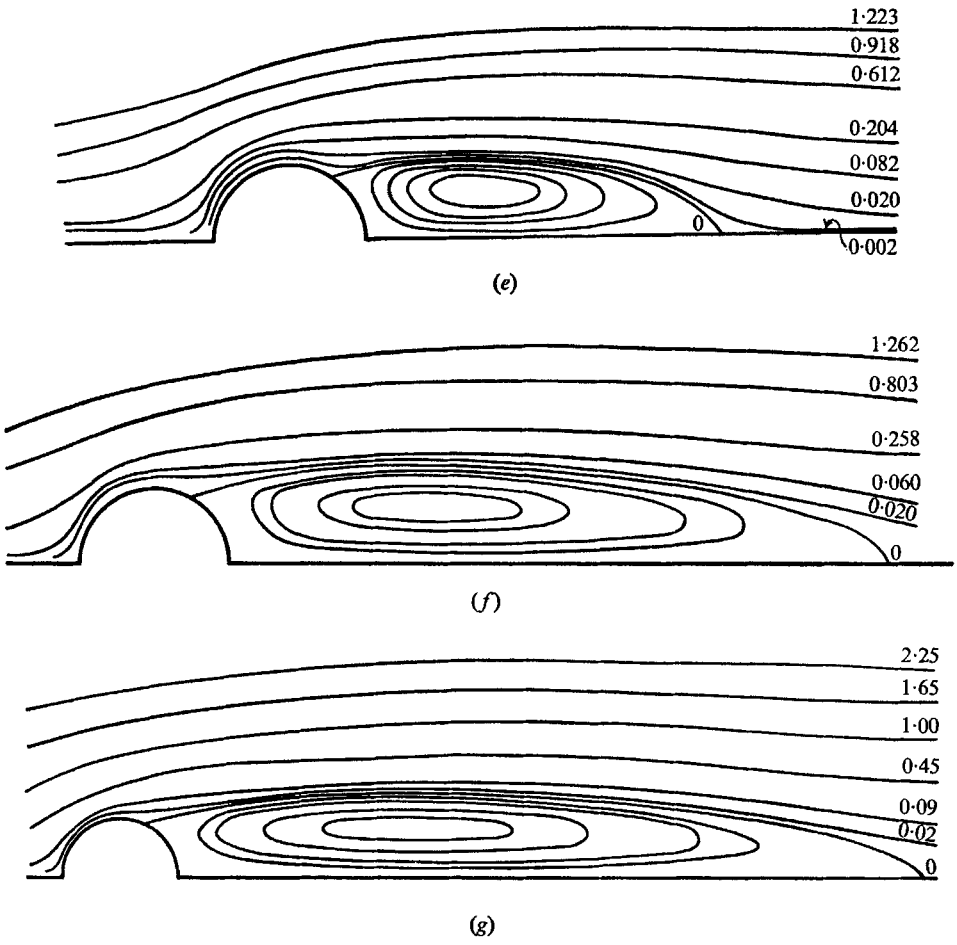


FIGURE 2. Streamlines for steady flow past a circular cylinder. Values of the dimensionless stream function, $\psi$, are shown for each streamline. Values of $\psi$ for the closed streamlines, $\psi_c$, are given following the Reynolds number, where appropriate, starting from the centre of the wake. (*a*) $R = 5$; (*b*) $R = 7$; (*c*) $R = 10$: $\psi_c = -0{\cdot}0002$; (*d*) $R = 20$: $\psi_c = -0{\cdot}008$, $-0{\cdot}0058$; (*e*) $R = 40$: $\psi_c = -0{\cdot}0328$, $-0{\cdot}0246$, $-0{\cdot}0164$, $-0{\cdot}0082$; (*f*) $R = 70$: $\psi_c = -0{\cdot}07$, $-0{\cdot}06$, $-0{\cdot}035$, $-0{\cdot}023$; (*g*) $R = 100$: $\psi_c = -0{\cdot}1$, $-0{\cdot}08$, $-0{\cdot}05$, $-0{\cdot}035$.

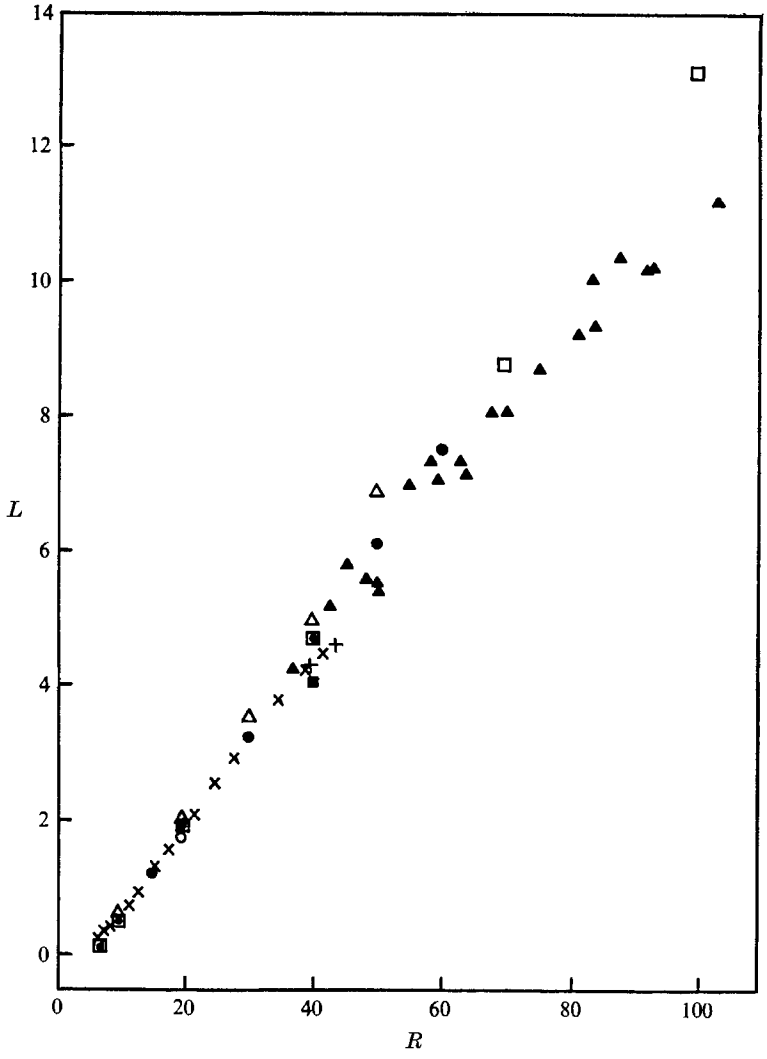


FIGURE 3. Calculated and experimental values for the wake length. Numerical solutions: □, this study; ●, Takami & Keller (1969); Δ, Kawaguti & Jain (1966); +, Apelt (1961); ■, Kawaguti (1953*b*); ○, Thom (1933). Experimental measurements: ▲, Acrivos *et al.* (1968): ×, Taneda (1956).

| $R$ | $L$ | $\theta_s$ | $C_f$ | $C_p$ | $C_D$ | $P(0)$ | $P(\pi)$ |
|---|---|---|---|---|---|---|---|
| 5 | — | — | 1·917 | 2·199 | 4·116 | −1·044 | 1·872 |
| 7 | 0·19 | 15·9 | 1·553 | 1·868 | 3·421 | −0·870 | 1·660 |
| 10 | 0·53 | 29·6 | 1·246 | 1·600 | 2·846 | −0·742 | 1·489 |
| 20 | 1·88 | 43·7 | 0·812 | 1·233 | 2·045 | −0·589 | 1·269 |
| 40 | 4·69 | 53·8 | 0·524 | 0·998 | 1·522 | −0·509 | 1·144 |
| 70 | 8·67 | 61·3 | 0·360 | 0·852 | 1·212 | −0·439 | 1·085 |
| 100 | 13·11 | 66·2 | 0·282 | 0·774 | 1·056 | −0·393 | 1·060 |

TABLE 2. Calculated properties of the numerical solutions. The angle of separation, $\theta_s$, is given in degrees

Calculated values of $\theta_s$ are given in table 2. They are in extremely good agreement with the calculations of Takami & Keller, who give the respective values $\theta_s = 14{\cdot}5°$, $29{\cdot}3°$, $43{\cdot}65°$, $53{\cdot}55°$, $56{\cdot}6°$, $59{\cdot}0°$ at the Reynolds numbers 7, 10, 20, 40, 50 and 60. Son & Hanratty's value at $R = 40$ is $\theta_s = 53{\cdot}9°$, while Kawaguti & Jain's is $53{\cdot}7°$. Separation first starts to take place at some critical Reynolds number between 5 and 7 for which $\theta_s = 0$. It may be deduced with the aid of (16) that this Reynolds number is that which makes the sum

$$B(R) = \sum_{n=1}^{\infty} n r_n(0)$$

vanish. The approximations $B(5) = 0{\cdot}100$ and $B(7) = -0{\cdot}068$ are obtained from the present results. A linear interpolation suggests the critical Reynolds number as $R = 6{\cdot}2$.

The dimensionless drag coefficient is defined by $C_D = D/\rho U^2 a$, where $D$ is the total drag on the cylinder, and $\rho$ is the density. The total drag may be obtained by integrating the total stress component in the direction of $x$ around the surface of the cylinder. If $p$ is the pressure and, as previously noted, $\zeta'$ is the dimensional scalar vorticity, then

$$D = -\int_0^{2\pi} (\rho\nu\zeta'_0 \sin\theta + p_0 \cos\theta)\, a\, d\theta,$$

where $\nu$ is the coefficient of kinematical viscosity and the subscript zero denotes a value at $\xi = 0$. The second term in the integral may be dealt with conveniently by integrating by parts and eliminating the pressure gradient using the equation of motion in the direction of $\theta$. It may then be shown that

$$C_D = \frac{4}{R}\int_0^{\pi} \zeta_0 \sin\theta\, d\theta - \frac{4}{R}\int_0^{\pi} (\partial\zeta/\partial\xi)_0 \sin\theta\, d\theta. \tag{21}$$

The first term on the right gives the friction drag coefficient and the second the pressure drag coefficient, denoted respectively by $C_f$ and $C_p$. If the result (16) is substituted, the simple expressions

$$C_f = 2\pi r_1(0)/R,$$

$$C_p = 2\pi\{2r_1(0) - r_1'(0)\}/R$$

are obtained, where the prime denotes differentiation with regard to $\xi$. Actually, it was found to be slightly more satisfactory to calculate $C_p$ by direct numerical evaluation of the second integral in (21) using values of $(\partial\zeta/\partial\xi)_0$ obtained by numerical differentiation. Calculated drag coefficients are given in table 2 and also in figure 4, where the total drag coefficient is compared with other numerical results obtained from integrations of the equations of steady motion and with the experimental measurements of Tritton (1959). A recent estimate of $C_D = 1{\cdot}172$ at $R = 100$ has been given by Hameliec & Raal, but the associated wake length of $L = 9{\cdot}48$ seems much too low and is likely to be due to the fact that the boundary $\xi = \xi_m$ has been taken too close to the cylinder.

The drag coefficient calculated from (21) enables some check to be made on the corresponding numerical solution in view of the fact that the nature of the

flow at large distances is known. From the solution of Imai (1951) it is known that, as $\xi \to \infty$,

$$\psi(\xi, \theta) \sim e^{\xi} \sin\theta - \tfrac{1}{2} C_D (1 - \theta/\pi),$$

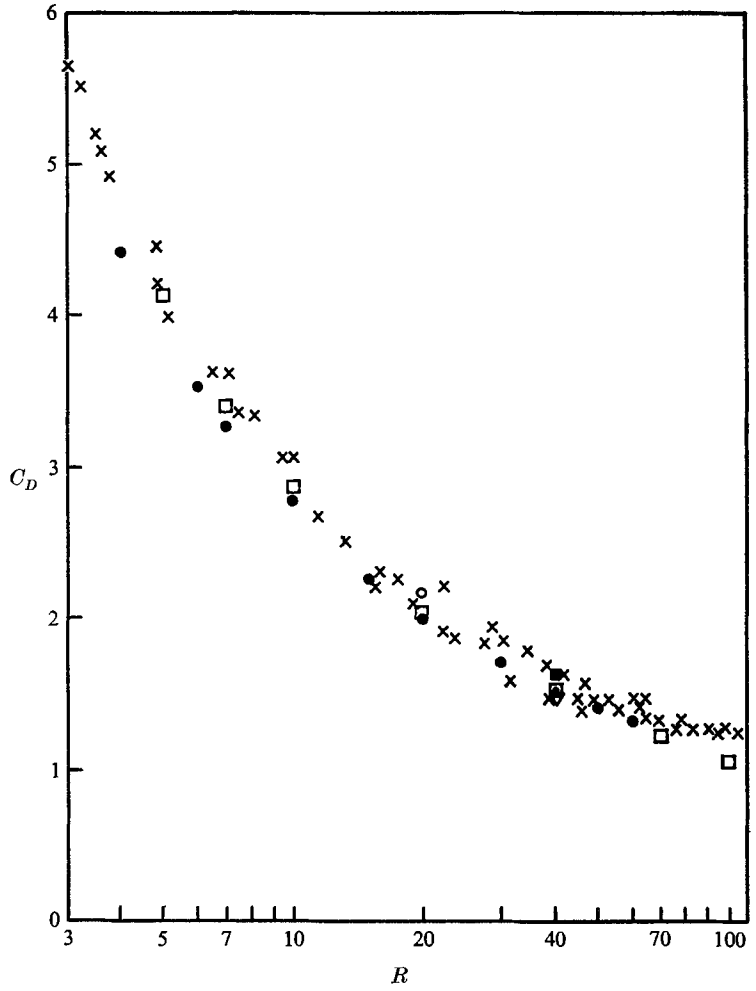


FIGURE 4. Calculated and experimental values for the total drag coefficient. Numerical solutions of the equations of steady motion: □, this study; ●, Takami & Keller (1969); ▽, Apelt (1961); ■, Kawaguti (1953*b*); ○, Thom (1933). Experimental measurements: ×, Tritton (1959).

except on $\theta = 0$, where a finite discontinuity exists. It follows that the solution of the set of equations (12) must be such that

$$f_n(\xi) \sim \delta_n e^{\xi} - C_D/\pi n, \tag{22}$$

where $\delta_n$ has the meaning already assigned in (15). In the numerical procedure, the coefficient of $1/n$ on the right side of (22) is not specified, but emerges as the result of the calculations. This gives the required check, although it is a stringent one and cannot be expected to be satisfied to high precision, since, effectively,

it checks the balance of outflow and inflow over a very large contour surrounding the cylinder. It may be applied to the numerical solutions, for example, by subtracting the exponential term from the right side of (22) when $n = 1$ and comparing the tendency of the remainder, as $\xi$ increases, with the value obtained using (21).

In all the computed results, a tendency consistent with (22) was observed, but the precision of the check is hindered by two factors. First, it is not known how closely the limiting behaviour should be approached at the finite upper limit, $\xi = \xi_m$, imposed on a given numerical solution. Further, any attempt to increase $\xi_m$ unduly leads to a fluctuation in the coefficient of $1/n$ in (22) as calculated by the numerical integration procedure. This is noticeable only near $\xi = \xi_m$ and is due to the increasingly poor finite-difference approximation to $\zeta$ in the wake. On the whole, however, the coefficient of $1/n$ as determined from the numerical integration was found to approach within about 10 % of the theoretical value consistent with calculation from (21), which is considered to be satisfactory in view of the two factors mentioned. Some other numerical checks were also carried out. For example, the effect of varying the number, $n_0$, of terms used to approximate the summation on the right side of (11) was considered. More terms are needed as $R$ is increased, but $n_0 = 40$ is still adequate at $R = 100$. If we take, as an illustration, the variation of wake length with $n_0$ at this Reynolds number we find $L = 9{\cdot}12$, $12{\cdot}03$ and $12{\cdot}99$ at values $n_0 = 10$, 20, 30. The final value (table 2) for $n_0 = 40$ is $L = 13{\cdot}1$.

One of the possible models for the limiting flow as $R \to \infty$ is the discontinuous potential flow of Kirchhoff type. Imai (1957) has given the large Reynolds number formula

$$C_D^{\frac{1}{2}} \sim C_{D\infty}^{\frac{1}{2}} + \alpha R^{-\frac{1}{2}} \tag{23}$$

based on this model. Here, $\alpha$ is an unknown constant and $C_{D\infty}$ is the drag coefficient of the limiting Kirchhoff flow. Brodetsky (1923) gives $C_{D\infty} = 0{\cdot}5$ for a circular cylinder. On the basis of this value, Takami & Keller have estimated $\alpha$ by evaluating it from (23) using their drag values at $R = 50$ and 60, and then extrapolating linearly in $R^{-1}$ as $R \to \infty$. The value obtained in this way is $\alpha = 3{\cdot}547$. A similar procedure carried out with the present values of $C_D$ at $R = 70$ and 100 gives $\alpha = 2{\cdot}99$. This discrepancy in estimates of $\alpha$ is a little too large to assume any reliable confirmation of the formula (23), and neither value of $\alpha$ gives values of $C_D$ which compare particularly well with the calculated values $C_D = 0{\cdot}924$ and $0{\cdot}60$ given by Son & Hanratty at $R = 200$ and 500. On the other hand, if we assume an asymptotic boundary-layer-type expansion for the friction drag in powers of $R^{-\frac{1}{2}}$, and fit the first two terms to the present results for $R = 70$ and 100, we obtain

$$C_f \sim 1{\cdot}83R^{-\frac{1}{2}} + 9{\cdot}95R^{-1}.$$

This not only fits the value at $R = 40$, but gives respective values $C_f = 0{\cdot}18$ and $0{\cdot}10$ at $R = 200$ and 500. These compare well with Son & Hanratty's respective values $C_f = 0{\cdot}19$ and $0{\cdot}09$.

The dimensionless pressure coefficient

$$P(\theta) = \frac{p_0(\theta) - p_\infty}{\frac{1}{2}\rho U^2}, \tag{24}$$

where $p_0(\theta)$ is the pressure on the cylinder surface and $p_\infty$ the uniform pressure at large distances, is calculated from the formula

$$P(\theta) = 1 - \frac{4}{R}\int_0^\infty \left(\frac{\partial\zeta}{\partial\theta}\right)_{\theta=\pi} d\xi + \frac{4}{R}\int_\theta^\pi \left(\frac{\partial\zeta}{\partial\xi}\right)_{\xi=0} d\theta. \tag{25}$$

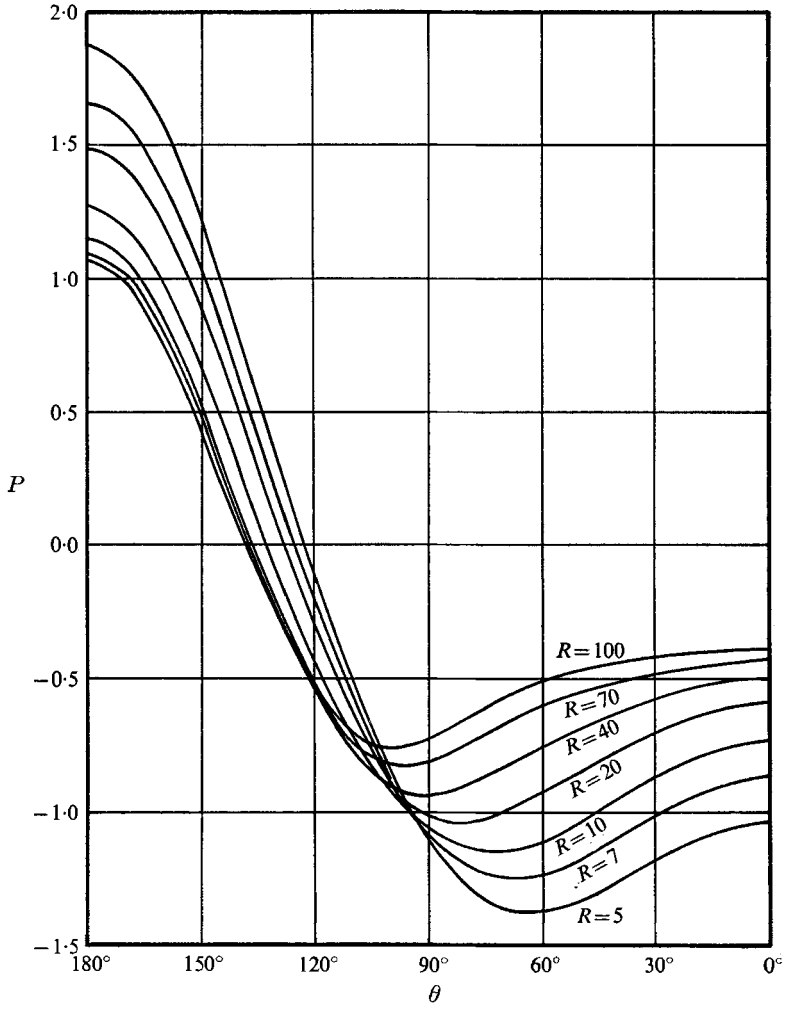


FIGURE 5. Pressure coefficient on the cylinder surface.

Curves of the pressure coefficient are given in figure 5, and its values at the rear and the front of the cylinder are given in table 2. Both of these values are of interest. According to the exact solution for stagnation point flow (see Schlichting 1960), the coefficient at the front of the cylinder should behave, for large Reynolds number, like

$$P(\pi) \sim 1 + \beta R^{-1}, \tag{26}$$

where $\beta$ is a constant. Takami & Keller have estimated $\beta = 5{\cdot}985$ by calculation from (26) at $R = 50$ and 60, followed by linear extrapolation in $R^{-1}$ as $R \to \infty$.

A similar extrapolation from the present results at $R = 70$ and 100 gives $\beta = 6{\cdot}09$, which is in reasonable agreement.

The variation with $R$ of the pressure coefficient at the rear of the cylinder is of interest in view of two models which have been proposed for the separated flow at high Reynolds number. In a model suggested by Roshko and by Sychev (1967), the behaviour for large Reynolds numbers should be

$$P(0) \sim AR^{-\frac{1}{2}}, \tag{27}$$

where $A$ is a constant. The model of Acrivos *et al.* (1965) suggests that $P(0)$ becomes constant as the Reynolds number increases. Recent experimental observations of Acrivos *et al.* (1968) tend to confirm this. It is found that the

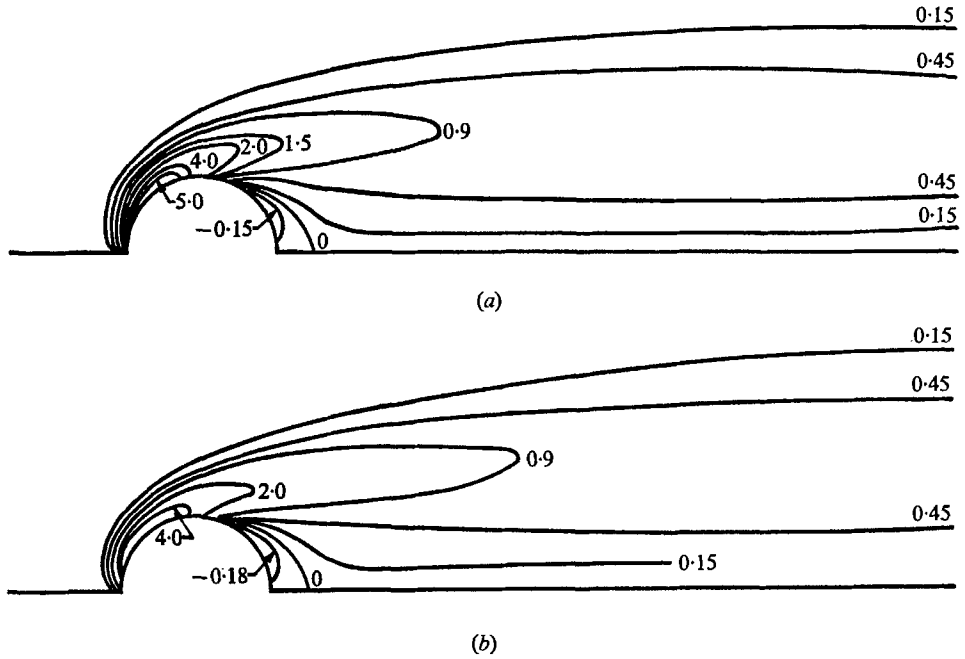


FIGURE 6. Equi-vorticity lines for steady flow past a circular cylinder. Values of the negative dimensionless vorticity, $\zeta$, are shown for each equi-vorticity line. (*a*) $R = 70$; (*b*) $R = 100$.

observed coefficient tends to become constant at quite moderate values of $R$, of the order of 100. Unfortunately, the results of the present calculations do not give any definite information one way or the other. The variation of $P(0)$ is not rapid enough to fit (27). Neither is this coefficient obviously approaching a constant, at least, certainly not in the range $-0{\cdot}47$ to $-0{\cdot}43$ suggested by the experimental results for circular cylinders. This point requires further elucidation.

The variation of vorticity throughout the flow field for Reynolds numbers 70 and 100 is indicated by equi-vorticity lines in figure 6. For lower Reynolds numbers, the vorticity distributions are, in essence, the same as those given by Takami & Keller. The dimensionless negative vorticity on the surface of the cylinder is shown in figure 7. No reasonable prediction can be made as to its

tendency for large Reynolds number and, in particular, as to the ultimate position of the separation point. Son & Hanratty have noted that in their solutions for late times, the vorticity near the front stagnation point is significantly less than that predicted by boundary-layer theory with the potential solution for the

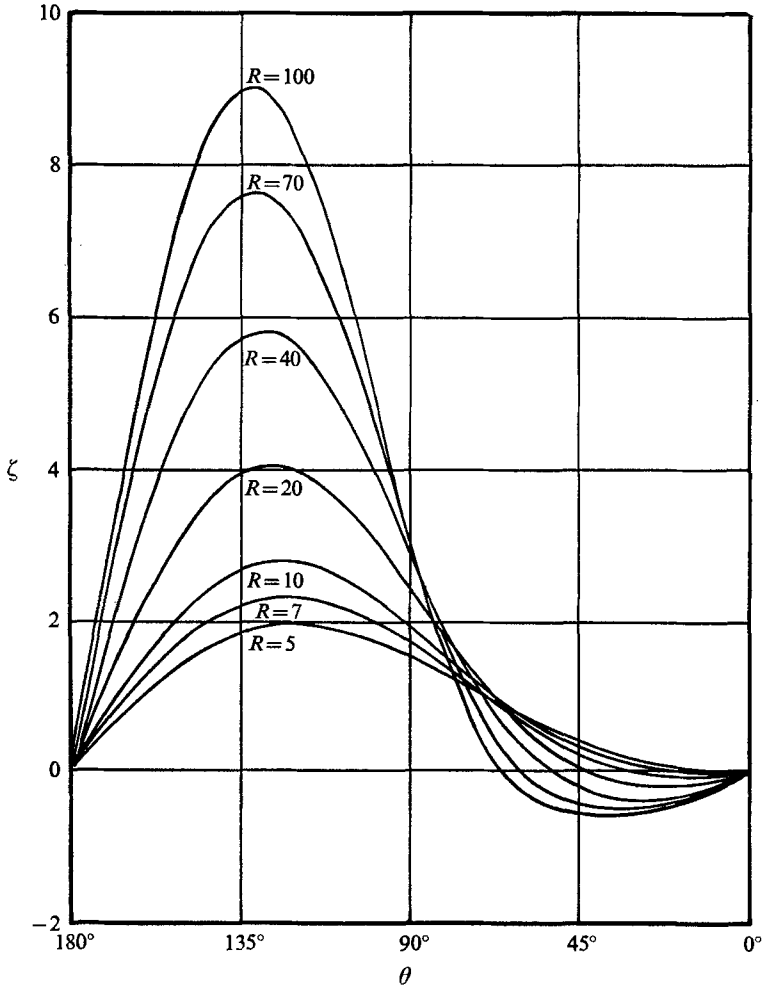


FIGURE 7. Vorticity distribution over the surface of the cylinder.

external flow. The same effect has been noted in the present solutions and may be indicated as follows. The local coefficient of skin friction is $c_f = \tau_0/\frac{1}{2}\rho U^2$, where $\tau_0$ is the local shearing stress, and it follows that

$$c_f = 4R^{-1}\zeta(0,\theta).$$

In the neighbourhood of the front stagnation point we put $\theta = \pi - \phi$, and it may then be deduced from (16) that, for small $\phi$,

$$R^{\frac{1}{2}}c_f \sim S\phi, \tag{28}$$

where

$$S(R) = 4R^{-\frac{1}{2}} \sum_{n=1}^{\infty} (-1)^{n+1} n r_n(0).$$

As $R \to \infty$, $S(R)$ should tend to the constant value of approximately 9·861 consistent with stagnation point flow (Schlichting 1960, p. 153). For the three highest Reynolds numbers $R = 40$, 70 and 100, the series $S(R)$ converges rapidly, and we obtain the respective values

$$S(R) = 6{\cdot}59,\ 6{\cdot}70,\ 6{\cdot}89.$$

The discrepancy with boundary-layer flow at these Reynolds numbers is therefore substantial.

Part of the work described in this paper was carried out while one author (S.C.R.D.) was a visitor to the Mathematics Research Centre, U.S. Army, University of Wisconsin. A detailed account of the investigation, including full details of the numerical method, is given in the report by Dennis & Chang (1969*a*) which has been cited. Copies of this report can be obtained from the Mathematics Research Centre, and a copy has been deposited in the editorial office of the Journal of Fluid Mechanics.

Part of the work was supported by Contract no. DA-31-124-ARO-D-462, and part was sponsored by the National Research Council of Canada. The numerical calculations were performed on the CDC 3600 of the University of Wisconsin and on the IBM 7040 of the University of Western Ontario.

## REFERENCES

Acrivos, A., Leal, L. G., Snowden, D. D. & Pan, F. 1968 *J. Fluid Mech.* **34**, 25.

Acrivos, A., Snowden, D. D., Grove, A. S. & Petersen, E. E. 1965 *J. Fluid Mech.* **21**, 737.

Allen, D. N. De G. & Southwell, R. V. 1955 *Quart. J. Mech. Appl. Math.* **8**, 129.

Apelt, C. J. 1961 *Aero. Res. Counc. R. & M.* no. 3175.

Batchelor, G. K. 1956 *J. Fluid Mech.* **1**, 388.

Brodetsky, S. 1923 *Proc. Roy. Soc.* A **102**, 542.

Dennis, S. C. R. & Chang, G. Z. 1969*a* *Mathematics Research Centre, U.S. Army, Madison, Wisconsin, Technical Summary Report*, no. 859.

Dennis, S. C. R. & Chang, G. Z. 1969 *Phys. Fluids Suppl.* II, **12**, II–88.

Dennis, S. C. R., Hudson, J. D. & Smith, N. 1968 *Phys. Fluids*, **11**, 933.

Dennis, S. C. R. & Shimshoni, M. 1965 *Aero. Res. Counc. Current Paper*, no. 797.

Filon, L. N. G. 1928 *Proc. Roy. Soc. Edinb.* **49**, 38.

Fox, L. 1947 *Proc. Roy. Soc.* A **190**, 31.

Hamielec, A. E. & Raal, J. D. 1969 *Phys. Fluids*, **12**, 11.

Hirota, I. & Miyakoda, K. 1965 *J. Met. Soc. Japan*, Ser. II, **43**, 30.

Imai, I. 1951 *Proc. Roy. Soc.* A **208**, 487.

Imai, I. 1957 *University of Maryland Tech. Note*, no. BN-104.

Ingham, D. B. 1968 *J. Fluid Mech.* **31**, 815.

Kawaguti, M. 1953*a* *J. Phys. Soc. Japan*, **8**, 403.

Kawaguti, M. 1953*b* *J. Phys. Soc. Japan*, **8**, 747.

Kawaguti, M. & Jain, P. 1966 *J. Phys. Soc. Japan*, **21**, 2055.

Keller, H. B. & Takami, H. 1966 In *Numerical Solutions of Nonlinear Differential Equations*. (Ed. D. Greenspan.) Englewood Cliffs, N.J.: Prentice-Hall.

Payne, R. B. 1958 *J. Fluid Mech.* **4**, 81.

Roshko, A. 1967 *Proc. Canadian Congress of Applied Mechanics*, **3**, 81.

SCHLICHTING, H. 1960 *Boundary Layer Theory*. New York: McGraw-Hill.

SON, J. S. & HANRATTY, T. J. 1969 *J. Fluid Mech.* **35**, 369.

SQUIRE, H. B. 1934 *Phil. Mag.* **17**, 1150.

SYCHEV, V. V. 1967 *Symposium on Modern Problems in Fluid and Gas Dynamics*. Tarda, Poland.

TAKAMI, H. & KELLER, H. B. 1969 *Phys. Fluids Suppl.* II, **12**, II–51.

TANEDA, S. 1956 *J. Phys. Soc. Japan*, **11**, 302.

THOM, A. 1928 *Aero. Res. Counc. R. & M.* no. 1194.

THOM, A. 1933 *Proc. Roy. Soc.* A **141**, 651.

THOMAN, D. C. & SZEWCZYK, A. A. 1966 *Heat Transfer and Fluid Mech. Lab., University of Notre Dame Tech. Rep.* no. 66–14.

TRITTON, D. J. 1959 *J. Fluid Mech.* **6**, 547.

VAN DYKE, M. 1964 *Perturbation Methods in Fluid Mechanics*. New York: Academic.

*J. Fluid Mech.* (1970), *vol.* 42, *part* 3, *pp.* 491–495
*Printed in Great Britain*



# The bed configuration of straight sand-bed channels when flow is nearly critical

By H. Y. CHANG

San Diego State College, San Diego, California

AND D. B. SIMONS

Colorado State University, Fort Collins, Colorado

(Received 19 March 1969 and in revised form 30 January 1970)

The diagonal pattern of bed form which appears in sand-bed channels when the channel width to depth ratio is great and the flow is nearly critical is discussed from the theoretical viewpoint by using the method of characteristics. Some photographs illustrate the phenomenon.

## 1. Introduction

The diagonal sand waves occur in straight sand-bed channels with smooth walls, when the flow is nearly critical (or the Froude number is near unity) with a certain depth to width ratio. This phenomenon has been observed previously by Vanoni & Brooks (1957), Shen (1961) and Guy, Simons & Richardson (1966) in their studies of resistance to flow and bed-material discharge in an 8 foot wide flume at Colorado State University during the period 1956–1958. According to Shen, this kind of diagonal pattern is probably due to water-surface fluctuations.

From further observations by the authors, the diagonal sand waves on a sand bed are associated with the water-surface undulation which is a type of disturbance that occurs when flow changes from supercritical to subcritical or vice versa. Flow bounded within the diagonal disturbances is essentially continuous, whereas a discontinuity exists for flow across the disturbances, see figure 1. The discontinuity in a flow field is usually determined by the method of characteristics which is used most often for problems in the field of gas dynamics (Owczarek 1964).

## 2. Theoretical considerations

In a straight alluvial channel with a large width/depth ratio, the vertical motion is neglected and the equations of motion in the longitudinal and transverse directions are

$$\frac{1}{g}\left(\frac{\partial U}{\partial t}+U\frac{\partial U}{\partial x}+W\frac{\partial U}{\partial z}\right)=S-\frac{\partial h}{\partial x}-\frac{\tau_0}{\gamma h}, \tag{1}$$

$$\frac{1}{g}\left(\frac{\partial W}{\partial t}+U\frac{\partial W}{\partial x}+W\frac{\partial W}{\partial z}\right)=-\frac{\partial h}{\partial z}-\frac{W}{U}\frac{\tau_0}{\gamma h}, \tag{2}$$

where $U$ and $W$ are average velocities per unit width in the longitudinal and transverse directions, $S$ is the channel slope, $h$ the local depth of flow, and $\tau_0 = \gamma h S$ (shear stress at channel bottom).

The continuity equation for water discharge is

$$\frac{\partial}{\partial x}(Uh)+\frac{\partial}{\partial z}(Wh)=-\frac{\partial h}{\partial t}. \tag{3}$$

The continuity for sediment transport requires

$$\frac{\partial q_1}{\partial x}+\frac{\partial q_3}{\partial z}=-(1-\lambda)\frac{\partial h_0}{\partial t},$$

where $q_1$ and $q_3$ are the discharges of sands per unit width in the longitudinal and transverse directions, $\lambda$ is the porosity of sands, and $h_0$ is the channel-bed elevation.

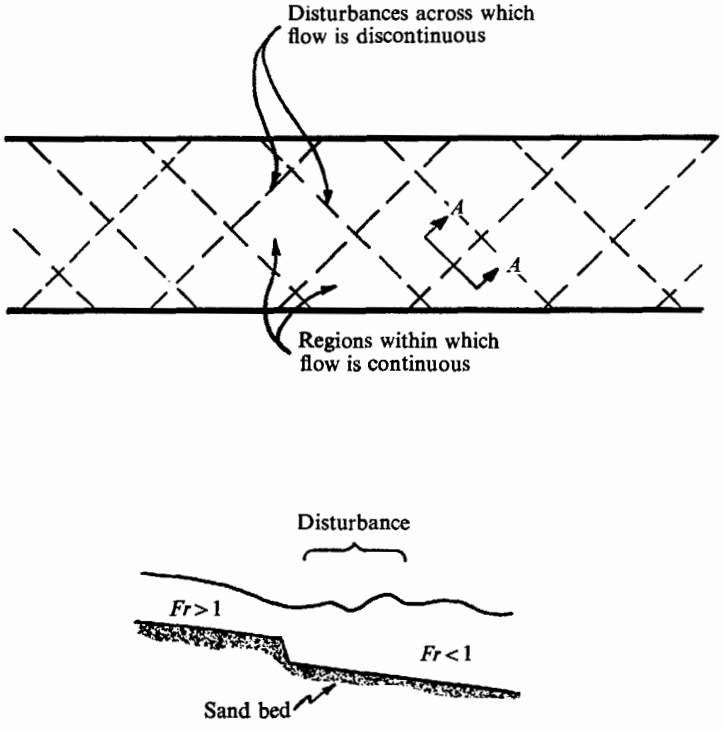


FIGURE 1. Schematic drawing showing diagonal lines in shallow channel flow with Froude number near unity.

The discharge of sands in a sand-bed channel depends on many variables. Colby (1964) has found that in streams where differences in depth, water temperature, and size of bed sand are not excessively large, the discharge of sands per unit width is proportional to the average velocity. If we assume that the discharges of sands are proportional to the velocity components, i.e.

$$U/W = q_1/q_3,$$

then

$$\frac{\partial q_1}{\partial x}+\frac{\partial}{\partial z}\left(\frac{W}{U}q_1\right)=-(1-\lambda)\frac{\partial h_0}{\partial t}. \tag{4}$$

The movement of diagonal sand waves has been observed to be very slow, hence the unsteady terms in the above equations can be neglected. The above four equations, together with the equations for total differentials can be written as

$$U\frac{\partial U}{\partial x}+W\frac{\partial U}{\partial z}=F_1(h,x), \tag{5}$$

$$U\frac{\partial W}{\partial x}+W\frac{\partial W}{\partial z}=F_2(h,z), \tag{6}$$

$$h\frac{\partial U}{\partial x}+h\frac{\partial W}{\partial z}+U\frac{\partial h}{\partial x}+W\frac{\partial h}{\partial z}=0, \tag{7}$$

$$\frac{Wq_1}{U^2}\frac{\partial U}{\partial z}-\frac{q_1}{U}\frac{\partial W}{\partial z}-\frac{\partial q_1}{\partial x}-\frac{W}{U}\frac{\partial q_1}{\partial z}=0, \tag{8}$$

$$dx\frac{\partial U}{\partial x}+dz\frac{\partial U}{\partial z}=dU, \tag{9}$$

$$dx\frac{\partial W}{\partial x}+dz\frac{\partial W}{\partial z}=dW, \tag{10}$$

$$dx\frac{\partial h}{\partial x}+dz\frac{\partial h}{\partial z}=dh, \tag{11}$$

$$dx\frac{\partial q_1}{\partial x}+dz\frac{\partial q_1}{\partial z}=dq_1. \tag{12}$$

This system of simultaneous equations for the partial derivatives $\partial U/\partial x$, $\partial U/dz$, $\partial W/\partial x$, $\partial W/\partial z$, $\partial h/\partial x$, $\partial h/\partial z$, $\partial q_1/\partial x$ and $\partial q_1/\partial z$ has independent variables $x$ and $z$, and dependent variables $U$, $W$, $h$ and $q_1$. The coefficients of the partial derivatives in (5) to (8) are functions of dependent variables only. This system of equations is called quasi-linear because each equation is linear with respect to the derivatives of the highest (in this case, first) order. Therefore, these equations can be analyzed by the method of characteristics.

Using Cramer's rule, the derivative $\partial U/\partial x$ can be determined from the quotient of two determinants

$$\partial U/\partial x = k_1/N,$$

where

$$k_1=\begin{vmatrix} F_1 & W & 0 & 0 & g & 0 & 0 & 0 \\ F_2 & 0 & U & W & 0 & g & 0 & 0 \\ 0 & 0 & 0 & h & U & W & 0 & 0 \\ 0 & \dfrac{Wq_1}{U^2} & 0 & -\dfrac{q_1}{U} & 0 & 0 & -1 & -\dfrac{W}{U} \\ dU & dz & 0 & 0 & 0 & 0 & 0 & 0 \\ dW & 0 & dx & dz & 0 & 0 & 0 & 0 \\ dh & 0 & 0 & 0 & dx & dz & 0 & 0 \\ dq_1 & 0 & 0 & 0 & 0 & 0 & dx & dz \end{vmatrix},$$

and
$$N = \begin{vmatrix} U & W & 0 & 0 & g & 0 & 0 & 0 \\ 0 & 0 & U & W & 0 & g & 0 & 0 \\ h & 0 & 0 & h & U & W & 0 & 0 \\ 0 & \frac{Wq_1}{U^2} & 0 & -\frac{q_1}{U} & 0 & 0 & -1 & -\frac{W}{U} \\ dx & dz & 0 & 0 & 0 & 0 & 0 & 0 \\ 0 & 0 & dx & dz & 0 & 0 & 0 & 0 \\ 0 & 0 & 0 & 0 & dx & dz & 0 & 0 \\ 0 & 0 & 0 & 0 & 0 & 0 & dx & dz \end{vmatrix}$$

Similarly, other derivatives are

$$\frac{\partial U}{\partial z} = \frac{k_2}{N}, \quad \frac{\partial W}{\partial x} = \frac{k_3}{N}, \quad \frac{\partial W}{\partial z} = \frac{k_4}{N}, \quad \frac{\partial h}{\partial x} = \frac{k_5}{N}$$

$$\frac{\partial h}{\partial z} = \frac{k_6}{N}, \quad \frac{\partial q_1}{\partial x} = \frac{k_7}{N}, \quad \text{and} \quad \frac{\partial q_1}{\partial z} = \frac{k_8}{N},$$

where $k_2, k_3, \ldots, k_8$ are appropriate determinants.

The necessary condition for the partial derivatives to be indeterminate, or there would be a discontinuity in the flow field, is that the determinant $N = 0$. The directions in the $(x, z)$ plane in which the determinant $N = 0$ are called characteristic directions and curves along which $N = 0$ are called characteristic curves. If the flow under consideration permits the existence of discontinuities in the form of water surface undulations, their paths can only be represented by the characteristic curves. Hence, the characteristic curves may represent the diagonal paths of disturbances.

Letting $N = 0$, we obtain

$$(W\,dx - U\,dz)^2[(W\,dx - U\,dz)^2 - gh(dx)^2] = 0. \tag{13}$$

The four roots of the above equation are

$$\frac{dx}{dz} = \frac{U}{W}, \quad \frac{dx}{dz} = \frac{U}{W}, \quad \frac{dx}{dz} = \frac{U}{W + \sqrt{(gh)}} \quad \text{and} \quad \frac{dx}{dz} = \frac{U}{W - \sqrt{(gh)}}.$$

They are independent of the sediment discharge. The first two roots are stream lines, and the characteristic direction represented by the last two roots is of principal interest to us. These roots can be written as

$$\frac{dx}{dz} = \frac{U}{W \pm \sqrt{(gh)}}. \tag{14}$$

In this equation, if we assume that $W$ is small and hence negligible, then

$$dx/dz = \pm\, U/\sqrt{(gh)}. \tag{15}$$

Since water surface undulations occur when the flow is nearly critical, or $U \doteq \sqrt{(gh)}$, then

$$dx/dz \doteq \pm 1. \tag{16}$$

Equation (16) indicates that the disturbances occur on lines approximately 45° from the flow direction. Thus, we have verified that the sand-wave patterns

associated with the accompanying water surface undulations are diagonal. Figure 2, plates 1 and 2, shows the diagonal bed form of channel flows when the water had been shut off, as observed by Guy, Simons & Richardson in an 8 foot wide laboratory flume. The Froude numbers ($F_r = U/\sqrt{(gh)}$) and width to depth ratios for all runs are also listed.

## 3. Conclusions

The diagonal bed form usually occurs in alluvial channels with a large width to depth ratio and with the flow nearly critical (or the Froude number near unity). The diagonal bed form is associated with the water-surface undulation which is a disturbance across which the flow changes from supercritical to subcritical or vice versa. It has been verified in this paper that the disturbance or the sand wave occurs on lines approximately 45° from the flow direction.

## REFERENCES

COLBY, B. R. 1964 Discharge of sands and mean-velocity relationships in sand-bed streams. *U.S. Geological Survey Professional Paper* 462-A, *Washington, D.C.*

GUY, H. P., SIMONS, D. B. & RICHARDSON, E. V. 1966 Summary of alluvial channel data from flume experiments, 1956–61. *U.S. Geological Survey Professional Paper* 461–1, *Washington, D.C.*

OWCZAREK, J. A. 1964 *Fundamentals of Gas Dynamics*. New York: International Textbook Company.

SHEN, H. W. 1961 A study on meandering and other bed patterns in straight alluvial channels. *Water Resources Center, Contribution*, no. 33, *University of California, Berkeley.*

VANONI, V. A. & BROOKS, N. H. 1957 Laboratory studies of the roughness and suspended load of alluvial streams. *Report* no. 68, *California Institute of Technology, Pasadena.*


(*a*)

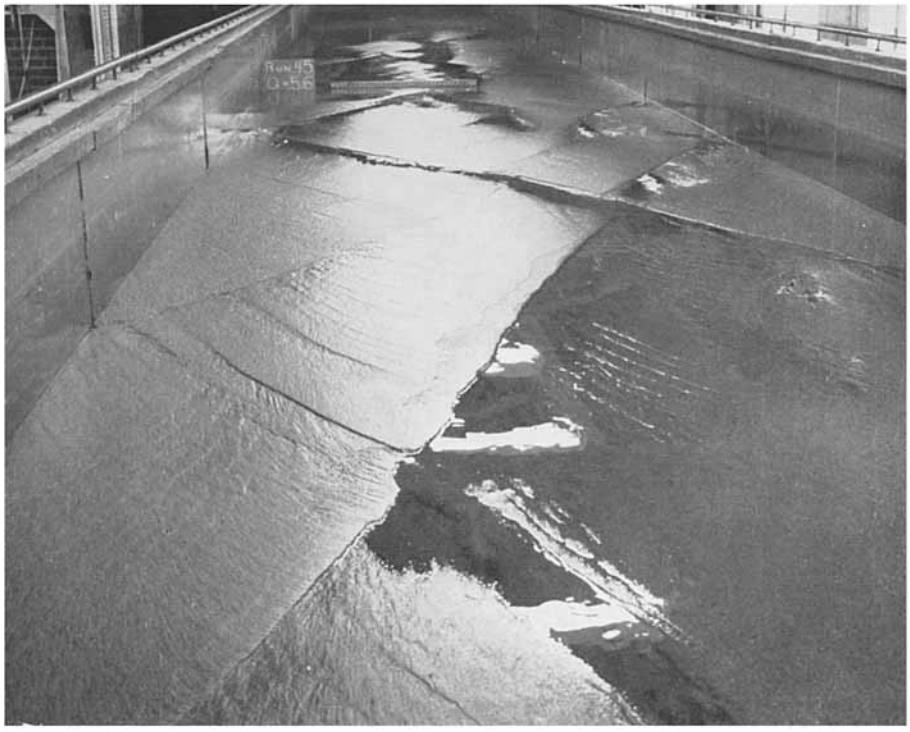


(*b*)

FIGURE 2(*a*), (*b*). For legend see plate 2.

(*c*)

FIGURE 2. Diagonal bed patterns in a laboratory flume with large width to depth ratios and with the flow nearly critical. (*a*) Froude number = 0·92, width to depth ratio = 24. (*b*) Froude number = 0·83, width to depth ratio = 28·5. (*c*) Froude number = 1·12, width to depth ratio = 18.

*J. Fluid Mech.* (1970), *vol.* 42, *part* 3, *pp.* 497–511
*Printed in Great Britain*



# The development of horizontal boundary layers in stratified flow. Part 1. Non-diffusive flow

By R. E. KELLY AND L. G. REDEKOPP†

School of Engineering and Applied Science,
University of California, Los Angeles, California 90024

(Received 15 September 1969)

The development of the boundary layer on the upper surface of a horizontal flat plate in a non-diffusive, stratified flow is described. It is shown that the flow can be characterized by two basic parameters, the Reynolds ($R_L$) and Russell ($Ru_L$) numbers, and that, depending on the relative magnitude of these two parameters, three different régimes of flow can be defined. The delineation of these régimes and the description of the flow in each of them is obtained by deriving a uniformly valid first approximation to the Boussinesq equations of motion for a flow contained in the two-dimensional parameter space $Ru_L > 0, R_L > 1$. The critical stratification for the self-blocking of a horizontal boundary layer is shown to be given by the condition $Ru_L = O(R_L^{\frac{1}{2}})$.

## 1. Introduction

Stratified flows in a gravitational field exhibit many remarkable phenomena which are nonexistent in the flow of homogeneous fluids. The development of the boundary layer on a horizontal plate is one example. When the stratification is large and the motion of the fluid is slow, a boundary layer whose thickness decreases in the downstream direction appears and a viscous wake exists upstream of the plate. This is in striking contrast to the familiar downstream growing boundary layer and downstream viscous wake existing when the fluid is homogeneous.

Long (1959) first observed experimentally and described theoretically the existence of a viscous wake with a multiple jet-like structure upstream of a body moving horizontally in a stratified fluid. He derived a similarity solution which is valid far upstream of an obstacle and showed that velocity perturbations relative to the horizontal free stream decay algebraically ($x^{-\frac{3}{4}}$) with distance measured upstream from the obstacle. The solution characterizes the blocking of the flow ahead of a body.

Martin (1966) and Martin & Long (1968) subsequently investigated the boundary layer above a slowly moving horizontal plate under conditions for which an upstream wake occurred. Their experiments, as well as those performed by Pao

† Present address: Department of Aerospace Engineering, University of Colorado, Boulder, Colorado 80302.

(1968), showed the remarkable result that the boundary-layer thickness decreased in the downstream direction. They were able to describe this flow structure theoretically by solving the equations of motion in which the advective terms and density diffusion were neglected. They also demonstrated that, when density diffusion is allowed, the diffusion boundary layer continues to grow in the downstream direction just as in the case of homogeneous flows.

The purpose of this investigation is to provide a parametric study of the influence of density stratification on the development and structure of horizontal boundary-layer regions. The appearance of upstream wakes and upstream growing boundary layers implies that a critical stratification exists for which the thickness of a downstream growing boundary layer becomes sufficiently large to induce blocking. Blocking of a flow ahead of an obstacle can be understood on the basis of energy considerations, but the occurrence of a self-blocking due solely to the action of viscosity is more difficult to understand. The establishment of a criterion for determining which boundary-layer structure appears for specified flow conditions is one of the objectives of this study.

Another interesting aspect of boundary layers in stratified media concerns the coupling between the viscous boundary layer and the outer inviscid flow. From existing studies of boundary layers in homogeneous flows, we know that the boundary layer displaces the outer flow in a direction transverse to the external flow. Since stratification effectively inhibits vertical motions, the question arises as to the interaction between the outer stratified flow and a horizontal boundary layer. Furthermore, since any non-trivial stratified flow is rotational, the boundary-layer induced perturbation on the external flow establishes a possible vorticity interaction with the boundary layer. These effects are investigated for the flow over a horizontal plate by deriving a uniformly valid solution to first order, with the magnitude of the density stratification $|d\ln\rho/dx_3|$ appearing as a parameter.

## 2. Formulation

We consider the development of a viscous boundary layer on the upper surface of a horizontal flat plate of length $L$ in a stably stratified flow (as shown in figure 1). Taking the viscosity $\mu_0$, the specific heat $c_{p_0}$, and the thermal conductivity $k_0$ to be constant, the dimensionless equations of motion for steady, low speed ($M^2 \ll 1$; $M$ = Mach number), thermally stratified flow are

$$\nabla\cdot(\rho\mathbf{q}) = 0, \tag{1}$$

$$\rho(\mathbf{q}\cdot\nabla)\mathbf{q} = -\nabla p - \frac{\rho}{F_L}\hat{\mathbf{k}} - \frac{1}{R_L}\nabla\times(\nabla\times\mathbf{q}), \tag{2}$$

$$\rho(\mathbf{q}\cdot\nabla)T = \frac{1}{P_0 R_L}\nabla^2 T, \tag{3}$$

and

$$\rho = \rho(T). \tag{4}$$

The equations have been made dimensionless by scaling the independent variables with the plate length $L$, the velocity with its free-stream value $U_0$, the density and temperature by their respective values at the level of the plate ($\rho_0$ and $T_0$),

and the pressure by the dynamic head ($\rho_0 U_0^2$). The three dimensionless parameters appearing in the above equations, the Froude number $F_L$, the Prandtl number $P_0$, and the Reynolds number $R_L$ are defined as

$$F_L = \frac{U_0^2}{gL}, \quad P_0 = \frac{\mu_0 c_{p_0}}{k_0} \quad \text{and} \quad R_L = \frac{\rho_0 U_0 L}{\mu_0}. \tag{5}$$

The equation of state (4) denotes that the fluid is incompressible in that changes in pressure induce negligible changes in density. This is consistent with the restriction of the analysis to low speed ($M^2 \ll 1$) flows.

The above equations are written explicitly for thermally stratified flows, but they also describe molecularly stratified flows if $T$ is replaced by the mass fraction of the biasing species and the Schmidt number is substituted for the Prandtl number.

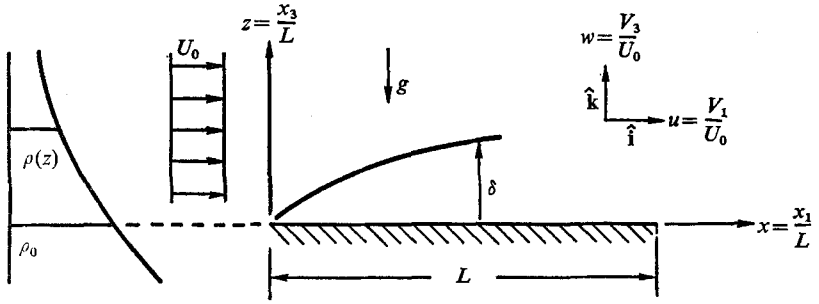


FIGURE 1. A schematic of the flow model.

The structure of the velocity field above the plate is studied first for the limiting case of a large Prandtl number. In this limit ($P_0 \to \infty$), the diffusion of heat can be neglected and the energy equation reduces to

$$(\mathbf{q}\cdot\nabla)T = 0, \tag{6}$$

or by use of the equation of state (4),

$$(\mathbf{q}\cdot\nabla)\rho = 0. \tag{7}$$

The diffusive case (arbitrary Prandtl number) is studied in part 2 of this analysis.

Combining (1) and (7), the continuity equation reduces to the incompressible form

$$\nabla\cdot\mathbf{q} = 0. \tag{8}$$

Assuming the plate is infinitely wide so that the flow can be taken as two-dimensional, (8) permits the introduction of a stream function $\psi$ defined by

$$\mathbf{q} = -(\nabla\times\hat{\mathbf{j}})\psi(x,z) = \hat{\mathbf{i}}\frac{\partial\psi}{\partial z} - \hat{\mathbf{k}}\frac{\partial\psi}{\partial x}. \tag{9}$$

Equations (6) and (7) can then be integrated to yield

$$T = T(\psi) \quad \text{and} \quad \rho = \rho(\psi). \tag{10}$$

The analytic forms of $\rho(\psi)$ and $T(\psi)$ are determined by the boundary conditions far upstream of the plate. Results (9) and (10) provide a great simplification and

permit the system of equations (2), (7) and (8) to be written in terms of a single equation for the stream function $\psi$.

Considering a density stratification given by

$$\rho(x \to -\infty, z) = \rho_s(z) = e^{-\beta z} = e^{-(\beta_0 L) x_3 / L}, \tag{11}$$

and invoking the Boussinesq approximation, the vorticity equation is obtained in the form

$$\left[ L(x, z, \psi) - \frac{1}{R_L} \nabla^2 \right] \nabla^2 \psi + Ru_L^2 \psi_x = 0, \tag{12}$$

where

$$L(x, z, \psi) = \psi_z \frac{\partial}{\partial x} - \psi_x \frac{\partial}{\partial z}. \tag{13}$$

The operator $L(x, z, \psi)$ appears extensively throughout the succeeding analysis and, for convenience, is written in shorthand form where the symbols in the parenthesis indicate the horizontal and vertical co-ordinate variables and the dependent variable of the operator in that order. The parameter $Ru_L$ represents the Russell number, a designation originally ascribed by Miles (1968). It is defined as

$$Ru_L^2 = \left( \frac{NL}{U_0} \right)^2 = \frac{\beta}{F_L}, \tag{14}$$

where

$$N = \left( -g \frac{d \ln \rho_s}{dx_3} \right)^{\frac{1}{2}} = (g\beta_0)^{\frac{1}{2}}, \tag{15}$$

$N$ denoting the intrinsic frequency. Two independent parameters appear in (12); the first parameter, $R_L^{-1}$, scales the viscous terms relative to the inertia terms, and the second, $Ru_L^2$, scales the buoyancy term relative to the inertia terms. Their relative magnitudes can be expected to play an important role in determining the flow structure in the vicinity of the plate.

The boundary conditions applicable to (12) for the problem depicted in figure 1 are

$$\begin{aligned} &\psi(x, 0) = 0, \quad (x < 0), \\ &\psi(x, 0) = \psi_z(x, 0) = 0, \quad (0 \leqslant x \leqslant L), \\ \text{and} \quad &\psi_z(x \to -\infty, z) = \psi_z(x, z \to \infty) = 1. \end{aligned} \tag{16}$$

We now seek a uniformly valid first approximation to the solution of (12), subject to the conditions (16), for large Reynolds numbers but with the Russell number varying from small to large values.

## 3. The boundary-layer approximation

Consider first the flow region in the immediate vicinity of the plate where viscosity has a first-order effect. Anticipating that the vertical scale of this region is small relative to the horizontal length of the plate, we introduce the boundary-layer transformation

$$y = z/\epsilon, \quad \epsilon = \epsilon(R_L, Ru_L) \cong \delta/L \ll 1,$$

and

$$\psi(x, z) = \epsilon \Psi(x, y), \tag{17}$$

where $\epsilon$ is a function of the parameters that appear in the differential equation (12). The functional form of $\epsilon$ is determined by requiring the coefficient of the highest order viscous term to be unity and all remaining terms in the vorticity equation to be of order unity or smaller.

Introducing the transformation (17) into the vorticity equation (12) yields the boundary-layer equation

$$\left[L(x,y,\Psi)-\frac{\epsilon^{-2}}{R_L}\left(\epsilon^2\frac{\partial^2}{\partial x^2}+\frac{\partial^2}{\partial y^2}\right)\right]\left(\epsilon^2\frac{\partial^2}{\partial x^2}+\frac{\partial^2}{\partial y^2}\right)\Psi+\epsilon^2 Ru_L^2\Psi_x=0. \tag{18}$$

Buoyancy contributes to the vorticity balance in the boundary layer in proportion to the square of the Russell number based on the boundary-layer thickness $\delta$, since

$$\epsilon^2 Ru_L^2=\frac{\delta^2}{L^2}\frac{N^2L^2}{U_0^2}=Ru_\delta^2. \tag{19}$$

The Russell number based on a representative vertical dimension of an obstacle characterizes the structure of the flow over the obstacle (cf. Long 1953, 1954, 1955, 1959; Miles 1968) and, when that Russell number becomes large, the flow is blocked upstream of the obstacle.

Two limiting cases of (18) are now considered. First, when the Russell number is small (small stratification, $R_L > Ru_L^2$), the boundary layer is characterized by a balance between the inertia and viscous terms with the familiar scale

$$\epsilon=\epsilon_{iv}=R_L^{-\frac{1}{2}}. \tag{20}$$

The buoyancy term is then of order $(Ru_L^2/R_L)$. Writing the stream function as a perturbation sequence in $\epsilon$,

$$\Psi(x,y;\epsilon)=\Psi^{(1)}(x,y)+\alpha(\epsilon)\Psi^{(2)}(x,y)+\ldots, \tag{21}$$

and substituting into (18), we obtain for $\Psi^{(1)}$ the equation

$$\left[L(x,y,\Psi^{(1)})-\frac{\partial^2}{\partial y^2}\right]\frac{\partial^2\Psi^{(1)}}{\partial y^2}=0. \tag{22}$$

This equation can be integrated once with respect to $y$ to yield the Blasius equation (cf. Rosenhead 1963, p. 222). The solution, $\Psi_B$, say, obtained by means of the similarity transformation

$$\eta=\frac{y}{x^{\frac{1}{2}}},$$

$$\Psi^{(1)}(x,y)=\Psi_B=x^{\frac{1}{2}}f_1(\eta), \tag{23}$$

is well-known. A property of $\Psi_B$ which has important consequences in the subsequent development is that the solution is not uniformly valid since

$$\left.\begin{aligned}\lim_{y\to\infty} w(x,y)&=0{\cdot}865\,\epsilon_{iv}x^{-\frac{1}{2}},\\ \text{or}\qquad \Psi^{(1)}(x,\infty)&=y-1{\cdot}730x^{\frac{1}{2}}.\end{aligned}\right\} \tag{24}$$

The second case we consider is the limit of large Russell numbers (large stratification, $R_L < Ru_L^2$). The boundary-layer scaling is then given by

$$\epsilon=\epsilon_{bv}=(R_LRu_L^2)^{-\frac{1}{4}}. \tag{25}$$

Since inertia terms are then of order $(R_L^{\frac{1}{2}}/Ru_L)$, the first-order boundary-layer vorticity equation becomes

$$\Psi^{(1)}_x - \Psi^{(1)}_{yyyy} = 0, \tag{26}$$

which corresponds to a balance between the diffusion of vorticity and the baroclinic generation of vorticity. Equation (26) was first derived by Long (1959) in his analysis of a viscous wake upstream of an obstacle. Later, a similarity solution to (26) was obtained by Martin & Long (1968) describing the boundary layer on a horizontal flat plate. They showed that, in order to obtain a physically meaningful solution to the parabolic equation (26), the direction of the time-like variable $x$ had to be reversed, leading to a boundary layer with upstream growth and an upstream wake. If we let

$$\bar{x} = 1 - x,$$

so that

$$\Psi^{(1)}_{\bar{x}} + \Psi^{(1)}_{yyyy} = 0,$$

the similarity solution is of the form

$$\eta = y/\bar{x}^{\frac{1}{4}},$$

$$\Psi^{(1)}(\bar{x}, y) = \Psi_L = \bar{x}^{\frac{1}{4}} f_1(\eta). \tag{27}$$

Their solution, $\Psi_L$, is uniformly valid in that the vertical velocity approaches zero exponentially fast at the outer edge of the boundary layer.

A useful representation of the above results which clarifies the interplay between the two parameters $Ru_L$ and $R_L$ is obtained by replacing the Russell number by a power of the Reynolds number,

$$Ru_L^2 = R_L^n. \tag{28}$$

The vertical scale $\epsilon$ of the first-order boundary layers for the inertia-viscous balance (22) and the buoyancy-viscous balance (27) are then given by

$$\epsilon_{iv} = R_L^{-\frac{1}{2}},$$

$$\epsilon_{bv} = R_L^{-\frac{1}{4}(n+1)},$$

so that

$$\frac{\epsilon_{bv}}{\epsilon_{iv}} = R_L^{\frac{1}{4}(1-n)}. \tag{29}$$

Using the latter relation, we can delineate three distinct boundary-layer types depending on the relative magnitude of the Russell and Reynolds numbers. For $n < 1$, $\epsilon_{iv} < \epsilon_{bv}$ and the first-order boundary layer is the Blasius one (22), in which convection and diffusion of vorticity are balanced. When $n > 1$, $\epsilon_{bv} < \epsilon_{iv}$, and the first-order boundary layer is described by Long's equation (27). The third boundary-layer type occurs when the condition $n = 1$ is satisfied. In this case $\epsilon_{iv} = \epsilon_{bv}$ and convection, diffusion, and baroclinic generation of vorticity are all of equal order in the boundary layer. The governing first-order equation then becomes

$$\left[L(x, y, \Psi^{(1)}) - \frac{\partial^2}{\partial y^2}\right] \frac{\partial^2 \Psi^{(1)}}{\partial y^2} + \Psi^{(1)}_x = 0. \tag{30}$$

We refer to this case as the critical boundary layer since it is transitional between a downstream growing boundary layer ($n < 1$) and an upstream growing boundary layer ($n > 1$). A similarity solution of (30) is possible only for the case of an accelerated flow ($U_e \sim x^{\frac{1}{2}}$).

The above three equations, (22), (27), and (30) describe all the possible first-order boundary layers on a horizontal surface in a stratified flow. Their classification depends strongly on the relative magnitude of the Russell and Reynolds numbers. To obtain a uniformly valid approximation to the entire flow structure, however, we must also examine the outer flow, to which the solutions of the above equations must match.

## 4. The outer flow

In considering the outer flow, we use the Russell–Reynolds number relation (28) and equation (12). The stream function expansion for the outer flow is

$$\psi(x,z;\epsilon) = z + \delta_1(\epsilon)\psi^{(1)}(x,z) + \ldots, \tag{31}$$

where the first term on the right describes the zeroth-order motion. The gauge function $\delta_1(\epsilon)$ is equal to $\epsilon$ and takes on the value dictated by the first-order boundary layer as given in (29). Substituting the above expansion into (12) yields the following equation for the outer flow

$$\left[\frac{\partial}{\partial x} - \frac{1}{R_L}\nabla^2\right]\nabla^2\psi^{(1)} + R_L^n\psi_x^{(1)} = O(\epsilon). \tag{32}$$

Examining this equation, we again find that there are three different cases depending on the value of the exponent $n$, i.e. on the magnitude of the Russell number. When $n < 0$, the last term on the left-hand side is smaller than unity and, in fact, vanishes in the limit ($R_L \to \infty$). The first-order outer flow is then governed by the equation

$$\frac{\partial}{\partial x}\nabla^2\psi^{(1)} = 0 \quad (n < 0). \tag{33}$$

The outer flow in this case is determined by a balance between the inertia and pressure forces while the buoyancy and viscous terms appear only in higher order equations. When $n = 0$, the inertia and buoyancy terms are of equal importance, and the first-order outer flow is described by the equation

$$\frac{\partial}{\partial x}[\nabla^2 + 1]\psi^{(1)} = 0 \quad (n = 0). \tag{34}$$

The stratification is now sufficiently large that the boundary-layer displacement effect renders the baroclinic generation of vorticity a first-order role in the outer flow. Thirdly, when $n > 0$, the buoyancy term in equation (32) dominates, and the first-order flow is governed by the equation

$$\frac{\partial\psi^{(1)}}{\partial x} = 0 \quad (n > 0). \tag{35}$$

This relation is analogous to the Taylor–Proudman theorem in rotating flows and expresses the fact that the constraining influence of stratification is sufficiently large to inhibit vertical motions. The outer flow is then in hydrostatic balance regardless of the boundary-layer displacement effect.

An incompatability in the above set of equations is immediately apparent. For $n < 1$, the first-order boundary layer is described by the Blasius equation which requires that the first-order outer flow satisfy the matching condition

$$\psi^{(1)}(x, 0) = -1{\cdot}730x^{\frac{1}{2}} \quad (n < 1). \tag{36}$$

However, for $n > 0$ the outer flow is governed by (35), which clearly does not admit a solution satisfying condition (36). Hence, we must conclude that for $0 < n < 1$ either the steady flow breaks down into some unsteady structure or a more complicated coupling exists involving an intermediate layer through which the Blasius solution and the solution $\psi^{(1)} = 0$ of (35) can be properly matched. We assume the latter to be true and re-examine (12) and (18) in the parameter range $0 < n < 1$. For $n > 1$, no difficulty occurs since the boundary-layer solution $\psi_L$ from (27) is uniformly valid.

## 5. The intermediate layer

Examining the boundary-layer equation (22) and the outer-flow equation (35), it is clear that the outer flow is governed by a pressure-buoyancy (hydrostatic) balance, while the boundary layer is characterized by a balance between the inertia, pressure, and viscous stress terms. The importance of the buoyancy term must diminish as one approaches the plate from the free stream, and the importance of the inertia terms must diminish as one proceeds away from the plate toward the free stream. Intuitively then, one expects that a region exists between the boundary layer and the external flow wherein an inertia-pressure-buoyancy balance occurs.

To derive the correct first-order approximation to the flow in the intermediate region, we introduce the transformation

$$\hat{y} = \sigma(R_L, n)y = \frac{z}{\epsilon/\sigma}, \quad \epsilon = R_L^{-\frac{1}{2}},$$

and

$$\psi(x, z) = (\epsilon/\sigma)\hat{\Psi}(x, \hat{y}). \tag{37}$$

Substituting (37) into (12) we obtain the equation

$$\left[L(x, \hat{y}, \hat{\Psi}) - \sigma^2\left\{(\epsilon/\sigma)^2\frac{\partial^2}{\partial x^2} + \frac{\partial^2}{\partial \hat{y}^2}\right\}\right]\left\{\left(\frac{\epsilon}{\sigma}\right)^2\frac{\partial^2}{\partial x^2} + \frac{\partial^2}{\partial \hat{y}^2}\right\}\hat{\Psi} + \sigma^2 R_L^{n-1}\hat{\Psi}_x = 0. \tag{38}$$

Choosing $\sigma$ so that a proper balance of terms is maintained leads to the condition

$$\sigma = R_L^{-\frac{1}{2}(1-n)}, \tag{39}$$

whereby the inertia and buoyancy terms are balanced and the viscous stress terms are at most of order $\sigma^2$. The characteristic vertical scale $\Delta_I$ of the intermediate region is

$$\Delta_I/L = (\epsilon/\sigma) = R_L^{-\frac{1}{2}n} \quad (0 \leqslant n < 1). \tag{40}$$

When $n = 0$, the intermediate layer contains the entire outer flow and, as the stratification is increased (increasing $n$), the vertical extent of the layer decreases until it is completely contained within the primary boundary layer when $n = 1$.

Thus, an intermediate region described by the scaling (40) and equation (38) can be defined. However, to conclusively demonstrate the existence of a double structure for $0 < n < 1$, it is necessary to show that solutions of (38) are possible satisfying the conditions

$$\hat{\Psi}^{(1)}(x, 0) = -1{\cdot}730x^{\frac{1}{2}} \quad \text{and} \quad \hat{\Psi}^{(1)}(x, \infty) = 0. \tag{41}$$

This topic has been considered in detail by Redekopp (1969), who demonstrated that such solutions are impossible unless the horizontal co-ordinate is scaled along with the vertical co-ordinate. The $x$ scaling that is required is exactly equivalent to the $z$ scaling, i.e.

$$\hat{x} = \frac{x}{\epsilon/\sigma} = xR_L^{\frac{1}{2}n} \quad (0 \leqslant n \leqslant 1). \tag{42}$$

This is the only scaling which allows a consistent matching between the boundary layer and the outer flow. Observe that when $n = 1$, $\hat{x}$ is of the same order as the boundary-layer thickness, which suggests that perhaps the complete Navier–Stokes equations are required to describe the $n = 1$ case. This presents a plausible explanation as to how the transition between the two parabolic cases (22) for ($n < 1$) and (29) for ($n > 1$) is accomplished.

A justification for the scaling (42) is provided by the following consideration. Outside the primary boundary layer, the representative length for the flow is no longer that of the body ($L$), but the characteristic wavelength of internal waves. This is precisely what the scaling (42) accomplishes, as can be seen by defining a length $\lambda$ equivalent to the length of a wave oscillating at the intrinsic frequency $N$ and moving with velocity $U_0$,

$$\lambda = \frac{U_0}{N} = \frac{L}{Ru} = LR_L^{-\frac{1}{2}n}.$$

Rescaling the $x$ variable with $\lambda$ we obtain

$$\hat{x} = x \Big/ \left(\frac{\lambda}{L}\right) = xR_L^{\frac{1}{2}n}. \tag{43}$$

The order of magnitude of the viscous terms is then

$$\epsilon\sigma = R_L^{-1+\frac{1}{2}n} \tag{44}$$

which is of order ($R_L^{-1}$) as in the case of homogeneous flow when $n = 0$ and of order ($R_L^{-\frac{1}{2}}$) when $n = 1$.

The stream function expansion for the intermediate layer is of the form

$$\psi(x, z; R_L) = \frac{\epsilon}{\sigma}\hat{\Psi}(\hat{x}, \hat{y}) = R_L^{-\frac{1}{2}n}[\hat{y} + \gamma(R_L)\hat{\Psi}^{(1)}(\hat{x}, \hat{y}) + \ldots], \tag{45}$$

where the form of $\gamma(R_L)$ is chosen so that $\hat{\Psi}^{(1)}(\hat{x}, \hat{y})$ matches to the Blasius solution $\Psi_B$. Carrying through the matching yields

$$\gamma(R_L) = \epsilon\left(\frac{\epsilon}{\sigma}\right)^{-\frac{1}{2}} = R_L^{-\frac{1}{2}+\frac{1}{4}n}$$

and

$$\hat{\Psi}^{(1)}(\hat{x}, \hat{y} = 0) = -1{\cdot}730\hat{x}^{\frac{1}{2}}. \tag{46}$$

The first-order equation for the intermediate layer then becomes

$$\frac{\partial}{\partial \hat{x}}[\hat{\nabla}^2 + 1]\hat{\Psi}^{(1)} = 0. \tag{47}$$

This equation is applicable for the parameter range $0 < n < 1$. Its form, together with the boundary conditions, is identical to the first-order equation for $n = 0$.

## 6. The flow due to boundary-layer displacement

In this section we present the solution for the first-order outer flow induced by the displacement effect of the Blasius boundary layer. Since the exact shape of the displacement body in the downstream wake is unknown, we calculate the outer flow as if the plate were semi-infinite.

For Russell numbers less than unity ($n < 0$), the outer flow is potential (equation (33)), and the solution satisfying the matching condition (36) is given by Van Dyke (1964, p. 134). It can be written in the form

$$\psi^{(1)}(x, z) = -0{\cdot}865\,((x+iz)^{\frac{1}{2}} + (x-iz)^{\frac{1}{2}}) = -1{\cdot}730 r^{\frac{1}{2}} \cos \tfrac{1}{2}\theta. \tag{48}$$

For $0 \leqslant n < 1$, the outer flow is described by the Helmholtz equation (equations (34) and (47)) which we write in the form

$$\nabla^2 \phi + a^2 \phi = 0, \tag{49}$$

with the boundary conditions

$$\phi = o(z) \quad \text{as} \quad (x^2 + z^2) \to \infty,$$

$$\phi(x, 0) = 0 \quad \text{for} \quad x < 0,$$

and

$$\phi(x, 0) = -1{\cdot}730 x^{\frac{1}{2}} \quad \text{for} \quad x > 0. \tag{50}$$

It is understood that $(\hat{x}, \hat{y})$ are substituted for $(x, z)$ when $0 < n < 1$ and that $\phi$ denotes either $\psi^{(1)}$ or $\hat{\Psi}^{(1)}$ depending on the value of $n$. The parameter $a$ is included to indicate explicitly the role of the Russell number.

The solution of the Helmholtz equation describing the flow of a stratified fluid over various shaped obstacles has been the concern of a number of investigators, particularly as it relates to the phenomena of internal waves in the lee of mountain ranges. Queney *et al.* (1960) and Miles (1968) have given comprehensive reviews of the existing solutions. For the solution of the boundary-value problem (49) and (50), we follow the development by Graham (1966) for the flow over an arbitrarily shaped slender body. Graham's solution is given in the form

$$\phi(x, z) = \int_0^\infty f(\xi)\, \phi_D(x - \xi, z)\, d\xi, \tag{51}$$

where $f(x)$ is the dipole density and $\phi_D(x, z)$ denotes the solution of (49) for an isolated dipole of strength $b$

$$\phi_D(x, z) = bz \frac{Y_1(a[z^2 + x^2]^{\frac{1}{2}})}{[z^2 + x^2]^{\frac{1}{2}}} + \frac{b}{\pi} \sum_{m=1}^{\infty} \frac{8m}{4m^2 - 1} J_{2m}(a[z^2 + x^2]^{\frac{1}{2}}) \sin\left(2m \tan^{-1}\frac{z}{x}\right). \tag{52}$$

In the framework of small disturbance theory, which is clearly applicable, the dipole density is related to the vertical perturbation velocity $w^{(1)}$ at the altitude $z = 0$ by

$$f(x, 0) = \int_0^x \tfrac{1}{2}a\, w^{(1)}(\xi, 0)\, d\xi = \tfrac{1}{2}a(1{\cdot}730x^{\frac{1}{2}}). \tag{53}$$

Note that the dipole strength depends directly on $a$, or, using the basic parameters of the problem, the Russell number $Ru_L$. This reflects the fact that the scale of the flow outside the boundary layer must change as the Russell number increases. Since the boundary-layer displacement is independent of the stratification to this order, (53) requires that the independent variable $x$ be scaled in such a way that the dipole strength is always comparable to the magnitude of the boundary-layer displacement velocity $w^{(1)}(x, 0)$, even when the Russell number is large ($0 < n < 1$). This is precisely what the intermediate layer scaling (43) accomplishes.

Substituting the results (52) and (53) into (51), the solution for $\phi(x, z)$ becomes

$$\phi(x, z) = -1{\cdot}730r^{\frac{1}{2}} \cos\tfrac{1}{2}\theta + \frac{1{\cdot}730a}{\pi} \sum_{m=1}^{\infty} \frac{4m}{4m^2 - 1} \int_0^{\infty} J_{2m}(a[z^2 + (x-\xi)^2]^{\frac{1}{2}}) \times \sin\left(2m \tan^{-1} \frac{z}{x-\xi}\right) d\xi. \tag{54}$$

The first term, which is identical to the solution (48) for potential flow, derives from the integration of the first term in (52). The effect of density stratification is then contained solely in the integral term of (54).

The integral and sum in (54) were evaluated numerically by integrating between the limits $\xi = 0$ to $\xi = 100$ and taking ten terms of the sum. An upper limit of ten for the summation was chosen because it corresponds to approximately a ten-fold decrease in magnitude between the first and tenth terms. Since there is no characteristic geometrical length for a semi-infinite plate, all lengths are scaled by the stratification length

$$L = \beta_0^{-1} = \left| \frac{d \ln \rho_s}{dx_3} \right|^{-1}. \tag{55}$$

Numerical values were computed for $x$ ranging between $x = -5$ and $x = 20$ in increments of $\Delta x = 0{\cdot}2$ with $z$ ranging between $z = 0{\cdot}25$ and $z = 3{\cdot}0$. The first-order, uniformly valid solutions for $a = 1{\cdot}0$ and Reynolds numbers of 100 and 1000 are shown in figure 2, where

$$\psi(x, z) = z + \epsilon\psi^{(1)}(x, z) + \epsilon(y - \Psi^{(1)}(x, y)),$$

and

$$\epsilon = R_{\beta_0}^{-\frac{1}{2}} = \left(\frac{\nu_0 \beta_0}{U_0}\right)^{\frac{1}{2}}. \tag{56}$$

No wave pattern appears and the streamlines exhibit the same general shape that exists for homogeneous flow. This is somewhat surprising in light of Lyra's (1943) solution for the flow over a semi-infinite plateau (forward facing step) which shows a very distinct pattern of waves. A possible explanation for this is that there is a critical bluntness for a monotonic, semi-infinite body which must be exceeded if waves are to be generated. For the flow over a finite flat plate, the

thickness of the displacement body decreases downstream of the trailing edge of the plate and it is quite likely that a wave pattern would appear in the downstream flow field.

Another interesting feature of the solution (54) is that the horizontal perturbation velocity vanishes as $z$ tends to zero indicating that there is no coupling between the first-order outer flow and the second-order boundary layer. It is worth noting that a coupling between the outer flow and the second-order boundary layer does exist when the non-Boussinesq terms are included in the outer flow equations. As will be demonstrated in part 2 of this analysis, a coupling enters via the thermal field when diffusion is allowed, even in the Boussinesq approximation.

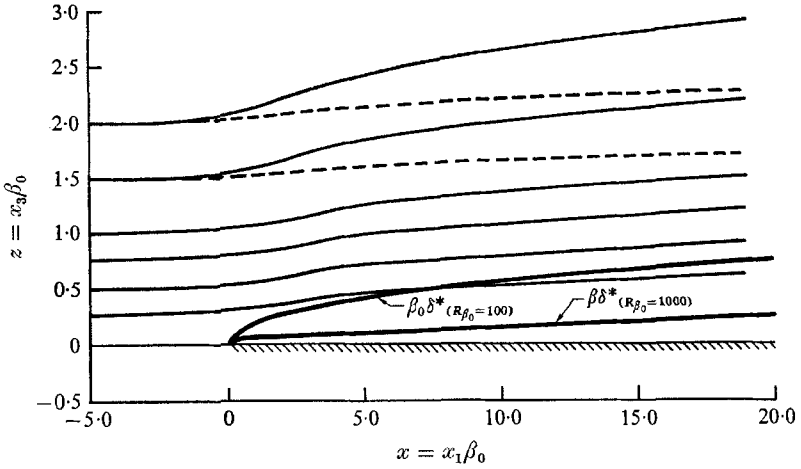


FIGURE 2. The first-order streamline pattern for the case $n = 0$. —, streamlines for $R_{\beta_0} = 100$; – – –, streamlines for $R_{\beta_0} = 1000$.

## 7. The second-order boundary layer

In the parameter range $0 < n < 1$, the boundary-layer expansion is given by

$$\psi(x,z) = R_L^{-\frac{1}{2}}[\Psi^{(1)}(x,y) + \alpha(R_L)\Psi^{(2)}(x,y) + \ldots], \tag{57}$$

and, from (45) and (46), the corresponding outer-flow expansion is

$$\psi(x,z) = R_L^{-\frac{1}{2}n}[\hat{y} + R_L^{-\frac{1}{2}+\frac{1}{4}n}\hat{\Psi}^{(1)}(x,y) + \ldots]. \tag{58}$$

Substituting (57) into the boundary-layer form of the vorticity equation (18), we obtain the equation

$$\left[L(x,y,\Psi^{(1)}) - \frac{\partial^2}{\partial y^2}\right]\frac{\partial^2\Psi^{(2)}}{\partial y^2} + L(x,y,\Psi^{(2)})\frac{\partial^2\Psi^{(1)}}{\partial y^2} + \frac{R_L^{n-1}}{\alpha(R_L)}\Psi_x^{(1)} = 0. \tag{59}$$

If there is a forcing of the second-order boundary layer arising from the first-order outer flow ($\hat{\Psi}^{(1)}$), the gauge function $\alpha$ is given by

$$\alpha = R_L^{-\frac{1}{4}n}. \tag{60a}$$

On the other hand, the forcing arising from the baroclinic term requires that

$$\alpha = R_L^{n-1}. \tag{60b}$$

The contributions from these two forcing effects are equal when $n = \frac{4}{5}$. When $n < \frac{4}{5}$ the baroclinic generation term has no influence on the solution to first order. However, when $n > \frac{4}{5}$ the second-order boundary-layer contribution due to the baroclinic generation of vorticity is more significant than the correction to the outer flow due to the displacement effect of the first-order (Blasius) boundary layer. A uniformly valid solution to first order, then, requires that $\Psi^{(2)}(x, y)$ be evaluated for $\frac{4}{5} \leqslant n < 1$ using (59) with homogeneous boundary conditions and $\alpha$ given by (60*b*). For the flow over a flat plate, $\Psi^{(2)}$ has the same form throughout the range $0 < n < 1$ since the displacement induced horizontal velocity vanishes at the plate surface (at least in the Boussinesq approximation) so that the boundary conditions and the differential equation are the same for the entire range.

Using the Blasius solution (equation (23)), a similarity solution of (59) is possible and has the form

$$\Psi^{(2)}(x, y) = x^{\frac{3}{2}} f_2(\eta), \tag{61}$$

where $f_2(\eta)$ satisfies the equation

$$f_2^{\mathrm{iv}} + \tfrac{1}{2} f_1 f_2''' - \tfrac{1}{2} f_1' f_2'' + \tfrac{1}{2} f_1'' f_2' + \tfrac{3}{2} f_1''' f_2 = \tfrac{1}{2}(f_1 - \eta f_1'). \tag{62}$$

The forcing term on the right-hand side is known from the Blasius solution and corresponds to the streamwise derivative of the temperature as expressed by (10). It is equal to the negative of the first-order vertical velocity and, therefore, approaches a constant value as $\eta$ becomes large. Consequently, (62) reveals that the second-order shear approaches a constant for large $\eta$

$$\lim_{\eta \to \infty} f_2'' = - \lim_{\eta \to \infty} (f_1 - \eta f_1') = 1{\cdot}730. \tag{63}$$

This violates the definition of a boundary layer and indicates that another intermediate layer must exist in which the shear decays to zero. It appears that the same difficulty is encountered in higher-order terms for $n \leqslant 0$ as well. We are investigating this problem further in an attempt to resolve the difficulty (solutions for the second-order boundary layer for Prandtl number of order unity are given in part 2).

## 8. Summary

We have found that two characteristic parameters describe the boundary-layer flow of a stratified fluid, the Reynolds and Russell numbers, and that their relative magnitude define three different régimes of flow. These régimes are given by (i) $Ru_L < O(1)$, (ii) $O(1) \leqslant Ru_L < O(R_L^{\frac{1}{2}})$, and (iii) $Ru_L > O(R_L^{\frac{1}{2}})$. The ranges of applicability of each of these régimes are shown schematically in figure 3. In the first case the inner flow is the familiar Blasius boundary layer and the outer flow is potential. In the second case, the primary boundary-layer flow is still described by the Blasius equation, but an intermediate region exists in which the flow induced by the displacement effect of the boundary layer adjusts to a parallel outer flow. Both dependent variables must be scaled with the wavelength of waves oscillating at the natural frequency and moving with the free stream velocity in order to obtain a consistent representation of the outer flow in this

régime. In the third case, the boundary layer changes from one with downstream growth to one with upstream growth. The upstream flow is then changed and, in order to maintain a balance between the diffusion of vorticity and the baroclinic generation of vorticity, the streamlines must diverge in the downstream direction and an upstream wake appears.

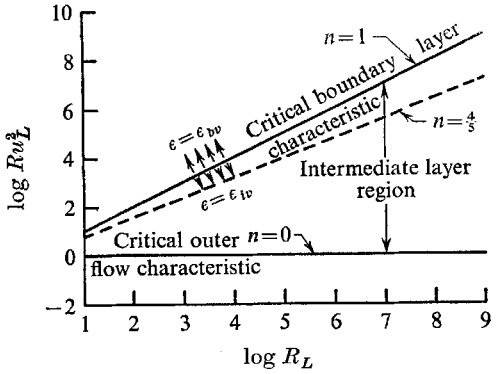


FIGURE 3. The various flow régimes in Russell number–Reynolds number parameter space.

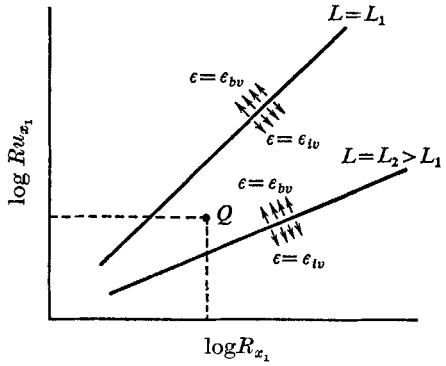


FIGURE 4. The qualitative effect of the plate length on the critical ($n = 1$) boundary-layer flow characteristic.

Another useful representation of the flow is obtained by writing the Russell–Reynolds number relation (28) in terms of the running length $x_1$

$$Ru_{x_1}^2 = \left(\frac{x_1}{L}\right)^{2-n} R_{x_1}^n = R_L^{n-2} R_{x_1}^2.$$

The magnitude of the Reynolds number based on the total plate length and the *relative* magnitude of the Russell and Reynolds numbers (characterized by $n$) define the slope of the flow characteristics in the two-dimensional parameter space $Ru_{x_1} - R_{x_1}$. Suppose we observe the flow at a fixed position on a plate, which we denote as the point $Q$ in figure 4. Furthermore, suppose that this point lies below the critical boundary-layer characteristic ($n = 1$) for a plate of length $L_1$ so that the boundary layer grows in the downstream direction. Then, if the

plate length is increased to $L_2$, $L_2 > L_1$, the slope of the critical characteristic decreases and we see that, if $L_2$ is sufficiently large, self-blocking occurs and an upstream wake and upstream growing boundary layer appear. Hence, for given flow conditions, one can always find a plate sufficiently long so that blocking occurs.

Discussions of this research with Dr A. F. Charwat and Dr A. G. Hammitt are gratefully acknowledged. The research was supported by the National Science Foundation under grants GK 1244 and GK 4213.

## REFERENCES

GRAHAM, E. W. 1966 The two-dimensional flow of an inviscid density-stratified liquid past a slender body. *Boeing Scientific Research Laboratories* Document DL-72-0550, Flight Sciences Laboratory Report no. 108.

LONG, R. R. 1953 Some aspects of the flow of stratified fluids. I. A theoretical investigation. *Tellus*, **5**, 42–57.

LONG, R. R. 1954 Some aspects of the flow of stratified fluids. II. Experiments with a two-fluid system. *Tellus*, **6**, 97–115.

LONG, R. R. 1955 Some aspects of the flow of stratified fluids. III. Continuous density gradients. *Tellus*, **7**, 432–457.

LONG, R. R. 1959 The motion of fluids with density stratification. *J. Geophys. Res.* **64**, 2151–2163.

LYRA, G. 1943 Theorie der stationären Leewellenstromung in freier Atmosphäre. *Z. angew. Math. Mech.* **23**, 1–23.

MARTIN, S. 1966 The slow motion of a finite flat plate in a viscous stratified fluid. *The John Hopkins University Technical Report* no. 21, ONR series Nonr-4010 (01).

MARTIN, S. & LONG, R. R. 1968 The slow motion of a flat plate in a viscous stratified fluid. *J. Fluid Mech.* **31**, 669–688.

MILES, J. W. 1968 Waves and wave drag in stratified flows. Presented at the *Twelfth International Congress of Applied Mechanics*. Stanford.

PAO, Y.-H. 1968 Laminar flow of a stably stratified fluid past a flat plate. *J. Fluid Mech.* **34**, 795–808.

QUENEY, P., CORBY, R., GERBIER, N., KOSCHMIEDER, H. & ZIEREP, J. 1960 The airflow over mountains. *World Meteorological Organization, Technical Note* no. 34.

REDEKOPP, L. G. 1969 Horizontal boundary layers in density stratified flows. Ph.D. Thesis, University of California, Los Angeles.

ROSENHEAD, L. (Ed.) 1963 *Laminar boundary layers*. Oxford University Press.

VAN DYKE, M. D. 1964 *Perturbation Methods in Fluid Mechanics*. New York: Academic.

*J. Fluid Mech.* (1970), *vol.* 42, *part* 3, *pp.* 513–525
*Printed in Great Britain*



# The development of horizontal boundary layers in stratified flow. Part 2. Diffusive flow

By L. G. REDEKOPP

Department of Aerospace Engineering
University of Colorado
Boulder, Colorado 80302

(Received 15 September 1969)

The boundary layer on the upper surface of a horizontal plane in a diffusive, stratified flow is examined. The analysis shows that density diffusion increases the role of the buoyancy forces and causes a significant change in the properties of the boundary layer when compared to the non-diffusive case. A uniformly valid first approximation for moderate Russell numbers is derived, and the effects of buoyancy and diffusion are evaluated by solving the resulting equations numerically.

## 1. Introduction

In part 1 of this series (Kelly & Redekopp 1970, hereafter referred to as I), we examined the boundary-layer structure for steady, stratified fluid motions on the assumption that the Prandtl (or Schmidt) number was very large, whereby the effects of density diffusion could be neglected. The results showed that three different régimes of flow are possible, depending on the relative magnitudes of the Reynolds and Russell numbers, and demonstrated that the coupling between the boundary layer and the external flow plays a crucial role in determining the overall features of the flow.

Martin & Long (1968) considered the effect of diffusion for the flow over a flat plate when the velocity boundary layer grows in the upstream direction. They show that the diffusion boundary layer grows from the leading edge irrespective of the Russell number. Obviously then, the diffusion and velocity layers intersect somewhere over the plate surface, and diffusion can strongly affect the trailing-edge singularity and the existence of a downstream wake. The analysis of Martin & Long (1968), however, was limited to large Schmidt (Prandtl) numbers and to the flow region near the leading edge of the plate where the velocity boundary layer is thick relative to the diffusion boundary layer.

In the present paper, the restriction to large Prandtl numbers imposed in I is relaxed in order to establish the effect of density diffusion on the flow structure in general and the boundary-layer properties in particular. It is known that the relative thickness of the viscous and diffusion boundary layers is determined solely by the magnitude of the Prandtl number. Hence, when the Prandtl number is of order unity or smaller, the coupling between the velocity and thermal fields can be expected to be important, especially within the boundary layer. Also,

heat diffusion can contribute significantly to the magnitude of buoyancy forces in the boundary layer and furthermore, as the Prandtl number decreases, the vertical scale over which these buoyancy forces act is increased. The combination of these effects is investigated for the flow over a horizontal plane. The general flow structure above a finite plate with diffusion is discussed in § 3 and a similarity solution of the boundary-layer equations with buoyancy and heat diffusion is derived in § 4. Numerical results are presented in § 5.

## 2. Formulation

We consider the development of the velocity and thermal boundary layers on the upper surface of an isothermal, horizontal plate of length $L$ immersed in a fluid that is in uniform motion with velocity $U_0$. The fluid is assumed to be stably stratified, and the stratification is assumed to derive from a linear space-distribution of temperature given by

$$T_{s(x_3)} = T_0(1+\beta_0 x_3). \tag{1}$$

A schematic of the flow configuration is given in figure 1. The fluid motion is assumed to obey the Boussinesq equations, which for the steady flow of a viscous, heat-conducting fluid are

$$\nabla . \mathbf{q} = 0, \tag{2}$$

$$(\mathbf{q}.\nabla)\mathbf{q} = -\frac{1}{\rho_0}\nabla p - \frac{\rho}{\rho_0} g\hat{\mathbf{k}} + \nu_0 \nabla^2 \mathbf{q}, \tag{3}$$

$$(\mathbf{q}.\nabla)T = \kappa_0 \nabla^2 T \tag{4}$$

and

$$\rho = \rho_0[1-\alpha_0(T-T_0)]. \tag{5}$$

The quantities $\mathbf{q}, p, \rho$, and $T$ are, respectively, the velocity, pressure, density, and temperature of the fluid at the point $(x_1, x_3)$; $\nu_0$ and $\kappa_0$ denote the kinematic viscosity and thermal diffusivity (which are constants in the limit of the Boussinesq approximation; $\alpha_0$ represents the coefficient of thermal expansion; and $\hat{\mathbf{k}}$ is a unit vector in the vertical direction. Symbols with the subscript '0' correspond to undisturbed values at the altitude of the plate ($x_3 = 0$). Use of the linear density-temperature relation (5) and a linear stratification in an unbounded flow is consistent with the Boussinesq approximation providing $(\alpha_0 T_0 \beta_0)^{-1}$ is large compared to a characteristic vertical dimension of the phenomena being described (e.g. the boundary-layer thickness).

Introducing the dimensionless state variables

$$T^* = \frac{T_{(x_1,x_3)}-T_0}{T_w-T_0} - \frac{T_0\beta_0 x_3}{T_w-T_0} = \frac{T-T_0}{T_w-T_0} - \frac{\beta}{\theta} z, \tag{6}$$

$$\rho^* = \frac{\rho}{\rho_0} = 1-\alpha(\beta z + \theta T^*) \tag{7}$$

and

$$p^* = \frac{p-p_0}{\rho_0 U_0^2} + \frac{1}{F_L}[z - \tfrac{1}{2}\alpha\beta z^2], \tag{8}$$

and following a procedure similar to that used in I, the system of equations (2) to (4) can be reduced to the set of coupled equations

$$\left[L(x,z,\psi)-\frac{1}{R_L}\nabla^2\right]\nabla^2\psi+\frac{\alpha\theta}{F_L}T_x=0, \tag{9}$$

and

$$\left[L(x,z,\psi)-\frac{1}{P_0R_L}\nabla^2\right](z\beta/\theta+T)=0. \tag{10}$$

The stream function $\psi$, Froude number $F_L$, Prandtl number $P_0$, Reynolds number $R_L$, and operator $L(x,z,\psi)$ are defined in I, $\theta$ represents the thermal driving potential across the boundary layer

$$\theta=\frac{T_w-T_0}{T_0}, \tag{11}$$

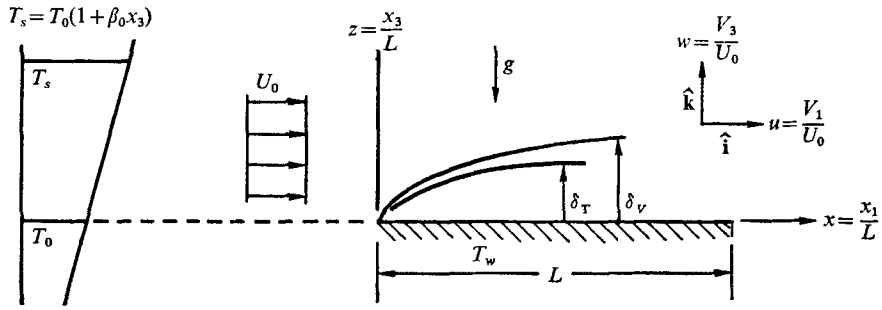


FIGURE 1. A schematic of the flow model.

$\beta$ is a dimensionless stratification scale ($\beta_0 L$), and $\alpha$ denotes a dimensionless thermal expansion coefficient ($\alpha_0 T_0$). The asterisk has been deleted from the temperature since all the variables are clearly dimensionless. In what follows, $\alpha$ will be taken to be unity, which is the case for a perfect gas, and the ratio $\beta/\theta$ is taken to be of order unity. The results can be applied to any fluid with arbitrary $\alpha$ by multiplying $\theta$ and $\beta$ by $\alpha$ as can be seen from (9) and (10). Both ($\alpha\theta$) and ($\alpha\beta$) must be smaller than unity for the Boussinesq approximation to be valid. The limiting case of $\theta$ approaching zero requires that a new dimensionless temperature ($\theta T^*$) be defined, but then the boundary conditions will depend on $\theta$.

In I we were able to combine the three parameters $\theta$, $\beta$, and $F_L$ into one parameter, the Russell number. That is possible only in the limit of infinite Prandtl number whereby the temperature is constant along a streamline. When the Prandtl number is finite, heat diffuses across streamlines and the simplified representation for $T$ is destroyed. In the diffusive case, then, four basic parameters are required to describe the flow, and the characterization of the flow in a two-dimensional space ($R_L$, $Ru_L$) as in I is no longer possible.

The boundary conditions for the flow depicted in figure 1 are

$$\psi(x,0)=0, \tag{12a}$$

$$\psi_z(x,z\to\infty)=\psi_z(x\to-\infty,z)=1, \tag{12b}$$

$$T(x,z\to\infty)=T(x\to-\infty,z)=0, \tag{12c}$$

$$\psi_z(x,0)=0 \quad \text{for} \quad 0\leqslant x\leqslant 1 \tag{12d}$$

and

$$T(x,0)=1 \quad \text{for} \quad 0\leqslant x\leqslant 1. \tag{12e}$$

These conditions complete the specification of the problem under consideration.

Now we seek to obtain an approximate solution to equations (9) and (10) subject to (12) for the case when the Reynolds number is large compared to unity. The objective is to establish the effect stratification has on the velocity and temperature field near a horizontal boundary and also on the friction and heat transfer at the boundary.

## 3. The flow structure for arbitrary Russell number

The approximate solution of (9) and (10) for infinite Reynolds number satisfying the far-field conditions (12$a, b, c$) is

$$\psi = z \quad \text{and} \quad T = 0. \tag{13}$$

This solution fails near the plate surface due to the neglect of diffusion effects. In the immediate vicinity of the plate the diffusion of vorticity and heat are essential to a description of the flow. We emphasize this explicitly by expanding the vertical scale in the manner

$$y = z/\epsilon(R_L), \tag{14}$$

where $\epsilon(R_L)$ scales the thickness of the viscous boundary layer and tends to zero in the limit as $R_L$ tends to infinity. Another scale $\epsilon_T(P_0, R_L)$ characteristic of the thermal-diffusion boundary-layer thickness can be defined, but, at least for the Blasius boundary layer, it is directly related to $\epsilon(R_L)$ by the expression

$$\frac{\epsilon}{\epsilon_T} = P_0^{\frac{1}{2}} = \frac{\delta_v}{\delta_T}. \tag{15}$$

This relation portrays clearly the role of the Prandtl number. In subsequent sections we take the Prandtl number to be of order unity whereby the distinction between the two scales is irrelevant.

Substituting (14) into (9) and (10) yields the boundary-layer vorticity and energy equations in the forms

$$\left[L(x,y,\Psi) - \frac{\epsilon^{-2}}{R_L}\left(\epsilon^2\frac{\partial^2}{\partial x^2} + \frac{\partial^2}{\partial y^2}\right)\right]\left(\epsilon^2\frac{\partial^2}{\partial x^2} + \frac{\partial^2}{\partial y^2}\right)\Psi + \epsilon(\theta/\beta)\,Ru_L^2\,\tilde{T}_x = 0, \tag{16}$$

and

$$\left[L(x,y,\Psi) - \frac{\epsilon^{-2}}{P_0 R_L}\left(\epsilon^2\frac{\partial^2}{\partial x^2} + \frac{\partial^2}{\partial y^2}\right)\right]\tilde{T} - \epsilon(\beta/\theta)\Psi_x = 0. \tag{17}$$

The new dependent variables are defined by

$$\psi(x,z) = \epsilon(R_L)\Psi(x,y) = \epsilon[\Psi^{(1)}(x,y) + \alpha(R_L)\Psi^{(2)}(x,y) + \ldots] \tag{18a}$$

and

$$T(x,z) = \tilde{T}(x,y) = \tilde{T}^{(1)}(x,y) + \Delta(R_L)\tilde{T}^{(2)}(x,y) + \ldots, \tag{18b}$$

and the Russell number $\beta/F_L$ has been introduced for comparison with the results of I. The transformations (18) arise from the matching requirements between the boundary layer and external stream (13). Using the parameter representation

$$Ru_L^2 = R_L^n \tag{19}$$

as in I, we see that the inertia-viscous (Blasius) boundary-layer balance with the familiar scale $\epsilon = R_L^{-\frac{1}{2}}$ holds for $n < \frac{1}{2}$, in contrast with $n = 1$ in the non-diffusive

case. Diffusion increases the role of buoyancy forces within the boundary layer and thereby can significantly alter the structure of the flow field. Recalling that $\beta/\theta$ is of order one, the direct effect of stratification (the last term in (17)) is at most a second-order quantity, and the scale of the diffusion boundary layer ($\epsilon_T = (P_0 R_L)^{-\frac{1}{2}}$) is unaffected by the stratification.

The region of applicability of the non-diffusive approximation is now clear. It requires that the Prandtl number be larger than $\epsilon^{-1} = R_L^{\frac{1}{2}}$ for the first-order boundary-layer analysis when $n < \frac{1}{2}$. For $n > \frac{1}{2}$, the buoyancy and viscous terms in (16) must balance leading to the scale

$$\epsilon = \epsilon_{bv} = (R_L R u_L^2)^{-\frac{1}{3}} = R_L^{-\frac{1}{3}(1+n)}, \tag{20}$$

and the first-order vorticity equation becomes

$$\Psi^{(1)}_{yyyy} - \tilde{T}^{(1)}_x = 0. \tag{21}$$

The energy equation (17) for the corrresponding scale is

$$\left[P_0 L(z, y, \Psi) - R_L^{\frac{1}{3}(2n-1)} \left(\epsilon_{bv}^2 \frac{\partial^2}{\partial x^2} + \frac{\partial^2}{\partial y^2}\right)\right] \tilde{T} - P_0 \epsilon_{bv} (\beta/\theta) \Psi_x = 0. \tag{22}$$

which shows that, for Prandtl numbers satisfying the condition

$$P_0 = R_L^{\frac{1}{3}(2n-1)} \quad (n > \tfrac{1}{2}), \tag{23}$$

the first-order equation is a balance between convection and diffusion. However, for Prandtl numbers smaller than that given in (23), the flow is diffusive on this scale. For Prandtl numbers greater than the condition (23), the first-order energy equation is non-diffusive on the scale of (20), but a diffusion layer does exist with a scale smaller than (20). Similarly, one can show that when the Prandtl number is larger than $R_L^{\frac{1}{2}(3n-1)}$, $n > 1$, the boundary-layer flow correct to first-order is described by the non-diffusive solution of Martin & Long (1968) and, when the Prandtl number is smaller than $R_L^{-1}$, the entire flow is diffusive ($\epsilon_T = O(1)$). A unified view of these results is given in figure 2 where $n$ is defined by (19) and $m$ is defined by the relation

$$P_0 = R_L^m. \tag{24}$$

The first-order flow characteristics are indicated in the respective domains on the figure.

In the outer flow where diffusion effects are negligible (at least to second order), (9) and (10) yield

$$L(x, z, \psi) \nabla^2 \psi + R u_L^2 \psi_x = 0, \tag{25a}$$

and

$$T = (\beta/\theta)(\psi - z). \tag{25b}$$

These equations are identical to the outer flow equations in I and, therefore, exhibit the same characteristics depending on the magnitude of the Russell number. However, since the first-order boundary layer is the Blasius one for all $n < \frac{1}{2}$, another scaling of the equations (9) and (10) is required for the parameter range $0 < n < \frac{1}{2}$ as compared to the range $0 < n < 1$ for the non-diffusive case. The correct intermediate-layer scaling for the diffusive case is the same as in I, namely,

$$(\hat{x}, \hat{y}) = (x, y) R_L^{\frac{1}{2}n} \quad (0 \leqslant n < \tfrac{1}{2}). \tag{26}$$

The matching conditions require that the expansions for the dependent variables in the intermediate layer have the form

$$\psi(x,z) = R_L^{-\frac{1}{2}n}\hat{\Psi}(\hat{x},\hat{y}) = R_L^{-\frac{1}{2}n}[\hat{y} + R_L^{-\frac{1}{2}(1-\frac{1}{2}n)}\hat{\Psi}^{(1)}(\hat{x},\hat{y}) + \ldots], \tag{27a}$$

and

$$T(x,z) = R_L^{-\frac{1}{2}(1+\frac{1}{2}n)}\hat{T}^{(1)}(\hat{x},\hat{y}) + \ldots \quad (0 \leqslant n < \tfrac{1}{2}). \tag{27b}$$

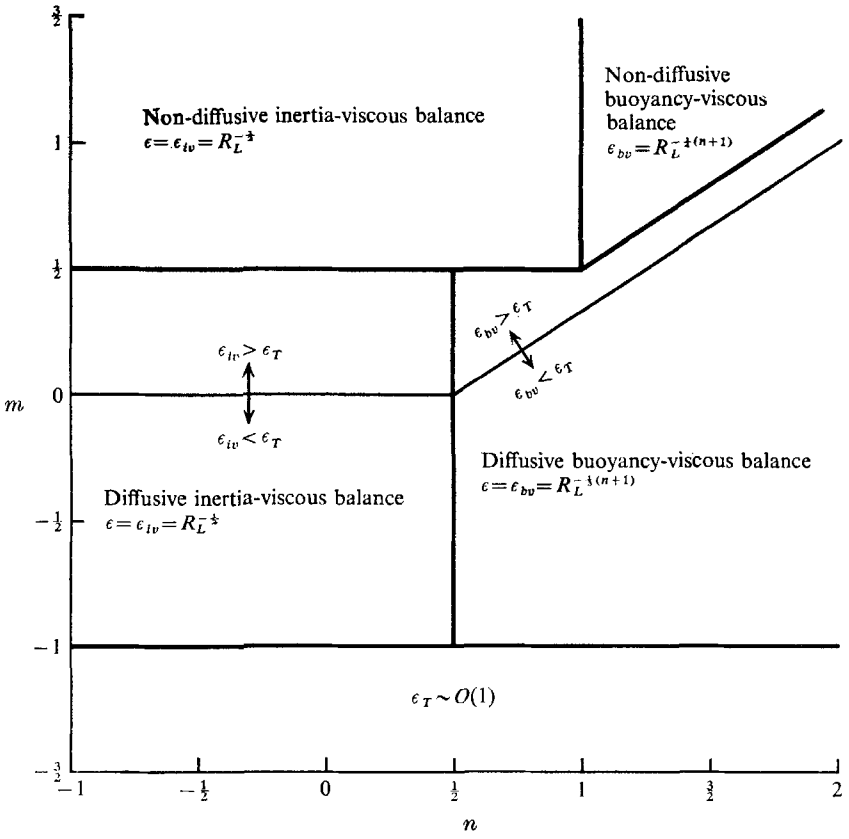


FIGURE 2. A unified representation of the first-order flow characteristics in Prandtl number–Russell number space.

The function $\hat{\Psi}^{(1)}$ is determined from the solution of the Helmholtz equation as in I (§6) and

$$\hat{T}^{(1)}(\hat{x},\hat{y}) = (\beta/\theta)\hat{\Psi}^{(1)}(\hat{x},\hat{y}). \tag{28}$$

With these transformations, a uniformly valid first approximation to (9) and (10) is possible for all Russell numbers greater than or equal to zero. The condition $n = \frac{1}{2}$ is the critical stratification for the diffusive boundary layer and corresponds to a smaller stratification than the case $n = 1$ which is the critical condition for the non-diffusive boundary layer.

## 4. A similarity solution for the case $n = 0$

We now consider the particular case when the Russell number is of order unity ($n = 0$). Since the Reynolds number is presumed to be large, the parameter $\epsilon = R_L^{-\frac{1}{2}}$ is small, and it is reasonable to seek solutions of equations (16) and (17) by means of a perturbation analysis. The boundary-layer variables are expanded in a sequence of the form given by (18*a*, *b*). Similarly, the outer flow variables are expressed as

$$\psi(x,z) = z + \gamma(R_L)\psi^{(1)}(x,z) + \ldots, \tag{29a}$$

and

$$T(x,z) = 0 + \gamma(R_L)T^{(1)}(x,z) + \ldots, \tag{29b}$$

where the first terms on the right-hand side are known from (13). The functions $\gamma(R_L)$, $\alpha(R_L)$, $\Delta(R_L)$ are part of an asymptotic sequence and are determined by matching the two expansions (18) and (29). In this study we carry the expansion procedure only to the order indicated in (18) and (29).

Substituting (18) into (16) and (17) yields the first-order boundary-layer equations

$$\left[L(x,y,\Psi^{(1)}) - \frac{\partial^2}{\partial y^2}\right]\Psi^{(1)}_{yy} = 0 \tag{30a}$$

and

$$\left[L(x,y,\Psi^{(1)}) - \frac{1}{P_0}\frac{\partial^2}{\partial y^2}\right]\tilde{T}^{(1)} = 0. \tag{30b}$$

Introducing the variables

$$\eta = y/x^{\frac{1}{2}}, \Psi^{(1)}(x,y) = x^{\frac{1}{2}}f_1(\eta) \quad \text{and} \quad \tilde{T}^{(1)}(x,y) = h_1(\eta), \tag{31}$$

the above equations reduce to the familiar similarity forms

$$f_1''' + \tfrac{1}{2}f_1 f_1'' = 0 \tag{32a}$$

and

$$h_1'' + \tfrac{1}{2}P_0 f_1 h_1' = 0. \tag{32b}$$

The appropriate boundary conditions are

$$f_1(0) = f_1'(0) = h_1(\infty) = 0 \quad \text{and} \quad f_1'(\infty) = h_1(0) = 1. \tag{32c}$$

Note that the first-order problem depends only on one parameter, the Prandtl number. The solutions for $f_1$ and $h_1$ are known (cf. Schlichting 1968, pp. 126, 280). Using the properties of these solutions, we find the matching conditions

$$\gamma(R_L) = \epsilon = R_L^{-\frac{1}{2}} \quad \text{and} \quad \psi^{(1)}(x,0) = -1{\cdot}730x^{\frac{1}{2}} \quad (x > 0). \tag{33}$$

Consequently, $\psi^{(1)}$ is given by the solution of the Helmholtz equation (see I, §6) and $T^{(1)}$ obeys an equation analogous to (28).

Since the displacement thickness in the downstream wake is unknown, we assume that the outer flow can be calculated as if the plate were semi-infinite. The solution for $\psi^{(1)}$ (I, §6) shows that, for a semi-infinite plate, the induced horizontal velocity vanishes as $z$ tends to zero. Within this approximation, there is no coupling between $\psi^{(1)}$ and $\Psi^{(2)}$ and the gauge function $\alpha(R_L)$ is undetermined. However, examining the relation for the temperature, we see that

$$T^{(1)}(x,0) = (\beta/\theta)\psi^{(1)}(x,0) = -1{\cdot}730(\beta/\theta)x^{\frac{1}{2}} \tag{34}$$

so that there is a coupling between the outer flow and the second-order boundary layer via the temperature field. The coupling is a direct consequence of the diffusion of heat. This requires that $\Delta(R_L) = \epsilon$ and, by substituting the respective expansions into the boundary-layer equations, one finds that $\alpha(R_L) = \epsilon$ as well.

By virtue of the above results, the second-order boundary-layer equations have the form

$$\left[L(x,y,\Psi^{(1)}) - \frac{\partial^2}{\partial y^2}\right]\Psi^{(2)}_{yy} + L(x,y,\Psi^{(2)})\,\Psi^{(1)}_{yy} + (\theta/\beta)\,Ru_L^2\,\tilde{T}^{(1)}_x = 0 \tag{35a}$$

and

$$\left[L(x,y,\Psi^{(1)}) - \frac{1}{P_0}\frac{\partial^2}{\partial y^2}\right]\tilde{T}^{(2)} + L(x,y,\Psi^{(2)})\,\tilde{T}^{(1)} - (\beta/\theta)\,\Psi^{(1)}_x = 0, \tag{35b}$$

with boundary conditions

$$\left.\begin{aligned} &\Psi^{(2)}(x,0) = \Psi^{(2)}_y(x,0) = \Psi^{(2)}_y(x,\infty) = \Psi^{(2)}_{yy}(x,\infty) = \tilde{T}^{(2)}(x,0) = 0 \\ \text{and}\quad &\tilde{T}^{(2)}(x,\infty) = -(\beta/\theta)1{\cdot}730x^{\frac{1}{2}}, \end{aligned}\right\} \tag{35c}$$

where the Russell number has been included to indicate explicitly its role, but its order of magnitude is assumed to be unity. Similarity forms are possible for these equations also if we write

$$\Psi^{(2)} = xf_2(\eta) \quad \text{and} \quad \tilde{T}^{(2)} = x^{\frac{1}{2}}h_2(\eta). \tag{36}$$

The equations for $f_2$ and $h_2$ are given by

$$2f'''_2 + f_1 f''_2 - f'_1 f'_2 + 2f''_1 f_2 = -(\theta/\beta)\,Ru_L^2\left[\eta h_1 + \int_\eta^\infty h_1\,d\eta\right], \tag{37a}$$

$$2h''_2 + P_0\{f_1 h'_2 - f'_1 h_2 + 2f_2 h'_1\} = P_0(\beta/\theta)\,(\eta f'_1 - f_1), \tag{37b}$$

subject to the conditions

$$f_2(0) = f'_2(0) = f'_2(\infty) = h_2(0) = 0 \quad \text{and} \quad h_2(\infty) = -(\beta/\theta)\,(1{\cdot}730). \tag{37c}$$

The first equation has been integrated once to reduce it to a third-order equation. The right-hand sides are known from the first-order solution (32) and comprise the primary forcing functions for the second-order boundary layer. A one-way coupling exists between (32) and (37) which proceeds from the first-order momentum equation (32$a$) to the second-order energy equation (37$b$). Furthermore, all equations except (32$a$) are linear. The combination of these facts simplifies considerably the numerical solution of the above equations.

Before discussing the numerical solutions to the above equations, it is worth pointing out that the boundary-layer expansion for the parameter range $0 < n < \frac{1}{2}$ has the form

$$\psi(x,z) = R_L^{-\frac{1}{2}}[\Psi^{(1)}(x,y) + R_L^{n-\frac{1}{2}}\Psi^{(2)}(x,y) + \ldots], \tag{38a}$$

and

$$T(x,z) = \tilde{T}^{(1)}(x,y) + R_L^{n-\frac{1}{2}}\tilde{T}^{(2)}(x,y) + \ldots. \tag{38b}$$

The equations for $\Psi^{(2)}$ and $\tilde{T}^{(2)}$ are identical to (35$a$, $b$) except that the term multiplied by the parameter $\beta/\theta$ in the energy equation (35$b$ and 37$b$) does not appear. Thus, the solution of (37$a$) yields the second-order velocity field for the entire range $0 \leqslant n < \frac{1}{2}$. Furthermore, comparison of the expansions (27) and (38) shows that the second-order boundary-layer stream function $\Psi^{(2)}$ containing

the effect of buoyancy in the boundary layer is more significant than the correction due to the displacement effect on the outer flow for $n > \frac{2}{5}$. For the non-diffusive case, this occurred for $n > \frac{4}{5}$.

The above analysis can be shown to reduce to the non-diffusive case discussed in (I) by considering the limit of (32) and (37) as the Prandtl number becomes large. When the Prandtl number is large, the first-order temperature field $h_1$ decays exponentially to zero in a thermal boundary which is of order $P_0^{-\frac{1}{3}}$ times the scale of the velocity boundary layer. The forcing term on the right-hand side of (37*a*) then vanishes, and $f_2$ vanishes as well since it satisfies a homogeneous equation with homogeneous boundary conditions. Thus, noting that $h_1'$ and $h_2''$ are zero outside a very thin thermal layer near the wall, the solution of (37*b*) is

$$h_2(\eta) = (\beta/\theta)\,(f_1(\eta) - \eta). \tag{39}$$

The expansion for the stream function must then take the form

$$\psi(x,z) = R_L^{-\frac{1}{2}}\,[x^{\frac{1}{2}} f_1(\eta) + R_L^{n-\frac{1}{2}} x(0) + R^{n-1} x^{\frac{3}{2}} f_3(\eta) + \ldots], \tag{40}$$

and $f_3$ is identical with the function noted as $f_2$ in I(§7, equations (61) and (62)). Consequently, the difficulty encountered there (see I, equation (63)) appears in the diffusive solutions also, for an extension of the preceding analysis ($P_0 \simeq O(1)$) to the next higher-order term in the boundary-layer expansion would result in a vorticity equation containing a non-zero forcing term at the edge of the boundary layer. This difficulty may be peculiar to the geometry of the problem, since, as shown in I, the boundary-layer solution is valid only for a plate of finite length.

## 5. Numerical results

Equations (32) and (37) were integrated numerically using Hamming's modified predictor-corrector method for the solution of general initial value problems (cf. Ralston & Wilf 1960, pp. 95–109). The integration was accomplished by transforming (32*a*) to an equivalent initial-value problem (cf. Rosenhead 1963, p. 223), solving for $f_1$, and then solving (32*b*), (37*a*), and (37*b*) successively in that order. A maximum error bound of $10^{-4}$ was imposed in the numerical approximation. If the absolute error exceeded the specified bound, the integration step-size was halved. Numerical solutions were obtained for a range of each of the three parameters $Ru_L$, $P_0$, and $\beta/\theta$ in order to determine their individual influence on the properties of the boundary layer.

A measure of the effect of stratification on the boundary layer is obtained by evaluating its influence on the shear and heat transfer at the plate surface. Using the previous results, the following expressions for the skin-friction and heat-transfer coefficients can be derived:

$$C_f = \frac{\tau_0}{\rho_0 U_0^2} = \frac{f_1''(0)}{R_{x_1}^{\frac{1}{2}}}\left[1 + x^{\frac{1}{2}} R_L^{n-\frac{1}{2}} \frac{f_2''(0)}{f_1''(0)}\right] \quad (0 \leqslant n < \tfrac{1}{2}), \tag{41}$$

and

$$C_h = \frac{q_0}{\rho_0 c_{p_0} U_0 (T_0 - T_w)} = \frac{h_1'(0)}{P_0 R_{x_1}^{\frac{1}{2}}}\left[1 + x^{\frac{1}{2}} R_L^{-\frac{1}{2}} \frac{q_2(0)}{h_1'(0)}\right] \quad (n = 0), \tag{42}$$

where $R_{x_1}$ is the Reynolds number based on the dimensional length $x_1$ measured from the leading edge of the plate, and $q_2(0)$ is defined by the relation

$$q_2(0) = h_2'(0) + \beta/\theta. \tag{43}$$

The symbols $\tau_0$ and $q_0$ denote the shear and heat flux, respectively, at the plate surface. Stratification and buoyancy have an effect only in the second-order terms. The second-order temperature field was evaluated only for the case $n = 0$, but the velocity field is computed for the range $0 \leqslant n < \frac{1}{2}$.

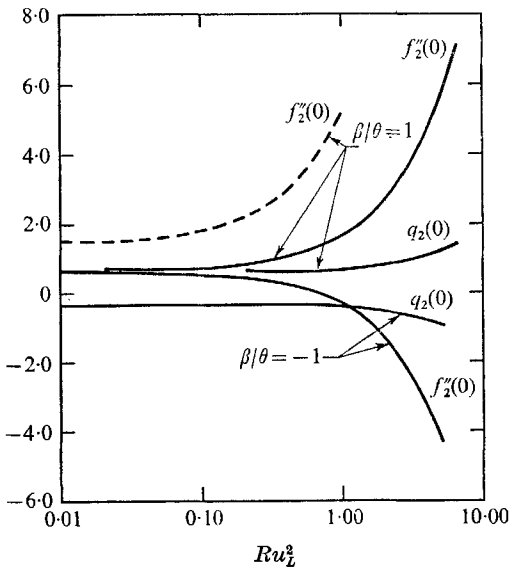


FIGURE 3

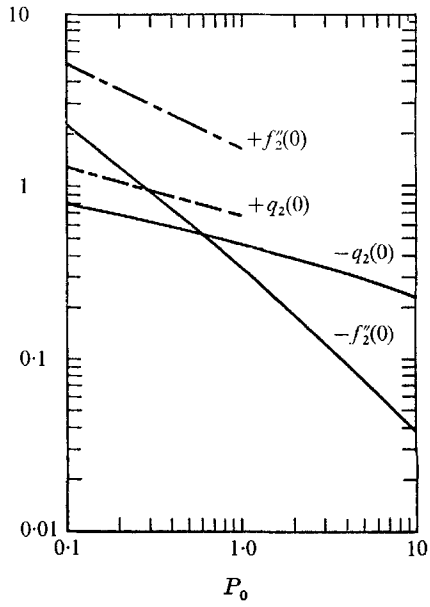


FIGURE 4

FIGURE 3. The variation of the second-order shear and heat transfer with the Russell number. —, $P_0 = 1{\cdot}0$; - - -, $P_0 = 0{\cdot}1$.

FIGURE 4. The variation of the second-order shear and heat transfer with the Prandtl number ($Ru_L = 1{\cdot}0$). —, $\beta/\theta = -1$; ———, $\beta/\theta = 1$.

The results show that the Russell number has a very significant effect on the structure of the boundary layer. Figure 3 exhibits the influence of $Ru_L$ on the skin-friction and heat transfer for both a heated and cooled wall. The second-order contribution to the shear changes profoundly when the Russell number is of order unity or larger. When the boundary is heated relative to the external stream, the skin-friction increases as the Russell number increases and vice versa for a cooled boundary. Stratification then acts to prevent separation on heated boundaries and promotes separation, at least for large Russell numbers, on cooled boundaries.

Figure 4 portrays the influence of the Prandtl number on the boundary-layer properties for a fixed Russell number and wall to free-stream temperature ratio. The Prandtl numer has a very strong effect on the shear at the boundary. This is attributable to the fact that the thermal boundary-layer thickness and the first-

order temperature field depend strongly on the Prandtl number and, therefore, affect the second-order velocity field through the right-hand side of (37*a*).

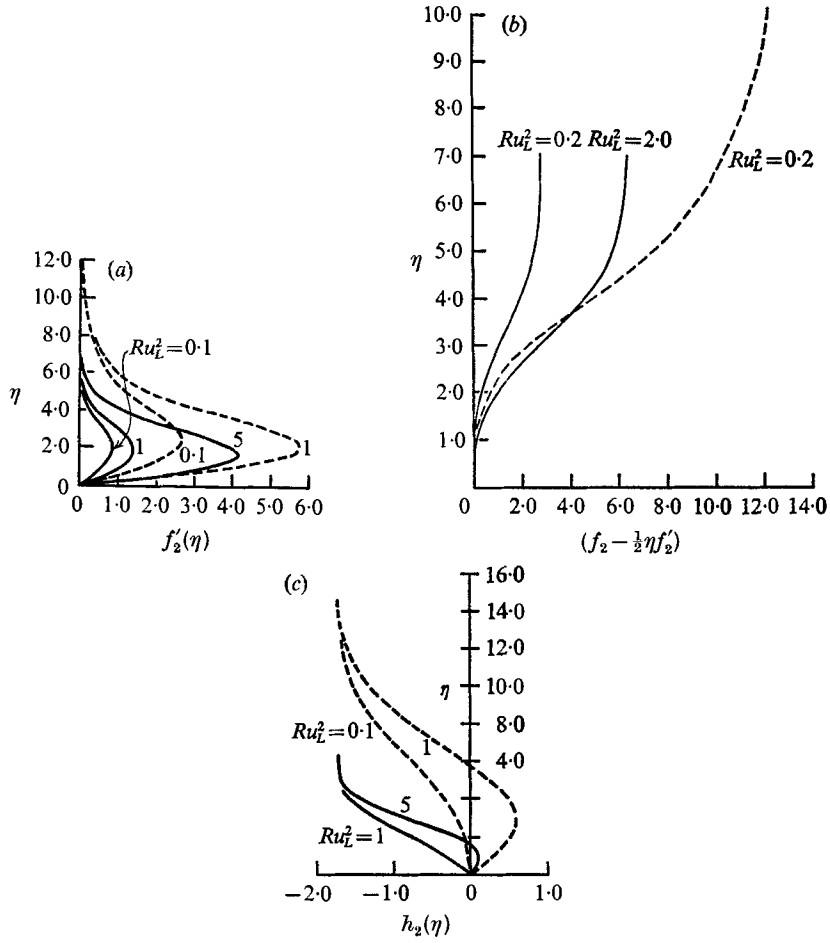


FIGURE 5. The effect of the Russell and Prandtl numbers on the boundary-layer profiles: (*a*) horizontal velocity, (*b*) vertical velocity, and (*c*) temperature. $\beta/\theta = 1$. —, $P_0 = 1{\cdot}0$; - - -, $P_0 = 0{\cdot}1$.

Representative second-order horizontal and vertical velocity profiles and temperature profiles are shown in figure 5. The total velocity and temperature in the boundary layer can be computed from the relations

$$u = f_1'\left[1 + x^{\frac{1}{2}}R_L^{n-\frac{1}{2}}\frac{f_2'}{f_1'}\right] \quad (0 \leqslant n < \tfrac{1}{2}), \tag{44}$$

$$w = -\tfrac{1}{2}R_{x_1}^{\frac{1}{2}}(f_1 - \eta f_1')\left[1 + 2x^{\frac{1}{2}}R_L^{n-\frac{1}{2}}\left(\frac{f_2 - \frac{1}{2}\eta f_2'}{f_1 - \eta f_1'}\right)\right] \quad (0 \leqslant n < \tfrac{1}{2}), \tag{45}$$

and

$$T = h_1\left[1 + x^{\frac{1}{2}}R_L^{-\frac{1}{2}}\frac{h_2}{h_1}\right] \quad (n = 0). \tag{46}$$

The figure clearly shows that buoyancy ($Ru_L$) and diffusion ($P_0$) have a strong influence on the velocity profile, especially for large Russell numbers and small

Prandtl numbers. Since the second-order contribution grows with distance from the leading edge, these effects may be quite pronounced near the trailing edge of the plate. Also, when the Russell number is large ($n$ close to $\frac{1}{2}$), the mean velocity profile is significantly different from the Blasius profile. Stratification, therefore,

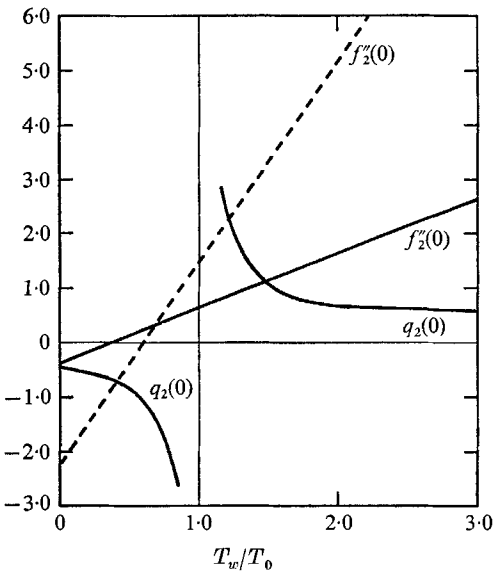


FIGURE 6

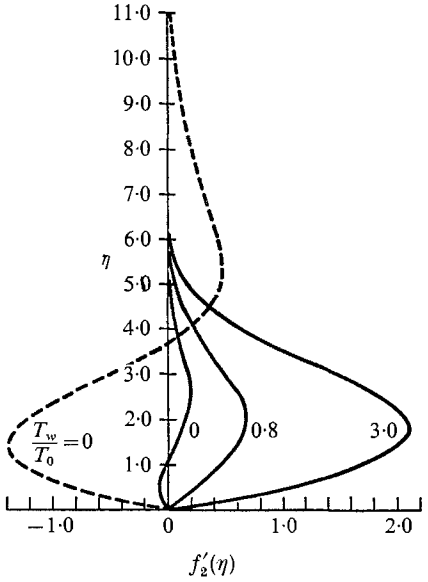


FIGURE 7 (*a*)

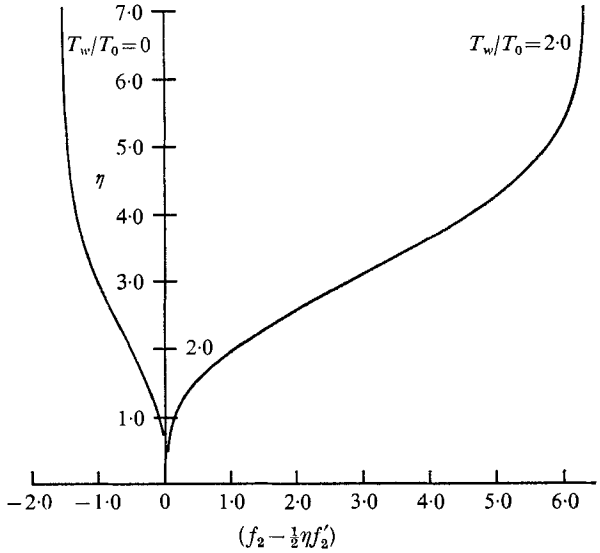


FIGURE 7 (*b*)

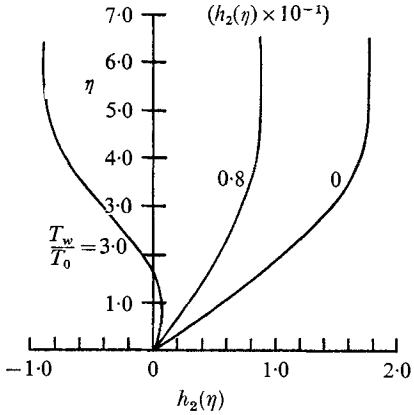


FIGURE 7 (*c*)

FIGURE 6. The second-order shear and heat transfer as a function of the wall-to-free-stream temperature ratio: ($Ru_L = 1·0$, $\beta = 1·0$). —, $P_0 = 1·0$; - - -, $P_0 = 0·1$.

FIGURE 7. The effect of the wall-to-free-stream temperature ratio on the boundary-layer profiles. (*a*) Horizontal velocity: $Ru_L = 1·0$; —, $P_0 = 1·0$; - - -, $P_0 = 0·1$. (*b*) Vertical velocity: $Ru_L^2 = 2·0$, $P_0 = 1·0$. (*c*) Temperature: $Ru_L = 1·0$, $P_0 = 1·0$.

can have an important effect on the stability of a boundary layer through its modification of the mean profile as well as through the effect of buoyancy on the velocity perturbations superimposed on the mean flow.

The wall to free-stream temperature ratio also plays a role in determining the characteristics of the stratified boundary layer. Its importance is depicted in figures 6 and 7 which contain results for a fixed stratification ($\beta_0 L = 1$) and fixed Russell number. The function $q_2(0)$ is singular at $T_w/T_0 = 1$ because the parameter $\beta/\theta$ in (37*b*, *c*) goes to infinity as $T_w$ approaches $T_0$. This is a consequence of the temperature scaling expressed in (6). The shear is seen to increase rapidly as the wall is heated.

## 6. Summary

In summary, the combined effect of thermal stratification and buoyancy on a horizontal boundary layer is greatest when the wall is heated and the Prandtl number is small. The Prandtl number is particularly important since it determines the vertical scale (the thickness of the thermal boundary layer) over which buoyancy forces can act. Also, stratification can either enhance or impede separation depending on the relative temperature of the boundary and free-stream and the magnitude of the Froude number.

Diffusion has a very significant effect in that it serves to emphasize the importance of the buoyancy term by coupling the velocity and thermal fields. This is of primary importance when the Froude number is small (or large Russell number) which indicates that diffusion may considerably alter the structure of the upstream boundary layer studied by Martin & Long (1968) and Pao (1968), especially in the vicinity of the trailing edge of a plate of finite length. Furthermore, since the diffusion boundary layer always grows from the leading edge, a downstream momentum wake arising from the resultant density variation should exist even in the case when the viscous boundary layer grows in the upstream direction.

The author acknowledges the many helpful discussions with Professors R. E. Kelly and A. F. Charwat during the course of this investigation. The research was supported by the National Science Foundation under Grant GK-4213 and was performed as part of the author's doctoral dissertation at the School of Engineering and Applied Science, UCLA.

REFERENCES

KELLY, R. E. & REDEKOPP, L. G. 1970 The development of horizontal boundary layers in stratified flow. Part 1. Non-diffusive flow. *J. Fluid Mech.* **42**, 497.

MARTIN, S. & LONG, R. R. 1968 The slow motion of a flat plate in a viscous stratified fluid. *J. Fluid Mech.* **31**, 669–688.

PAO, Y. H. 1968 Laminar flow of a stably stratified fluid past a flat plate. *J. Fluid Mech.* **34**, 795–808.

RALSTON, A. & WILF, H. S. 1960 *Mathematical Methods for Digital Computers.* New York: Wiley.

ROSENHEAD, L. (Ed.) 1963 *Laminar Boundary Layers.* Oxford University Press.

SCHLICHTING, H. 1968 *Boundary Layer Theory.* New York: McGraw-Hill.

*J. Fluid Mech.* (1970), *vol.* 42, *part* 3, *pp.* 527–548
*Printed in Great Britain*



# Extensions of extremum principles for slow viscous flows

By RICHARD SKALAK

Department of Civil Engineering and Engineering Mechanics
Columbia University, New York, N.Y.

(Received 6 May 1969 and in revised form 31 October 1969)

Several generalizations of theorems of the types originally stated by Helmholtz concerning the dissipation of energy in slow viscous flow have been given recently by Keller, Rubenfeld & Molyneux (1967). These generalizations included cases in which the fluid contains one or more solid bodies and drops of another liquid assuming the drops do not change shape. Some further extensions are given herein which allow for drops which may be deformed by the flow and include the effect of surface tension. The admissible boundary conditions have also been extended and particular theorems applicable to infinite domains, spatially periodic flows and to flows in infinite cylindrical pipes are derived. Uniqueness theorems are also proved.

## 1. Introduction

The history of extremum principles for slow viscous flow (Stokes flow) is given briefly by Keller *et al.* (1967) and they prove several theorems which include and extend previous results. These theorems establish upper and lower bounds for the excess dissipation rate which is defined to be the rate of energy dissipation in the fluid minus twice the power of the external body forces and given surface tractions. One of the principal generalizations introduced was to include suspended solid particles and drops of another liquid whose motion is not known in advance. However, the shapes of the drops were assumed to be constant during the motion.

In the present paper it is shown that if minus twice the power delivered by surface tension is included in the definition of the excess dissipation rate, that minimum and maximum principles can be derived for suspensions containing deformable drops as well as rigid particles.

The motivation for the present paper stems from a study of capillary blood flow in which the red blood cells may be represented by a line of flexible particles suspended in viscous flow in a tube. Spatially periodic flows are of interest for this application and the extremum principles have also been appropriately specialized for this purpose. Simplifications in the specification of the problem are possible, namely, it is sufficient to specify certain integral quantities such as the discharge rather than pointwise data such as velocity on the boundaries of the typical periodic cell. These results can be applied to uniform flows in cylindrical pipes also.

Specific theorems are proved for infinite domains assuming body forces are conservative. It is shown that the rate of decrease of the velocity at infinity can be predicted rather than assumed and this allows a more general statement of uniqueness and extremum principles.

All of the theorems proved below, like those already in the literature, consider that the configurations of the droplets and particles are known at the instant that the fluid motion is to be found.

## 2. Statement of the problem

Consider a domain $V$ which contains a viscous fluid in which there are $N_L$ liquid drops or bubbles and $N_K$ rigid, solid particles. The boundary $S$ of $V$ is assumed not to intersect any of the suspended drops or particles. The boundary conditions in the sense of prescribed velocity and traction components are assumed to be specified only on $S$ which will be subdivided into $S_1$, $S_2$, $S_3$, $S_4$ according to the particular components specified.

Let the domain $V$ be subdivided into $V_0$ occupied by the suspending fluid, $V_L^{(l)}$ $(l = 1, \ldots, N_L)$ occupied by the fluid drops, and $V_K^{(k)}$ $(k = 1, \ldots, N_K)$ occupied by the solid particles. Let $S_0$, $S_L^{(l)}$ and $S_K^{(k)}$ denote the surfaces of $V_0$, $V_L^{(l)}$ and $V_K^{(k)}$ respectively. Then $S_0$ is the sum of $S$, $S_L^{(l)}$ $(l = 1, \ldots, N_L)$ and $S_K^{(k)}$ $(k = 1, \ldots, N_K)$. Let $\mathbf{n}$ denote the normal to $S_0$ directed outward from $V_0$.

Each of the fluids in $V_0$ and $V_L^{(l)}$ $(l = 1, \ldots, N_L)$ is assumed to be a uniform, incompressible, Newtonian fluid but the viscosity $\mu(\mathbf{x})$ may be different in each of these domains. Let $\sigma^{(l)}$ $(l = 1, \ldots, N_L)$ denote the surface tension in $S_L^{(l)}$; $\sigma^{(l)}$ may be different for each $S_L^{(l)}$.

It is convenient to define a single velocity field $\mathbf{u}(\mathbf{x})$ for the entire domain $V$. The motions of the drops and solid particles are not known in advance but are to be found as part of the solution. The requirement of zero relative velocity of the fluids and solids on the two sides of each $S_L^{(l)}$ and $S_K^{(k)}$ is met by stipulating that $\mathbf{u}(\mathbf{x})$ be continuous in $V$. Within each solid particle, the velocity $\mathbf{u}(\mathbf{x})$ is defined to be that of the rigid body motion consistent with the fluid velocity on its boundary.

Let $\mathbf{f}(\mathbf{x})$ denote the body force per unit volume defined throughout $V$. Let $p(\mathbf{x})$ and $\tau_{ij}(\mathbf{x})$ denote the pressure and stress tensor which are defined only in the fluid domains $V_0$ and $V_L^{(l)}$ $(l = 1, \ldots, N_L)$. The pressure and stress are required to be continuous except across the surfaces $S_L^{(l)}$ of the drops where the difference of the value outside minus the value inside the drop will be denoted by $\Delta p$ and $\Delta\tau_{ij}$ respectively.

Let $\mathbf{j}(x)$, $\mathbf{t}(x)$, $\mathbf{m}(x)$ be three unit vectors which are specified at each point of $S$ as part of the boundary conditions of the problem. The $\mathbf{j}, \mathbf{t}, \mathbf{m}$ must be mutually orthogonal, but may be otherwise arbitrarily oriented at each point.

The problem is to find $\mathbf{u}(\mathbf{x})$ in $V$ satisfying the following equations and boundary conditions:

$$u_{i,i} = 0, \quad \mathbf{x} \text{ in } V; \tag{2.1}$$

$$\tau_{ij,j} + f_i = 0, \quad \mathbf{x} \text{ in } V_0 \text{ and } V_L^{(l)} \quad (l = 1, \ldots, N_L); \tag{2.2}$$

$$u_i = g_i(\mathbf{x}), \quad \mathbf{x} \text{ on } S_1; \tag{2.3}$$

$$u_i j_i = h(\mathbf{x}), \quad u_i t_i = b(\mathbf{x}), \quad \mathbf{x} \quad \text{on} \quad S_2; \tag{2.4a}$$

$$\tau_{ij} n_j m_i = \beta(\mathbf{x}), \quad \mathbf{x} \quad \text{on} \quad S_2; \tag{2.4b}$$

$$u_i j_i = h(\mathbf{x}), \quad \mathbf{x} \quad \text{on} \quad S_3; \tag{2.5a}$$

$$\tau_{ij} n_j t_i = \alpha(\mathbf{x}), \quad \tau_{ij} n_j m_i = \beta(\mathbf{x}), \quad \mathbf{x} \quad \text{on} \quad S_3; \tag{2.5b}$$

$$\tau_{ij} n_j = \gamma_i(\mathbf{x}), \quad \mathbf{x} \quad \text{on} \quad S_4; \tag{2.6}$$

$$\Delta\tau_{ij} n_i n_j = \sigma^{(l)} \left( \frac{1}{R_1} + \frac{1}{R_2} \right), \quad \mathbf{x} \quad \text{on} \quad S_L^{(l)} \quad (l = 1, \ldots, N_L); \tag{2.7}$$

$$\Delta\tau_{ij} n_j - \Delta\tau_{qm} n_q n_m n_i = 0, \quad \mathbf{x} \quad \text{on} \quad S_L^{(l)} \quad (l = 1, \ldots, N_L); \tag{2.8}$$

$$\int_{V_K^{(k)}} f_i dV - \int_{S_K^{(k)}} n_j \tau_{ij} dS = 0, \quad (k = 1, \ldots, N_K); \tag{2.9}$$

$$\int_{V_K^{(k)}} e_{ijm} x_j f_m dV - \int_{S_K^{(k)}} e_{ijm} x_j n_q \tau_{qm} = 0 \quad (k = 1, \ldots, N_K); \tag{2.10}$$

$$\tau_{ij} = -p\delta_{ij} + 2\mu e_{ij}, \quad \mathbf{x} \quad \text{in} \quad V_0 \quad \text{and} \quad V_L^{(l)} \quad (l = 1, \ldots, N_L); \tag{2.11}$$

$$e_{ij} = \tfrac{1}{2}(u_{j,i} + u_{i,j}), \quad \mathbf{x} \quad \text{in} \quad V; \tag{2.12}$$

$$e_{ij} = 0, \quad \mathbf{x} \quad \text{in} \quad V_K^{(k)} \quad (k = 1, \ldots, N_K); \tag{2.13}$$

where $e_{ijk}$ is the alternating tensor and $\delta_{ij}$ is the Kronecker delta. $R_1$ and $R_2$ denote the two principal radii of curvature of $S_L^{(l)}$ reckoned positive when they extend into the drop. The functions $\alpha$, $\beta$, $\gamma$, $g$, $h$, $b$ are given as part of the boundary conditions.

Equations (2.1) and (2.2) are the equations of continuity and motion for the Stokes flow in the fluid domains.

The boundary conditions (2.3), (2.4*a*), (2.5*a*) and (2.6) specify 3, 2, 1 or 0 components of the velocity on $S_1$, $S_2$, $S_3$, $S_4$ respectively. In each case, a sufficient number of traction components are also specified by (2.4*b*), (2.5*b*) and (2.6) to make the solution unique, as will be shown in the derivations below.

Equation (2.7) equates the difference of the normal components of the tractions on the two sides of $S_L^{(l)}$ to the effect of surface tension $\sigma^{(l)}$. Equation (2.8) states that the tangential component of the surface traction is continuous across $S_L^{(l)}$.

The equations of motion of the solid particles are expressed by (2.9) and (2.10).

Equations (2.11) and (2.12) define the stress tensor $\tau_{ij}$ and $e_{ij}$ for a Newtonian fluid and (2.13) ensures that the motion within $S_K^{(k)}$ is that of a rigid body.

Only solutions $\mathbf{u}(\mathbf{x})$ which are continuous throughout $V$ will be considered; derivatives of $\mathbf{u}$ may be discontinuous on $S_L^{(l)}$ ($l = 1, \ldots, N_L$) and on $S_K^{(k)}$ ($k = 1, \ldots, N_K$).

The domain $V$ is considered to be finite until §6 where infinite domains are specifically considered. Spatially periodic flows are treated in §7.

## 3. A minimum principle

Let the rate of dissipation of energy into heat by viscosity in $V$ be denoted $D[\mathbf{u}]$. It is defined by

$$D[\mathbf{u}] = \int_{V_0} 2\mu(e_{ij}[\mathbf{u}])^2 dV + \sum_{l=1}^{N_L} \int_{V_L^{(l)}} 2\mu(e_{ij}[\mathbf{u}])^2 dV. \tag{3.1}$$

The excess dissipation rate $D_e[\mathbf{u}]$ is defined to be the rate of viscous energy dissipation minus twice the power of the external body forces, the given surface traction components and the surface tensions:

$$D_e[\mathbf{u}] = D[\mathbf{u}] - 2\int_V f_i u_i dV - 2\int_{S_2} u_i m_i \beta dS - 2\int_{S_3} (u_i t_i \alpha + u_i m_i \beta) dS - 2\int_{S_4} u_i \gamma_i dS + 2\sum_{l=1}^{N_L} \sigma^{(l)} \dot{A}^{(l)}, \tag{3.2}$$

where $\dot{A}^{(l)}$ is the time rate of change of the area $A^{(l)}$ of $S_L^{(l)}$ ($l = 1, \ldots, N_L$). The product $(-\sigma^{(l)}\dot{A}^{(l)})$ is the rate at which surface tension does work on the adjacent fluids and is also the rate at which the surface energy $\sigma^{(l)}A^{(l)}$ decreases. At any time, $\dot{A}^{(l)}$ is given by (cf. Landau & Lifshitz 1959)

$$\dot{A}^{(l)} = -\int_{S_L^{(l)}} u_i n_i \left(\frac{1}{R_1} + \frac{1}{R_2}\right) dS. \tag{3.3}$$

The minus sign in (3.3) is due to the fact that $\mathbf{n}$ is the normal taken outward from $V_0$ which is inward to $V_L^{(l)}$.

THEOREM 1. *A minimum principle. Let* $\mathbf{u}(\mathbf{x})$ *be a continuous solution of a Stokes flow problem satisfying* (2.1)–(2.13). *Let* $\tilde{\mathbf{u}}(\mathbf{x})$ *be any continuous velocity field which is piecewise continuously differentiable and satisfies* (2.1), (2.3), (2.4*a*), (2.5*a*), *and* (2.13). *Then*

$$D_e[\mathbf{u}] \leqslant D_e[\tilde{\mathbf{u}}] \tag{3.4}$$

The equality holds only if $\tilde{\mathbf{u}} = \mathbf{u}$ or $\tilde{\mathbf{u}} = \mathbf{u} + \mathbf{u}_0$ where $\mathbf{u}_0$ is a rigid body motion.

(Note that the configurations of the droplets and solid particles are identical for both flows $\mathbf{u}$ and $\tilde{\mathbf{u}}$ at the instant considered.)

*Proof.* Let $\tilde{\mathbf{u}} = \mathbf{u} + \tilde{\mathbf{u}}$. Then from (3.1)

$$D[\tilde{\mathbf{u}}] = D[\mathbf{u} + \tilde{\mathbf{u}}] = D[\mathbf{u}] + D[\tilde{\mathbf{u}}] + \int_{V_0} 4\mu e_{ij}[\mathbf{u}] e_{ij}[\tilde{\mathbf{u}}] dV + \sum_{l=1}^{N_L} \int_{V_L^{(l)}} 4\mu e_{ij}[\mathbf{u}] e_{ij}[\tilde{\mathbf{u}}] dV. \tag{3.5}$$

In (3.5), $2\mu e_{ij}[\mathbf{u}]$ may be replaced by $\tau_{ij}[\mathbf{u}]$ because the trace of $e_{ij}[\tilde{\mathbf{u}}]$ is zero. Also, $e_{ij}[\tilde{\mathbf{u}}]$ may be replaced by $\tilde{u}_{i,j}$ because $\tau_{ij}[\mathbf{u}]$ is symmetric. Then using (2.2), (3.5) becomes

$$D[\tilde{\mathbf{u}}] = D[\mathbf{u}] + D[\tilde{\mathbf{u}}] + \int_{V_0} (2(\partial_j \tilde{u}_i \tau_{ij}[\mathbf{u}]) + 2 f_i \tilde{u}_i) dV + \sum_{l=1}^{N_L} \int_{V_L^{(l)}} (2\partial_j(\tilde{u}_i \tau_{ij}[\mathbf{u}]) + 2 f_i \tilde{u}_i) dV. \tag{3.6}$$

Now replacing $\mathbf{u}$ in (3.2) by $\tilde{\mathbf{u}}$ and using (3.6) and Gauss's theorem, yields (3.7), below. In applying Gauss's theorem the surfaces on which the derivatives of $\tilde{\mathbf{u}}$ are discontinuous give no net contributions. The contributions from the two sides cancel because $\tilde{\mathbf{u}}$ and $\tilde{\mathbf{u}}$ are continuous. Thus

$$\begin{aligned} D_e[\tilde{\mathbf{u}}] = D[\mathbf{u}] + D[\tilde{\mathbf{u}}] + 2\int_{S_0} \tilde{u}_i \tau_{ij}^{(0)}[\mathbf{u}] n_j dS + 2\int_{V_0} f_i \tilde{u}_i dV \\ - 2\sum_{l=1}^{N_L} \int_{S_L^{(l)}} \tilde{u}_i \tau_{ij}^{(l)}[\mathbf{u}] n_j dS + 2\sum_{l=1}^{N_L} \int_{V_L^{(l)}} f_i \tilde{u}_i dV \\ - 2\int_V f_i(u_i + \tilde{u}_i) dV - 2\int_{S_2} (u_i + \tilde{u}_i) m_i \beta dS \\ - 2\int_{S_3} (u_i + \tilde{u}_i)(t_i \alpha + m_i \beta) dS - 2\int_{S_4} (u_i + \tilde{u}_i)\gamma_i dS \\ + 2\sum_{l=1}^{N_L} \sigma^{(l)}(\dot{A}^{(l)} + \dot{\tilde{A}}^{(l)}), \end{aligned} \tag{3.7}$$

where $\dot{A}^{(l)}$ is given by (3.3) and $\dot{\tilde{A}}^{(l)}$ is the rate of change of $A^{(l)}$ under the velocity $\tilde{\mathbf{u}}$. Since (3.3) is linear in $\mathbf{u}$, $\dot{\tilde{A}}^{(l)}$ is given by (3.3) with $\mathbf{u}$ replaced by $\tilde{\mathbf{u}}$. In (3.7) the superscripts in $\tau_{ij}^{(0)}[\mathbf{u}]$ and $\tau_{ij}^{(l)}[\mathbf{u}]$ have been added to denote the stress tensors on the two sides of the surfaces $S_L^{(l)}$ facing $V_0$ and $V_L^{(l)}$ respectively. The difference $(\tau_{ij}^{(0)}[\mathbf{u}] - \tau_{ij}^{(l)}[\mathbf{u}])$ is $\Delta\tau_{ij}$ as used in (2.7) and (2.8).

Since $\mathbf{u}$ and $\tilde{\mathbf{u}}$ both satisfy (2.3), (2.4*a*) and 2.5*a*), the components of $\tilde{\mathbf{u}}$ corresponding to the specified components of $\mathbf{u}$ on $S$ are zero. Further, $\tau_{ij}[\mathbf{u}]$ satisfies (2.4*b*), (2.5*b*) and (2.6). As a result, the surface integrals in (3.7) over $S_1$, $S_2$, $S_3$ and $S_4$ involving $\tilde{\mathbf{u}}$ all cancel. The surviving terms of (3.7) may be written

$$\begin{aligned} D_e[\tilde{\mathbf{u}}] = D_e[\mathbf{u}] + D[\tilde{\mathbf{u}}] + 2\sum_{l=1}^{N_L} \int_{S_L^{(l)}} \tilde{u}_i \Delta\tau_{ij} n_j dS \\ - 2\sum_{k=1}^{N_K} \int_{V_K^{(k)}} \tilde{u}_i f_i dV + 2\sum_{k=1}^{N_K} \int_{S_K^{(k)}} \tilde{u}_i \tau_{ij} n_j dS + 2\sum_{l=1}^{N_L} \sigma^{(l)} \dot{\tilde{A}}^{(l)}. \end{aligned} \tag{3.8}$$

The integrals over $V_K^{(k)}$ and $S_K^{(k)}$ in (3.8) are the rate of work done on the solid particles by the body forces $f_i$ and surface tractions $\tau_{ij}[\mathbf{u}]$ under the motion $\tilde{\mathbf{u}}$. Since $\tilde{\mathbf{u}}$ is a rigid body motion within each $V_K^{(k)}$ it has the form

$$\tilde{u}_i = \tilde{u}_i^{(k)} + \epsilon_{ilm}(\tfrac{1}{2}\epsilon_{ljk}\tilde{u}_{k,j}) x_m, \quad \mathbf{x} \text{ in } V_K^{(k)}, \tag{3.9}$$

where $\tilde{\mathbf{u}}^{(k)}$ is a constant vector and the angular velocity $(\frac{1}{2}\epsilon_{ljk}\tilde{u}_{k,j})$ which appears in (3.9) is also constant within $V_K^{(k)}$. Using (3.9), (2.9) and (2.10) it follows that the sum of the integrals over $V_K^{(k)}$ and $S_K^{(k)}$ is zero in (3.8).

The surface integrals over $S_L^{(l)}$ and the surface tension terms in (3.8) may be rewritten using (3.3), (2.7) and (2.8) as

$$\begin{aligned} 2\sum_{l=1}^{N_L} \int_{S_L^{(l)}} \tilde{u}_i \Delta\tau_{ij} n_j dS + 2\sum_{l=1}^{N_L} \sigma^{(l)} \dot{\tilde{A}}^{(l)} \\ = 2\sum_{l=1}^{N_L} \int_{S_L^{(l)}} \tilde{u}_i n_i \left\{ \Delta\tau_{qm} n_q n_m - \sigma^{(l)} \left( \frac{1}{R_1} + \frac{1}{R_2} \right) \right\} dS, \end{aligned} \tag{3.10}$$

where $\tilde{u}_i \Delta\tau_{ij} n_j$ has been replaced by $\tilde{u}_i n_i \Delta\tau_{qm} n_q n_m$ because the tangential component of $\Delta\tau_{ij} n_j$ is zero by (2.8). The last integrand in (3.10) is zero by (2.7). Hence (3.8) becomes

$$D_e[\bar{\mathbf{u}}] = D_e[\mathbf{u}] + D[\tilde{\mathbf{u}}]. \tag{3.11}$$

Since $D[\tilde{\mathbf{u}}]$ is never negative and is zero only if $\tilde{\mathbf{u}} = 0$ or if $\tilde{\mathbf{u}}$ is a rigid body motion, theorem 1 follows.

If the boundary conditions are such that no rigid body motion is possible satisfying (2.3), (2.4$a$) and (2.5$a$) when the given functions $g, h, b$ are replaced by zeros, then $\tilde{\mathbf{u}}$ cannot be a rigid body motion. In this case $D_e[\bar{\mathbf{u}}] = D_e[\mathbf{u}]$ only if $\bar{\mathbf{u}} = \mathbf{u}$. This is the case, for example, if $S_1$ contains at least three non-colinear points.

## 4. A maximum principle

A maximum principle for the Stokes flow problem stated in § 2 can be obtained in terms of a functional $H[\tau_{ij}]$ of the stress tensor $\tau_{ij}$. This functional will be called the excess power. It is defined as twice the power delivered by surface tractions on $S$ acting through the given velocity components $g$, $b$, $h$ minus the dissipation expressed in terms of the stress:

$$\begin{aligned} H[\tau_{ij}] = {} & 2\int_{S_1} g_i \tau_{ij} n_j dS + 2\int_{S_2} (h j_i \tau_{ij} n_j + b t_i \tau_{ij} n_j) dS \\ & + 2\int_{S_3} h j_i \tau_{ij} n_j dS - \int_{V_0} \frac{1}{2\mu} (\tau_{ij} - \tfrac{1}{3}\tau_{kk}\delta_{ij})^2 dV \\ & - \sum_{l=1}^{N_L} \int_{V_L^{(l)}} \frac{1}{2\mu} (\tau_{ij} - \tfrac{1}{3}\tau_{kk}\delta_{ij})^2 dV. \end{aligned} \tag{4.1}$$

When $\tau_{ij}$ is the stress tensor corresponding to a solution $\mathbf{u}$ of (2.1)–(2.13), then

$$H[\tau_{ij}] = D_e[\mathbf{u}]. \tag{4.2}$$

To prove (4.2), consider first that for a solution $\tau_{ij}[\mathbf{u}]$, the volume integrals over $V_0$ and $V_L^{(l)}$ in (4.1) become equal to those in (3.1) and add up to $D[\mathbf{u}]$. Next, by use of the boundary conditions (2.3)–(2.6) the surface integrals over $S_1$, $S_2$ and $S_3$ in (4.1) may be written:

$$\int_{S_1} g_i \tau_{ij} n_j dS = \int_{S_1} u_i \tau_{ij} n_j dS, \tag{4.3}$$

$$\int_{S_2} (h j_i \tau_{ij} n_j + b t_i \tau_{ij} n_j) dS = \int_{S_2} u_i \tau_{ij} n_j dS - \int_{S_2} u_i m_i \beta dS, \tag{4.4}$$

$$\int_{S_3} h j_i \tau_{ij} n_j dS = \int_{S_3} u_i \tau_{ij} n_j dS - \int_{S_3} (u_i t_i \alpha + u_i m_i \beta) dS. \tag{4.5}$$

Using (4.3)–(4.5) in (4.1) and adding and subtracting twice the integral of $u_i \tau_{ij} n_j$ over $S_4$ gives

$$\begin{aligned} H[\tau_{ij}] = {} & 2\int_S u_i \tau_{ij} n_j dS - 2\int_{S_2} u_i m_i \beta dS \\ & - 2\int_{S_3} (u_i t_i \alpha + u_i m_i \beta) dS - 2\int_{S_4} u_i \gamma_i dS - D[\mathbf{u}]. \end{aligned} \tag{4.6}$$

The first integral in (4.6) is the rate at which surface tractions on $S$ do work on the fluid in $V$. This integral may be evaluated by expressing conservation of energy in the form

$$\int_S u_i \tau_{ij} n_j dS + \int_V f_i u_i dV = D[\mathbf{u}] + \sum_{l=1}^{N_L} \sigma^{(l)} \dot{A}^{(l)}. \tag{4.7}$$

Equation (4.7) is not an independent postulate here since it may be shown to follow from (2.1) to (2.13). Using (4.7) in (4.6) to eliminate the integral of $u_i \tau_{ij} n_j$ over $S$ gives $H[\tau_{ij}]$ in a form which is identical to (3.2) so (4.2) is proved.

THEOREM 2. *A maximum principle. Let* $\mathbf{u}(\mathbf{x})$ *be a continuous solution of a Stokes flow problem satisfying* (2.1)–(2.13). *Let* $\bar{\tau}_{ij}$ *be any stress tensor defined in* $V_0$ *and* $V_L^{(l)}$ *which is piecewise continuous and piecewise continuously differentiable and satisfies* (2.2), (2.4*b*), (2.5*b*), (2.6), (2.7), (2.8), (2.9) *and* (2.10); *on surfaces of discontinuity of* $\bar{\tau}_{ij}$ *the traction* $n_i' \bar{\tau}_{ij}$ *is required to be continuous where* $n_i'$ *is the normal to the surface of discontinuity of* $\bar{\tau}_{ij}$ (*other than the surfaces* $S_L^{(l)}$ *of the drops*). *Then*

$$D_e[\mathbf{u}] \geqslant H[\bar{\tau}_{ij}]. \tag{4.8}$$

The equality in (4.8) holds only if $\bar{\tau}_{ij} = \tau_{ij}$ or $\bar{\tau}_{ij} = \tau_{ij} + p_0 \delta_{ij}$ where $p_0$ is a constant.

*Proof.* Let $\bar{\tau}_{ij} = \tau_{ij} + \tilde{\tau}_{ij}$, where $\tau_{ij}$ is the stress tensor corresponding to the solution $\mathbf{u}$. In (4.8), $H[\bar{\tau}_{ij}]$ is given by (4.1) with $\tau_{ij}$ replaced by $\bar{\tau}_{ij}$:

$$\begin{aligned} H[\bar{\tau}_{ij}] = {} & 2\int_{S_1} g_i \bar{\tau}_{ij} n_j dS + 2\int_{S_2} (hj_i \bar{\tau}_{ij} n_j + bt_i \bar{\tau}_{ij} n_j) dS \\ & + 2\int_{S_3} hj_i \bar{\tau}_{ij} n_j dS - \int_{V_0} \frac{1}{2\mu} (\bar{\tau}_{ij} - \tfrac{1}{3}\bar{\tau}_{kk}\delta_{ij})^2 dV \\ & - \sum_{l=1}^{N_L} \int_{V_L^{(l)}} \frac{1}{2\mu} (\bar{\tau}_{ij} - \tfrac{1}{3}\bar{\tau}_{kk}\delta_{ij})^2 dV. \end{aligned} \tag{4.9}$$

The integral over $V_0$ in (4.9) is

$$\begin{aligned} \int_{V_0} \frac{1}{2\mu} (\bar{\tau}_{ij} - \tfrac{1}{3}\bar{\tau}_{kk}\delta_{ij})^2 dV = {} & \int_{V_0} \frac{1}{2\mu} (\tau_{ij} - \tfrac{1}{3}\tau_{kk}\delta_{ij})^2 dV \\ & + \int_{V_0} \frac{1}{\mu} (\tau_{ij} - \tfrac{1}{3}\tau_{kk}\delta_{ij})(\tilde{\tau}_{ij} - \tfrac{1}{3}\tilde{\tau}_{kk}\delta_{ij}) dV \\ & + \int_{V_0} \frac{1}{2\mu} (\tilde{\tau}_{ij} - \tfrac{1}{3}\tilde{\tau}_{kk}\delta_{ij})^2 dV. \end{aligned} \tag{4.10}$$

An expansion similar to (4.10) can be written for the integrals over $V_L^{(l)}$ in (4.9). Using these expansions in (4.9) and comparing to (4.1) gives

$$\begin{aligned} H[\bar{\tau}_{ij}] = H[\tau_{ij}] & - \int_{V_0} \frac{1}{2\mu} (\tilde{\tau}_{ij} - \tfrac{1}{3}\tilde{\tau}_{kk}\delta_{ij})^2 dV \\ & - \sum_{l=1}^{NL} \int_{V_L^{(l)}} \frac{1}{2\mu} (\tilde{\tau}_{ij} - \tfrac{1}{3}\tilde{\tau}_{kk}\delta_{ij})^2 dV \\ & - 2\int_{V_0} e_{ij} (\tilde{\tau}_{ij} - \tfrac{1}{3}\tilde{\tau}_{kk}\delta_{ij}) dV \end{aligned}$$

$$-2\sum_{l=1}^{N_L}\int_{V_L^{(l)}} e_{ij}(\tilde{\tau}_{ij}-\tfrac{1}{3}\tilde{\tau}_{kk}\delta_{ij})\,dV$$
$$+2\int_{S_1} g_i\tilde{\tau}_{ij}n_j\,dS+2\int_{S_2}(hj_i\tilde{\tau}_{ij}n_j+bt_i\tilde{\tau}_{ij}n_j)\,dS$$
$$+2\int_{S_3} hj_i\tilde{\tau}_{ij}n_j\,dS. \tag{4.11}$$

In (4.11), (2.11) has been used to replace $\tau_{ij}$ in terms of $e_{ij}$. The integral over $V_0$ containing $e_{ij}$ in (4.11) may be written

$$\int_{V_0} e_{ij}(\tilde{\tau}_{ij}-\tfrac{1}{3}\tilde{\tau}_{kk}\delta_{ij})dV=\int_{V_0} e_{ij}\tilde{\tau}_{ij}dV=\int_{V_0} u_{i,j}\tilde{\tau}_{ij}dV$$
$$=\int_{V_0}\partial_j(u_i\tilde{\tau}_{ij})\,dV=\int_{S_0} u_i\tilde{\tau}_{ij}n_j\,dS. \tag{4.12}$$

In deriving (4.12), account is taken of the facts that $u_i$ is an incompressible flow and that $\partial_j(\tilde{\tau}_{ij})=0$, since both $\tau_{ij}$ and $\bar{\tau}_{ij}$ satisfy (2.2). The surfaces of discontinuity of $\bar{\tau}_{ij}$ would also enter in (4.12) but since $\bar{\tau}_{ij}n_j'$ and $\tau_{ij}n_j'$ are both continuous across such surfaces, the contributions over the two sides of these surfaces cancel.

A transformation similar to (4.12) yields

$$\int_{V_L^{(l)}} e_{ij}(\tilde{\tau}_{ij}-\tfrac{1}{3}\tilde{\tau}_{kk}\delta_{ij})\,dV=-\int_{S_L^{(l)}} u_i\tilde{\tau}_{ij}n_j\,dS, \tag{4.13}$$

where $n_j$ is again the normal outward from $V_0$. The surface $S_0$ in (4.12) is the sum of $S_1$, $S_2$, $S_3$, $S_4$, $S_L^{(l)}$ and $S_K^{(k)}$. When (4.12) and (4.13) are substituted into (4.11), all the surface integrals, except those contained in $H[\tau_{ij}]$, are found to cancel leaving

$$H[\bar{\tau}_{ij}]=H[\tau_{ij}]-\int_{V_0}\frac{1}{2\mu}(\tilde{\tau}_{ij}-\tfrac{1}{3}\tilde{\tau}_{kk}\delta_{ij})^2dV$$
$$-\sum_{l=1}^{N_L}\int_{V_L^{(l)}}\frac{1}{2\mu}(\tilde{\tau}_{ij}-\tfrac{1}{3}\tilde{\tau}_{kk}\delta_{ij})^2dV. \tag{4.14}$$

In the reduction of (4.11) to (4.14), the surface integrals over $S_2$ which arise are:

$$2\int_{S_2}(hj_i\tilde{\tau}_{ij}n_j+bt_i\tilde{\tau}_{ij}n_j)\,dS-2\int_{S_2} u_i\tilde{\tau}_{ij}n_j\,dS$$
$$=2\int_{S_2}(hj_i\tilde{\tau}_{ij}n_j+bt_i\tilde{\tau}_{ij}n_j)\,dS$$
$$-2\int_{S_2}(u_qj_qj_i\tilde{\tau}_{ij}n_j+u_ql_ql_i\tilde{\tau}_{ij}n_j+u_qm_qm_i\tilde{\tau}_{ij}n_j)\,dS. \tag{4.15}$$

The sum of the integrals in (4.15) is zero because $\mathbf{u}$ satisfies (2.4$a$) and both $\tau_{ij}$ and $\bar{\tau}_{ij}$ satisfy (2.4$b$) so that $\tilde{\tau}_{ij}n_jm_i=0$ on $S_2$. The cancellation of integrals over $S_1$, $S_3$ and $S_4$ follows similarly.

Surface integrals over $S_L^{(l)}$ arise from (4.12) and (4.13) which combine in (4.11) to give terms of the form

$$\int_{S_L^{(l)}} u_i \Delta\tilde{\tau}_{ij} n_j dS, \tag{4.16}$$

where $\Delta\tilde{\tau}_{ij}$ is the jump of $\tilde{\tau}_{ij}$ across the surfaces $S_L^{(l)}$. The tangential components of $\tau_{ij}n_j$ and $\bar{\tau}_{ij}n_j$ are continuous across $S_L^{(l)}$ since both satisfy (2.8). The normal components of $\tau_{ij}n_j$ and $\bar{\tau}_{ij}n_j$ take the same jump, as prescribed by (2.7). Hence $\Delta\tilde{\tau}_{ij}n_j$ is zero and (4.16) vanishes.

On the surfaces $S_K^{(k)}$ ($k = 1, \ldots, N_K$), the integrals arising from (4.12) are of the form

$$\int_{S_K^{(k)}} u_i \tilde{\tau}_{ij} n_j dS. \tag{4.17}$$

Since $u_j$ has the form (3.9) on $S_K^{(k)}$ and both $\tau_{ij}$ and $\bar{\tau}_{ij}$ satisfy (2.9) and (2.10), it follows after substitution of (3.9) in (4.17) that (4.17) also vanishes.

In (4.14) the volume integrals involving $\tilde{\tau}_{ij}$ are positive unless $\tilde{\tau}_{ij}$ is zero or of the form $p_0\delta_{ij}$ where $p_0$ is a constant. Hence

$$H[\bar{\tau}_{ij}] \leqslant H[\tau_{ij}] \tag{4.18}$$

and the equality holds only if $\bar{\tau}_{ij} = \tau_{ij}$ or if $\bar{\tau}_{ij} = \tau_{ij} + p_0\delta_{ij}$. Theorem 2 follows from (4.18) and (4.2).

The constant $p_0$ will be zero if no uniform pressure field can satisfy the stress conditions (2.4*b*), (2.5*b*) and (2.6) when the given $\alpha$, $\beta$, $\gamma$ are replaced by zeros. In this case $D_e[u] = H[\bar{\tau}_{ij}]$ only if $\bar{\tau}_{ij} = \tau_{ij}$. This is the case, for example, if $S_4$ contains at least one point.

Theorems 1 and 2 contain the minimum and maximum principles given by Keller *et al.* (1967) as special cases in which the drops are of constant shape, $S_2$ is absent, and **j** is coincident with **n**.

The theorems 1 and 2 also apply to drops or regions of constant volume of one or more immiscible fluids in another fluid where the surface tensions are negligible ($\sigma^{(l)} = 0$). Then deformation of drops is to be expected in general.

## 5. Uniqueness theorem

THEOREM 3. *The solution* **u** *of a Stokes flow problem posed by* (2.1)–(2.13) *is unique to within a rigid body motion and the stress* $\tau_{ij}$ *is unique within a uniform pressure.*

*Proof.* Let $\mathbf{u}^{(1)}$ and $\mathbf{u}^{(2)}$ be two solutions. Then (3.4) holds with $\mathbf{u} = \mathbf{u}^{(1)}$ and $\bar{\mathbf{u}} = \mathbf{u}^{(2)}$ and vice versa so the equality in (3.4) would hold. The first part of theorem 3 then follows from theorem 1.

Similarly, let $\tau_{ij}^{(1)}$ and $\tau_{ij}^{(2)}$ be the stresses corresponding to $\mathbf{u}^{(1)}$ and $\mathbf{u}^{(2)}$. Then (4.18) holds with $\tau_{ij} = \tau_{ij}^{(1)}$ and $\bar{\tau}_{ij} = \tau_{ij}^{(2)}$ and vice versa so the equality would hold in (4.18). The second part of theorem 3 follows from theorem 2.

The arbitrary rigid body motion and the arbitrary uniform pressure implied in theorem 3 will be zero under the same conditions as discussed below (3.11) and (4.18).

Theorems 1, 2 and 3 can be applied to a single homogeneous fluid by deleting all references to suspended drops and particles.

The theorems also apply if any one, two, or three of the surfaces $S_1$, $S_2$, $S_3$, $S_4$ are absent. However, every point of $S$ must be a point of one of the surfaces $S_1$, $S_2$, $S_3$, $S_4$. The boundary conditions on $S$ which are permitted by (2.3)–(2.6) specify just enough components of velocity and traction to make the solution unique. This requires that sufficient components of velocity and/or traction be specified at each point of $S$ that if $\tilde{u}_i$ and $\tilde{\tau}_{ij}$ are differences between two fields which both satisfy the boundary conditions on $S$, then the work rate $\tilde{u}_i\tilde{\tau}_{ij}n_j$ is zero at every point of $S$.

## 6. Infinite domains

In the theorems 1, 2 and 3, the domain $V$ is assumed to be finite. The theorems can be applied to infinite domains if it is assumed that the velocity and stress fields decay fast enough so that the surface integrals which arise over a sphere at infinity vanish. The situation is similar to that of linear elastostatics for exterior domains treated by Gurtin & Sternberg (1961). As they point out, the rate at which a solution approaches specified values at infinity is an item of information which one would legitimately expect to infer from the solution, rather than a condition to be imposed on the solution in advance. A uniqueness theorem resting on an assumption of the rate of decay at infinity leaves in doubt the existence of solutions which approach the specified values at infinity less rapidly.

In the present section, generalizations of theorems 1, 2 and 3 are proved for infinite domains without assumptions of the rates of decay of the solutions at infinity. It is also shown that the comparison flows for the various theorems must be subject to a specification of the rate of dilation of the internal boundaries.

The nomenclature of § 2 will be used also for infinite domains with the understanding that the region $V$ is now an exterior domain bounded internally by the surface $S$. The surface $S$ is assumed to consist of a finite number of closed surfaces which lie within a finite sphere, $r = r_0$ where $r_0$ is a constant and $r$ is the distance from the origin. The surface $S$ is again considered in four parts $S_1$, $S_2$, $S_3$, $S_4$ according to the boundary conditions specified. It is assumed that the number of liquid drops, $N_L$, and the number of solid particles, $N_K$, in suspension in $V$ are finite and that they also lie within the sphere $r = r_0$. The suspending fluid occupies the region $V_0$ which is the portion of $V$ not occupied by solid particles or liquid drops. The surface $S_0$ of $V_0$ consists of $S_1$, $S_2$, $S_3$, $S_4$, $S_L^{(l)}$ ($l = 1, \ldots, N_L$) and $S_K^{(k)}$ ($k = 1, \ldots, N_K$).

The only boundary condition at infinity which will be considered is that the velocity approach a constant vector uniformly at infinity, i.e.

$$\lim_{r\to\infty} u_i = U_i, \tag{6.1}$$

where $U_i$ is a given constant vector. Whenever the boundary condition (6.1) is imposed, a system of axes translating with velocity $U_i$ may be used so that the condition (6.1) is replaced by

$$\lim_{r\to\infty} u_i = 0. \tag{6.2}$$

The condition (6.2) will be assumed to apply in all cases below.

An additional restriction that will be imposed for infinite domains is that the body force within $V_0$ be conservative, meaning there exists a single valued potential, $\Omega(\mathbf{x})$, such that

$$f_i = -\Omega_{,i}, \quad \mathbf{x} \quad \text{in} \quad V_0. \tag{6.3}$$

The boundary conditions on the interior boundaries $S_1$, $S_2$, $S_3$, $S_4$ are the same as for finite domains detailed by (2.3)-(2.6). It will be shown that for an infinite domain the total rate of expansion, $\theta^*$, must also be specified for uniqueness of the solution. Hence the statement of the problem will be augmented by the requirement

$$-\int_S u_i n_i \, dS = \theta^*, \tag{6.4}$$

where $\theta^*$ may be a given function of time in general.

A complete statement of the problem considered in this section is to find $\mathbf{u}(\mathbf{x})$ in the infinite domain, $V$, described above satisfying (2.1)-(2.13), (6.2), (6.3) and (6.4).

The dissipation rate $D[\mathbf{u}]$ is again defined by (3.1) with the understanding that the integral over $V_0$ is now interpreted as the limit

$$\int_{V_0} 2\mu(e_{ij}[\mathbf{u}])^2 dV = \lim_{\rho\to\infty} \int_{V_{0\rho}} 2\mu(e_{ij}[\mathbf{u}])^2 dV. \tag{6.5}$$

where $V_{0\rho}$ is the portion of $V_0$ within a sphere $r = \rho$.

The excess dissipation rate $D_e^*[\mathbf{u}]$ for an infinite domain $V$ is defined by

$$\begin{aligned} D_e^*[\mathbf{u}] = D[\mathbf{u}] &+ 2\int_{S_0} \Omega u_i n_i \, dS - 2\sum_{l=1}^{N_L} \int_{V_L^{(l)}} f_i u_i \, dV \\ &- 2\sum_{k=1}^{N_K} \int_{V_K^{(k)}} f_i u_i \, dV - 2\int_{S_2} u_i m_i \beta \, dS \\ &- 2\int_{S_3} (u_i t_i \alpha + u_i m_i \beta) dS - 2\int_{S_4} u_i \gamma_i \, dS + 2\sum_{l=1}^{N_L} \sigma^{(l)} \dot{A}^{(l)}. \end{aligned} \tag{6.6}$$

This definition (6.6) differs from (3.2) in that the rate of work done by body forces in $V_0$ has been replaced in (6.6) by the rate of change of potential energy due to the motion of the boundary $S_0$ of $V_0$. If the domain $V_0$ were finite, this potential energy term would be equal to the integral of $f_i u_i$ over $V_0$ by Gauss's theorem, (2.1) and (6.3). Then (6.6) would be equivalent to (3.2).

The counterpart of theorem 1 for infinite domains requires a representation theorem for $u_i$ which is developed first below.

The velocity field $\mathbf{u}(\mathbf{x})$ is assumed to be continuous and to possess continuous derivatives up to second order within each of the domains $V_0$, $V_L^{(l)}$ ($l = 1, \ldots, N_L$). At the boundaries of $V_L^{(l)}$ and $V_K^{(k)}$ the velocity $\mathbf{u}(\mathbf{x})$ is required to be continuous but its derivatives may be discontinuous. Then as shown in the appendix, $u_i$ must be analytic within $V_0$ and $V_L^{(l)}$.

Equations (2.2) and (2.11) may be combined to give the usual equations of motion within $V_0$ and $V_L^{(l)}$.

$$u_{i,jj} - \frac{1}{\mu} p_{,i} + \frac{1}{\mu} f_i = 0. \tag{6.7}$$

Taking $(\partial/\partial x_i)\,\partial/\partial x_k$ of (6.7) and using (6.3) and (2.1) yields

$$p_{,ik} + \Omega_{,ik} = 0. \tag{6.8}$$

Taking $(\partial/\partial x_l)\,\partial/\partial x_l$ of (6.7) and using (6.8) shows that the velocity is biharmonic,

i.e. $$\nabla^4 u_i = 0. \tag{6.9}$$

A representation of biharmonic functions in an exterior domain has been developed by Gurtin & Sternberg (1961). A region $\mathscr{R}$ is defined as a deleted neighbourhood of infinity characterized by

$$r_0 < r < \infty, \tag{6.10}$$

where $r_0$ is a constant. For such a region they prove

THEOREM 4. *Let $F(r,\theta,\phi)$ be biharmonic in $\mathscr{R}$, where $(r,\theta,\phi)$ are spherical polar co-ordinates. Then*

*(a) $F(r,\theta,\phi)$ admits the representation*

$$F(r,\theta,\phi) = \sum_{k=-\infty}^{\infty} h^{(k)}(r,\theta,\phi) + r^2 \sum_{k=-\infty}^{\infty} H^{(k)}(r,\theta,\phi), \tag{6.11}$$

*where $h^{(k)}(r,\theta,\phi)$ and $H^{(k)}(r,\theta,\phi)$ are solid harmonics of degree $k$ and both infinite series are uniformly convergent in every closed subregion of $\mathscr{R}$;*

*(b) $F(r,\theta,\phi)$ in $\mathscr{R}$ has partial derivatives of all orders, series representations of which may be obtained by performing the corresponding termwise differentiations of* (6.11), *the resulting expansions being also uniformly convergent in every closed subregion of $\mathscr{R}$;*

*(c) if $n$ is a fixed integer, the three statements*

$$\text{(i)} \quad F(r,\theta,\phi) = O(r^{n-1}), \tag{6.12}$$

$$\text{(ii)} \quad F(r,\theta,\phi) = o(r^n), \tag{6.13}$$

$$\text{(iii)} \quad h^{(k)}(r,\theta,\phi) = H^{(k-2)}(r,\theta,\phi) = 0 \quad \text{for} \quad k \geqslant n \tag{6.14}$$

*are equivalent and imply*

$$\text{(iv)} \quad F_{,i}(r,\theta,\phi) = O(r^{n-2}). \tag{6.15}$$

The orders of magnitude $F = O(r^n)$ and $F = o(r^n)$ indicate, as usual, that $|r^{-n}F|$ remains bounded uniformly and $|r^{-n}F|$ approaches zero uniformly, respectively, as $r \to \infty$.

The following theorem follows from theorem 4.

THEOREM 5. *Suppose $u_i(x)$, $e_{ij}(x)$, $\tau_{ij}(x)$ and $f_i$ in $\mathscr{R}$ satisfy* (2.1), (2.2), (2.11), (2.12) *and* (6.3). *Then if $n$ is a fixed integer*

$$u_i(x) = o(r^n) \tag{6.16}$$

*implies*

$$\text{(i)} \quad u_i(x) = O(r^{n-1}), \tag{6.17}$$

$$\text{(ii)} \quad e_{ij} = O(r^{n-2}), \tag{6.18}$$

$$\text{(iii)} \quad p_{,i} + \Omega_{,i} = O(r^{n-3}). \tag{6.19}$$

*Proof.* Since $u_i(\mathbf{x})$ is biharmonic, theorem 4 applies with $F$ replaced by $u_i$. Then (6.16), (6.13) and (6.12) imply (6.17). The definition (2.12) and (6.15) yield (6.18). Substituting (2.12), (2.11) and (6.3) into (2.2) and applying (6.15) again gives (6.19).

THEOREM 6. *A minimum principle for infinite domains. Let $V$ be an exterior domain containing $N_L$ liquid particles, $N_K$ solid particles and internal boundaries $S$ within a finite sphere $\mathrm{r} = r_0$. Let $\mathbf{u}(\mathbf{x})$ be a continuous solution of the Stokes flow problem satisfying* (2.1)–(2.13), (6.2), (6.3) *and* (6.4). *Let $\bar{\mathbf{u}}(\mathbf{x})$ be any continuous velocity field which is piecewise continuously differentiable and satisfies* (2.1), (2.3), (2.4$a$), (2.5$a$), (2.13), (6.4) *and*

$$\bar{u}_i = O(r^{-1}) \quad \text{as} \quad r \to \infty. \tag{6.20}$$

*Then*

$$D_e^*[\mathbf{u}] \leqslant D_e^*[\bar{\mathbf{u}}], \tag{6.21}$$

*where $D_e^*[\mathbf{u}]$ is defined by* (6.6). *The equality in* (6.21) *holds only if $\bar{\mathbf{u}} = \mathbf{u}$.*

*Proof.* Let $\bar{\mathbf{u}} = \mathbf{u} + \tilde{\mathbf{u}}$. From (3.1) the forms (3.5) and (3.6) follow as before with the understanding that the integrals over $V_0$ are interpreted in the sense of (6.5). Replacing $\mathbf{u}$ by $\tilde{\mathbf{u}}$ in (6.6) and using (3.6) and Gauss's theorem yields (6.22) below. In applying Gauss's theorem to $V_0$ in (3.6), the surface of $V_0$ is considered to consist of $S_0$ plus $S_\rho$ where $S_\rho$ is the surface of a sphere $r = \rho$, $\rho \to \infty$. Then

$$\begin{aligned}
D_e^*[\bar{\mathbf{u}}] = {} & D[\mathbf{u}] + D[\tilde{\mathbf{u}}] + 2\int_{S_0} \tilde{u}_i \tau_{ij}^{(0)}[\mathbf{u}] n_j dS + 2\int_{V_0} f_i \tilde{u}_i dV \\
& - 2\sum_{l=1}^{N_L} \int_{S_L^{(l)}} \tilde{u}_i \tau_{ij}^{(l)}[\mathbf{u}] n_j dS + 2\sum_{l=1}^{N_L} \int_{V_L^{(l)}} f_i \tilde{u}_i dV \\
& + 2\int_{S_\rho} \tilde{u}_i \tau_{ij}[\mathbf{u}] n_j dS + 2\int_{S_0} \Omega(u_i + \tilde{u}_i) n_i dS \\
& - 2\sum_{l=1}^{N_L} \int_{V_L^{(l)}} f_i (u_i + \tilde{u}_i) dV - 2\sum_{k=1}^{N_K} \int_{V_K^{(k)}} f_i (u_i + \tilde{u}_i) dV \\
& - 2\int_{S_1} (u_i + \tilde{u}_i) m_i \beta dS - 2\int_{S_2} (u_i + \tilde{u}_i)(t_i \alpha + m_i \beta) dS \\
& - 2\int_{S_4} (u_i + \tilde{u}_i) \gamma_i dS + 2\sum_{l=1}^{N_L} \sigma^{(l)}(\dot{A}^{(l)} + \dot{\tilde{A}}^{(l)}),
\end{aligned} \tag{6.22}$$

where the notation is the same as in (3.7). Since $\mathbf{u}$ and $\bar{\mathbf{u}}$ both satisfy (2.3), (2.4$a$) and (2.5$a$) and $\tau_{ij}$ satisfies (2.4$b$), (2.5$b$) and (2.6), the surface integrals over $S_1$, $S_2$, $S_3$ and $S_4$ involving $\tilde{\mathbf{u}}$ and $\tau_{ij}$ all cancel in (6.22). The surviving terms may be written

$$\begin{aligned}
D_e^*[\bar{\mathbf{u}}] = {} & D_e^*[\mathbf{u}] + D[\tilde{\mathbf{u}}] + 2\sum_{l=1}^{N_L} \int_{S_L^{(l)}} \tilde{u}_i \Delta\tau_{ij} n_j dS + 2\int_{V_0} f_i \tilde{u}_i dV \\
& - 2\sum_{k=1}^{N_K} \int_{V_K^{(k)}} \tilde{u}_i f_i dV + 2\sum_{k=1}^{N_K} \int_{S_K^{(k)}} \tilde{u}_i \tau_{ij} n_j dS + 2\sum_{l=1}^{N_L} \sigma^{(l)} \dot{\tilde{A}}^{(l)} \\
& + 2\int_{S_\rho} \tilde{u}_i \tau_{ij}[\mathbf{u}] n_j dS + 2\int_{S_0} \Omega \tilde{u}_i n_i dS.
\end{aligned} \tag{6.23}$$

Equation (6.23) is the counterpart of (3.8). The terms in (6.23) which are summed over $l$ and $k$ pertain to the liquid and solid particles and add up to zero as shown below (3.8). Applying Gauss's theorem to the region $V_0$ considered bounded by $S_0$ internally and $S_\rho$ externally and using (6.3) and (2.1) yields

$$\int_{S_0} \Omega \tilde{u}_i n_i dS = -\int_{V_0} f_i \tilde{u}_i dV - \int_{S_\rho} \Omega \tilde{u}_i n_i dS. \tag{6.24}$$

Substituting (6.24) in (6.23) gives

$$D_e^*[\bar{\mathbf{u}}] = D_e^*[\mathbf{u}] + D[\tilde{\mathbf{u}}] + 2\int_{S_\rho} \tilde{u}_i(\tau_{ij}[\mathbf{u}] - \delta_{ij}\Omega) n_j dS. \tag{6.25}$$

Using (2.11) the integral over $S_\rho$ in (6.25) is

$$\int_{S_\rho} \tilde{u}_i(\tau_{ij}[\mathbf{u}] - \delta_{ij}\Omega) n_j dS = \int_{S_\rho} \mu \tilde{u}_i e_{ij}[\mathbf{u}] n_j dS - \int_{S_\rho} (p + \Omega)\tilde{u}_i n_i dS. \tag{6.26}$$

Theorem 5 applies to $u_i$ with $n = 0$ by virtue of (6.2). Hence $e_{ij}[\mathbf{u}] = O(r^{-2})$ by (6.18). Further, $\tilde{u}_i = O(r^{-1})$ by (6.20) and (6.17). It follows that the first integral on the right of (6.26) is zero in the limit $\rho \to \infty$.

If the integration of (6.19) is considered along a path lying on the sphere $S_\rho$, it follows that on $r = \rho$

$$p + \Omega = p^* + F(r, \theta, \phi), \tag{6.27}$$

where $p^*$ is a constant and $F(r, \theta, \phi)$ is a function of order $O(r^{-2})$. Hence

$$\int_{S_\rho} (p + \Omega)\tilde{u}_i n_i dS = p^* \int_{S_\rho} \tilde{u}_i n_i dS + \int_{S_\rho} F(\rho, \theta, \phi)\tilde{u}_i n_i dS. \tag{6.28}$$

The first integral on the right of (6.28) is zero since $\mathbf{u}$ and $\bar{\mathbf{u}}$ satisfy (6.4) and the second integral is zero in the limit $\rho \to \infty$. Hence (6.28) and (6.26) are zero and theorem 6 follows from (6.25). In the present case, $u_i$ and $\bar{u}_i$ cannot differ by a rigid body motion because of the boundary condition at infinity so the equality holds in (6.21) only if $\bar{\mathbf{u}} = \mathbf{u}$.

A maximum principle for infinite domains corresponding to theorem 2 for finite domains can be derived if the excess power is redefined for infinite domains as follows

$$\begin{aligned} H^*[\tau_{ij}] = {} & 2\int_{S_1} g_i \tau_{ij} n_j dS + 2\int_{S_2} (hj_i \tau_{ij} n_j + bt_i \tau_{ij} n_j) dS \\ & + 2\int_{S_3} hj_i \tau_{ij} n_j dS - 2\theta^* p^* \\ & - \int_{V_0} \frac{1}{2\mu}(\tau_{ij} - \tfrac{1}{3}\tau_{kk}\delta_{ij})^2 dV \\ & - \sum_{l=1}^{N_L} \int_{V_L^{(l)}} \frac{1}{2\mu}(\tau_{ij} - \tfrac{1}{3}\tau_{kk}\delta_{ij})^2 dV. \end{aligned} \tag{6.29}$$

The difference between (6.29) and (4.1) is that the term $-2\theta^*p^*$ has been added in (6.29). The total rate of expansion, $\theta^*$, defined by (6.4) is a part of the given kinematic data and the work done by the pressure and body forces at infinity represented by $p^*$ is therefore included in the excess power. $H_e^*[\tau_{ij}]$ is defined only when $p^*$ exists as defined by

$$p^* = \lim_{r\to\infty}(p+\Omega) = \lim_{r\to\infty}(-\tfrac{1}{3}\tau_{kk}+\Omega). \tag{6.30}$$

When $\tau_{ij}$ is the stress tensor corresponding to a solution of (2.1)-(2.13), (6.2), (6.3) and (6.4), then

$$H^*[\tau_{ij}] = D_e^*[\mathbf{u}], \tag{6.31}$$

where $D_e^*[\mathbf{u}]$ is given by (6.6). To prove (6.31), we proceed as in proving (4.2). In the present case, (4.3), (4.4) and (4.5) hold also. Using (4.3)–(4.5) in (6.29) and subtracting twice the integral of $u_i\tau_{ij}n_j$ over $S_4$ gives

$$\begin{aligned} H^*[\tau_{ij}] = {} & 2\int_S u_i\tau_{ij}n_j dS - 2\int_{S_2} u_i m_i\beta\, dS \\ & - 2\int_{S_3}(u_i t_i\alpha + u_i m_i\beta)dS - 2\int_{S_4} u_i\gamma_i dS \\ & - 2\theta^*p^* - D[\mathbf{u}]. \end{aligned} \tag{6.32}$$

Instead of (4.7), the conservation of energy now takes the form

$$\int_S u_i\tau_{ij}n_j dS + \int_{S_\rho} u_i\tau_{ij}n_j dS + \int_V f_i u_i dV = D[\mathbf{u}] + \sum_{l=1}^{N_L}\sigma^{(l)}\dot{A}^{(l)}, \tag{6.33}$$

where the integrals over $S_\rho$ and $V$ are interpreted as the limits for $\rho\to\infty$. Using (6.3) and Gauss's theorem these terms may be written

$$\begin{aligned} \int_{S_\rho} u_i\tau_{ij}n_j dS + \int_V f_i u_i dV = {} & -\int_{S_\rho} u_i p n_i dS - \int_{S_\rho}\Omega u_i n_i dS \\ & - \int_{S_0}\Omega u_i n_i dS + \sum_{l=1}^{N_L}\int_{V_L^{(l)}} f_i u_i dV + \sum_{k=1}^{N_K}\int_{V_K^{(k)}} f_i u_i dV. \end{aligned} \tag{6.34}$$

The two integrals over $S_\rho$ on the right of (6.34) may be replaced by $-\theta^*p^*$ in view of (6.27) and the fact that $u_i = O(r^{-1})$. Substituting (6.34) into (6.33) and using (6.33) to eliminate the integral over $S$ in (6.32) yields $H^*[\tau_{ij}]$ in a form identical to (6.6) so (6.31) is proved.

THEOREM 7. *A maximum principle for infinite domains. Let $V$ be an exterior domain containing $N_L$ liquid particles, $N_K$ solid particles and internal boundaries $S$ within a finite sphere $r = r_0$. Let $\mathbf{u}(\mathbf{x})$ be a continuous solution of the Stokes flow problem satisfying* (2.1)–(2.13), (6.2), (6.3), (6.4). *Let $\bar{\tau}_{ij}$ be any stress tensor defined in $V_0$ and $V_L^{(l)}$ which is piecewise continuous and piecewise continuously differentiable and satisfies* (2.2), (2.4*b*), (2.5*b*), (2.6)–(2.10). *On surfaces of discontinuity of $\bar{\tau}_{ij}$ the traction $n_i'\bar{\tau}_{ij}$ is required to be continuous where $n_i'$ is the normal to the surface of the discontinuity of $\bar{\tau}_{ij}$. Further, the limit, $\bar{p}^*$, defined by* (6.30) *must exist and*

$$\bar{\tau}_{ij} - \tfrac{1}{3}\bar{\tau}_{kk}\delta_{ij} = O(r^{-2}) \quad \text{as} \quad r\to\infty. \tag{6.35}$$

*Then*
$$D_e^*[\mathbf{u}] \geqslant H^*[\bar{\tau}_{ij}]. \tag{6.36}$$

The equality in (6.36) holds only if $\bar{\tau}_{ij} = \tau_{ij}$ or $\bar{\tau}_{ij} = \tau_{ij} + p_0\delta_{ij}$ where $p_0$ is a constant.

*Proof.* Let $\bar{\tau} = \tau_{ij} + \tilde{\tau}_{ij}$, where $\tau_{ij}$ is the stress tensor corresponding to the solution $\mathbf{u}$. In (6.36), $H^*[\bar{\tau}_{ij}]$ is given by (6.29) with $[\tau_{ij}]$ replaced by $[\bar{\tau}_{ij}]$ and $p^*$ replaced by $\bar{p}^*$. The same steps that were used to convert (4.9) to (4.11) yield

$$\begin{aligned} H^*[\bar{\tau}_{ij}] = H^*[\tau_{ij}] &- \int_{V_0} \frac{1}{2\mu}(\tilde{\tau}_{ij} - \tfrac{1}{3}\tilde{\tau}_{kk}\delta_{ij})^2 dV \\ &- \sum_{l=1}^{N_L} \int_{V_L^{(l)}} \frac{1}{2\mu}(\tau_{ij} - \tfrac{1}{3}\tau_{kk}\delta_{ij})^2 dV \\ &- 2\int_{V_0} e_{ij}(\tilde{\tau}_{ij} - \tfrac{1}{3}\tilde{\tau}_{kk}\delta_{ij})\, dV \\ &- 2\sum_{l=1}^{N_L} \int_{V_L^{(l)}} e_{ij}(\tilde{\tau}_{ij} - \tfrac{1}{3}\tilde{\tau}_{kk}\delta_{ij}) dV \\ &+ 2\int_{S_1} g_i\tilde{\tau}_{ij}n_j dS + 2\int_{S_2} (hj_i\tilde{\tau}_{ij}n_j + bt_i\tilde{\tau}_{ij}n_j) dS \\ &+ 2\int_{S_3} hj_i\tilde{\tau}_{ij}n_j dS - 2\theta^*\tilde{p}^*, \end{aligned} \tag{6.37}$$

where $\tilde{p}^* = \bar{p}^* - p^*$. The integral over $V_0$ containing $e_{ij}$ in (6.37) may be rewritten by the same steps as in (4.12) to yield

$$\int_{V_0} e_{ij}(\tilde{\tau}_{ij} - \tfrac{1}{3}\tau_{kk}\delta_{ij})\, dV = \int_{S_0} u_i\tilde{\tau}_{ij}n_j dS + \int_{S_\rho} u_i\tilde{\tau}_{ij}n_j dS. \tag{6.38}$$

The integral over $S_\rho$ in (6.38) may be written

$$\int_{S_\rho} u_i\tilde{\tau}_{ij}n_j dS = \int_{S_\rho} u_i(\tilde{\tau}_{ij} - \tfrac{1}{3}\tilde{\tau}_{kk}\delta_{ij})n_j dS - \int_{S_\rho} u_i\tilde{p}^*n_i d\tau. \tag{6.39}$$

The first integral on the right of (6.39) is zero in the limit $\rho \to \infty$ due to (6.2) and (6.35); the second integral is equal to $-2\theta^*\tilde{p}^*$. Substituting (6.39) and (6.38) into (6.37) and using the same arguments as used in connexion with (4.14) gives

$$\begin{aligned} H^*[\bar{\tau}_{ij}] = H^*[\tau_{ij}] &- \int_{V_0} \frac{1}{2\mu}(\tilde{\tau}_{ij} - \tfrac{1}{3}\tilde{\tau}_{kk}\delta_{ij})^2 dV \\ &- \sum_{l=1}^{N_L} \int_{V_L^{(l)}} \frac{1}{2\mu}(\tilde{\tau}_{ij} - \tfrac{1}{3}\tilde{\tau}_{kk}\delta_{ij})^2 dV. \end{aligned} \tag{6.40}$$

The integrals in (6.40) are positive unless $\tilde{\tau}_{ij}$ is zero or of the form $p_0\delta_{ij}$ where $p_0$ is a constant throughout $V_0$ and $V_L^{(l)}$. Hence

$$H^*[\bar{\tau}_{ij}] \leqslant H^*[\tau_{ij}] \tag{6.41}$$

and the equality holds only if $\bar{\tau}_{ij} = \tau_{ij}$ or if $\bar{\tau}_{ij} = \tau_{ij} + p_0\delta_{ij}$. Theorem 7 follows from (6.41) and (6.31). The constant $p_0$ will be zero under the same conditions discussed below (4.18).

THEOREM 8. *Uniqueness theorem for infinite domains. Let $V$ be an exterior domain containing $N_L$ liquid particles, $N_K$ solid particles and internal boundaries $S$ within a finite sphere $r = r_0$. Then the solution* $\mathbf{u}$ *of a Stokes flow problem posed by* (2.1)–(2.13), (6.2), (6.3) *and* (6.4) *is unique and the stress $\tau_{ij}$ is unique to within a uniform pressure.*

*Proof.* The proof follows from theorems 6 and 7 by the same arguments by which theorem 3 follows from theorems 1 and 2.

In theorems 6, 7 and 8 the requirement that $\theta^*$ be specified as part of the given data may be redundant if sufficient velocity components are specified by (2.3)–(2.5) to compute the integral in (6.4). In this case, the separate requirement (6.4) may be deleted.

The physical significance of specifying $\theta^*$ is illustrated by the following simple problem.

A hollow spherical cavity of radius $r_0$, centred at the origin, is surrounded by a uniform viscous liquid extending to infinity. Suppose the body forces are zero and the internal pressure in the cavity is $p_0$, a given constant. Find the creeping motion of the fluid.

The solution of this problem is

$$u_r = (p_0 - c_1) r_0^2 / 4\mu r^2, \tag{6.42}$$

which is not unique because $c_1$ is an arbitrary constant equal to the pressure at infinity which was not specified.

If the problem is augmented by requiring $\theta^*$ to be a given value, the solution is

$$u_r = \theta^* / 4\pi r^2, \tag{6.43}$$

which is unique. The stress tensor is now also unique. In effect, specifying $\theta^*$ determines the pressure at infinity.

## 7. Spatially periodic flows

Consider an infinite pipe whose cross-section is variable, but periodic with respect to a co-ordinate $x_1$ with periodicity $\lambda$. The walls of the pipe are fixed and rigid and may contain additional internal boundaries provided they are also fixed and rigid. Let the remaining space be filled with a viscous liquid containing liquid drops and solid particles which are also distributed periodically in $x_1$. Body forces $f_i$ are assumed to be periodic in $x_1$ also. It is assumed that the velocity field of any Stokes flow in the pipe under these conditions is periodic in $x_1$ and consists of a series of identical cells.

Each cell has two identical surfaces, say $S_a$ and $S_b$ in order of increasing $x_1$, spaced $\lambda$ apart. $S_a$ and $S_b$ need not be plane, but are chosen to extend entirely across the flow and not to intersect any liquid drops or solid particles. The remaining surface of the cell, say $S_c$, consists entirely of fixed boundaries. Hence

$$u_i = 0 \quad \text{on} \quad S_c. \tag{7.1}$$

Let the volume of a typical flow cell be $V$ with boundary $S$ equal to the sum of $S_a$, $S_b$ and $S_c$. Let $V$ contain $N_L$ liquid drops and $N_K$ rigid, solid particles. Let $V_0$, $V_L^{(l)}$, $V_K^{(k)}$ be the parts of $V$ occupied by suspending fluid, liquid drops and solid particles respectively with surfaces $S_0$, $S_L^{(l)}$ and $S_K^{(k)}$.

The discharge, $Q$, through the pipe must be the same for all cross-sections, i.e.

$$\int_{S'} u_n \, dS = Q \quad \text{all } S', \tag{7.2}$$

where $S'$ is any cross-section of the flow cell and $u_n$ is the component of velocity normal to $S'$. The discharge $Q$ includes suspending fluid, liquid drops and solid particles. The general problem considered is to find $\mathbf{u}(\mathbf{x})$ in $V$ satisfying (2.1), (2.2), (2.7)–(2.13), (7.1) and (7.2) with $Q$ given.

Substituting (2.11) in (2.2), it may be seen that since $f_i$ and $u_i$ are periodic, $p_{,i}$ is periodic in $x_1$ and $\partial p/\partial s$ is identical for corresponding paths on $S_a$ and $S_b$. Then by integrating along $S_a$ and $S_b$ it follows that any difference of pressures at corresponding points of $S_a$ and $S_b$ is the same constant, say $\Delta p$, for all pairs of corresponding points. A mean pressure gradient, $p_x$, is defined by

$$p_x = \Delta p/\lambda. \tag{7.3}$$

The dissipation $D[\mathbf{u}]$ in $V$ is given by (3.1). The excess dissipation $D_e'[\mathbf{u}]$ for the present case is defined by

$$D_e'[\mathbf{u}] = D[\mathbf{u}] - 2\int_V f_i u_i \, dV + 2\sum_{l=1}^{N_L} \sigma^{(l)} \dot{A}^{(l)}, \tag{7.4}$$

where $\dot{A}^{(l)}$ is given by (3.3).

THEOREM 9. *A minimum principle. Let* $\mathbf{u}(\mathbf{x})$ *be a continuous solution of a periodic Stokes flow problem satisfying* (2.1), (2.2), (2.7)–(2.13), (7.1) *and* (7.2). *Let* $\tilde{\mathbf{u}}(\mathbf{x})$ *be any continuous periodic velocity field which is piecewise continuously differentiable and satisfies* (2.1), (2.13), (7.1) *and* (7.2). *Then*

$$D_e'[\mathbf{u}] \leqslant D_e'[\tilde{\mathbf{u}}]. \tag{7.5}$$

The equality holds only if $\mathbf{u} = \tilde{\mathbf{u}}$.

*Proof.* Let $\tilde{\mathbf{u}} = \mathbf{u} + \tilde{\mathbf{u}}$. Then (3.5) and (3.6) apply in the present case also. Replacing $\mathbf{u}$ by $\tilde{\mathbf{u}}$ in (7.4), using (3.6) and Gauss's theorem yields

$$\begin{aligned} D_e'[\tilde{\mathbf{u}}] = {} & D[\mathbf{u}] + D[\tilde{\mathbf{u}}] + 2\int_{S_0} \tilde{u}_i \tau_{ij}^{(0)}[\mathbf{u}] n_j \, dS + 2\int_{V_0} f_i \tilde{u}_i \, dV \\ & - 2\sum_{l=1}^{N_L} \int_{S_L^{(l)}} \tilde{u}_i \tau_{ij}^{(l)}[\mathbf{u}] n_j \, dS + 2\sum_{l=1}^{N_L} \int_{V_L^{(l)}} f_i \tilde{u}_i \, dV \\ & - 2\int_V f_i (u_i + \tilde{u}_i) \, dV + 2\sum_{l=1}^{N_L} \sigma^{(l)} (\dot{A}^{(l)} + \dot{\tilde{A}}^{(l)}), \end{aligned} \tag{7.6}$$

where the notation is the same as in (3.7) except that in (7.6) $S_0$ is the sum of $S_a$, $S_b$, $S_c$, $S_L^{(l)}$ and $S_K^{(k)}$. The portion of the integral over $S_0$ in (7.6) associated with

$S_L^{(l)}$ and $S_K^{(k)}$ combines to nullify the same terms as in (3.7); the portion over $S_c$ is zero by (7.1). This leaves only the integrals over $S_a$ and $S_b$ which may be written

$$2\int_{S_a} \tilde{u}_i \tau_{ij}[\mathbf{u}] n_j dS + 2\int_{S_b} \tilde{u}_i \tau_{ij}[\mathbf{u}] n_i dS$$

$$= 2\int_{S_b} \tilde{u}_i [\tau_{ij}^{(b)}[\mathbf{u}] - \tau_{ij}^{(a)}[\mathbf{u}]] n_j dS. \tag{7.7}$$

The difference of the stress tensors on $S_b$ and $S_a$ represented by $\tau_{ij}^{(b)} - \tau_{ij}^{(a)}$ in (7.7) is equal to $\Delta p \delta_{ij}$ at every point. Further, the integral of $\tilde{u}_i n_i$ is zero over $S_b$ because $\tilde{\mathbf{u}}$ and $\mathbf{u}$ satisfy (7.2). Hence (7.7) is zero and (7.6) reduces to

$$D_e'[\tilde{\mathbf{u}}] = D_e'[\mathbf{u}] + D[\tilde{\mathbf{u}}]. \tag{7.8}$$

Then (7.5) follows from (7.8).

A maximum principle similar to theorem 2 for spatially periodic flows can be derived for suitably restricted comparison stress fields, $\bar{\tau}_{ij}$. The stress deviator of $\bar{\tau}_{ij}$ is required to be periodic in $x_1$ and the pressure $\bar{p}$ must exhibit a constant difference $\Delta\bar{p}$ for all pairs of corresponding points on $S_a$ and $S_b$ of the typical cell. Thus

$$\bar{\tau}_{ij} - \tfrac{1}{3}\bar{\tau}_{kk}\delta_{ij} = \text{periodic in } x_1, \tag{7.9}$$

$$[-\tfrac{1}{3}\bar{\tau}_{kk}]_A - [-\tfrac{1}{3}\bar{\tau}_{kk}]_B = \Delta\bar{p}, \tag{7.10}$$

where $\Delta\bar{p}$ is a constant and $A$ and $B$ are any pair of corresponding points on $S_a$ and $S_b$.

The excess power $H'[\tau_{ij}]$ is defined for a periodic Stokes flow having a discharge $Q$ and any stress field $\tau_{ij}$ satisfying (7.10) by

$$H'[\tau_{ij}] = 2Q\Delta p - \int_{V_0} \frac{1}{2\mu}(\tau_{ij} - \tfrac{1}{3}\tau_{kk}\delta_{ij})^2 dV$$

$$- \sum_{l=1}^{N_L} \int_{V_L^{(l)}} \frac{1}{2\mu}(\tau_{ij} - \tfrac{1}{3}\tau_{kk}\delta_{ij})^2 dV, \tag{7.11}$$

where $V_0$ and $V_L^{(l)}$ refer to the typical cell of the flow.

When the stress tensor $\tau_{ij}$ and concomitant pressure drop $\Delta p$ are those of a solution $\mathbf{u}(\mathbf{x})$ of the periodic Stokes flow problem with discharge $Q$, then

$$H'[\tau_{ij}] = D_e'[\mathbf{u}]. \tag{7.12}$$

To prove (7.12), we use (4.7) to show that

$$Q\Delta p = D[\mathbf{u}] + \sum_{l=1}^{N_L} \sigma^{(l)} \dot{A}^{(l)} - \int_V f_i u_i dV. \tag{7.13}$$

Substituting (7.13) in (7.11) and identifying terms with (7.4) yields (7.12).

THEOREM 10. *A maximum principle. Let* $\mathbf{u}(\mathbf{x})$ *be a continuous solution of a periodic Stokes flow problem satisfying* (2.1), (2.2), (2.7)-(2.13), (7.1) *and* (7.2). *Let* $\bar{\tau}_{ij}$ *be any stress tensor defined in* $V_0$ *and* $V_L^{(l)}$ *which is piecewise continuous*

*and piecewise continuously differentiable and satisfies* (2.2), (2.7)–(2.10), (7.9) *and* (7.10). *On surfaces of discontinuity of* $\bar{\tau}_{ij}$ *the traction* $n_i'\bar{\tau}_{ij}$ *is required to be continuous. Then*

$$D_e'[u] \geqslant H'[\bar{\tau}_{ij}]. \tag{7.14}$$

The equality holds only if $\bar{\tau}_{ij} = \tau_{ij}$ or $\bar{\tau}_{ij} = \tau_{ij} + p_0\delta_{ij}$ where $p_0$ is a constant.

*Proof.* Let $\bar{\tau}_{ij} = \tau_{ij} + \tilde{\tau}_{ij}$. Substituting $\bar{\tau}_{ij}$ in (7.11), using (4.10) and collecting terms as in (4.11) yields

$$\begin{aligned} H'[\bar{\tau}_{ij}] = H'[\tau_{ij}] &- \int_{V_0} \frac{1}{2\mu}(\tilde{\tau}_{ij} - \tfrac{1}{3}\tilde{\tau}_{kk}\delta_{ij})^2 dV \\ &- \sum_{l=1}^{N_L} \int_{V_L^{(l)}} \frac{1}{2\mu}(\tilde{\tau}_{ij} - \tfrac{1}{3}\tilde{\tau}_{kk}\delta_{ij})^2 dV \\ &- 2\int_{V_0} e_{ij}(\tilde{\tau}_{ij} - \tfrac{1}{3}\tilde{\tau}_{kk}\delta_{ij}) dV \\ &- 2\sum_{l=1}^{N_L} \int_{V_L^{(l)}} e_{ij}(\tilde{\tau}_{ij} - \tfrac{1}{3}\tilde{\tau}_{kk}\delta_{ij}) dV \\ &+ 2Q\Delta\tilde{p}, \end{aligned} \tag{7.15}$$

where $\Delta\tilde{p}$ is defined by (7.10) with $\bar{\tau}_{ij}$ replaced by $\tilde{\tau}_{ij}$. Equations (4.12) and (4.13) apply in the present case with $S_0$ equal to the sum of $S_a$, $S_b$, $S_c$, $S_L^{(l)}$ and $S_K^{(k)}$. Considering the fact that $\tilde{\tau}_{ij}$ satisfies conditions of the form (7.9) and (7.10), it is found that after substitution of (4.12) and (4.13) in (7.15) that (7.15) can be reduced to

$$\begin{aligned} H'[\bar{\tau}_{ij}] = H'[\tau_{ij}] &- \int_{V_0} \frac{1}{2\mu}(\tilde{\tau}_{ij} - \tfrac{1}{3}\tilde{\tau}_{kk}\delta_{ij})^2 dV \\ &- \sum_{l=1}^{N_L} \int_{V_L^{(l)}} \frac{1}{2\mu}(\tilde{\tau}_{ij} - \tfrac{1}{3}\tilde{\tau}_{kk}\delta_{ij})^2 dV. \end{aligned} \tag{7.16}$$

Theorem 10 follows from (7.16) and (7.12).

A uniqueness theorem for periodic Stokes flow can be derived from theorems 9 and 10 by the same arguments used to prove theorem 3. The result is

THEOREM 11. *Uniqueness theorem for periodic flows. A periodic solution* $\mathbf{u}(\mathbf{x})$ *of a periodic Stokes flow problem satisfying* (2.1), (2.2), (2.7)–(2.13), (7.1) *and* (7.2) *is unique for a given discharge* $Q$ *and the stress* $\tau_{ij}$ *is unique to within a uniform pressure.*

If $f_i$ is conservative so that it has a potential $\Omega$ and the solid particles and liquid drops are neutrally buoyant, theorems 9–11 can be simplified.

The condition that the suspended drops and particles be neutrally buoyant particles is equivalent to the requirement that $\Omega$ be continuous in $V$. Since $f_i$ is assumed to be periodic in $x_1$, any difference of $\Omega$ at corresponding points of $S_a$ and $S_b$ is a constant, i.e.

$$[\Omega]_A - [\Omega]_B = \Delta\Omega, \tag{7.17}$$

where $\Delta\Omega$ is a constant and $A$ and $B$ are any pair of corresponding points on $S_a$ and $S_b$. It follows that

$$\int_V u_i f_i dV = \int_V \bar{u}_i f_i dV, \tag{7.18}$$

where $u_i$ and $\bar{u}_i$ are the velocity fields in theorem 9. Proof of (7.18) follows by use of Gauss's theorem, (7.1), (7.2) and (7.17). Adding twice (7.18) to (7.5) yields

THEOREM 12. *If the suspended liquid drops and solid particles are neutrally buoyant and the body forces are conservative, then theorem* 9 *holds with* (7.5) *replaced by*

$$D[\mathbf{u}] + 2\sum_{l=1}^{N_L} \sigma^{(l)}\dot{A}^{(l)} \leqslant D[\bar{\mathbf{u}}] + 2\sum_{l=1}^{N_L} \sigma^{(l)}\dot{\bar{A}}^{(l)}. \tag{7.19}$$

Similarly, theorem 10 may be replaced by

THEOREM 13. *If the suspended liquid drops and solid particles are neutrally buoyant and the body forces are conservative, then theorem* 10 *holds with* (7.14) *replaced by*

$$D[\mathbf{u}] + 2\sum_{l=1}^{N_L} \sigma^{(l)}\dot{A}^{(l)} \geqslant H'[\bar{\tau}_{ij}] + 2Q\Delta\Omega. \tag{7.20}$$

The uniqueness theorem for periodic Stokes flows, theorem 11, remains unchanged whether the suspended drops and particles are neutrally buoyant or not.

If there are no liquid drops present, or if the shape of the liquid drops is assumed to be constant, the terms involving $\sigma^{(l)}$ in (7.19) and (7.20) do not appear and theorems 12 and 13 give bounds on the dissipation $D[\mathbf{u}]$ directly. In this case theorem 9 can be reformulated as follows:

THEOREM 14. *The solution* $\mathbf{u}(\mathbf{x})$ *of a periodic Stokes flow problem satisfying* (2.1), (2.2), (2.7)–(2.13), (7.1) *and* (7.2) *produces less dissipation than any other periodic flow* $\bar{\mathbf{u}}(\mathbf{x})$ *satisfying* (2.1), (7.1) *and* (7.2) *for the same discharge* $Q$ *provided* (i) $\bar{\mathbf{u}}(\mathbf{x})$ *is continuous and piecewise continuously differentiable*; (ii) *body forces are conservative*; (iii) *suspended solid particles and liquid drops are neutrally buoyant and of constant shape.*

Theorem 14 can be applied to the steady laminar flow of a uniform liquid with no suspended particles in an infinite pipe of any uniform cylindrical cross-section. Such a flow may be considered periodic with any periodicity $\lambda$, $0 < \lambda < \infty$. Then theorem 14 states that the laminar flow solution of this problem has less dissipation than any spatially periodic comparison flow of the same discharge. This is a result that was proved previously by Thomas (1942) for the case of uniform flow in a circular pipe.

Theorem 14 is also of interest for approximate computation of the pressure drop in a model of capillary blood flow in which the red blood cells are represented as deformed liquid drops of constant shape spaced periodically in a uniform circular tube.

This work was supported by the Office of Naval Research under Project NR 062-393.

## Appendix. Analyticity of $u_i$

The equations of motion (6.7) and continuity (2.1) may be written

$$\nabla^2 u_i = \frac{\partial F}{\partial x_i} \tag{A 1}$$

and $$u_{i,i} = 0, \tag{A 2}$$

where $$F = \frac{1}{\mu}(p + \Omega). \tag{A 3}$$

The equations (A 1) and (A 2) are identical in form to the equations of linear elasticity with Poisson's ratio equal to $\frac{1}{2}$ and zero body forces, as discussed by Duffin (1956). Assuming only that the derivatives in (A 1) and (A 2) exist and are continuous in an open domain $E$, Duffin (1956) proves that $F$ is harmonic, i.e. $\nabla^2 F = 0$ and hence $F$ is analytic in $E$. Now (A 1) may be regarded as Poisson's equation on $u_i$ where $F_{,i}$ is analytic. The differentiability theorem given by Courant & Hilbert (1962, p. 345) for a general second-order elliptic equation then ensures that $u_i$ is also analytic. Thus $F$ and $u_i$ possess derivatives of all orders.

## REFERENCES


Courant, R. & Hilbert, D. 1962 *Methods of Mathematic Physics*, vol. 2, New York: Interscience.

Duffin, R. J. 1956 *J. Rat. Mech. and Anal.* **5**, 939–950.

Gurtin, M. E. & Sternberg, E. 1961 *Arch. Rat. Mech. and Anal.* **8**, 99–119.

Keller, J. B., Rubenfeld, L. A. & Molyneux, J. E. 1967 *J. Fluid Mech.* **30**, 97–125.

Landau, L. D. & Lifshitz, E. M. 1959 *Fluid Mechanics*. London: Pergamon.

Thomas, T. Y. 1942 *Am. J. Math.* **64**, 754–67

*J. Fluid Mech.* (1970), *vol.* 42, *part* 3, *pp.* 549–559
*Printed in Great Britain*



# Shallow three-dimensional flows with variable surface tension

By J. ADLER AND L. SOWERBY
Department of Mathematics, Imperial College, London S.W. 7

(Received 8 August 1969)

The three-dimensional steady flow of a shallow viscous liquid with non-uniform surface tension has been considered when the variation in surface tension results from the presence of an insoluble chemical contaminant on the surface. Similarly solutions for the particular problem of a channel flowing into a semi-infinite lake have been obtained, the depth and surface concentration at infinity being specified.

## 1. Introduction

There are many physical situations in which fluid motion takes place with variable surface tension, and in recent years there has been considerable interest in such phenomena; Kenning (1968) refers to a hundred publications relating to work in this field. The variation of surface tension along the interface of a fluid gives rise to tangential stresses which effect the motion of the fluid. Variation in the surface tension can occur for several reasons; examples cited by Levich (1962) are variations in the surface temperature and electric charge and changes in concentration of a surface active material.

Fluid flow with a surface active contaminant is of industrial importance and also takes place under natural conditions. A variable surface tension has probably the greatest influence on shallow flows and a two-dimensional problem of this kind has been considered by Yih (1968). In Yih's problem two reservoirs of fluid are connected by an open shallow channel with the depths of fluid and surface concentration of contaminant maintained in each reservoir. Steady motion takes place in the channel under the action of liquid head and surface tension variation.

## 2. Statement of the problem

The purpose of our paper is the extension of Yih's analysis to three-dimensional flows. A thin layer of insoluble surface active material is assumed to lie on the surface of a region of shallow liquid, the thickness of the layer being negligible compared to the depth so that it is permissible to define the concentration in terms of the density $c$ per unit area. There is no transport of contaminant into the main body of the liquid; this occurs only along the surface. The surface tension $\sigma'$ is assumed to be related linearly to the concentration, namely

$$\sigma' = \sigma'_0 + \gamma c,$$

in which $\sigma_0'$ and $\gamma$ are constants. For the purpose of our analysis it is convenient to introduce the relative surface tension $\sigma$ where

$$\sigma = \sigma' - \sigma_0',$$

and we note that $\sigma$ generally takes negative values.

The variation of concentration and hence surface tension gives rise to tractive forces along the surface which through the action of viscosity are transmitted to the bulk of the fluid. The spatial variation of hydrostatic head and surface tension will produce a steady flow of varying depth, but we shall assume that such changes are sufficiently small for the surface curvature to be neglected.

The steady state problem considered by Yih is the determination of $\sigma$ and the depth $h$ of liquid in the channel connecting the two reservoirs. Depending on the depths of the reservoirs and the direction of flow of the contaminant, two distinct situations are possible, where the bulk flow is in the direction of increasing surface tension and where it is in the direction of decreasing surface tension. In this paper we shall consider in particular the corresponding problem in which a channel of fluid flows into a semi-infinite lake, with the surface material either flowing from or into the lake depending on the relative states of contamination.

## 3. Equations of motion

With $(x, y, z)$ as Cartesian co-ordinates, $z$ is measured vertically from the horizontal bed of the liquid, which is locally of depth $h(x, y)$. If $(u, v, w)$ are Cartesian components of velocity, the diffusion equation for the surface material can be written in terms of $\sigma(= \gamma c)$, and is

$$\frac{\partial}{\partial x}(u\sigma) + \frac{\partial}{\partial y}(v\sigma) = \frac{\partial}{\partial x}\left(D\frac{\partial \sigma}{\partial x}\right) + \frac{\partial}{\partial y}\left(D\frac{\partial \sigma}{\partial y}\right) \tag{3.1}$$

at $z = h$. Here $D$ is the diffusivity of the material in the surface, and this will be assumed to be constant, as also will be the viscosity $\mu$ and density $\rho$ of the liquid.

The equations of motion of the liquid are simplified, as in the case of lubrication theory, in that inertia terms are negligible and also the dominant element only in the viscosity terms need be retained. Thus, if $p$ denotes the difference between the fluid pressure and the atmospheric pressure, the equations become

$$\left.\begin{aligned} \frac{\partial p}{\partial x} &= \mu \frac{\partial^2 u}{\partial z^2}, \\ \frac{\partial p}{\partial y} &= \mu \frac{\partial^2 v}{\partial z^2}, \\ \frac{\partial p}{\partial z} &= -\rho g, \end{aligned}\right\} \tag{3.2}$$

with the equation of continuity

$$\frac{\partial u}{\partial x} + \frac{\partial v}{\partial y} + \frac{\partial w}{\partial z} = 0. \tag{3.3}$$

Boundary conditions at $z = 0$ are

$$u = v = w = 0, \tag{3.4}$$

and at the free surface $z = h$, continuity of stress components requires that

$$\left.\begin{aligned} \mu \frac{\partial u}{\partial z} &= \frac{\partial \sigma}{\partial x}, \\ \mu \frac{\partial v}{\partial z} &= \frac{\partial \sigma}{\partial y}, \\ p &= 0, \end{aligned}\right\} \tag{3.5}$$

and

in which the assumption of small surface curvature is implicit. Finally, there is the kinematical boundary condition at the free surface, namely at $z = h$,

$$w = u\frac{\partial h}{\partial x} + v\frac{\partial h}{\partial y}. \tag{3.6}$$

## 4. The field equations for $\sigma$ and $h$

Both $\sigma$ and $h$ are functions of $x$ and $y$ only, and so also are $\partial p/\partial x$, $\partial p/\partial y$ (from equations (3.2)). Thus a solution of equations (3.2) for $u$ and $v$, satisfying the boundary conditions (3.4) and (3.5), is

$$\left.\begin{aligned} u &= \frac{1}{\mu}\frac{\partial \sigma}{\partial x} z - \frac{1}{2\mu}\frac{\partial p}{\partial x} z(2h - z), \\ v &= \frac{1}{\mu}\frac{\partial \sigma}{\partial y} z - \frac{1}{2\mu}\frac{\partial p}{\partial y} z(2h - z), \end{aligned}\right\} \tag{4.1}$$

and the solution for $p$ is clearly

$$p = \rho g(h - z). \tag{4.2}$$

Levich (1962) and Yih (1968) obtained expressions similar to these for the two-dimensional channel flow problem.

With the introduction of the two-dimensional gradient operator

$$\nabla \equiv (\partial/\partial x, \partial/\partial y, 0),$$

result (4.2) yields

$$\nabla p = \rho g \nabla h,$$

and thus from (4.1), the velocity components in the surface are given by

$$(u_h, v_h) = \frac{h}{\mu}\nabla(\sigma - \tfrac{1}{4}\rho g h^2).$$

These surface values, when substituted in the diffusion equation (3.1), give the equation

$$\frac{\partial}{\partial x}\left\{\frac{h\sigma}{\mu}\frac{\partial}{\partial x}(\sigma - \tfrac{1}{4}\rho g h^2)\right\} + \frac{\partial}{\partial y}\left\{\frac{h\sigma}{\mu}\frac{\partial}{\partial y}(\sigma - \tfrac{1}{4}\rho g h^2)\right\} = D\left(\frac{\partial^2 \sigma}{\partial x^2} + \frac{\partial^2 \sigma}{\partial y^2}\right). \tag{4.3}$$

The equation of continuity (3.3), when integrated with respect to $z$ between the limits $z = 0, h$, yields with use of result (3.6),

$$\frac{\partial}{\partial x}\int_0^h u\,dz + \frac{\partial}{\partial y}\int_0^h v\,dz = 0.$$

After performing the integration with respect to $z$ of expressions (4.1), this last equation becomes

$$\frac{\partial}{\partial x}\left\{h^2\frac{\partial}{\partial x}(\sigma - \tfrac{1}{3}\rho g h^2)\right\} + \frac{\partial}{\partial y}\left\{h^2\frac{\partial}{\partial y}(\sigma - \tfrac{1}{3}\rho g h^2)\right\} = 0. \tag{4.4}$$

Equations (4.3) and (4.4) are thus the required field equations.

## 5. Similarity solution of the field equations

The field equations appear to be intractable as they stand, but it is possible to derive solutions of physical interest in the following manner. Postulate the existence of scalar fields $\phi(x, y)$, $\psi(x, y)$ defined by

$$h\sigma\nabla(\sigma - \tfrac{1}{4}\rho g h^2) - \mu D\nabla\sigma = \mu\nabla\phi, \tag{5.1}$$

$$h^2\nabla(\sigma - \tfrac{1}{3}\rho g h^2) = 2\mu\nabla\psi. \tag{5.2}$$

Equations (4.3), (4.4) imply therefore that

$$\nabla^2\phi = \nabla^2\psi = 0. \tag{5.3}$$

Further, on forming the curl of either (5.1) or (5.2) we derive the result

$$\nabla h \times \nabla\sigma = 0;$$

i.e.

$$J(\sigma, h) \equiv \frac{\partial\sigma}{\partial x}\frac{\partial h}{\partial y} - \frac{\partial\sigma}{\partial y}\frac{\partial h}{\partial x} = 0. \tag{5.4}$$

Thus $h$ and $\sigma$ are functionally related, so there exists a family of curves in the $(x, y)$ plane on each member of which $h$ and $\sigma$ assume constant values. We may thus introduce a curvilinear co-ordinate $\xi(x, y)$ so that the family is the system

$$\xi(x, y) = \text{const.},$$

and $h$ and $\sigma$ are functions of $\xi$ alone. If further we set $\phi = k_1(\xi - 1)$, $\psi = k_2(\xi - 1)$, where $k_1$, $k_2$ are constant, then $\xi$ must be harmonic, and equations (5.1), (5.2) become the ordinary differential equations

$$h\sigma\frac{d}{d\xi}(\sigma - \tfrac{1}{4}\rho g h^2) - \mu D\frac{d\sigma}{d\xi} = k_1\mu, \tag{5.5}$$

$$h^2\frac{d}{d\xi}(\sigma - \tfrac{1}{3}\rho g h^2) = 2k_2\mu, \tag{5.6}$$

and these are equivalent to the equations derived by Yih for the two-dimensional problem. We note also, from expressions (4.1), that the component of fluid velocity parallel to the base $z = 0$ is everywhere in the direction $\nabla\xi$.

The nature of the constants $k_1$, $k_2$ is not apparent from this approach, but alternatively the direct postulation of a similarity solution of (4.3), (4.4), namely $\sigma = \sigma(\xi)$, $h = h(\xi)$ leads to the conclusion that $\xi$ must be harmonic and (4.3), (4.4) then have first integrals as exhibited in (5.5), (5.6). Thus $k_1$, $k_2$ are constants associated with the surface and bulk flows respectively.

## 6. The characteristic equation

Equations (5.5) and (5.6) can be rewritten in the form

$$(h\sigma - 4\mu D)\frac{d\sigma}{d\xi} = \mu\left(4k_1 - \frac{6\sigma}{h}k_2\right), \tag{6.1}$$

$$(h\sigma - 4\mu D)\frac{dh}{d\xi} = \frac{6\mu}{\rho g h}\left\{k_1 + \frac{2k_2}{h^2}(\mu D - h\sigma)\right\}. \tag{6.2}$$

It is clear from the form of these equations that it is necessary only to consider the two cases $k_1, k_2 > 0$ and $k_1 < 0$, $k_2 > 0$. The co-ordinate $\xi$ is already dimensionless, and the following substitutions may be used to reduce equations (6.1), (6.2) to non-dimensional form:

(i) $k_1, k_2 > 0$.

$$\left.\begin{aligned} B &= 6\mu D k_1 k_2, \quad \alpha = \frac{3k_1 k_2}{2DB^{\frac{1}{2}}}, \quad \beta = \frac{k_1^3}{2\rho g D B}, \\ \sigma &= \frac{2B^{\frac{1}{2}}Y}{3k_2}, \quad h = \frac{B^{\frac{1}{2}}X}{k_1}. \end{aligned}\right\} \tag{6.3}$$

The above equations now become:

$$(XY - 1)\frac{dY}{d\xi} = \frac{\alpha}{X}(X - Y), \tag{6.4}$$

$$(XY - 1)\frac{dX}{d\xi} = \frac{\beta}{X^3}(3X^2 - 4XY + 1). \tag{6.5}$$

The characteristic, or phase-plane, equation deduced from this pair is thus

$$\frac{dY}{dX} = \frac{CX^2(X - Y)}{3X^2 - 4XY + 1}, \tag{6.6}$$

where $C = \alpha/\beta$.

(ii) $k_1 < 0$, $k_2 > 0$.

In this case the substitutions

$$\left.\begin{aligned} B &= -6\mu D k_1 k_2, \quad \alpha = \frac{3k_1 k_2}{2DB^{\frac{1}{2}}}, \quad \beta = \frac{k_1^3}{2\rho g D B}, \\ \sigma &= \frac{2B^{\frac{1}{2}}Y}{3k_2}, \quad h = -\frac{B^{\frac{1}{2}}X}{k_1}, \end{aligned}\right\} \tag{6.7}$$

lead to the equations

$$(XY - 1)\frac{dY}{d\xi} = \frac{\alpha}{X}(X + Y), \tag{6.8}$$

$$(XY - 1)\frac{dX}{d\xi} = \frac{\beta}{X^3}(3X^2 + 4XY - 1), \tag{6.9}$$

with characteristic equation

$$\frac{dY}{dX} = \frac{CX^2(X+Y)}{3X^2+4XY-1}, \tag{6.10}$$

and $C = \alpha/\beta$.

Since $h$ is essentially positive and $\sigma$ negative, the region of physical interest in both (i) and (ii) corresponds to $X > 0$, $Y < 0$. Also $C$ is positive in both cases, with $\alpha$, $\beta$ positive in (i), and negative in (ii).

## 7. Diffusion from a channel into a semi-infinite lake

The lake occupies the region $x \geqslant 0$ in the $(x, y)$ plane and the channel extends in the negative $x$ direction, its mouth being represented by the line $x = 0$, $-a \leqslant y \leqslant a$. It is supposed that $k_1, k_2 > 0$, and that the following boundary conditions apply:

$\sigma$ and $h$ have constant prescribed values on $x = 0$, $|y/a| \leqslant 1$; $\sigma \to \sigma_1$, $h \to h_1$ ($\sigma_1, h_1$ constant) as $x/a$ and $|y/a| \to \infty$; $\sigma \to \sigma_1$, $h \to h_1$ on $x = 0$, $|y/a| > 1$.

Clearly $x$, $y$ can be made non-dimensional by a simple change of variable, so that if they are now interpreted in this dimensionless form, the harmonic function $\xi$ can be set to have boundary conditions

$$\begin{aligned} &\xi = 0, \quad \text{for} \quad x = 0, \quad |y| \leqslant 1, \\ &\xi = 1, \quad \text{for} \quad x = 0, \quad |y| > 1, \\ &\xi \to 1 \quad \text{as} \quad x, \quad |y| \to \infty. \end{aligned}$$

(The region in which a solution is required is $x \geqslant 0$.)

A solution of Laplace's equation suitable for these boundary conditions can be written

$$\xi(x, y) = 1 - \left(\frac{2}{\pi}\right)^{\frac{1}{2}} \int_0^\infty f(\lambda)\, e^{-\lambda x} \cos \lambda y \, d\lambda.$$

Thus

$$\xi(0, y) = 1 - \left(\frac{2}{\pi}\right)^{\frac{1}{2}} \int_0^\infty f(\lambda) \cos \lambda y \, d\lambda,$$

and hence from the theory of Fourier transforms,

$$f(\lambda) = \left(\frac{2}{\pi}\right)^{\frac{1}{2}} \int_0^\infty \{1 - \xi(0, y)\} \cos \lambda y \, dy = \left(\frac{2}{\pi}\right)^{\frac{1}{2}} \int_0^1 \cos \lambda y \, dy$$

$$= \left(\frac{2}{\pi}\right)^{\frac{1}{2}} \frac{\sin \lambda}{\lambda}.$$

Hence

$$\xi = 1 - \frac{2}{\pi} \int_0^\infty e^{-\lambda x} \frac{\sin \lambda}{\lambda} \cos \lambda y \, d\lambda,$$

and evaluation of the integral now leads to the result

$$\xi = 1 - \frac{1}{\pi} \tan^{-1}\left(\frac{2x}{x^2+y^2-1}\right). \tag{7.1}$$

The curves $\xi = \text{const.}$ are thus

$$(x + \cot(\pi\xi))^2 + y^2 = \operatorname{cosec}^2(\pi\xi), \tag{7.2}$$

which is a system of coaxal circles, with common points $(0, \pm 1)$, centres $(-\cot(\pi\xi), 0)$ and radii $\operatorname{cosec}(\pi\xi)$.

Some degree of idealization is involved in solving the problem subject to the above boundary conditions. What one would expect physically are rapid changes in contaminant concentration and liquid depth along the boundary near the mouth of the channel but that these quantities remain nearly constant thereafter. Our solution has transformed the changes into the singular points $(0, 1)$ and $(0, -1)$ at the corners of the channel. Such an assumption does in fact imply that the solution is not valid near the corners since the surface curvature will not be negligible in these regions.

We show that the boundary conditions are compatible with the requirement that the components of surface velocity at the edge of the lake shall vanish. The conditions

$$u_h = v_h = 0, \quad \text{for} \quad x = 0, \quad |y| > 1,$$

imply that

$$\xi = 1: \quad \frac{d\sigma}{d\xi} - \tfrac{1}{2}\rho g h \frac{dh}{d\xi} = 0. \tag{7.3}$$

With changes of variable (6.3), this is equivalent to

$$\xi = 1: \quad \frac{dY}{d\xi} - \tfrac{1}{4}CX\frac{dX}{d\xi} = 0. \tag{7.4}$$

The condition (7.4) must be compatible with differential equation (6.6), so that

$$\xi = 1: \quad \frac{dY}{dX} = \tfrac{1}{4}CX = \frac{CX^2(X-Y)}{3X^2 - 4XY + 1}, \tag{7.5}$$

from which it follows that $X = 1$, for all $Y$. This boundary value for $X$ has been used in subsequent numerical integrations.

## 8. Numerical results

This section refers to the solution of equations (6.4) and (6.5), but for the purpose of discussion it is convenient to refer also to the particular physical problem of §7. The trapezoidal rule, with one iteration, was used to solve the equations, and the calculations were performed on the IBM 7094 computer at Imperial College.

For given physical parameters, the ratio $k_1/k_2$ determines the dimensionless height $X$ in terms of the physical height $h$, and also the value of $C$. Equations (6.4), (6.5) were solved for $X$ and $Y$ in the range $0 \leqslant \xi \leqslant 1$, corresponding to the whole of the physical space in §7. As explained in §7 the fixed height $X = 1$ was taken at $\xi = 1$; the value of $Y$ at the same point was set at $-1$. For the solutions presented here, the value of $C$ $(= \alpha/\beta)$ was set at 1, 10, and 0·1 respectively, but $\alpha$ and $\beta$ were increased separately for each case. The corresponding graphs of $X$, $Y$ *versus* $\xi$ are displayed in figures 1, 2, and 3. From the viewpoint of the problem considered in §7, these solutions represent a situation in which the outflow from the channel has a lower concentration of surface contaminant than that existing on the lake at great distances from the channel mouth. Thus $Y$ decreases from a

small negative value at $\xi = 0$ to the value $-1$ at $\xi = 1$, and in each case the decrease appears to be monotonic. Essentially, in place of prescribing $X$ and $Y$ at $\xi = 0$, the values of $\alpha$ and $\beta$ have been prescribed. Thus the solutions yield the corresponding values of $X$ and $Y$ at $\xi = 0$. In particular the computations were

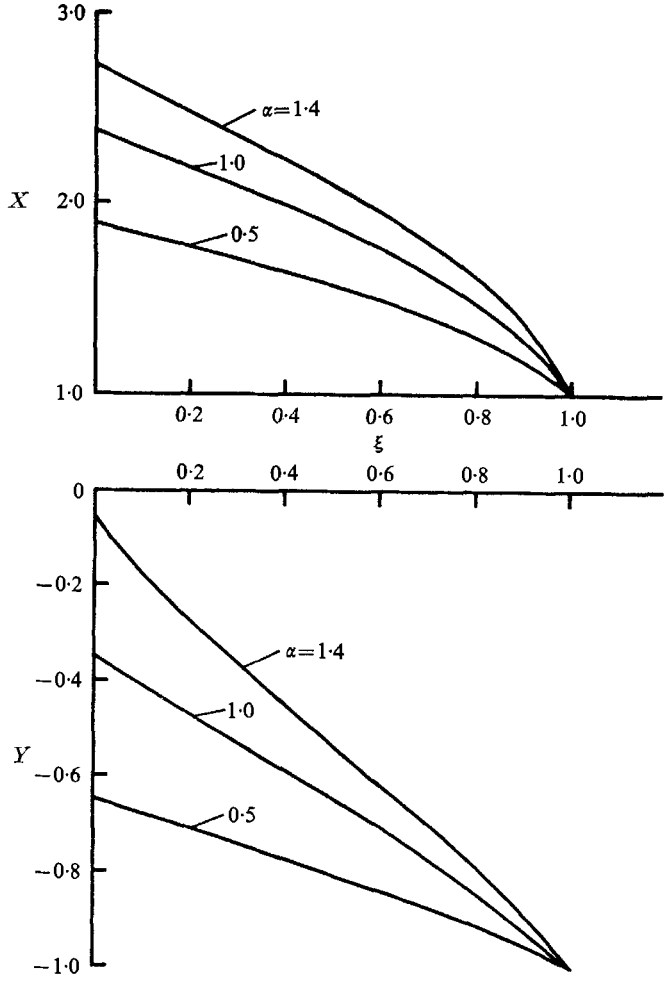


FIGURE 1. Curves of $X$ and $Y$ *versus* $\xi$ for $C = 1$.

arranged to produce, for each value of $C$, one solution for which the value of $Y$ was close to zero at $\xi = 0$. Such a solution can be seen in each of the three figures, and represents a situation in which the outflow from the channel is almost free of surface contaminant.

## 9. Discussion

The comparison of equations (5.5) and (5.6) with the corresponding equations of the two-dimensional problem shows that the constants, $k_1$, $k_2$ are associated with the surface and bulk flows respectively. In the case of flow from a channel

into a semi-infinite lake they are proportional to the constant surface flux and constant bulk flux per unit width of channel. In view of the relationship between surface tension and surface concentration, the condition $k_1 > 0$ implies that surface material is flowing out of the lake and here the bulk flow is in the direction of falling surface tension. Similarly $k_1 < 0$ implies that contaminant is flowing into the lake, with the bulk flow in the direction of increasing surface tension.

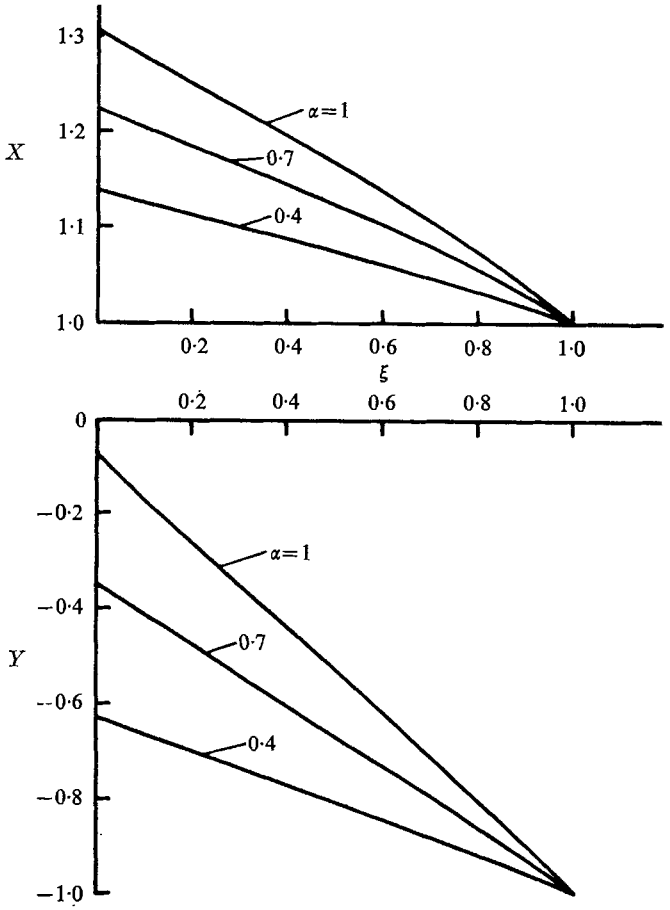


FIGURE 2. Curves of $X$ and $Y$ *versus* $\xi$ for $C = 10$.

Solutions of the flow equations have been obtained in similarity form, but such solutions will not always exist since it may not be possible to satisfy the boundary conditions. In the problem of a channel flowing into a semi-infinite lake the situation has been idealized to some extent by assuming a constant depth and constant concentration of contaminant across the mouth of the channel. The similarity solution implies that maximum changes in surface tension occur along lines of greatest slope in the surface, which appears to be a reasonable result on physical grounds.

In his analysis of the two-dimensional channel flow problem, Yih considered

two physical situations—where the bulk flow is zero, and where the velocity component in the surface is zero, respectively. The solutions corresponding to zero surface flow appear to be inconsistent since the equation of continuity is not satisfied. A more serious error arises in connexion with equation (1) of Yih's paper, which is essentially the transport equation for the surface contaminant. The quantity $\sigma$ used by Yih is the relative surface tension, which for an insoluble

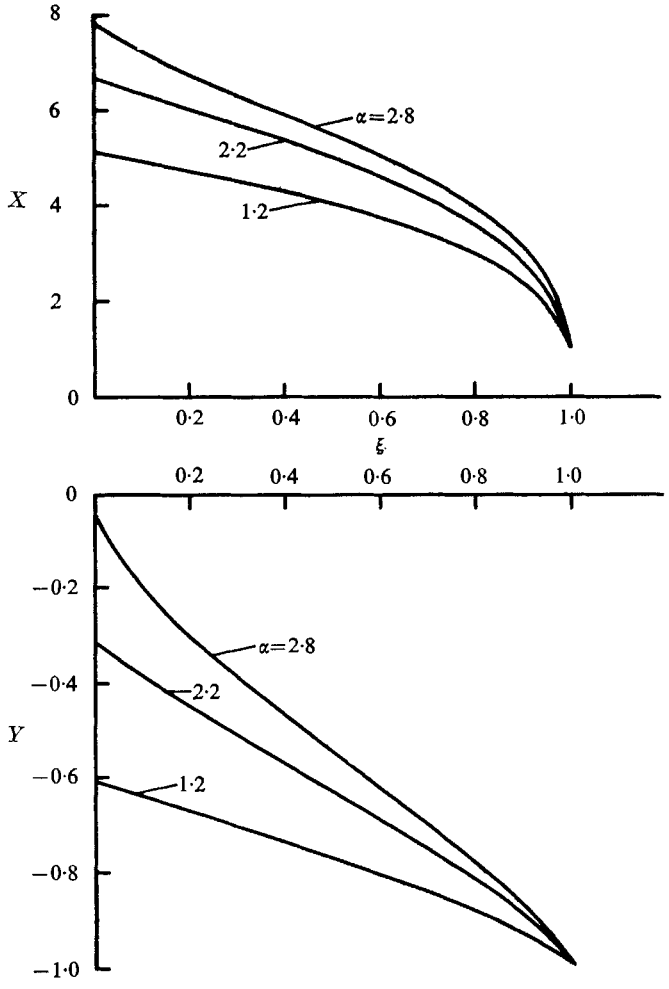


FIGURE 3. Curves of $X$ and $Y$ *versus* $\xi$ for $C = 0{\cdot}1$.

surface active agent is generally negative. This invalidates the discussion concerning the possible instability of the flow, since inequalities of the kind considered, equation (20), can no longer arise. The result that the flow is always stable may be obtained by examining the phase plane equation (6.6) of our paper, the region of physical interest being $X \geqslant 0$, $Y \leqslant 0$. Possible cusp-like solutions are associated with integral curves crossing the curve $XY = 1$. Associated with equation (6.6) are two singular points, (1, 1) and $(-1, -1)$; for a certain range of the parameter $C$ a limit cycle encloses the point (1,1) but this lies entirely in the

region $X > 0$, $Y > 0$. It follows that flow instabilities associated with the cusp curve or with a limit cycle cannot arise.

Yih (1969) has recently considered the three-dimensional motion of a shallow liquid layer with variable surface tension, for the situation where $\Delta\sigma \gg \rho g h_0^2$, $\Delta\sigma$ being a characteristic change in $\sigma$ and $h_0$ a vertical scale. Under these conditions the flow is independent of gravity and the pressure constant throughout the fluid. He finds the depth and surface tension to be functionally related and shows that a simple polynomial of the depth is a harmonic function of the horizontal co-ordinates $x$ and $y$. The flow near vertical boundaries is dealt with by considering a velocity boundary layer whose thickness is of the same order as the depth. An explicit solution for the velocity distribution in the layer is given, for the case where the angle of contact between the free surface and the boundary is $\frac{1}{2}\pi$.

## REFERENCES

KENNING, D. B. R. 1968 Two-phase flow with nonuniform surface tension. *Appl. Mech. Rev.* **21**, 1101–1111.

LEVICH, V. G. 1962 *Physicochemical Hydrodynamics*. New Jersey: Prentice Hall.

YIH, C-S. 1968 Fluid motion induced by surface tension variation. *Phys. Fluids*, **11**, 477–480.

YIH, C-S. 1969 Three-dimensional motion of a liquid film induced by surface tension variation or gravity. *Phys. Fluids*, **12**, 1982–1987.

*J. Fluid Mech.* (1970), *vol.* 42, *part* 3, *pp.* 561–584
*Printed in Great Britain*



# Trailing-edge stall

By S. N. BROWN AND K. STEWARTSON
Department of Mathematics, University College, London W.C. 1

(Received 18 July 1969)

A study is made of the laminar flow in the neighbourhood of the trailing edge of an aerofoil at incidence. The aerofoil is replaced by a flat plate on the assumption that leading-edge stall has not taken place. It is shown that the critical order of magnitude of the angle of incidence $\alpha^*$ for the occurrence of separation on one side of the plate is $\alpha^* = O(R^{-\frac{1}{16}})$, where $R$ is a representative Reynolds number, for incompressible flow, and $\alpha^* = O(R^{-\frac{1}{4}})$ for supersonic flow. The structure of the flow is determined by the incompressible boundary-layer equations but with unconventional boundary conditions. The complete solution of these fundamental equations requires a numerical investigation of considerable complexity which has not been undertaken. The only solutions available are asymptotic solutions valid at distances from the trailing edge that are large in terms of the scaled variable of order $R^{-\frac{3}{8}}$, and a linearized solution for the boundary layer over the plate which gives the antisymmetric properties of the aerofoil at incidence. The value of $\alpha^*$ for which separation occurs is the trailing-edge stall angle and an estimate is obtained from the asymptotic solutions. The linearized solution yields an estimate for the viscous correction to the circulation determined by the Kutta condition.

## 1. Introduction

The flow near the trailing edge of a flat plate aligned with a uniform stream in an incompressible viscous fluid has recently been studied by both Stewartson (1969) and Messiter (1969). Both authors showed that when the Reynolds number $R$ is large the flow in the neighbourhood of the trailing edge of the plate has a complicated three-layer or triple-deck structure. This triple deck is similar to that encountered by Stewartson & Williams (1969) in their investigation of the self-induced separation of supersonic flow. In the sublayer, of thickness $O(R^{-\frac{5}{8}})$, the appropriate equations are the incompressible boundary-layer equations but with boundary conditions involving a match with the main deck, which is essentially inviscid; additionally, in the trailing-edge problem, matching is necessary both with the Blasius (1908) solution upstream and the Goldstein (1930) wake solution downstream. The numerical solution of the sublayer equations successfully carried out by Stewartson & Williams (1969) was aided by the fact that the upper-deck equation in the supersonic case is the wave equation rather than the potential equation. This leads to a slightly simplified outer boundary condition in the lower deck.

The cause of this triple deck in the trailing-edge problem is the change in boundary condition at the trailing edge $O$ from zero tangential velocity to zero stress on the line of symmetry. The effect of the triple deck is to induce a favourable pressure gradient upstream of $O$. The transition of the solution through $O$ is achieved by the Rott & Hakkinen (1965) similarity solution. Downstream of the trailing edge the pressure increases, slightly overshooting its main-stream value before tending to it from above.

The present paper extends the work of Stewartson (1969) to the case when the plate is at a small angle of incidence to the oncoming stream. The purpose of the study is to estimate the circulation around a two-dimensional aerofoil at incidence when the effect of viscosity is taken into account. When the viscosity is zero this is determined by the Kutta condition. We also aim to elucidate some of the phenomena of trailing-edge stall. We make the assumption that the ratio of the thickness of the aerofoil to the angle of incidence is large enough for the fluid not to separate at the leading edge, and that the flow remains attached over the forward part of the body. Thus the boundary layer approaches the trailing edge in an adverse pressure gradient on the upper side of the aerofoil, though the incidence induces a favourable pressure gradient on the lower side. Within a distance $O(R^{-\frac{3}{8}})$ of $O$ the effect of the triple deck, discussed above for the symmetrically disposed plate, makes itself felt. The boundary layer on the upper side of the aerofoil thus experiences a favourable pressure gradient which tends to counteract the adverse gradient due to the incidence. If the angle of incidence is large the flow separates before it is influenced by the triple deck, and if the angle is too small the effect of the triple deck outweighs that of the incidence and the boundary layer remains attached right to the trailing edge. If, however, the angle of incidence $\alpha^*$ is $O(R^{-\frac{1}{16}})$ the two effects are comparable, and we postulate the existence of a critical angle $R^{-\frac{1}{16}}\alpha_s$ at which trailing-edge stall is liable to occur since the flow just separates on the upper side of the aerofoil.

In order to bring out the essential features of the trailing-edge problem unencumbered by complicated geometry, we replace the aerofoil by a flat plate at incidence in a uniform stream. This simplifies the main-stream velocity, and justification for the replacement is discussed in § 2. The flow upstream of the trailing edge is then the Blasius flow plus a perturbation that is $O(\alpha^*)$. At this stage the flow on the lower side of the plate is obtained from that on the upper side by changing the sign of $\alpha^*$. These two boundary layers then separately enter the triple deck which is centred on $O$ and of thickness $O(R^{-\frac{3}{8}})$. The equations that then hold in the lower deck have more complicated boundary conditions than in the case of the symmetrically disposed plate, as the unknown functions that appear in them are no longer the same on both sides of the plate. At $O$ the boundary condition of zero velocity on the plate is abandoned and instead the pressure must be continuous across the wake. Downstream the solution must finally become that of the Goldstein wake though with the centre line displaced. The equations for the fundamental problem of the lower deck are set up, though a full numerical solution has not yet been undertaken. However, it is shown that the partial differential equations have the correct asymptotic behaviour both upstream, where they match with the perturbed Blasius solution, and

downstream where they match with the modified Goldstein wake mentioned above. In this asymmetric problem the transition through the trailing edge itself is achieved by an extension of the Rott & Hakkinen (1965) solution for the symmetrically disposed plate.

Although the complete solution remains to be computed for the plate at both zero and non-zero incidence, the asymmetry of the flow about the aerofoil at incidence enables some of the features of the flow to be deduced from a linearized solution of the equation. Upstream of the trailing edge it is reasonable to linearize about the linear shear with which the streamwise velocity must match at the outer edge of the lower deck. A solution of the resulting equation for the difference in the streamwise velocity components on the top and bottom of the plate is then obtainable by Wiener–Hopf arguments without the need to solve for the boundary layer in the wake. This equation involves the anti-symmetric part of the unknown pressure which must vanish downstream of the trailing edge. The resulting solution, whose asymptotic form is correct both upstream and downstream of $O$, is consistent with the predicted behaviour of the solution of the full non-linear equations and leads to an estimate of the viscosity correction to the circulation given by the Kutta condition.

The final section of the paper describes the modifications required if the fluid is compressible. If the flow is subsonic the incompressible results carry over with a scaling involving the Mach number and temperature at infinity. If it is supersonic the critical angle of incidence for separation and trailing-edge stall to occur is $\alpha^* = O(R^{-\frac{1}{4}})$. In this case the boundary conditions for the lower-deck problem are similar to those of Stewartson & Williams (1969).

## 2. The exterior inviscid flow

Consider a two-dimensional aerofoil of length $l$ with a sharp trailing edge in an infinite incompressible fluid of density $\rho$ and kinematic viscosity $\nu$. At infinity the velocity of the fluid is uniform and of magnitude $U_\infty$, and the aerofoil, which is without camber, is fixed at an angle $\alpha^*$ to the direction of the undisturbed stream. The design of the aerofoil is such that the flow over it is smooth and attached except possibly in the immediate neighbourhood of the trailing edge. For leading-edge separation to be avoided it is necessary to have the thickness ratio $\tau$ of the body very much greater than the angle of attack. If $\tau = O(\alpha^*)$, so that the two quantities are of the same order, the initial stagnation point is followed by a region of rapid pressure fall on one side of the aerofoil and then by a region of adverse pressure gradient which can provoke separation and long or short bubbles of reversed flow. Here we wish to exclude this phenomenon so that we can concentrate on trailing-edge stall and so we take $\tau \gg \alpha^*$. However, we wish to keep the external inviscid flow as simple as possible and consequently it would be convenient to replace the aerofoil by a flat plate at incidence $\alpha^*$ since this is sufficient to bring out the essential features of the trailing-edge flow. Since trailing-edge stall is estimated to occur when $\alpha^* = O(R^{-\frac{1}{10}})$, consideration of this simpler geometry may formally be justified if we suppose, for example, that the aerofoil has thickness ratio $\tau = O(R^{-\frac{1}{32}})$ in which case leading-edge separation

will not occur. Here $R = U_\infty l/\nu$ is the Reynolds number and is taken to be large, though the flow is assumed to remain laminar and steady throughout. The effect of a non-zero trailing-edge angle $\beta^*$ is of secondary importance if $\beta^*$ is sufficiently small since, as shown by Riley & Stewartson (1969), the flow does not separate over a symmetrically-disposed wedge if $\beta^* \ll R^{-\frac{1}{4}}$. A similar situation occurs for a cusped trailing edge. We take $\beta^* \ll R^{-\frac{1}{4}}$, so that the effect of the trailing-edge angle is negligible compared with that of the incidence. Although we shall concentrate on a flat plate from now on, our results may easily be generalized to include aerofoils of thickness ratio $\tau = O(1)$. The only modification necessary is to the external inviscid flow, which in the neighbourhood of the trailing edge has the same structure as for a flat plate.

The plate is taken to occupy the strip $-l < x^* < 0$ of the $x^*$ axis with the origin of co-ordinates at the trailing edge. The velocity components in the $x^*$, $y^*$ directions are $u^*$, $v^*$ respectively and at an infinite distance upstream, i.e. as $x^* \to -\infty$, we have, making use of the assumption that $\alpha^* \ll 1$,

$$u^* \to U_\infty, \quad v^* \to U_\infty \alpha^*. \tag{2.1}$$

Since leading-edge separation has not occurred, and the Reynolds number is large, it is legitimate to expect that the flow is inviscid almost everywhere, the exceptions being the neighbourhood of the flat plate and the wake extending downstream from the trailing edge. The inviscid solution outside these regions is well-known and has the properties that on the flat plate ($y^* = 0$, $-l < x^* < 0$)

$$v^* = 0, \quad u^* = U_\infty - U_\infty \alpha^* \frac{x^* + B}{[(-x^*)(l + x^*)]^{\frac{1}{2}}} \operatorname{sgn} y^*, \tag{2.2}$$

and on the wake centre line ($y^* = 0$, $x^* > 0$)

$$u^* = U_\infty, \quad v^* = U_\infty \alpha^* \frac{x^* + B}{[x^*(l + x^*)]^{\frac{1}{2}}}, \tag{2.3}$$

where $B$ is a constant to be determined.

The constant $B$ is usually determined by the Kutta condition applied at the trailing edge. An interpretation of this condition, which implies $B = 0$, is that a stagnation point on the upper side of the plate near the trailing edge is to be excluded. If such a stagnation point occurs it is argued that the boundary layer must separate further upstream on that side of the plate. The lift coefficient derived from (2.2) is

$$C_L = 2\pi\alpha^* \left(1 - \frac{2B}{l}\right), \tag{2.4}$$

and if $B = 0$ it is broadly in line with experiment for small $\alpha^*$. However, the inviscid theory, in conjunction with the Kutta condition, does not explain why, at some value of $\alpha^*$, usually between 5° and 15°, catastrophic stall, nevertheless, sets in. The contribution to the theoretical explanation of the observed flow properties to be made here may be summarized as follows. First, if $\alpha^*$ is sufficiently small no separation occurs. The reason for this is that the change in character of the boundary layer as the trailing edge is approached induces a favourable pressure gradient which dominates the adverse pressure gradient implied by (2.2). Secondly, when $\alpha^*$ is of a critical order of magnitude, in fact

when $\alpha^* = O(R^{-\frac{1}{16}})$, the boundary layer associated with the main stream (2.2) must always separate before $x^* = 0$. Stall begins, therefore, when $\alpha^*$ is large enough to cause the boundary layer to separate before the induced favourable pressure gradient is able to make its impact. In these circumstances it emerges that the constant $B = O(R^{-\frac{3}{8}}l)$ which results in a stagnation point of the inviscid flow at a distance $-x^*/l = O(R^{-\frac{7}{8}})$ upstream of the trailing edge. In order to quantify this argument we now consider the boundary layer corresponding to the main stream (2.2).

## 3. The perturbed Blasius flow

Apart from the immediate neighbourhood of the leading and trailing edges the velocity of slip implied by (2.2) is virtually uniform. For the reasons outlined in the previous section the singularity in (2.2) at $x^* = -l$, the leading edge of the plate, is ignored, and on the upper side of the plate, to which we shall restrict attention in this section, we replace the main-stream velocity by $U_1(x^*)$ where

$$U_1(x^*) = U_\infty + U_\infty \alpha^* (-x^*/l)^{\frac{1}{2}}. \tag{3.1}$$

Thus we have simplified the slip velocity and set $B = 0$. The first modification leads to an error in both the slip velocity and its derivative that is small over the whole of the plate, except for the leading edge, and therefore will not make a significant contribution to the theory below. The second modification anticipates that $B = O(R^{-\frac{3}{8}}l)$ and may be justified *a posteriori*. We note, however, that even if $B = O(l)$ the main properties of the perturbed Blasius flow can easily be inferred from the discussion when $B = 0$.

We define the parameter $e$ by

$$e^{-8} = R = U_\infty l/\nu, \tag{3.2}$$

and introduce the non-dimensional variables

$$\xi = 1 + x^*/l, \quad \bar{y} = y^*/le^4, \quad u = u^*/U_\infty, \quad \bar{v} = v^*/U_\infty e^4, \tag{3.3}$$

in terms of which the boundary-layer equations appropriate to the main stream (3.1) are

$$\frac{\partial u}{\partial \xi} + \frac{\partial \bar{v}}{\partial \bar{y}} = 0, \quad u\frac{\partial u}{\partial \xi} + \bar{v}\frac{\partial u}{\partial \bar{y}} = \frac{-\alpha^*}{2(1-\xi)^{\frac{1}{2}}}[1 + \alpha^*(1-\xi)^{\frac{1}{2}}] + \frac{\partial^2 u}{\partial \bar{y}^2}. \tag{3.4}$$

These equations are to be solved subject to the boundary conditions

$$u = \bar{v} = 0 \quad \text{on} \quad \bar{y} = 0; \quad u \to 1 + \alpha^*(1-\xi)^{\frac{1}{2}} \quad \text{as} \quad \bar{y} \to \infty, \tag{3.5}$$

and if $\alpha^* = 0$ the solution is $u = f_B'(\zeta)$ where $\zeta = \bar{y}/\xi^{\frac{1}{2}}$ and $f_B(\zeta)$ is the Blasius function with $f_B(0) = f_B'(0) = 0, f_B''(0) = \lambda = 0{\cdot}3321$. When $\alpha^*$ is small but non-zero we seek a perturbation to the Blasius solution in the manner described by Riley & Stewartson (1969) in their analogous investigation in the case of a wedge. We write

$$u = f_B'(\zeta) + \alpha^* \sum_{n=0}^{\infty} \xi^{n+1} f_n'(\zeta) + O(\alpha^{*2}) \tag{3.6}$$

in (3.3), and the equation satisfied by the function $f_n'(\zeta)$ is

$$f_n''' + \tfrac{1}{2} f_B f_n'' - (n+1) f_B' f_n' + (n+\tfrac{3}{2}) f_B'' f_n = \frac{(n-\frac{1}{2})!}{2\pi^{\frac{1}{2}} n!}, \tag{3.7}$$

with boundary conditions

$$f_n(0) = f_n'(0) = 0, \quad f_n'(\infty) = -\frac{(n-\frac{1}{2})!}{2\pi^{\frac{1}{2}}(n+1)!}. \tag{3.8}$$

Since we are interested in the singular behaviour of the solution (3.6) as $\xi \to 1$, the trailing edge of the plate, we examine the functions $f_n$ for large values of $n$ by writing

$$2\pi^{\frac{1}{2}} n^{\frac{3}{2}} f_n(\zeta) = \Phi_n(\zeta) + o(1). \tag{3.9}$$

The equation for $\Phi_n$ is exactly that considered by Riley & Stewartson (1969) and in the same way it follows that

$$\Phi_n'(\zeta) = -\frac{n^{\frac{1}{3}}(-\frac{2}{3})!}{3^{\frac{2}{3}}\lambda^{\frac{2}{3}}} f_B''(\zeta) \tag{3.10}$$

if $\zeta = O(1)$, but if $\zeta$ is small so that $n^{\frac{1}{3}}\zeta = O(1)$, then

$$\Phi_n'(\zeta) = -\frac{n^{\frac{1}{3}} 3^{\frac{1}{3}}(-\frac{2}{3})!}{\lambda^{\frac{1}{3}}} \int_0^{n^{\frac{1}{3}}\zeta} \mathrm{Ai}\,(\lambda^{\frac{1}{3}} t)\, dt, \tag{3.11}$$

since (3.10) does not satisfy the boundary condition at the wall. Here Ai is the Airy function.

Thus, near $\xi = 1$,

$$u \approx f_B'(\bar{y}) - \alpha^* \frac{(-\frac{2}{3})!}{3^{\frac{2}{3}} 2\pi^{\frac{1}{2}} \lambda^{\frac{2}{3}}} f_B''(\bar{y}) \sum_{n=1}^{\infty} \frac{\xi^n}{n^{\frac{7}{6}}} \tag{3.12}$$

for any fixed $\bar{y} > 0$, while the skin friction must be calculated from the expression

$$u \approx f_B'(\bar{y}) - \alpha^* \frac{3^{\frac{1}{3}}(-\frac{2}{3})!}{2\pi^{\frac{1}{2}}\lambda^{\frac{1}{3}}} \sum_{n=1}^{\infty} \frac{\xi^n}{n^{\frac{7}{6}}} \int_0^{n^{\frac{1}{3}}\bar{y}} \mathrm{Ai}\,(\lambda^{\frac{1}{3}} t)\, dt. \tag{3.13}$$

Since the terms in the series in (3.12), (3.13) were deduced from the properties of (3.7) for large $n$ only, these solutions may be augmented by any term $O(\alpha^*)$ having an expansion in powers of $\xi$ which, when $\xi = 1$, converges more rapidly than the term given. It follows from (3.12) that, near $\xi = 1$,

$$u \approx f_B'(\bar{y}) + \alpha^* \left\{ g_{\frac{1}{2}}(\bar{y}) + \frac{6^{\frac{1}{3}}(-\frac{1}{3})!}{\lambda^{\frac{5}{3}}} (1-\xi)^{\frac{1}{6}} f_B''(\bar{y}) \right\}, \tag{3.14}$$

where the singular part of $g_{\frac{1}{2}}(\bar{y})$ as $\bar{y} \to 0$ is obtained by letting $\xi \to 1$ in the expression for $u$ in (3.13). Thus for small $\bar{y}$ we have

$$g_{\frac{1}{2}}(\bar{y}) \approx -\frac{3^{\frac{1}{3}}(-\frac{2}{3})!}{2\pi^{\frac{1}{2}}\lambda^{\frac{1}{3}}} \sum_{n=1}^{\infty} n^{-\frac{5}{6}} \int_0^{\bar{y}} \mathrm{Ai}\,(n^{\frac{1}{3}}\lambda^{\frac{1}{3}} t)\, dt. \tag{3.15}$$

In (3.14) the error in replacing $f_B'(\zeta)$ by $f_B'(\bar{y})$ is $O(1-\xi)$, and the term in $\alpha^*$ is in error by powers of $1-\xi$ higher than $(1-\xi)^{\frac{1}{6}}$.

The behaviour of $g_{\frac{1}{2}}(\bar{y})$ for small $\bar{y}$ is most easily found by consideration of the shear stress which may be deduced from (3.13). It is proportional to $\partial u/\partial \bar{y}$ where

$$\frac{\partial u}{\partial \bar{y}} \approx f_B''(\bar{y}) - \alpha^* \frac{3^{\frac{1}{3}}(-\frac{2}{3})!}{2\pi^{\frac{1}{2}}\lambda^{\frac{1}{3}}} \sum_{n=1}^{\infty} \frac{\xi^n}{n^{\frac{5}{6}}} \mathrm{Ai}\,(n^{\frac{1}{3}}\lambda^{\frac{1}{3}}\bar{y}), \tag{3.16}$$

to which may be added any term $O(\alpha^*)$ which when $\bar{y} = 0$ and $\xi = 1$ diverges less strongly than $\sum_{n=1}^{\infty} n^{-\frac{5}{6}}$. Investigation of (3.16) reveals that the double limiting process $\bar{y} \to 0$, $\xi \to 1$ is non-commutative. If we let $\bar{y} \to 0$ first we obtain

$$\left.\frac{\partial u}{\partial \bar{y}}\right|_{\bar{y}=0} \approx \lambda - \alpha^* 6^{-\frac{1}{3}} \lambda^{-\frac{1}{3}} \left[\frac{(-\frac{2}{3})!}{(-\frac{1}{3})!}\right]^2 (1-\xi)^{-\frac{1}{6}}. \tag{3.17}$$

However $$\left.\frac{\partial u}{\partial \bar{y}}\right|_{\xi=1} \approx f_B''(\bar{y}) - \alpha^* \frac{3^{\frac{1}{3}}(-\frac{2}{3})!}{2\pi^{\frac{2}{3}}\lambda^{\frac{2}{3}}} \sum_{n=1}^{\infty} n^{-\frac{5}{6}} \int_0^{\infty} \cos\left(\frac{s^3}{3\lambda} + n^{\frac{1}{3}}\bar{y}s\right) ds, \tag{3.18}$$

where the Airy function has been replaced by an integral representation. In order to investigate the behaviour of (3.18) as $\bar{y} \to 0$ we consider the summation which is the real part of the integral

$$j(\bar{y}) = \int_0^{\infty} \exp(is^3/3\lambda) \sum_{n=1}^{\infty} \frac{\exp(i\bar{y}sn^{\frac{1}{3}})}{n^{\frac{5}{6}}} ds, \tag{3.19}$$

since the interchange of summation and integration may be justified. The series in (3.19) converges for all $\bar{y} > 0$, and because

$$\sum_{n=1}^{\infty} \frac{\exp(in^{\frac{1}{3}}\theta)}{n^{\frac{5}{6}}} = \int_1^{\infty} \frac{\exp(it^{\frac{1}{3}}\theta)}{t^{\frac{5}{6}}} dt + O(1) \quad \text{as} \quad \theta \to 0+ \tag{3.20}$$

it follows that, for small $\bar{y}$,

$$j(\bar{y}) \approx \frac{3\pi^{\frac{1}{2}} \exp(i\pi/4)}{\bar{y}^{\frac{1}{2}}} \int_0^{\infty} \frac{\exp(is^3/3\lambda)}{s^{\frac{1}{2}}} ds. \tag{3.21}$$

Hence finally, for small $\bar{y}$,

$$\left.\frac{\partial u}{\partial \bar{y}}\right|_{\xi=1} \approx \lambda - \alpha^* \frac{3^{\frac{1}{3}}(-\frac{2}{3})!\,(-\frac{5}{6})!}{4\pi\lambda^{\frac{1}{2}}} \bar{y}^{-\frac{1}{2}}, \tag{3.22}$$

so that $g_{\frac{1}{2}}(\bar{y})$ differs from $$-\frac{3^{\frac{1}{2}}(-\frac{2}{3})!}{\lambda^{\frac{1}{2}}(-\frac{1}{6})!}\bar{y}^{\frac{1}{2}} \tag{3.23}$$

by a constant as $\bar{y} \to 0$ and has a singular derivative at $\bar{y} = 0$.

It is at this stage that we first have confirmation of the prediction of § 2 regarding the order of magnitude of $\alpha^*$. We know (Stewartson 1969, to which we hereafter refer as I) that if $\alpha^* = 0$ the Blasius flow breaks down when $1 - \xi = O(\epsilon^3)$ since the trailing edge induces a favourable pressure gradient. If the adverse pressure gradient caused by the incidence is to be comparable, we see from (3.17) that $\alpha^* = O(\epsilon^{\frac{1}{2}})$. This is also consistent with (3.22) since within a distance $O(\epsilon^3)$. of the trailing edge the appropriate scale for $\bar{y}$ in the immediate neighbourhood of the wall is $\bar{y} = O(\epsilon)$.

The following section describes the modification to the trailing-edge triple deck of I to accommodate the singular behaviour of $\partial u/\partial \bar{y}$ as demonstrated in (3.17), (3.22) in the respective limits $\bar{y} \to 0$ for fixed $\xi \neq 1$ and $\xi \to 1$ for fixed $\bar{y} > 0$. It will emerge, as is indicated by (3.13), that the appropriate combination of co-ordinates in the neighbourhood of the wall is $\bar{y}/(1-\xi)^{\frac{1}{3}}$, a variable that remains $O(1)$ in the scaled co-ordinates of the lower deck.

## 4. The trailing-edge triple deck for $y^* > 0$

Even if $\alpha^* = 0$ and the Blasius flow is maintained over $-l < x^* < 0$, it has already been shown in I that it must break down within a distance $O(\epsilon^3 l)$ of the trailing edge. Also as $x^* \to 0-$ the work of the previous section already shows that the boundary layer is taking on the familiar properties of the lower and

main decks, of thicknesses $O(\epsilon^5 l)$ and $O(\epsilon^4 l)$ respectively. Further, the normal velocity associated with the main deck is seen from (3.14) to be

$$O(U_\infty \alpha^* \epsilon^4 (-x^*/l)^{-\frac{5}{6}}) \tag{4.1}$$

and is of the same order as the term $O(\alpha^*)$ in the slip velocity (3.1) when $-x^* = O(\epsilon^3 l)$. Now, as demonstrated in I, the increase in slip velocity induced by the change in boundary condition at $y^* = 0$ when $x^*$ changes sign is $O(\epsilon^2 U_\infty)$ which is comparable with (4.1) in the triple deck if $\alpha^* = O(\epsilon^{\frac{1}{2}})$. For larger values of $\alpha^*$ separation occurs for $-x^* \gg \epsilon^3 l$ on the upper side of the plate, and for smaller values of $\alpha^*$ the effect of the incidence is negligible in comparison with the trailing-edge effect. Accordingly, interest centres on values of $\alpha^*$ such that $\alpha = O(1)$ where

$$\alpha^* = \epsilon^{\frac{1}{2}} \lambda^{\frac{2}{3}} \alpha, \tag{4.2}$$

where $\lambda = f_B''(0) = 0{\cdot}3321$ and is introduced here merely to simplify the fundamental equation (3.14).

In setting up the triple deck the arguments given in Stewartson & Williams (1969) and in I are used extensively. The main modifications necessary are to the boundary conditions which depend on §§ 2, 3. Otherwise the structure is taken over, with notation, from I. We write

$$x^* = \epsilon^3 \lambda^{-\frac{5}{4}} l x, \quad y^* = \epsilon^4 \lambda^{-\frac{5}{8}} l y, \quad u^* = U_\infty u, \quad v^* = U_\infty \lambda^{\frac{5}{8}} v,$$
$$p^* = p_\infty + \rho U_\infty^2 \lambda^{\frac{5}{8}} p, \tag{4.3}$$

where $u$, $v$, $p$ are functions of $x$, $y$. Then in the main deck $x = O(1)$, $y = O(1)$ and we set up the following formal expansions for $u$, $v$, $p$:

$$u(x,y) = U_0(y) + \epsilon^{\frac{1}{2}} u_{\frac{1}{2}}(y) + \epsilon \log \epsilon u_{11}(y) + \epsilon u_1(x,y) + \ldots, \tag{4.4a}$$
$$v(x,y) = \epsilon^2 v_1(x,y) + \ldots, \tag{4.4b}$$
$$p(x,y) = \epsilon^2 p_2(x,y) + \ldots. \tag{4.4c}$$

Here $U_0(y) = f_B'(\bar{y})$ and is the velocity profile at $x^* = 0$ as given by the Blasius solution. The function $u_{\frac{1}{2}}(y)$ is a constant multiple of $g_{\frac{1}{2}}(\bar{y})$ as introduced in (3.14), and results from formally letting $x^*$ tend to zero in the perturbation of order $\epsilon^{\frac{1}{2}}$ caused by the pressure variation of the same order. This term and the term $O(\epsilon \log \epsilon)$ are the only ones that differ from I (equation (3.1)). The presence of the latter is indicated by the form taken by the solution at the outer edge of the inner deck, and reference to it is made again in § 5. Neither, however, makes a contribution to $u_1(x,y)$ since both are functions of $y$ alone. The boundary conditions satisfied by $u_1$, $v_1$, $p_2$ upstream of the triple-deck region are obtained from the part of the perturbation Blasius solution of § 3 that has a singular derivative as $x^* \to 0-$. The relevant matching is provided by (3.14) and we have

$$\frac{u_1}{(-x)^{\frac{1}{6}}} \to \alpha \frac{6^{\frac{1}{3}}(-\frac{1}{3})!\, dU_0}{\lambda^{\frac{1}{8}}\, dy}, \quad (-x)^{\frac{5}{6}} v_1 \to \frac{\alpha(-\frac{1}{3})!}{6^{\frac{2}{3}}\lambda^{\frac{1}{8}}} U_0(y), \quad \frac{p_2}{(-x)^{\frac{1}{2}}} \to -\frac{\alpha}{\lambda^{\frac{1}{8}}}, \tag{4.5}$$

as $x \to -\infty$ with $y = O(1)$. On substituting (4.4) into the full Navier–Stokes equations and equating the coefficients of the leading powers of $\epsilon$ to zero we obtain

$$u_1(x,y) = A_1(x) \frac{dU_0}{dy}, \quad v_1(x,y) = -A_1'(x)\, U_0(y), \quad p_2(x,y) = p_2(x,0), \tag{4.6}$$

as in I (equations (3.6) and (3.8)), where $A_1(x)$ is a function of $x$ to be determined. One equation connecting $p_2$ and $A_1$ follows from the upper deck in which $y^* = O(\epsilon^3 l)$ and in which the governing equations are essentially inviscid. To obtain this relation we introduce a new variable

$$Y = \epsilon\lambda^{\frac{5}{8}} y = \lambda^{\frac{1}{4}} y^*/l\epsilon^3, \tag{4.7}$$

and write

$$u = 1 + \epsilon^2 U_2(x, Y) + \ldots, \quad v = \epsilon^2 V_2(x, Y) + \ldots, \quad p = \epsilon^2 P_2(x, Y) + \ldots, \tag{4.8}$$

where the dots denote higher powers of $\epsilon$. Then it may easily be shown that $P_2 + iV_2$ is a function of $x + iY$ only and that

$$P_2(x, 0) = p_2(x, 0), \quad V_2(x, 0) = -A_1'(x). \tag{4.9}$$

In I it was straightforward to express $p_2$ in terms of $A_1'$ by means of a Hilbert integral but there is a slight complication here as $p_2(x, 0) \sim -\alpha(-x)^{\frac{1}{2}}\lambda^{-\frac{1}{8}}$ as $x \to -\infty$ and $A_1'(x) \sim \alpha x^{\frac{1}{2}}\lambda^{-\frac{1}{8}}$ as $x \to +\infty$ so that formally the Hilbert integrals do not converge. However the difficulty can be overcome by using Hadamard's notion of the finite part of the infinite integral and then we have

$$p_2(x, 0) = \frac{1}{\pi} \mathscr{F} \int_{-\infty}^{\infty} \frac{A_1'(x')}{x - x'} dx', \tag{4.10}$$

where $\mathscr{F}$ means that the finite part only is to be taken and that the integral is a Cauchy principal value. An alternative form is

$$p_2(x, 0) = \frac{-\alpha}{\lambda^{\frac{1}{8}}} (-x)^{\frac{1}{2}} H(-x) + \frac{1}{\pi}\int_{-\infty}^{0} \frac{A_1'(x')\, dx'}{x - x'} + \frac{1}{\pi}\int_{0}^{\infty} \frac{[A_1'(x') - \alpha\lambda^{-\frac{1}{8}} x'^{\frac{1}{2}}]}{x - x'} dx', \tag{4.11}$$

where $H$ is Heaviside's step function.

Turning now to the lower deck of thickness $O(\epsilon^5 l)$ we write

$$z = \lambda^{\frac{1}{8}} y/\epsilon = \lambda^{\frac{3}{4}} y^*/l\epsilon^5 \tag{4.12a}$$

and

$$u = \epsilon\lambda^{\frac{1}{4}} \tilde{u}_1(x, z) + \ldots, \quad v = \epsilon^3\lambda^{\frac{1}{8}} \tilde{v}_1(x, z) + \ldots, \quad p = \epsilon^2 \tilde{p}_2(x) + \ldots, \tag{4.12b}$$

where $\tilde{p}_2(x) = \lambda^{\frac{1}{8}} p_2(x, 0)$. Then $\tilde{u}_1$, $\tilde{v}_1$ satisfy

$$\tilde{u}_1 \frac{\partial \tilde{u}_1}{\partial x} + \tilde{v}_1 \frac{\partial \tilde{u}_1}{\partial z} = -\frac{d\tilde{p}_2}{dx} + \frac{\partial^2 \tilde{u}_1}{\partial z^2}, \quad \frac{\partial \tilde{u}_1}{\partial x} + \frac{\partial \tilde{v}_1}{\partial z} = 0, \tag{4.13}$$

with boundary conditions for $x < 0$,

$$\left.\begin{aligned} \tilde{u}_1 = 0 = \tilde{v}_1 \quad \text{if} \quad z = 0, \qquad \tilde{u}_1 - z \to \tilde{A}_1(x) \quad \text{as} \quad z \to \infty, \\ \tilde{u}_1 - z \to 0 \quad \text{as} \quad x \to -\infty, \end{aligned}\right\} \tag{4.14}$$

where $\tilde{A}_1(x) = \lambda^{\frac{1}{8}} A_1(x)$.

No boundary conditions have so far been given for (4.13) in $x > 0$ and before setting these out it is convenient to go through the analogous argument for the region $y^* < 0$. The only difference in the key equations (4.11), (4.13), (4.14) is that the sign of the term corresponding to $A_1(x)$ changes while the term corresponding to $p_2(x, 0)$ remains unaltered. Of course since we are dealing with an asymmetric problem the two boundary layers must be solved separately and no simple connecting relations can be expected. If we denote the value of $\tilde{p}_2(x)$ by $\tilde{p}_T(x)$ when $y^* > 0$ and by $\tilde{p}_B(x)$ when $y^* < 0$ with a corresponding notation for

$\tilde{A}_T(x)$ and $\tilde{A}_B(x)$ the fundamental problem of the triple deck for a lifting flat plate can be stated as follows.

Solve (4.13) with

$$\left.\begin{aligned}\tilde{p}_2(x) = \tilde{p}_T(x) &= \frac{1}{\pi}\mathscr{F}\int_{-\infty}^{\infty}\frac{\tilde{A}_T'(x')\,dx'}{x-x'} \quad \text{if} \quad z>0,\\ \tilde{p}_2(x) = \tilde{p}_B(x) &= -\frac{1}{\pi}\mathscr{F}\int_{-\infty}^{\infty}\frac{\tilde{A}_B'(x')\,dx'}{x-x'} \quad \text{if} \quad z<0,\end{aligned}\right\} \tag{4.15a}$$

subject to the following boundary conditions:

$$\tilde{u}_1 \to |z| \quad \text{as} \quad x\to-\infty; \tag{4.15b}$$

$$\tilde{u}_1 = 0 = \tilde{v}_1 \text{ at } z=0, \quad x<0, \quad \text{while } \partial\tilde{u}/\partial z \text{ is discontinuous;} \tag{4.15c}$$

$$\tilde{u}_1 - z \to \tilde{A}_T(x) \quad \text{as} \quad z\to+\infty, \quad \tilde{u}_1+z\to-\tilde{A}_B(x) \quad \text{as} \quad z\to-\infty; \tag{4.15d}$$

$\tilde{u}_1$, $\tilde{v}_1$ are smooth for all $z$ if $x>0$;

$$\tilde{p}_T(x) = \tilde{p}_B(x) \quad \text{if} \quad x>0. \tag{4.15e}$$

Finally $$\tilde{p}_T + \alpha(-x)^{\frac{1}{2}} \to 0, \quad \tilde{p}_B(x) - \alpha(-x)^{\frac{1}{2}} \to 0 \quad \text{as} \quad x\to-\infty. \tag{4.15f}$$

In the wake region a simple Galilean transformation can be made which, while not perhaps reducing the formidable numerical problem presented by (4.13), (4.15), makes it easier to see how to proceed and to understand the structure of the solution. In $x>0$ we write $$\tilde{z} = z-\theta(x), \tag{4.16}$$

where $\theta(x)$ is an arbitrary function of $x$, regard $\tilde{u}_1$ as a function of $x$, $\tilde{z}$, and replace $\tilde{v}_1$ by $\tilde{v}_1+\theta'(x)\tilde{u}_1$. Then (4.13) is unaltered but the boundary conditions in $x>0$ reduce to

$$\begin{aligned}\tilde{u}_1 - |\tilde{z}| \to{}& \tfrac{1}{2}[\tilde{A}_T(x)-\tilde{A}_B(x)]\\ &+\{\tfrac{1}{2}[\tilde{A}_T(x)+\tilde{A}_B(x)]+\theta(x)\}\operatorname{sgn}\tilde{z} \quad \text{as} \quad |\tilde{z}|\to\infty.\end{aligned} \tag{4.17}$$

One possible choice for $\theta(x)$ is $-\frac{1}{2}(\tilde{A}_T+\tilde{A}_B)$ which simplifies (4.17) but, with an iterative method as outlined below, it is undesirable to move the origin. Hence we shall choose $$\theta(0)=0, \quad \theta' = -\tfrac{1}{2}(\tilde{A}_T'+\tilde{A}_B') \quad (x>0), \tag{4.18}$$

so that $$\begin{aligned}\tilde{u}_1 - |\tilde{z}| \to{}& \tfrac{1}{2}[\tilde{A}_T(x)-\tilde{A}_B(x)]\\ &+\tfrac{1}{2}\{\tilde{A}_T(0)+\tilde{A}_B(0)\}\operatorname{sgn}\tilde{z} \quad \text{as} \quad |\tilde{z}|\to\infty.\end{aligned} \tag{4.19}$$

The numerical integration might now proceed as follows. Guess $\tilde{A}_T$, $\tilde{A}_B$ in $x<0$ and $\tilde{A}_T-\tilde{A}_B$ in $x>0$. Using (4.15$a$) determine $\tilde{p}_T$, $\tilde{p}_B$ in $x<0$ and $\tilde{p}_2$ in $x>0$ together with the values of $\tilde{A}_T'+\tilde{A}_B'$ which make $\tilde{p}_T=\tilde{p}_B$ in $x>0$. Then $\theta(x)$ is determined from (4.18). Now integrate (4.13) with these values of $\tilde{p}_2$ and $\theta$ to deduce new values of $\tilde{A}_T$, $\tilde{A}_B$ in $x<0$ and of $\tilde{A}_T-\tilde{A}_B$ in $x>0$. Hopefully this iterative procedure will converge to the required solution of the fundamental problem. Alternatively (4.15$a$) can be used in reverse, i.e. begin with $\tilde{p}_2$ and deduce $\tilde{A}_T'$, $\tilde{A}_B'$ from (4.15$a$). Then $\tilde{A}_T$, $\tilde{A}_B$ follow by integration, the additive constant being determined from the known properties of $\tilde{A}$ when $x$ is large and negative. The last step in the cycle is to use (4.13) to compute $\tilde{p}_2$.

## 5. The structure of the lower deck

(*a*) $|x| \gg 1$, $x < 0$

The elucidation of the structure of the solution of (4.13) subject to (4.14), (4.15) cannot proceed straightforwardly, even on an intuitive basis, because the behaviour of the pressures $\tilde{p}_T$ and $\tilde{p}_B$ depends on the overall properties of $\tilde{A}_T$ and $\tilde{A}_B$. However we can expect that $\frac{1}{2}(\tilde{p}_T - \tilde{p}_B)$, the anti-symmetric part of $\tilde{p}_2$, which is zero when $x > 0$ and is derived from a complex function of $x + iY$, has an asymptotic expansion for large negative $x$ containing terms of the form $a_n(-x)^{\frac{1}{2}-n}$ with $n = 0, 1, 2, \ldots$. For $n \geqslant 1$ the coefficients $a_n$ depend on the overall values of $\tilde{A}(x)$ while $a_0 = -\alpha$. Further, $\frac{1}{2}(\tilde{p}_T + \tilde{p}_B)$, the symmetric part of $\tilde{p}_2$, is, when $x$ is large and negative, mainly forced by the wake growth at large positive values of $x$. This would imply, from I (equation (5.14)), that it has an asymptotic expansion which starts with $-1{\cdot}7840/3^{\frac{2}{3}}(-x)^{\frac{2}{3}}$. The dependence of the symmetric part of $\tilde{p}_2$ on overall properties of $\tilde{A}$ results in multipole solutions giving terms like $(-x)^{-n}$ for integral $n$. Otherwise the various terms arise from the properties of $\tilde{A}(x)$ when $|x|$ is large which depend in turn on the properties of $\tilde{p}_2$ and the eigensolutions of (4.13). Finally, logarithmic terms may arise through a confluence of forced terms and eigensolutions. On the basis of this general argument we therefore assume that

$$\tilde{p}_T(x) = -\alpha(-x)^{\frac{1}{2}} + \frac{\alpha a_1}{(-x)^{\frac{1}{2}}} - \frac{1.7840}{3^{\frac{3}{2}}(-x)^{\frac{2}{3}}} + O((-x)^{-\frac{5}{6}}), \tag{5.1}$$

when $x$ is large and negative and verify *a posteriori* that it is a consistent assumption. The constant $a_1$ is related to the unknown circulation term $B$ of (2.2) by

$$B = \epsilon^3 l \lambda^{-\frac{5}{4}} a_1, \tag{5.2}$$

and in § 6 an estimate of its value is made.

Following the argument of § 5 in I we now assume that the solution of (4.13) for the region $z > 0$ of the lower deck can be obtained in the form

$$\tilde{u}_1 = z + \alpha(-x)^{\frac{1}{6}} H_1'(\eta) + \alpha^2 H_2'(\eta) + \alpha^3(-x)^{-\frac{1}{6}} H_3'(\eta) + O((-x)^{-\frac{1}{3}}) \tag{5.3}$$

when $x$ is large and negative. Here

$$\eta = z/3\,|2x|^{\frac{1}{3}}, \tag{5.4}$$

and the $H_n'(\eta)$ are functions of $\eta$ satisfying the boundary conditions

$$H_n(0) = H_n'(0) = 0, \quad H_n''(\eta) \to 0 \quad \text{as} \quad \eta \to \infty, \tag{5.5}$$

and the differential equations

$$H_n''' - 18\eta^2 H_n'' + 9(4-n)(\eta H_n' - H_n) = h_n(\eta). \tag{5.6}$$

Each $h_n(\eta)$ depends on the previous $H_m(\eta)$, $1 \leqslant m \leqslant n-1$, and

$$h_1(\eta) = 9 \cdot 2^{-\frac{1}{3}}, \quad h_2(\eta) = 3 \cdot 2^{-\frac{1}{3}}(3H_1 H_1'' - H_1'^2). \tag{5.7}$$

The second and third terms of (5.1) do not affect the expansion (5.3) until we reach $H_7(\eta)$, $H_8(\eta)$. The complementary functions of (5.6) are either exponentially large as $\eta \to \infty$, which is inadmissible, or linear, or, except for $n = 1, 2$, are such

that their first derivative vanishes at infinity. If $n = 1$ one complementary function is $O(\eta^{\frac{1}{2}})$ as $\eta \to \infty$ and indeed we find that, on solving (5.6) analytically in this case,

$$H_1'(\eta) = -\frac{3^{\frac{1}{2}}(-\frac{2}{3})!}{(-\frac{1}{6})!}\eta^{\frac{1}{2}} + 6^{\frac{1}{3}}(-\tfrac{1}{3})! + O(\eta^{-\frac{1}{2}}) \tag{5.8}$$

as $\eta \to \infty$. Also

$$H_1''(0) = 3^{\frac{2}{3}}\left[\frac{(-\frac{2}{3})!}{(-\frac{1}{3})!}\right]^2, \tag{5.9}$$

and this gives a contribution to the skin friction that exactly matches with the corresponding term in (3.17). The first term of (5.8) matches with the second term of (4.4$a$) as forecast in the discussion of § 3. We note that this term is independent of $x$ and so persists as $x \to +\infty$ and must appear in the expansion of $\tilde{u}_1$ about $x = \infty$. The second term of (5.8) gives a leading term in the asymptotic expansion of $\tilde{A}(x)$ so that

$$\tilde{A}_T(x) \approx \alpha 6^{\frac{1}{3}}(-\tfrac{1}{3})!\,(-x)^{\frac{1}{6}}. \tag{5.10}$$

The same term leads the asymptotic expansion of $\tilde{A}_B(x)$, and it follows from (4.15$a$) that (5.10) makes a contribution to $\tilde{p}_T(x)$ which is $O((-x)^{-\frac{5}{6}})$ and accounts for the last term of (5.1).

One complementary function of the equation for $H_2(\eta)$ is such that

$$H_2'(\eta) \sim \log \eta \quad \text{as} \quad \eta \to \infty,$$

and this presumably matches with the third term of (4.4$a$). This third term is $O(\log y)$ as $y \to 0$ and hence must be matched all the way along the lower deck even as $x \to +\infty$. The contribution to $\tilde{A}_T(x)$ arising from $H_2'(\eta)$ is a constant plus a term proportional to $\log|x|$, and gives a term in $\tilde{p}_T(x)$ which is proportional to $x^{-1}\log|x|$.

Thus, from conditions when $x$ is large and negative, it would seem that the expansion (5.3) is the correct one: we shall confirm below that it is also consistent with the expansion as $x \to +\infty$. Through the kind offices of Dr N. Riley the first four equations of (5.7) were integrated numerically with the same basic program as was used to calculate the corresponding functions in Riley & Stewartson (1969) and it was found that

$$\left.\frac{\partial \tilde{u}_1}{\partial z}\right|_{z=0} = 1 - 2{\cdot}1539\sigma - 0{\cdot}8940\sigma^2 - 1{\cdot}2256\sigma^3 - 2{\cdot}2452\sigma^4 - \ldots, \tag{5.11}$$

where $\sigma = \alpha/(-x)^{\frac{1}{6}}$. In order to have a smooth solution it seems important to prevent separation occurring in the lower deck. It is clear from (5.1) that as $x$ increases from $-\infty$ the pressure initially increases and so separation is a possibility. On the other hand the presence of the third term of (5.1) shows that the wake part of the lower deck provides a favourable pressure gradient which, although weak at large negative $x$, may well be enough to prevent separation if $\alpha$ is not too large. Certainly no separation occurs if $\alpha = 0$, and it is a reasonable hypothesis, in view of the existence of this term, to postulate the existence of an $\alpha_s$ such that if $\alpha < \alpha_s$ there is no separation and the triple-deck structure assumed here is correct, while if $\alpha > \alpha_s$ separation occurs and with it at least the partial collapse of the structure we have set up. We also postulate that $\alpha_s$ is associated

with stall and define $\alpha_s$ as the trailing-edge stall angle. Clearly the determination of $\alpha_s$ is the most important end-point of the present theory but equally it presents a numerical problem that is beyond our capabilities at present. A rough estimate of its value can however be obtained as follows.

We compute the position of separation on the assumption that $\tilde{p}_T(x)$ is exactly equal to $-\alpha(-x)^{\frac{1}{2}}$. This may be done on the same lines as in Riley & Stewartson (1969) and we find, from (5.11), that if $x = x_s$, $\sigma = \sigma_s$ at this point then

$$0{\cdot}307 < \sigma_s < 0{\cdot}364 \tag{5.12}$$

and that the probable value of $\sigma_s$ is near 0·326. We now set $a_1 = 0$ and determine the relative contribution of the third term of (5.1) to the pressure gradient at $x = x_s$. If

$$\alpha(-x_s)^{\frac{7}{6}} = 2 \tag{5.13}$$

this term is only about 20% of the first term and separation is unlikely to be inhibited. If

$$\alpha(-x_s)^{\frac{7}{6}} = 0{\cdot}45 \tag{5.14}$$

the pressure gradient has been reduced to zero at $x = x_s$ and separation is likely to have been inhibited. We infer that

$$0{\cdot}45 < \alpha_s^8/(0{\cdot}326)^7 < 2,$$

so that

$$0{\cdot}33 < \alpha_s < 0{\cdot}41. \tag{5.15}$$

With a Reynolds number of $10^6$ the relation (4.2) in conjunction with (5.15) gives an angle of incidence of approximately 2° for the onset of separation. Since experimentally trailing-edge stall does not occur until the angle of incidence is much larger, between 5° and 15°, this predicted angle is much too small. The discrepancy may in part be explained by the fact that the observed flow is probably turbulent. In turbulent flow the displacement effect is greater than in laminar flow, the adverse pressure gradient is thereby decreased, and the boundary layer will remain attached at the trailing edge of the aerofoil through increased angles of incidence.

On the lower side of the plate the pressure variation due to the incidence is favourable so no separation takes place there for any $\alpha$. The form of the expansions for $\tilde{u}_1$ and for $\tilde{p}_B$ are similar to (5.1) and (5.3) for the upper side of the plate, and the asymptotic structure of the skin friction may be obtained from (5.11) by changing the sign of $\sigma$.

### (*b*) $|x| \ll 1$

Turning now to the immediate neighbourhood of the trailing edge of the plate we first note that the conventional boundary-layer equations, with main stream as given by (3.1) with $\alpha^* < 0$ and $O(1)$, have been integrated numerically by Ackerberg (private communication) who finds a complicated singularity at $x^* = 0$ with an infinite skin friction there. In our case $\alpha^*$ is small and the interaction with the main stream is likely to keep the boundary-layer properties finite if $\alpha < \alpha_s$. We may expect, however, that as $x \to 0-$ the values of $\partial\tilde{u}_1/\partial z$ as $z \to 0\pm$ are different. We denote them by $\lambda_T(\alpha)$ and $\lambda_B(\alpha)$, and for reasons similar to those given in I they are expected to be finite with $\lambda_B < 0 < \lambda_T$.

Further, in view of the previous history of the boundary layers on the top and bottom of the plate, they will satisfy, for $\alpha > 0$,

$$|\lambda_B(\alpha)| > |\lambda_B(0)| = \lambda_1 = \lambda_T(0) > \lambda_T(\alpha), \tag{5.16}$$

where $\lambda_1$ is defined in I (§6). As was the case there, the pressure and pressure gradient should be bounded as $x \to 0-$, but as $x \to 0+$ the pressure gradient is $O(x^{-\frac{1}{3}})$ which is necessary to prevent $\tilde{A}'(x)$ from being singular at $x = 0+$. The transition of the solution from $x = 0-$ to $x = 0+$ is achieved by a generalization of the Rott & Hakkinen (1965) wake solution. We suppose that the velocity profile at $x = 0-$ is

$$\tilde{u}_1(0-, z) = \hat{u}_1(z) \quad \text{with} \quad \hat{u}_1'(0+) = \lambda_T, \quad \hat{u}_1'(0-) = \lambda_B, \tag{5.17}$$

where $\hat{u}_1(z)$ is to be computed, and also

$$d\tilde{p}_2/dx \quad \text{is finite at } x = 0-, \text{ and } \quad d\tilde{p}_2/dx \approx C_0 x^{-\frac{1}{3}} \quad \text{as} \quad x \to 0+, \tag{5.18}$$

where $C_0$ is a constant to be found. Then, if, near $z = 0$,

$$\tilde{u}_1(x, z) = \tfrac{1}{3}(\tfrac{1}{4}x)^{\frac{1}{3}} G_0'(\eta) \quad (x > 0), \tag{5.19}$$

$G_0(\eta)$ satisfies

$$G_0''' + 2G_0 G_0'' - G_0'^2 = 27 C_0 2^{\frac{4}{3}}, \tag{5.20}$$

with boundary conditions

$$\left.\begin{aligned} G_0'(\eta) - 18\lambda_T \eta \to 0 \quad &\text{as} \quad \eta \to \infty, \\ G_0'(\eta) - 18\lambda_B \eta \to 0 \quad &\text{as} \quad \eta \to -\infty. \end{aligned}\right\} \tag{5.21}$$

These conditions ensure that the velocity profile (5.19) matches with (5.17) as $x \to 0+$. This could of course be achieved if finite constants replaced the zeros on the right-hand sides of (5.21), but the additional restriction that these constants must be zero is necessary to ensure that $\tilde{A}_T'(x)$ and $\tilde{A}_B'(x)$ are bounded as $x \to 0+$. A discussion of this point is made in I (§6) for the special case $\lambda_T = -\lambda_B$, and the conclusions reached there are also applicable here.

Solutions of equation (5.20) with boundary conditions (5.21) have been kindly obtained for the authors by Mr P. G. Williams for a range of values of the positive parameter $-\lambda_T/\lambda_B$. The results are given in table 1, where $\eta_0$ is defined to be the value of $\eta$ at which $G_0$ vanishes.

| $-\lambda_T/\lambda_B$ | 1·0 | 0·8 | 0·6 | 0·4 | 0·2 | 0 |
|---|---|---|---|---|---|---|
| $\lambda_T^{\frac{1}{3}}\eta_0$ | 0 | 0·017 | 0·040 | 0·070 | 0·109 | 0·164 |
| $G_0'(\eta_0)/\lambda_T^{\frac{2}{3}}$ | 4·28 | 4·03 | 3·86 | 3·82 | 4·02 | 4·44 |
| $C_0/\lambda_T^{\frac{4}{3}}$ | 0·409 | 0·351 | 0·287 | 0·213 | 0·124 | 0 |

TABLE 1

If $\lambda_T < 0$ the governing equation has no solutions since $G_0 < 0$ for large enough positive $\eta$ and the method of solution completely breaks down in the neighbourhood of $x = 0$. Part of the reason is no doubt connected with the change in the direction of propagation of small disturbances, but at the present stage of development of the theory any attempts to overcome the difficulty are bound

to be speculative especially in view of the singularity at separation, which has also to be dealt with, and so we shall not pursue the matter.

Returning to the case $\lambda_T > 0$ we see that the streamline from the trailing edge is given by $\eta = \eta_0$, so that it has a vertical tangent there, and in addition the streamwise component of velocity on it is proportional to $x^{\frac{1}{3}}$. Its subsequent behaviour probably needs a complete numerical integration for elucidation but we note that as in the symmetrical problem, even if $\hat{u}_1$ and $\tilde{p}_2$ are completely known, the form of $\tilde{u}_1$ downstream is not fully determinate and depends on an infinite set of arbitrary constants. The reason of course is that $\tilde{A}(x)$ near $x = 0$ is not entirely dependent on the local values of $\tilde{p}_2(x)$, and in addition to the arbitrary constants mentioned in I (§6) there will be others associated with $\theta(x)$ as introduced in (4.16).

(*c*) $|x| \gg 1$, $x > 0$

Finally, we consider the properties of the solution when $x \gg 1$. Here it seems that the Goldstein solution for the inner wake (Goldstein 1930) is appropriate together with the transformation (4.16). For large $x$ we write

$$\tilde{u}_1 = \tfrac{1}{3}(\tfrac{1}{4}x)^{\frac{1}{3}} g_0'(\bar{\eta}) + \ldots, \tag{5.22}$$

the dots denoting terms which are smaller when $x$ is large, and

$$\bar{\eta} = \frac{z - \theta(x)}{3\,|2x|^{\frac{1}{3}}}. \tag{5.23}$$

Here $g_0$ satisfies the same differential equation (5.20) as $G_0$, except that $C_0 = 0$, together with boundary conditions

$$g_0(0) = g_0''(0) = 0, \quad g_0''(\infty) = 18, \tag{5.24}$$

and $\theta(x)$ is defined by (4.18). Physically this means that the lower deck terminates in a wake which is similar to that for a symmetrically disposed plate except that it is displaced a distance $\theta(x)$ upwards due to the upwash of the inviscid flow behind the inclined plate. From the relation between $\tilde{A}_1'(x)$ and $\tilde{p}_2(x)$ and the property $\tilde{p}_T = \tilde{p}_B$ where $x > 0$ we have

$$\theta(x) = \tfrac{2}{3}\alpha x^{\frac{3}{2}} + 2\alpha a_1 x^{\frac{1}{2}} + \ldots, \tag{5.25}$$

when $x$ is large, which is in accord with the above physical description of the flow. The properties of the Goldstein inner wake imply that

$$\tfrac{1}{2}[\tilde{A}_T(x) - \tilde{A}_B(x)] = 1{\cdot}416(\tfrac{1}{4}x)^{\frac{1}{3}} + \ldots, \tag{5.26}$$

which gives a pressure decaying like $x^{-\frac{2}{3}}$ as $x \to \infty$ as in the symmetrical situation. In order to determine further terms in (5.25), (5.26) we set up an asymptotic series for $\tilde{u}_1$ in descending powers of $x$, and ultimately of $\log x$ also, whose coefficients are functions of $\bar{\eta}$, the leading term being given by (5.22). Were it not for the boundary conditions due to the asymmetry of the problem the structure of this series would be the same as that in I (§5) and so we shall concentrate on the asymmetrical features which are in fact dominant. Of these the most important arises from the term $u_{\frac{1}{2}}(y)$ in (4.4*a*) which behaves like $|y|^{\frac{1}{2}} \operatorname{sgn} y$ as $y \to 0$ and which matches with (5.3) when $x$ is large and negative. Since it is

independent of $x$ it must match with the asymptotic series for $\tilde{u}_1$ when $x$ is large and positive. This can be achieved by taking the first two terms of the series for $\tilde{u}_1$ as

$$\tilde{u}_1 = \tfrac{1}{3}(\tfrac{1}{4}x)^{\frac{1}{3}} g_0'(\bar{\eta}) + \tfrac{1}{3}\alpha(\tfrac{1}{4}x)^{\frac{1}{6}} g_1'(\bar{\eta}), \tag{5.27}$$

where $g_1$ satisfies

$$g_1''' + 2g_0 g_1'' - \tfrac{3}{2}(g_0' g_1' - g_0'' g_1) = 0, \tag{5.28}$$

together with the boundary conditions

$$g_1'(\eta) + 9 \cdot 2^{\frac{1}{3}} \frac{(-\frac{2}{3})!}{(-\frac{1}{6})!} |\bar{\eta}|^{\frac{1}{2}} \to d_1 \operatorname{sgn} \bar{\eta} \quad \text{as} \quad |\bar{\eta}| \to \infty, \tag{5.29}$$

where $d_1$ is a constant which we now determine. The contribution to the asymptotic expansions of both $\tilde{A}_T(x)$ and $\tilde{A}_B(x)$ from the term in $d_1$ is

$$\tfrac{1}{3}\alpha(\tfrac{1}{4}x)^{\frac{1}{6}} d_1, \tag{5.30}$$

and we now obtain $d_1$ by noting that (5.30) in conjunction with (5.10) and the identical result for $\tilde{A}_B(x)$ gives a contribution to the pressure which must vanish for large positive $x$. Hence

$$d_1 = 2^{\frac{5}{3}} 3^{\frac{5}{6}} (-\tfrac{1}{3})!. \tag{5.31}$$

The solution of (5.28) may now be obtained uniquely and we find after numerical integration that $g_1(0) = 10{\cdot}0$, $g_1''(0) = 46{\cdot}0$. The consequent contribution to $\theta(x)$ is $O(x^{\frac{1}{3}})$ and is, as anticipated, smaller than both the terms in (5.25). Further terms in the expansion of $\tilde{u}_1$ may be found if necessary, but we shall not pursue the matter beyond noting that it will involve an infinite set of arbitrary constants.

## 6. An approximate solution for the antisymmetric part of the pressure

At the end of § 4 we outlined a possible procedure for the numerical solution of the fundamental problem presented by (4.13), (4.15), and in view of the considerable complexity of such a computation we feel it worthwhile to derive an approximate solution which would yield the antisymmetric part of the pressure and the symmetric part of the function $\tilde{A}_1(x)$. This is made possible by the fact that $\tilde{p}_T(x) = \tilde{p}_B(x)$ in the wake so that the antisymmetric part of the pressure, $\frac{1}{2}(\tilde{p}_T - \tilde{p}_B)$, is zero for $x > 0$. Equations (4.13) become tractable if they are linearized about the shear flow with which $\tilde{u}_1(x, z)$ merges at the outer edge of the lower deck. The resulting equation should yield a solution exhibiting the main properties of the flow if it is regarded as valid for $x < 0$ only, since it is not expected that the linear shear is a good first approximation in the wake. The method of Wiener and Hopf then enables the functions $\frac{1}{2}(\tilde{p}_T - \tilde{p}_B)$, $\frac{1}{2}(\tilde{A}_T + \tilde{A}_B)$ to be determined for all $x$, the former vanishing for $x > 0$, from a solution for the boundary layer over the plate which is independent of the boundary layer in the wake.

Denoting by $\tilde{u}_T(x, z)$, $\tilde{u}_B(x, z)$ the values of $\tilde{u}_1(x, z)$ for $z > 0$ and $z < 0$ respectively, we write

$$\tilde{u}_T(x, z) = Z + \tilde{w}_T(x, Z), \quad \tilde{u}_B(x, z) = Z + \tilde{w}_B(x, Z), \tag{6.1}$$

where $Z = |z|$, in the appropriate forms of (4.13), neglect the non-linear terms and subtract to obtain

$$\left.\begin{aligned} Z\frac{\partial}{\partial x}(\tilde{w}_T - \tilde{w}_B) + (\tilde{v}_T + \tilde{v}_B) &= -\frac{d}{dx}(\tilde{p}_T - \tilde{p}_B) + \frac{\partial^2}{\partial Z^2}(\tilde{w}_T - \tilde{w}_B), \\ \frac{\partial}{\partial x}(\tilde{w}_T - \tilde{w}_B) + \frac{\partial}{\partial Z}(\tilde{v}_T + \tilde{v}_B) &= 0. \end{aligned}\right\} \tag{6.2}$$

The fundamental equation, which is to be considered for $x < 0$ only, is then obtained from (6.2) as

$$Z\frac{\partial^2 w}{\partial x \partial Z} = \frac{\partial^3 w}{\partial Z^3} \quad (x < 0), \tag{6.3}$$

where $w = \frac{1}{2}(\tilde{w}_T - \tilde{w}_B)$, and is to be solved subject to the conditions

$$\frac{\partial^2 w}{\partial Z^2} = Q(x) \quad \text{on} \quad Z = 0; \quad w \to \tfrac{1}{2}(\tilde{A}_T + \tilde{A}_B) \quad \text{as} \quad Z \to \infty. \tag{6.4}$$

Here $Q(x) = \frac{1}{2}d(\tilde{p}_T - \tilde{p}_B)/dx$, and the boundary condition as $Z \to \infty$ follows from (4.15*d*).

If the Fourier transform of $w(x, Z)$ is denoted by $\bar{w}(\omega, Z)$ so that

$$\bar{w}(\omega, Z) = \int_{-\infty}^{\infty} w(x, Z)\, e^{-i\omega x}\, dx, \tag{6.5}$$

then, since $w(x, Z)$ satisfies (6.3) for $x < 0$, we have

$$\frac{\partial \bar{w}}{\partial Z} = \frac{\bar{Q}_+(\omega)\, e^{-\frac{1}{6}i\pi}}{\mathrm{Ai}'(0)\,(\omega - i\delta)^{\frac{1}{3}}} \mathrm{Ai}\{\exp[\tfrac{1}{6}i\pi]\,(\omega - i\delta)^{\frac{1}{3}} Z\} + M_-(\omega, Z). \tag{6.6}$$

The function $\bar{Q}_+(\omega)$ is the Fourier transform of $Q(x)$, and the suffix plus indicates that it is a regular function of the complex variable $\omega$ for $\mathrm{Re}\,\omega > 0$ since we require that $Q(x) \equiv 0$ for $x > 0$. The solution (6.6) satisfies the boundary condition on $Z = 0$ for $x < 0$, and contains the additional function $M_-(\omega, Z)$ regular for $\mathrm{Re}\,\omega < 0$ as the equation and boundary conditions satisfied by $w(x, Z)$ for $x > 0$ are unspecified. The parameter $\delta$ is introduced for convenience and the limiting process $\delta \to 0+$ will be made in conclusion. The branch of the cube root in (6.6) is to be chosen so that the argument of the Airy function has positive real part as $\mathrm{Re}\,\omega \to \pm\infty$.

A relationship between $\bar{Q}_+(\omega)$ and $\bar{C}(\omega)$, which is defined to be the Fourier transform of $\frac{1}{2}d^2(\tilde{A}_T + \tilde{A}_B)/dx^2$, is obtained from the upper deck. With an obvious extension of the notation of (4.7), (4.8) we have that in the upper deck

$$\frac{\partial}{\partial Y}(P_{2T} - P_{2B}) = -\frac{\partial}{\partial x}(V_{2T} + V_{2B}) \quad (Y \geqslant 0), \tag{6.7}$$

and that $P_{2T} - P_{2B}$ is harmonic in the variables $x$ and $Y$. Thus if $\bar{Q}_2(\omega, Y)$ is the Fourier transform of $\frac{1}{2}\partial(P_{2T} - P_{2B})/\partial x$ we obtain, using (4.9),

$$\bar{Q}_2(\omega, Y) = \lambda^{-\frac{1}{3}}\bar{Q}_+(\omega)\, e^{-|\omega| Y}. \tag{6.8}$$

The factor $\lambda^{-\frac{1}{8}}$ is required since $\tilde{p}_2(x) = \lambda^{\frac{1}{8}} p_2(x, 0)$. If we now differentiate (6.7) with respect to $x$ and let $Y \to 0$ we deduce that

$$\frac{\partial Q_2}{\partial Y} = \lambda^{-\frac{1}{8}} \frac{1}{2} \frac{d^3}{dx^3} (\tilde{A}_T + \tilde{A}_B). \tag{6.9}$$

Finally, combining (6.8), (6.9), we have

$$-|\omega| \, \bar{Q}_+(\omega) = i\omega \bar{C}(\omega), \tag{6.10}$$

where $C(\omega)$ is the transform of $\frac{1}{2} d^2(\tilde{A}_T + \tilde{A}_B)/dx^2$.

We are now in a position to apply the second of the boundary conditions (6.4). It becomes

$$-\omega^2 \bar{w}(x, Z) \to \bar{C}(\omega) \quad \text{as} \quad Z \to \infty, \tag{6.11}$$

so that, from (6.6),

$$-\frac{\bar{C}(\omega)}{\omega^2} = \int_0^\infty \frac{\partial \bar{w}}{\partial Z} dZ = \frac{\bar{Q}_+(\omega) \, e^{-\frac{1}{3} i\pi}}{3 \operatorname{Ai}'(0) \, (\omega - i\delta)^{\frac{2}{3}}} + N_-(\omega), \tag{6.12}$$

where

$$N_-(\omega) = \int_0^\infty M_-(\omega, Z) \, dZ.$$

The function $\bar{C}(\omega)$ may now be eliminated between (6.10) and (6.12), and, if $|\omega|$ is replaced by $(\omega - i\delta)^{\frac{1}{2}} (\omega + i\delta)^{\frac{1}{2}}$, the result of the elimination is

$$\bar{Q}_+(\omega) \, K_+(\omega) = \gamma \, e^{\frac{1}{3} i\pi} (\omega - i\delta)^{\frac{2}{3}} N_-(\omega) \, K_-(\omega), \tag{6.13}$$

where

$$\frac{K_+(\omega)}{K_-(\omega)} = K(\omega) = 1 + \gamma \, e^{-\frac{1}{6} i\pi} \frac{(\omega + i\delta)^{\frac{1}{2}}}{(\omega - i\delta)^{\frac{11}{6}}} \tag{6.14}$$

and

$$0 < \gamma = -3 \operatorname{Ai}'(0) = 3^{\frac{2}{3}} / (-\tfrac{2}{3})!. \tag{6.15}$$

Equation (6.13) has been written with the left-hand side regular for $\operatorname{Re} \omega > 0$ and the right-hand side regular for $\operatorname{Re} \omega < 0$ on the assumption that the factorization (6.14) has been made. We now make the additional assumption, which may be justified *a posteriori*, that the region of regularity of the left-hand side of (6.13) may be extended to $\operatorname{Re} \omega > -\delta$, and that of the right-hand side to $\operatorname{Re} \omega < \delta$. The two sides are now equal and regular on a dense set of points, so, by analytic continuation, together they define a function which is regular everywhere. Before proceeding further it is convenient to perform the factorization of $K(\omega)$.

The function $K(\omega)$ is regular and non-zero in the $\omega$ plane cut along the positive imaginary axis from $i\delta$ to $i\infty$, and along the negative imaginary axis from $-i\delta$ to $-i\infty$. The factorization is carried out in the usual way (see, for example, Noble 1958), and we obtain

$$\frac{K'_-(\omega)}{K_-(\omega)} = \frac{11}{6(\omega - i\delta)} + \frac{2\gamma}{3\pi i} \int_0^\infty \frac{\sigma^{\frac{1}{3}} \, d\sigma}{(\gamma^2 - 3^{\frac{1}{2}} \gamma \sigma^{\frac{4}{3}} + \sigma^{\frac{8}{3}}) \, (\sigma + i\omega)}, \tag{6.16}$$

and

$$\frac{K'_+(\omega)}{K_+(\omega)} = \frac{1}{2(\omega + i\delta)} + \frac{4\gamma}{3\pi i} \int_0^\infty \frac{\sigma^{\frac{1}{3}} \, d\sigma}{(\gamma^2 + \sigma^{\frac{8}{3}}) \, (\sigma - i\omega)}. \tag{6.17}$$

We shall require in particular the values of $K_-(\omega)$, $K_+(\omega)$ for $\omega = -it\gamma^{\frac{3}{4}}$, $\omega = is\gamma^{\frac{3}{4}}$ respectively where $t$, $s$ are real and positive. They are

$$K_-(-it\gamma^{\frac{3}{4}}) = t^{\frac{11}{6}} \exp\left[ -\frac{2}{3\pi} \int_0^\infty \frac{\sigma^{\frac{1}{3}} \log(\sigma + t) \, d\sigma}{1 - 3^{\frac{1}{2}} \sigma^{\frac{4}{3}} + \sigma^{\frac{8}{3}}} \right], \tag{6.18}$$

and
$$K_+(is\gamma^{\frac{3}{4}}) = -s^{\frac{1}{2}}\exp\left[\frac{4}{3\pi}\int_0^\infty \frac{\sigma^{\frac{1}{3}}\log(\sigma+s)\,d\sigma}{1+\sigma^{\frac{8}{3}}}\right], \tag{6.19}$$

where the arbitrary multiplicative constant is chosen so that

$$\frac{K_+(\omega)}{i\omega}\to\gamma^{-\frac{3}{4}}, \quad \frac{K_-(\omega)}{i\omega}\to\gamma^{-\frac{3}{4}} \quad \text{as} \quad \mathrm{Re}\,\omega\to+\infty. \tag{6.20}$$

We are now in a position to return to (6.13). We set both sides equal to a constant $D$ so that

$$Q(x) = \frac{D}{2\pi}\int_{-\infty}^{\infty}\frac{e^{i\omega x}}{K_+(\omega)}\,d\omega. \tag{6.21}$$

Since $K_+(\omega)$ as given by (6.17) is regular and non-zero for $\mathrm{Re}\,\omega \geqslant 0$ and is asymptotic to $\omega$ as $|\omega|\to\infty$, we see that $Q(x)\equiv 0$ for $x>0$ as required. Once $\bar{Q}_+(\omega)$ is known $\bar{C}(\omega)$ is given by (6.10) and $(\partial\bar{w}/\partial Z)|_{Z=0}$ by (6.6). With the use of (6.14) where necessary the three Fourier transforms are inverted to give

$$\left.\begin{aligned}\frac{1}{2}\frac{d}{dx}(\tilde{p}_T-\tilde{p}_B) &= -\frac{D\gamma^{\frac{3}{4}}}{\pi}\int_0^\infty \frac{\exp(\gamma^{\frac{3}{4}}xt)\exp[I(t)]}{t^{\frac{1}{2}}(1+t^{\frac{8}{3}})}\,dt \quad \text{if} \quad x<0\\ &= 0 \qquad\qquad\qquad\qquad\qquad\qquad\quad \text{if} \quad x>0\end{aligned}\right\} \tag{6.22}$$

$$\left.\begin{aligned}\frac{1}{2}\frac{d^2}{dx^2}(\tilde{A}_T+\tilde{A}_B) &= \frac{D\gamma^{\frac{3}{4}}}{\pi}\int_0^\infty \frac{\exp(\gamma^{\frac{3}{4}}xt)\,t^{\frac{5}{6}}\exp[I(t)]}{1+t^{\frac{8}{3}}}\,dt \quad \text{if} \quad x<0\\ &= \frac{D\gamma^{\frac{3}{4}}}{\pi}\int_0^\infty \frac{\exp(-\gamma^{\frac{3}{4}}xs)\exp[-J(s)]}{s^{\frac{1}{2}}}\,ds \quad \text{if} \quad x>0\end{aligned}\right\}, \tag{6.23}$$

$$\left.\frac{\partial w}{\partial\bar{Z}}\right|_{Z=0} = \frac{D\gamma^{\frac{1}{2}}}{\pi}\frac{(-\frac{2}{3})!}{3^{\frac{1}{3}}(-\frac{1}{3})!}\int_0^\infty \frac{\exp(\gamma^{\frac{3}{4}}xt)\exp[I(t)]}{t^{\frac{5}{6}}(1+t^{\frac{8}{3}})}\,dt \quad \text{if} \quad x<0. \tag{6.24}$$

Here $I(t)$, $J(s)$ are the integrals appearing in (6.18), (6.19):

$$I(t) = \frac{2}{3\pi}\int_0^\infty \frac{\sigma^{\frac{1}{3}}\log(\sigma+t)}{1-3^{\frac{1}{2}}\sigma^{\frac{4}{3}}+\sigma^{\frac{8}{3}}}\,d\sigma, \tag{6.25}$$

$$J(s) = \frac{4}{3\pi}\int_0^\infty \frac{\sigma^{\frac{1}{3}}\log(\sigma+s)}{1+\sigma^{\frac{8}{3}}}\,d\sigma. \tag{6.26}$$

No expression for $(\partial w/\partial Z)|_{Z=0}$ for $x>0$ is given in (6.24) since the original equation (6.3) only determines $w$ for $x<0$. The constant $D$ will be determined by the requirement (4.15$f$) which gives

$$(-x)^{\frac{1}{2}}d(\tilde{p}_T-\tilde{p}_B)/dx\to\alpha \quad \text{as} \quad x\to-\infty. \tag{6.27}$$

In order to deduce the forms taken by (6.22)–(6.24) for large and small $|x|$, we require the asymptotic expansions of $I(t)$, $J(s)$ for small and large values of $t$, $s$. Since we find, from (6.25), (6.26), that

$$I(t)-I(t^{-1}) = \tfrac{5}{6}\log t, \quad J(s)-J(s^{-1}) = \tfrac{1}{2}\log s, \tag{6.28}$$

we need only consider small values of the variables. The results are

$$I(t) = 2^{\frac{1}{2}}t\cos\frac{\pi}{8}-\frac{t^{\frac{4}{3}}}{3^{\frac{1}{2}}}-\frac{t^2}{2^{\frac{3}{2}}}+\frac{t^{\frac{8}{3}}}{2}-\frac{2^{\frac{1}{2}}}{3}t^3\sin\frac{\pi}{8}+\frac{t^4}{3\pi}(\log t-\tfrac{1}{4})+O(t^5). \tag{6.29}$$

$$J(s) = 2^{\frac{1}{2}}s\cos\frac{\pi}{8}-\frac{2}{3^{\frac{1}{2}}}s^{\frac{4}{3}}+\frac{s^2}{2^{\frac{3}{2}}}-\frac{2^{\frac{1}{2}}}{3}s^3\sin\frac{\pi}{8}-\frac{s^4}{3\pi}(\log s-\tfrac{1}{4})+O(s^5). \tag{6.30}$$

We now determine the constant $D$ by using (6.22), (6.27), (6.29) and obtain

$$D = -\frac{\alpha\pi^{\frac{1}{2}}}{2\gamma^{\frac{3}{8}}}. \tag{6.31}$$

The quantities $\frac{1}{2}(\tilde{p}_T - \tilde{p}_B)$, $\frac{1}{2}(\tilde{A}_T + \tilde{A}_B)$ are obtained from (6.22), (6.23) by integration. The arbitrary constant in the integration of (6.22) is determined by the requirement that the pressure be continuous at $x = 0$. Of the four arbitrary

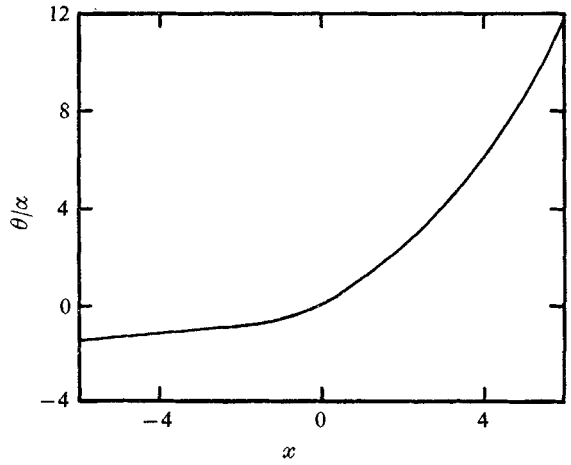


FIGURE 1. The function $\theta(x)/\alpha$.

constants that arise from (6.23), two are used to ensure that $\frac{1}{2}(\tilde{A}_T + \tilde{A}_B)$ and $\frac{1}{2}d(\tilde{A}_T + \tilde{A}_B)/dx$ are also continuous at the trailing edge, while with one of the remaining two we require that $\frac{1}{2}d(\tilde{A}_T + \tilde{A}_B)/dx \to 0$ as $x \to -\infty$ to comply with (5.10). The fourth constant is presumably determined by the constant in the asymptotic expansion of $H_2'(\eta)$ as $\eta \to \infty$ in (5.3), and is not at our disposal. However, since $\alpha^2 H_2'(\eta)$ represents a non-linear contribution to $\tilde{u}_1$ in (5.3) and the solution of this section embodies only the linear features of the fundamental problem of the trailing edge, we shall not match these two constants. The function plotted in figure 1 is $\theta(x)/\alpha$ with the definition of (4.18) extended to $x < 0$. For $x > 0$, $\theta(x)$ represents the deviation from the centre-line of the streamline that comes off the trailing edge of the plate. At $x = 0$, $\theta(x) = 0$ and $\theta'(x)$ is bounded, though $\theta''(x)$ is logarithmically infinite.

The resulting expressions for $(\tilde{p}_T - \tilde{p}_B)/2\alpha$, $(2\alpha)^{-1}\{(\partial\tilde{u}_1/\partial z)_T + (\partial\tilde{u}_1/\partial z)_B\}_{z=0}$ are illustrated in figure 2. As for $\theta(x)$, expansions were found for small and large values of $|x|$, and the integrals were evaluated numerically for intermediate values of $x$. For large $|x|$ the expansions follow easily from (6.29), (6.30) and we note the first few terms here in order to compare the results with the predictions of § 5.

If $x$ is large and negative the appropriate forms are

$$\tfrac{1}{2}(\tilde{p}_T - \tilde{p}_B) = -\alpha\left\{(-x)^{\frac{1}{2}} - \frac{(-x)^{-\frac{1}{2}}}{2^{\frac{1}{2}}\gamma^{\frac{3}{4}}}\cos\frac{\pi}{8} + \frac{(-\frac{1}{3})!}{6^{\frac{2}{3}}3^{\frac{1}{2}}}(-x)^{-\frac{5}{6}} + O((-x)^{-\frac{3}{2}})\right\}, \tag{6.32}$$

$$\tfrac{1}{2}(\tilde{A}_T + \tilde{A}_B) = \alpha\{6^{\frac{1}{3}}(-\tfrac{1}{3})!\,(-x)^{\frac{1}{6}} + O(1)\}, \tag{6.33}$$

and

$$\frac{1}{2}\left\{\left(\frac{\partial \tilde{u}_1}{\partial z}\right)_T + \left(\frac{\partial \tilde{u}_1}{\partial z}\right)_B\right\}_{z=0} = -\frac{\alpha}{6^{\frac{1}{3}}}\left[\frac{(-\frac{2}{3})!}{(-\frac{1}{3})!}\right]^2\left\{(-x)^{-\frac{1}{6}} + \frac{(-x)^{-\frac{7}{6}}}{3\,.\,2^{\frac{1}{2}}\gamma^{\frac{3}{4}}}\cos\frac{\pi}{8} + O((-x)^{-\frac{3}{2}})\right\}, \tag{6.34}$$

while for $x > 0$

$$\tfrac{1}{2}(\tilde{A}_T + \tilde{A}_B) = -\alpha\left\{\tfrac{2}{3}x^{\frac{3}{2}} + \frac{2^{\frac{1}{2}}x^{\frac{1}{2}}}{\gamma^{\frac{3}{4}}}\cos\frac{\pi}{8} - \frac{2^{\frac{4}{3}}}{3^{\frac{1}{6}}}(-\tfrac{1}{3})!\,x^{\frac{1}{6}} + O(1)\right\}. \tag{6.35}$$

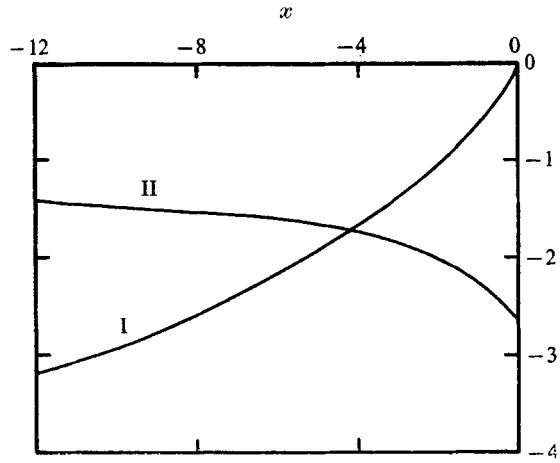


FIGURE 2. I, The anti-symmetric pressure $(\tilde{p}_T - \tilde{p}_B)/2\alpha$; II, The symmetric skin friction $\frac{1}{2\alpha}\left\{\left(\frac{\partial \tilde{u}_1}{\partial z}\right)_T + \left(\frac{\partial \tilde{u}_1}{\partial z}\right)_B\right\}_{z=0}$.

This linearized solution of the problem of the trailing edge is consistent with, and gives confidence in, the structure set out in the preceding sections. Comparison of (6.32) with (5.1) gives an estimate of the previously unknown constant $a_1$ as

$$a_1 = 2^{-\frac{1}{2}}\gamma^{-\frac{3}{4}}\cos\tfrac{1}{8}\pi = 0{\cdot}7898, \tag{6.36}$$

and then the two expressions are seen to agree except for the additional term $O((-x)^{-\frac{3}{2}})$ in (5.1). However, as this arises from the symmetric part of the pressure it is automatically excluded from (6.32). Similarly, we may compare (6.33) with (5.10), and (6.34) with (5.3) and (5.8). Finally, we note the agreement between (6.34) and (5.25) and (5.31).

The constant $a_1$ of which we have an estimate in (6.36) is related to the circulation term $B$ of (2.2) by (5.2), and the assumption of §3 that $B = O(\epsilon^3 l)$ is seen to be justified. Thus there is a stagnation point of the outer inviscid flow on the upper side of the plate at a distance from the trailing edge given by

$$-x^*/l = \epsilon^7\alpha^2 a_1^2\lambda^{-\frac{1}{4}}. \tag{6.37}$$

## 7. Supersonic trailing edges

It is of interest to compare and contrast the results for incompressible flow with those for supersonic flow. We suppose that the flat plate is fixed in a compressible fluid which has Mach number $M_\infty > 1$ at an infinite distance upstream. Thus at the leading edge of the plate an expansion fan is formed on the upper side and a shock on the lower side. According to inviscid theory the slip velocity and pressure on the plate are given by

$$\left.\begin{aligned} U_1(x^*) &= U_\infty + U_\infty \alpha^* \operatorname{sgn} y^*/(M_\infty^2 - 1)^{\frac{1}{2}}, \\ p^* &= p_\infty - U_\infty^2 \rho_\infty \alpha^* \operatorname{sgn} y^*/(M_\infty^2 - 1)^{\frac{1}{2}}. \end{aligned}\right\} \tag{7.1}$$

At the trailing edge a triple deck similar to that in incompressible flow is set up, the main difference arising from the inviscid-flow properties in the upper deck where the governing equation is the linear wave equation instead of the potential equation. The structure in fact is the same as that proposed by Stewartson & Williams (1969) for the closely related problem of self-induced separation and which is based on ideas introduced by Lighthill (1953). We write for $y^* > 0$ in the lower deck

$$\left.\begin{aligned} \frac{p^* - p_\infty}{\rho_\infty U_\infty^2} &= \epsilon^2 \frac{C^{\frac{1}{4}} \lambda^{\frac{1}{2}}}{(M_\infty^2 - 1)^{\frac{1}{4}}} \tilde{p}_T(x), \\ \frac{x^*}{l} &= \epsilon^3 \frac{C^{\frac{3}{8}} \lambda^{-\frac{5}{4}}}{(M_\infty^2 - 1)^{\frac{3}{8}}} \left(\frac{T_w}{T_\infty}\right)^{\frac{3}{2}} x, \\ \frac{y^*}{l} &= \epsilon^5 \frac{C^{\frac{5}{8}} \lambda^{-\frac{3}{4}}}{(M_\infty^2 - 1)^{\frac{1}{8}}} \left(\frac{T_w}{T_\infty}\right)^{\frac{3}{2}} z, \\ \frac{u^*(x^*, y^*)}{U_\infty} &= \epsilon \frac{C^{\frac{1}{8}} \lambda^{\frac{1}{4}}}{(M_\infty^2 - 1)^{\frac{1}{8}}} \left(\frac{T_w}{T_\infty}\right)^{\frac{1}{2}} \tilde{u}_1(x, z), \\ \frac{v^*(x^*, y^*)}{U_\infty} &= \epsilon^3 C^{\frac{3}{8}} \lambda^{\frac{3}{4}} (M_\infty^2 - 1)^{\frac{1}{8}} \left(\frac{T_w}{T_\infty}\right)^{\frac{1}{2}} \tilde{v}_1(x, z), \end{aligned}\right\} \tag{7.2}$$

as in (5.11)–(5.15) of Stewartson & Williams (1969), where $T_w$ is the wall temperature, $T_\infty$ the temperature at infinity, and $C$ is Chapman's constant which occurs in the linear viscosity law

$$\mu/\mu_\infty = CT/T_\infty, \quad C = \mu_w T_\infty / \mu_\infty T_w \tag{7.3}$$

discussed in Stewartson (1964, p. 35), for example, and $\mu$ is the coefficient of viscosity. With these assumptions the fundamental boundary-layer equation for the region $z > 0$ is the same as (4.13). The boundary conditions in $x < 0$ are the same as in (4.14) the only difference being the relation between $\tilde{p}_T(x)$ and $\tilde{A}_T(x)$. Instead of (4.15$a$) we now have

$$\tilde{p}_T(x) = -\frac{d\tilde{A}_T}{dx} - \alpha^* \frac{C^{-\frac{1}{4}} \lambda^{-\frac{1}{2}}}{\epsilon^2 (M_\infty^2 - 1)^{\frac{1}{4}}}, \tag{7.4}$$

the difference being due to the change in structure of the upper deck and to the fact that on leaving the triple deck in the upstream direction $\tilde{A}_T$ tends to zero but $\tilde{p}_T$ is given by (7.1). Similar results hold for the lower deck with some sign changes analogous to (4.15) [e.g. $\tilde{p}_T(x)$ is replaced by $-\tilde{p}_B(x)$ in (7.4)].

The form of the two lower decks in supersonic flow is quite different from that in incompressible flow because now there is no possibility of the solution at a particular station of $x$ directly affecting what happens farther upstream. Instead, on both the top and bottom of the plate, there occurs a self-induced flow due to the non-uniqueness of the governing equation (4.13) when subject to the condition (7.4). Some properties of this solution were discussed in Stewartson & Williams (1969) where it was shown that for a rising pressure the only disposable parameter is $x_0$ which fixes the position of separation. In the present problem, if $\alpha^* = 0$, we need the other solution in which the pressure falls as $x$ increases so that the skin friction increases. At the trailing edge the skin friction is greater than that given by Blasius and is the same on the upper and lower sides of the plate. Just downstream of the trailing edge the Rott & Hakkinen (1965) similarity solution holds in the neighbourhood of the line $z = 0$ with pressure gradient proportional to $x^{-\frac{1}{3}}$. Consequently $\tilde{A}_T(x)$ and $\tilde{p}_T(x)$ vary linearly as $x \to 0+$ but their second derivatives are singular. The formal solution is then continued by forward numerical integration and proceeds until, as $x \to \infty$, the Goldstein wake is approached with pressure gradient proportional to $x^{-\frac{5}{3}}$. Presumably the disposable parameter in this solution that fixes the pressure at $x = 0-$ is determined by the condition that $\tilde{p}_T(x) \to 0$ as $x \to \infty$.

When $\alpha^* > 0$ it is clear from (7.4) that the crucial parameter is $\alpha_c$ where

$$\alpha^* = \epsilon^2 C^{\frac{1}{4}} \lambda^{\frac{1}{2}} (M_\infty^2 - 1)^{\frac{1}{4}} \alpha_c. \tag{7.5}$$

If $\alpha_c \ll 1$ the effect of the inclination of the plate to the main stream may be neglected in comparison with that due to the trailing edge. If $\alpha_c = O(1)$, then there are two disposable constants $x_T$ and $x_B$ fixing the self-induced solutions of (4.13) on top and on the bottom of the plate. On the lower side the pressure will fall, and the appropriate solution is the same as for the trailing edge of a symmetrically disposed plate though $x_B \neq x_0$. On the top the pressure depends on the value of $\alpha_c$ and may fall or rise. The difference $x_T - x_B$ is determined by the condition that $\tilde{p}_T(0) = \tilde{p}_B(0)$. Thereafter the same procedure is used as when $\alpha_c = 0$ and $x_T$ is determined by the condition $\tilde{p}_T(\infty) = 0$. If the pressure rises there is a possibility of separation on the upper side and once this occurs the development of the flow is not clear. Although the separation is not accompanied by a singularity as explained in Stewartson & Williams (1969, § 9), the equation of Rott & Hakkinen (1965) does not appear to have a solution when reversed flow has occurred on one side of the plate. A further point to note is that it has not yet been determined what ultimately happens to the self-induced solution in which the pressure decreases with increasing $x$. It appears possible that $\tilde{p}(x) \to -\infty$ as $x \to \infty$ but further numerical work is required before firm conclusions may be drawn. All we can confirm at the moment is that separation occurs when $\alpha^*$, the angle of incidence of the wing, is such that

$$\alpha^* \sim \left[\frac{C(M_\infty^2 - 1)}{R}\right]^{\frac{1}{4}} \tag{7.6}$$

in contrast to the result $\alpha^* = O(R^{-\frac{1}{16}})$ in the incompressible case.

Finally we observe that, if the compressible flow is subsonic rather than supersonic, the appropriate scaling in the triple deck is the same as (7.2) except that $(M_\infty^2 - 1)$ is replaced by $(1 - M_\infty^2)$. In addition, in (3.1), $\alpha^*$ is replaced by $\alpha^*/(1 - M_\infty^2)^{\frac{1}{2}}$. The condition for separation then becomes

$$\alpha^* \sim \epsilon^{\frac{1}{2}} C^{\frac{1}{16}} \left(\frac{T_w}{T_\infty}\right)^{-\frac{3}{4}} (1 - M_\infty^2)^{\frac{7}{16}}. \tag{7.7}$$

We wish to thank Dr R. C. Lock for a helpful discussion on the nature of separation.

## REFERENCES

BLASIUS, H. 1908 Grenzschichten in Flüssigkeiten mit kleiner Reibung. *Z. Math. Phys.* **56**, 1–37.

GOLDSTEIN, S. 1930 Concerning some solutions of the boundary-layer equations in hydrodynamics. *Proc. Camb. Phil. Soc.* **26**, 1–30.

LIGHTHILL, M. J. 1953 On boundary layers and upstream influence. II. Supersonic flows without separation. *Proc. Roy. Soc.* A **217**, 478–507.

MESSITER, A. F. 1969 Boundary-layer flow near the trailing edge of a flat plate. To appear in *S.I.A.M. J. of Applied Mathematics.*

NOBLE, B. 1958 *The Wiener–Hopf technique.* Oxford: Pergamon.

RILEY, N. & STEWARTSON, K. 1969 Trailing-edge flows. *J. Fluid Mech.* **39**, 193–207.

ROTT, N. & HAKKINEN, R. J. 1965 Similar solutions for merging shear flows, II. *AIAA J.* **8**, 1553–4.

STEWARTSON, K. 1964 *The Theory of Laminar Boundary Layers in Compressible Fluids.* Oxford University Press.

STEWARTSON, K. 1969 On the flow near the trailing edge of a flat plate, II. *Mathematika*, **16**, 106–21.

STEWARTSON, K. & WILLIAMS, P. G. 1969 Self-induced separation. *Proc. Roy. Soc.* A **312**, 181–206.

*J. Fluid Mech.* (1970), *vol.* 42, *part* 3, *pp.* 585–608
*Printed in Great Britain*



# Diffraction of shock waves by a moving thin wing

By L. TING AND M. GUNZBURGER
New York University, Bronx, N.Y.

(Received 19 November 1969)

An analytical solution is obtained for the flow field due to the impinging of a plane shock wave of arbitrary strength by a thin wing moving in the opposite direction. The planform and the thickness distribution of the wing can be arbitrary and the speed of the wing can be either supersonic or subsonic relative to the undisturbed stream ahead of the shock or to that behind the shock. The solution is a generalization of the previous solution of Ting & Ludloff for the diffraction of shock wave by a two-dimensional stationary airfoil to a three-dimensional wing moving with supersonic or subsonic speed relative to the stream ahead of or behind the shock. The solution is employed for the analysis of the changes in aerodynamic forces when an airplane encounters a blast wave or a shock wave of another airplane. It is also used to study the diffraction of a shock wave or an $N$-wave advancing over flat terrains.

## 1. Introduction

The variations in aerodynamic forces on an airplane, when it encounters a shock wave due to an explosion or that of another vehicle nearby, are of practical interest (figure 1 (*a*)). The problem of the diffraction of a shock wave or an $N$-wave advancing over a flat terrain is an area of interest in the current sonic boom investigations (figure 1 (*b*)). The second problem can be considered as a special case of the first one, i.e. the diffraction of a shock wave advancing over a stationary symmetric thin wing. In this paper, analytical solutions for both problems are presented.

The solution for the conical flow field due to the diffraction of a shock wave advancing over a stationary thin wedge was obtained by Lighthill (1949). Extension to stationary wedges at yaw and to wedges moving head on with supersonic speed were obtained by Chester (1954) and by Smyrl (1963), respectively. Additional conical solutions have been developed by Blankenship (1965) for the diffraction of a shock wave by a slender cone moving with supersonic speed and by Ter-Minassiants (1969) for the diffraction of an oblique shock wave and its regular reflected wave by a small corner.

The solution for the diffraction of a shock wave by any stationary two-dimensional symmetric thin airfoil was obtained by Ting & Ludloff (1952) directly as a solution of the two-dimensional wave equation. The same method was applied to a stationary slender axially symmetric body by Ludloff & Friedman (1952). The boundary condition for the disturbance pressure $p'$ on the airfoil or the body behind the shock was fulfilled by an appropriate source distribution.

The homogeneous boundary condition across the shock, $D_{xt}p' = 0$, is replaced by an equivalent boundary condition or a fictitious source distribution on the plane of the wing or along the axis of the body ahead of the shock. The fictitious source distribution is related to the given source distribution behind the shock

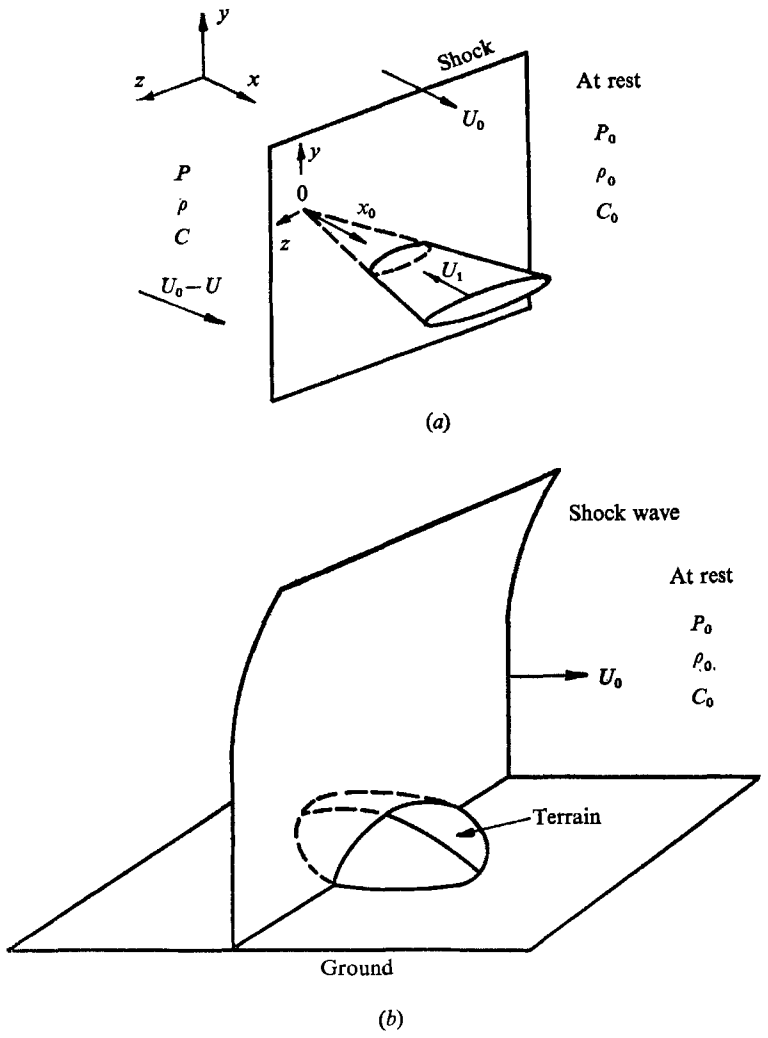


FIGURE 1. Diffraction problems: (*a*) diffraction of shock by a moving wing, (*b*) shock wave advancing over a flat terrain.

by a linear transform of the independent variables. The final solution is given by the known integral solution for unsteady linear source distributions.

Following the formulation of Ting & Ludloff (1952), Arora obtained analytic solutions for the diffraction of a shock wave by a slender body (1968) and by a planar symmetric thin wing (1969). The solutions of Arora, which were obtained by a different procedure using Laplace and Fourier transforms, can again be recognized as integral solutions of unsteady axial or planar source distributions.

In the present paper, the procedure used by Ting & Ludloff (1952) is extended to the unsteady three-dimensional problem, i.e. the diffraction of a shock wave by a moving planar symmetric thin wing. The governing differential equations and the boundary conditions are formulated in § 2. The shock condition is now of the form $D_{xt}p' = KC^2p'_{0,x_0x_0}$, where $C$ is the speed of sound behind the shock.

The inhomogeneous term is due to the disturbed pressure $p'_0$ created ahead of the shock by the moving wing. The pressure $p'_0$ is given by a steady flow solution without the shock and with the speed of sound the same as that of the stream ahead of the shock, $C_0$. In the appendix, a steady solution for an equivalent wing moving in a stream without a shock and with the speed of sound $C$ can be found so that the corresponding disturbance pressure $p^*$ creates the same inhomogeneous term in the shock condition, i.e. $D_{xt}p^* = KC^2p'_{0,x_0x_0}$. The difference between the disturbance pressure behind the shock, $p'$, and $p^*$ obeys the homogeneous shock condition and is obtained in § 3 by an extension of the procedure of Ting & Ludloff (1952). The complete analytic solution is given in § 4 together with a list of the relevant symbols. A physical interpretation of the individual terms in the solution as integral solutions for moving planar source distributions is also presented. In § 5 the analytical solution is reduced to a sum of 'quasi-steady' three-dimensional solutions, so that it is easier to carry out the integrations for a given wing. Furthermore, from the planform of the wing, a domain of influence of the shock can be defined, and outside that domain the analytic solution can be reduced to the sum of at most two steady three-dimensional solutions. In § 6, the integrals are evaluated for a simple semi-infinite swept back wing so that explicit solutions are presented. By the superposition of these explicit solutions, solutions for wings with complicated planforms and thickness distributions can be obtained in the same manner as in the steady flow problems (Donovan & Lawrence 1957). Several numerical examples are included, e.g. the diffraction of a shock wave by a flat terrain in the shape of a pyramid and the variation of the lift and drag of a triangular wing with supersonic edges impinging on a shock wave.

It should be pointed out here that the solutions of Smyrl (1963) and Arora (1968, 1969) are restricted to bodies or wings moving at supersonic speed relative to the flow ahead of the shock. The analytic solution presented in this paper is valid regardless of whether the wing is moving at supersonic or subsonic speed relative to the stream ahead of or behind the shock.

## 2. Formulation of the problem

Figure 1 (*a*) shows a thin wing lying in the $x$–$z$ plane and impinging head on to a plane shock wave moving in the direction of the $x$-axis. The undisturbed flow ahead of the shock is at rest with pressure $P_0$, density $\rho_0$ and speed of sound $C_0$ or $(\gamma P_0/\rho_0)^{\frac{1}{2}}$. The shock front is advancing with velocity $U_0$ and the undisturbed uniform stream behind the shock is moving with velocity $U_0 - U$, pressure $P$ and density $\rho$ and speed of sound $C$ or $(\gamma P/\rho)^{\frac{1}{2}}$. Relative to the shock front the Mach number ahead of the shock, $M_0 = U_0/C_0$ and that behind the shock, $M = U/C$, are related by the normal shock condition (Liepman & Roshko 1957) with

$M_0 > 1$ and $M < 1$. Likewise the pressure ratio, density ratio and the ratio of speed of sounds are related to $M_0$ or $M$ (Liepman & Roshko 1957).

The thin wing is moving in the direction of the negative $x$-axis with velocity $U_1$ relative to the undisturbed stream ahead of the shock. The velocity $U_1$ can be supersonic or subsonic relative to $C_0$. The velocity of the wing relative to the undisturbed stream behind the shock is $U_1+U_0-U$, which can be either supersonic or subsonic relative to $C$.

For a symmetric wing at zero angle of attack, the disturbed flow is symmetric with respect to the variable $y$. It suffices to consider only $y \geqslant 0$. With $\epsilon$ as the small thickness parameter, the linearized disturbance pressure, density and velocity components behind the shock will be denoted by $\epsilon p'$, $\epsilon\rho'$, $\epsilon u'$, $\epsilon v'$ and $\epsilon w'$ respectively. For the regions ahead of the shock, these disturbance quantities will be represented by the same symbols with subscript 0, namely, $\epsilon p'_0$, $\epsilon\rho'_0$, $\epsilon u'_0$, $\epsilon v'_0$ and $\epsilon w'_0$.

The linearized boundary condition on the plane of the wing is

$$ev' = e(U_1+U_0-U)f_{x_0}(x_0,z) \quad \text{for} \quad x_0 < (U_1+U_0)t, \tag{2.1}$$

and

$$ev'_0 = eU_1 f_{x_0}(x_0,z) \quad \text{for} \quad x_0 > (U_1+U_0)t, \tag{2.2}$$

where $x_0$ is fixed on the wing surface and $y = f(x_0,z)$ represents the upper surface of the wing inside the planform $S$. Outside the planform $S$, $f(x_0,z)$ vanishes.

Since the shock front is moving with supersonic speed ($M_0 > 1$) relative to the undisturbed stream ahead of the shock, the presence of the shock will not influence the flow field ahead of it. The flow field ahead of the shock is therefore a steady isentropic flow in variables $x_0, y, z$. The governing equations are,

$$\left.\begin{aligned} \rho_0 U_1 u'_0 = -p'_0, \quad \rho_0 U_1 (v'_0)_{x_0} = -(p'_0)_y, \\ \rho_0 U_1 (w'_0)_{x_0} = -(p'_0)_z, \quad C_0^2\rho'_0 = p'_0, \\ (M_1^2-1)(p'_0)_{x_0x_0} - (p'_0)_{yy} - (p'_0)_{zz} = 0. \end{aligned}\right\} \tag{2.3}$$

The boundary condition (2.2) yields a condition for $(p'_0)_y$ and the solution for the region ahead of the shock is given by the integral,

$$p'_0(x_0,y,z) = \frac{\rho_0 U_1^2}{\pi\nu}\iint \frac{f_{x_0x_0}(\xi_0,\zeta)\,d\xi_0\,d\zeta}{\{(x_0-\xi_0)^2-(M_1^2-1)[(z-\zeta)^2+y^2]\}^{\frac{1}{2}}}. \tag{2.4}$$

For the subsonic case $M_1 = U_1/C < 1$, the domain of integration is the planform of the wing and $\nu = 2$. For the supersonic case $M_1 > 1$, the domain of integration is the part of the planform of the wing inside the hyperbola,

$$\xi < x_0 - \{(M_1^2-1)[(z-\zeta)^2+y^2]\}^{\frac{1}{2}}.$$

For the region behind the shock, the flow field cannot be reduced to a steady flow and will be a function of time $t$ and three variables $x, y, z$. The co-ordinates are fixed on the undisturbed flow behind the shock. The linearized governing equations are,

$$\left.\begin{aligned} \rho'_t + \rho(u'_x+v'_y+w'_z) = 0, \\ \rho u'_t = -p'_x, \quad \rho v'_t = -p'_y, \quad \rho w'_t = -p'_z, \quad p'_t = C^2\rho'_t. \end{aligned}\right\} \tag{2.5}$$

By straightforward elimination, it is found that the disturbance pressure fulfils the simple wave equation

$$\Box p' = \left(\frac{\partial^2}{\partial x^2}+\frac{\partial^2}{\partial y^2}+\frac{\partial^2}{\partial z^2}-\frac{1}{C^2}\frac{\partial^2}{\partial t^2}\right)p' = 0, \tag{2.6}$$

while the other quantities fulfil the equation $(\partial/\partial t)(\Box g) = 0$, where $g$ stands for $u'$, $v'$, $w'$ or $\rho'$.

With (2.6) serving as the governing equation for $p'$ the next step is to state the initial conditions for the region behind the shock, i.e. $x < Ut$.

If the wing is moving at subsonic speed ($M_1 < 1$) relative to the stream ahead of the shock, the initial conditions are

$$p'(x < Ut, y, z, t) \to 0, \quad p'_t(x < Ut, y, z, t) \to 0 \quad \text{as} \quad t \to -\infty. \tag{2.7}$$

The boundary condition at infinity is

$$p'(x < Ut, y, z, t) \to 0, \quad \text{as} \quad (x^2+y^2+z^2)^{\frac{1}{2}} \to \infty. \tag{2.8}$$

For a stationary wing ($U_1 = 0$) or a wing moving with supersonic speed ($U_1/C_0 > 1$) the initial conditions and the boundary condition at infinity can be sharpened but it is not necessary to impose these sharpened ones instead of (2.7) and (2.8).

With $x_0$ related to $x$ by the translation $x_0 = x+(U_1+U_0-U)t$, the boundary conditions (2.1) and (2.5), yield a condition for $p'_y$

$$p'_y(x < Ut, 0^+, z, t) = -\rho(U_1+U_0-U)^2 f_{x_0 x_0}(x_0, z). \tag{2.9}$$

Relative to the undisturbed flow behind the shock, the air in front of the shock, the wing and the shock front are moving with velocity $-(U_0-U)$, $-(U_1+U_0-U)$ and $U$, respectively. The disturbed shock front can be expressed by the equation,

$$x = Ut+\epsilon\psi(y, z, t)+O(\epsilon^2). \tag{2.10}$$

Under the framework of linearized theory, the unit normal vector $\hat{n}$ and the shock velocity $U_s\hat{n}$ are related to $\psi(y, z, t)$ as follows,

$$\left.\begin{aligned} \hat{n} &= \hat{\imath}-\epsilon\psi_y\hat{\jmath}-\epsilon\psi_z\hat{k}, \\ U_s\hat{n} &= (U+\epsilon\psi_t)\hat{\imath}-\epsilon U\psi_y\hat{\jmath}-\epsilon U\psi_z\hat{k}. \end{aligned}\right\} \tag{2.11}$$

The continuity of tangential components of velocity across the shock yields

$$v'(x = Ut, y, z, t) = v'_0(x_0 = (U_1+U_0)t, y, z)-(U_0-U)\psi_y(y, z, t), \tag{2.12}$$

$$w'(x = Ut, y, z, t) = w'_0(x_0 = (U_1+U_0)t, y, z)-(U_0-U)\psi_z(y, z, t). \tag{2.13}$$

Solution of the continuity, normal momentum and energy equation across the shock for $\rho'$, $u'$ and $p'$ yields

$$\begin{aligned} C^2\rho'(x = Ut, y, z, t) = (1+\Omega_0)p'(x = Ut, y, z, t) \\ +\Omega_3 p'_0(x_0 = (U_1+U_0)t, y, z), \end{aligned} \tag{2.14a}$$

$$\begin{aligned} \rho C u'(x = Ut, y, z, t) = \Omega_1 p'(x = Ut, y, z, t) \\ +\rho C u'_0(x_0 = (U_1+U_0)t, y, z) \\ +\Omega_4 p'_0(x_0 = (U_1+U_0)t, y, z), \end{aligned} \tag{2.14b}$$

$$\begin{aligned} \rho(U-U_0)\psi_t(y, z, t) = \Omega_2 p'(x = Ut, y, z, t) \\ +\rho(U-U_0)u'_0(x_0 = (U_1+U_0)t, y, z) \\ +\Omega_5 p'_0(x_0 = (U_1+U_0)t, y, z), \end{aligned} \tag{2.14c}$$

where $\Omega_0 = \dfrac{-(\gamma-1)(M^2-1)^2}{M^2[2+(\gamma-1)M^2]}$,

$\Omega_1 = [(3\gamma-1)M^2+3-\gamma]/[2+(\gamma-1)M^2]$,

$\Omega_2 = -(1-M^2)/2M^2$,

$\Omega_3 = (\gamma-1)(M_0^2-1)(1-M^2)/M^2[2+(\gamma-1)M^2]$,

$\Omega_4 = -\{\gamma+1+M_0^2[2(\gamma-1)M^2+3-\gamma]\}/[2M^2(\gamma+1)]$,

$\Omega_5 = -[\gamma-3-2(\gamma-1)M^2+(\gamma+1)M_0^2(2M^2-1)]/[2M^2(\gamma+1)]$.

By using differential equations (2.3), (2.5), (2.6), the boundary conditions across the shock $x = Ut$ can be reduced to a single condition on $p'$,

$$D_{x,t}p'(x = Ut, y, z, t) = KC^2 p'_{0,x_0x_0}(x_0 = (U_1+U_0)t, y, z), \tag{2.15}$$

where

$$K = -[(\bar{M}_0+\bar{M}_1)^2[\Omega_4 - \bar{M}_0/(\bar{M}_1 M)] + (M_1^2-1)[\Omega_5 - (M^{-1}+\bar{M}_1^{-1})\bar{M}_0]M],$$

and $D_{x,t}$ is the linear differential operator defined as

$$D_{x,t} = (\Omega_1+M+\Omega_2 M)\frac{\partial^2}{\partial t^2} + (1+M^2+2M\Omega_1)C\frac{\partial^2}{\partial t\,\partial x} + (\Omega_1 M^2+M-M\Omega_2)C^2\frac{\partial^2}{\partial x^2}. \tag{2.16}$$

The differential operator $D_{x,t}$ is identical with that of the two-dimensional problem (Ting & Ludloff 1952). The inhomogeneous term is the contribution due to the disturbances created by the moving airfoil ahead of the shock.

The boundary conditions along the shock and that along the body surface creates a discontinuity in $p_y$ at their intersection, i.e. $x = Ut$, $y = 0$. Along the shock, (2.12) yields

$$(U-U_0)\psi_y(0^+, z, t) = v'(x = Ut^-, 0^+, z, t) - v'_0(x_0 = (U_1+U_0)t^+, 0^+, z).$$

Since the velocity components are continuous on either side of the shock near its intersection with the body, (2.1), (2.2) and the preceding equation give

$$(U-U_0)\psi_{yt}(0^+, z, t) = (U_1+U_0)(U_0-U)f_{x_0x_0}(x_0 = (U_1+U_0)t, z).$$

From (2.14*c*) along the shock, the following is obtained:

$$p'_y(x = Ut, y = 0^+, z, t) = [4(\gamma+1)^{-1}\rho(U_1+U_0) + \rho_0 U_1^2\Omega_5/\Omega_2]f_{x_0x_0}[(U_0+U_1)t, z]. \tag{2.17}$$

On the other hand (2.1) implies

$$p'_y(x = Ut^-, y = 0, z, t) = -\rho(U_1+U_0-U)^2 f_{x_0x_0}[(U_0+U_1)t, z]. \tag{2.18}$$

Equations (2.17) and (2.18) define the discontinuity in $p'_y$ behind the shock at its intersection with the body. It should be pointed out that in the neighbourhood ahead of the shock there is no such discontinuity in $p'_{0,y}$ since the solution $p'_0$ is not influenced by the presence of the shock.

The moving front, $x = Ut$, suggests the introduction of new variables $\bar{x}, \bar{y}, \bar{z}, \bar{t}$ from the old variables by the Lorentz transformation (Ting & Ludloff 1952).

$$\left.\begin{aligned} \bar{x} &= (x-Ut)/(1-M^2)^{\frac{1}{2}}, \quad & \bar{y} &= y, \\ \bar{t} &= (Ct-Mx)/(1-M^2)^{\frac{1}{2}}, \quad & \bar{z} &= z. \end{aligned}\right\} \tag{2.19}$$

The region behind the shock, $x < Ut$, becomes the region $\bar{x} < 0$. In this region, the wave equation remains of the same type,

$$p'_{\bar{x}\bar{x}} + p'_{\bar{y}\bar{y}} + p'_{\bar{z}\bar{z}} - p'_{\bar{t}\bar{t}} = 0. \tag{2.20}$$

The initial conditions are

$$p' = p'_{\bar{t}} = 0, \quad \text{as} \quad \bar{t} \to -\infty. \tag{2.21}$$

The boundary conditions become

$$p' \to 0, \quad \text{as} \quad \bar{x}^2 + \bar{y}^2 + \bar{z}^2 \to \infty, \tag{2.22}$$

$$p'_{\bar{y}}(\bar{x}, 0, \bar{z}, \bar{t}) = \rho C^2 A_0 f_{x_0 x_0}[x_0 = \bar{a}(\bar{t} + \bar{\lambda}_0 \bar{x}), \bar{z}], \tag{2.23}$$

$$\bar{D}_{\bar{x},\bar{t}} p'(\bar{x} = 0, \bar{y} > 0, \bar{z}, \bar{t}) = \bar{K} p'_{x_0 x_0}[x_0 = \bar{a}\bar{t}, \bar{y} > 0, \bar{z}], \tag{2.24}$$

and

$$p'_{\bar{y}}(\bar{x} = 0^-, \bar{y} = 0, \bar{z}, \bar{t}) = \rho C^2 A_0 f_{x_0 x_0}[x_0 = \bar{a}\bar{t}, \bar{z}], \tag{2.25}$$

$$p'_{\bar{y}}(\bar{x} = 0, \bar{y} = 0^+, \bar{z}, \bar{t}) = \rho C^2 \mu f_{x_0 x_0}[x_0 = \bar{a}\bar{t}, \bar{z}], \tag{2.26}$$

where

$$\bar{a} = (\bar{M}_1 + \bar{M}_0)/(1 - M^2)^{\frac{1}{2}}, \quad \bar{M}_0 = U_0/C, \tag{2.27}$$

$$\bar{\lambda}_0 = M + (1 - M^2)/(\bar{M}_0 + \bar{M}_1), \quad \bar{M}_1 = U_1/C, \tag{2.28}$$

$$A_0 = -(\bar{M}_1 + \bar{M}_0 - M)^2, \tag{2.29}$$

$$\mu = -4M(2\bar{M}_1 + \bar{M}_0)/(\gamma + 1) + M_1^2 M \Omega_5/(\bar{M}_0 \Omega_2), \tag{2.30}$$

$$\bar{D}_{\bar{x}\bar{t}} = \frac{\partial^2}{\partial \bar{x}^2} + 2M \frac{\partial^2}{\partial \bar{x}\, \partial \bar{t}} + \frac{1}{M_0^2} \frac{\partial}{\partial \bar{t}^2}, \tag{2.31}$$

$$\bar{K} = -2M(1 - M^2)^{-1}\{(\bar{M}_0 + \bar{M}_1)^2 [\Omega_4 - \bar{M}_0/(M\bar{M}_1)] + M(M_1^2 - 1)[\Omega_5 - (M^{-1} + \bar{M}_1^{-1})\bar{M}_0]\}, \tag{2.32}$$

and $\Omega_2$, $\Omega_4$, $\Omega_5$ are defined by the equations following (2.14*c*). Equations (2.20) to (2.26) summarize the mathematical formulation of the problem.

## 3. The analytic solution

The solution for the wave equation, (2.20) subjected to the initial condition, (2.21), and the boundary condition at infinity, (2.22), can be related to its normal derivative on the plane $\bar{y} = 0$ by the Kirchhoff formula (Baker & Copson 1950),

$$p'(\bar{x}, \bar{y}, \bar{z}, \bar{t}) = -\frac{1}{2\pi} \int\int_{-\infty}^{\infty} \frac{p'_{\bar{y}}(\xi, 0, \zeta, \bar{t} - \bar{r})}{\bar{r}}\, d\xi\, d\zeta, \tag{3.1}$$

where $\bar{r} = [(\bar{x} - \xi)^2 + \bar{y}^2 + (\bar{z} - \zeta)^2]^{\frac{1}{2}}$. The region where $p'_y(\bar{x}, 0, \bar{y}, \bar{t})$ is non-zero will in general be bounded.

For the left half of the plane $y = 0$ ($x < 0$), $p'_0$ is given by the boundary condition, (2.23). For the right half of the plane $\bar{y} = 0$ ($\bar{x} > 0$) $p'_y$ is undefined. The next step is to find a differential equation for $p'_y(\bar{x} > 0, 0, \bar{z}, \bar{t})$ such that the solution given by (3.1) fulfils the condition across the shock (2.24) and possesses the proper discontinuity at $\bar{x} = 0$, $\bar{y} = 0$ of (2.25), (2.26). Prior to doing this, the inhomogeneous terms in the shock condition (2.24) will be removed by splitting

the pressure disturbance $p'$ into two terms, each of which is a solution of the wave equation (2.20).

$$p' = \bar{p} + p^*; \tag{3.2}$$

$p^*$ is a solution of the type (3.1) yielding the inhomogeneous term in (2.24).

In the inhomogeneous term the pressure $p_0'(x_0, y, z)$ is given by a steady flow solution of (2.4) with speed of sound $C_0$. If the co-ordinate $x_0$ is related to $x$ and then to $\bar{x}$ so that they represent the same point for all $x_0$, the solution $p_0'$ in the new variables will not fulfil the wave equation with the speed of sound $C$ nor the equivalent equation (2.20). Since it is necessary only to reproduce the inhomogeneous term at $x_0 = (U_0 + U_1)t$ or at $\bar{x} = 0$ with $\bar{t} = Ct(1-M^2)^{\frac{1}{2}}$, a linear transformation $x_0 = \bar{a}(\bar{t} + \bar{\lambda}^* \bar{x})$ can be introduced with $\bar{\lambda}^*$ to be defined and

$$\bar{a} = (\bar{M}_0 + \bar{M}_1)/(1-M^2)^{\frac{1}{2}}. \tag{3.3}$$

The pressure $p^*$ is then defined by an integral of the type in (3.1),

$$p^* = -\frac{\rho C^2 A^*}{2\pi} \iint_{-\infty}^{\infty} \frac{d\xi\, d\zeta}{\bar{r}} f_{x_0 x_0}[\bar{a}(\bar{\lambda}^* \xi + \bar{t} - \bar{r}), \zeta]. \tag{3.4}$$

The constants $A^*$ and $\bar{\lambda}^*$ are defined by the condition,

$$D_{\bar{x}\bar{t}}\, p^*(\bar{x} = 0, \bar{y}, \bar{z}, \bar{t}) = \bar{K} p'_{0, x_0 x_0}(x_0 = \bar{a}\bar{t}, \bar{y}, \bar{z}). \tag{3.5}$$

In the appendix it is shown that this condition is fulfilled if

$$\bar{\lambda}^* = [1 - (M_1^2 - 1)/\bar{a}^2]^{\frac{1}{2}}, \tag{3.5a}$$

and

$$A^* = -(M/\bar{M}_0)\, \bar{M}_1^2 \bar{K}/[\bar{a}^2 H(-\bar{\lambda}^*)]. \tag{3.5b}$$

In the integrand of (3.4), $f[\bar{a}(\bar{\lambda}^* \bar{x} + \bar{t}), \bar{z}]$ represents an equivalent wing moving with velocity $1/\bar{\lambda}^*$.

Since the wing impinges on the shock at $t = 0$, the particular solution $p^*$ given by (3.4) fulfils all the boundary conditions and initial conditions for the region behind the shock for $t < 0$. For a wing moving at supersonic speed ($M_1 > 1$), $p^*$ is identically zero behind the shock for $t < 0$. At subsonic speed ($M_1 < 1$), $p^*$ gives the disturbance pressure behind the shock for $t < 0$. In either case, it is correct to write,

$$p' = p^* \quad \text{and} \quad \bar{p} = 0, \quad \text{for} \quad x < Mt \quad (t < 0). \tag{3.6}$$

After the impingement of the shock by the wing, $\bar{t} > 0$, the solution $p^*$ alone will not fulfil the boundary condition at $\bar{y} = 0$, $\bar{x} < 0$, (2.23). The additional contribution $\bar{p}$ should also fulfil the wave equation, (2.20), the initial condition (2.21) and the condition at infinity (2.22). The remaining boundary conditions for $p'$, (2.23) to (2.26), become respectively,

$$\bar{p}_{\bar{y}}(\bar{x} < 0, 0, \bar{z}, \bar{t}) = \rho C^2 \{A_0 f_{x_0 x_0}[\bar{a}(\bar{t} + \bar{\lambda}_0 \bar{x}), \bar{z}] + A_5 f_{x_0 x_0}[\bar{a}(\bar{t} + \bar{\lambda}_5 \bar{x}), \bar{z}], \tag{3.7}$$

$$\bar{D}_{\bar{x}, \bar{t}}\, \bar{p}(\bar{x} = 0, \bar{y} > 0, \bar{z}, \bar{t}) = 0, \tag{3.8}$$

and

$$\bar{p}_{\bar{y}}(\bar{x} = 0^-, \bar{y} = 0, \bar{z}, \bar{t}) = \rho C^2 [A_0 + A_5] f_{x_0 x_0}(\bar{a}\bar{t}, \bar{z}), \tag{3.9}$$

$$\bar{p}_{\bar{y}}(\bar{x} = 0, \bar{y} = 0^+, \bar{z}, \bar{t}) = \rho C^2 [\mu + A_5] f_{x_0 x_0}(\bar{a}\bar{t}, \bar{z}), \tag{3.10}$$

where

$$A_5 = -A^* \quad \text{and} \quad \bar{\lambda}_5 = \bar{\lambda}^*.$$

The condition (3.8) across the shock for $\bar{p}$ is homogeneous and the solution for $\bar{p}$ will be obtained in the same manner as that for a two-dimensional stationary

wing (Ting & Ludloff 1952). $\bar{p}$ will be expressed in terms of $\bar{p}_{\bar{y}}$ on the plane $y = 0$ by Kirchhoff's formula,

$$\bar{p}(\bar{x} < 0, \bar{y}, \bar{z}, \bar{t}) = -\frac{\rho C^2}{2\pi}\int_{-\infty}^{\infty} d\zeta \int_{-\infty}^{0} d\xi \{A_0 f_{\xi_0 \xi_0}[\xi_0, \zeta] + A_5 f_{\xi_5 \xi_5}[\xi_5, \zeta]\}/\bar{r}$$
$$-\frac{\rho C^2}{2\pi}\int_{-\infty}^{\infty} d\zeta \int_{0}^{\infty} d\xi \{\bar{p}_{\bar{y}}(\xi, 0, \zeta, \bar{t}-\bar{r})\}\bar{r}, \tag{3.11}$$

where $$\xi_i = (\bar{\lambda}_i \xi + \bar{t} - \bar{r})\bar{a} \quad (i = 1, 5).$$

The unknown distribution $\bar{p}_{\bar{y}}(\bar{x}, 0, \bar{z}, \bar{t})$ ahead of the shock, $\bar{x} > 0$, will be defined by the remaining boundary conditions (3.8) and (3.10). By observing the identity $[g(\xi, \zeta, \bar{t}-\bar{r})/\bar{r}]_{\bar{x}} = -[g(\xi, \zeta, \bar{t}-\bar{r})/\bar{r}]_{\xi} + [g_{\xi}(\xi, \zeta, \tau)_{\tau=\bar{t}-\bar{r}}]/\bar{r}$, the differential operator $\bar{D}_{\bar{x},\bar{t}}$, is applied to $\bar{p}$,

$$\bar{D}_{\bar{x},\bar{t}}\,\bar{p}(\bar{x} = 0, \bar{y} > 0, \bar{z}, \bar{t}) = -\frac{\rho C^2 \bar{a}^2}{2\pi}\int_{-\infty}^{\infty} d\zeta \int_{-\infty}^{0} d\xi \{A_0 H(-\bar{\lambda}_0) f^{(\mathrm{IV})}(\xi_0, \zeta)$$
$$+ A_5 H(-\bar{\lambda}_5) f^{(\mathrm{IV})}(\xi_5, \zeta)\}/\bar{r} - \frac{1}{2\pi}\int_{-\infty}^{\infty} d\zeta \int_{0}^{\infty} d\xi [\bar{D}_{\xi\tau}\bar{p}_{\bar{y}}(\xi, 0, \zeta, \tau)]_{\tau=\bar{t}-\bar{r}}/\bar{r}$$
$$-\frac{1}{2\pi}\int_{-\infty}^{\infty} d\zeta \{[\Delta_2(\zeta, \bar{t}-\bar{r}) + 2M\Delta_{1,\bar{t}}(\zeta, \bar{t}-\bar{r})]/\bar{r}\}_{\xi=0}, \tag{3.12}$$

where $$H(\bar{\lambda}) = 1/M_0^2 - 2M\bar{\lambda} + \bar{\lambda}^2,$$
$$\Delta_1(\zeta, \bar{t}) = \bar{p}_{\bar{y}}(0^+, 0, \zeta, \bar{t}) - \bar{p}_{\bar{y}}(0^-, 0, \zeta, \bar{t}),$$
$$\Delta_2(\zeta, \bar{t}) = \bar{p}_{\bar{y}\bar{x}}(0^+, 0, \zeta, \bar{t}) - \bar{p}_{\bar{y}\bar{x}}(0^-, 0, \zeta, \bar{t}),$$

and $f^{(\mathrm{IV})}$ means the fourth derivative of $f$ with respect to its first argument. Boundary condition (3.8) implies that the expression (3.12) vanishes. This will be the case if,

$$\bar{D}_{\bar{x}\bar{t}}\bar{p}_{\bar{y}}^{(1)}(\bar{x} > 0, \bar{z}, \bar{t})$$
$$= -\rho C^2 \bar{a}^2 \{A_0 H(-\bar{\lambda}_0) f^{(\mathrm{IV})}[\bar{a}(\bar{t} - \bar{\lambda}_0 \bar{x}), \bar{z}] + A_5 H(-\bar{\lambda}_0) f^{(\mathrm{IV})}[\bar{a}(\bar{t} - \bar{\lambda}_5 \bar{x}), \bar{z}]\}/2\pi, \tag{3.13}$$

and $$\Delta_2(\bar{z}, \bar{t}) = -2M\Delta_{1,t}(\bar{z}, \bar{t}). \tag{3.14}$$

For the fulfilment of the boundary condition (3.10), it is necessary to specify the appropriate limit $\bar{p}_{\bar{y}}$ as $\bar{x} \to 0^+$ along the $\bar{x}$–$\bar{z}$ plane. The limit is defined by applying a kind of 'mean value theorem' for $\bar{p}_{\bar{y}}$, namely,

$$\tfrac{1}{2}[\bar{p}_{\bar{y}}(0^+, 0, \bar{z}, \bar{t}) + \bar{p}_{\bar{y}}(0^-, 0, \bar{z}, \bar{t})] = \bar{p}_{\bar{y}}(0, 0^+, \bar{z}, \bar{t}). \tag{3.15}$$

The proof can be carried out in the same manner as that for the two-dimensional case (Ting & Ludloff 1952). A simple proof will be given here by splitting the solution $\bar{p}$, and hence $\bar{p}_{\bar{y}}$, into even and odd solutions of $\bar{x}$. For the even solution there is no discontinuity in $\bar{p}_{e,\bar{y}}$ across the $z$-axis in the $\bar{x}$–$\bar{z}$ plane. The limit of $\bar{p}_{e,\bar{y}}$ as $\bar{x} \to 0$ is unique and is equal to the value on the left side of (3.15). The odd solution, $\bar{p}_{\mathrm{odd}}$, vanishes on the plane $\bar{x} = 0$, therefore the $\bar{y}$ derivative of $\bar{p}_{\mathrm{odd}}$ vanishes on the plane $\bar{x} = 0$ for $y > 0$. From the sum of the even and odd solution, (3.15) is verified.

With the aid of (3.15) and (3.9) condition (3.10) is replaced by the following condition,

$$\bar{p}_{\bar{y}}(0^+, 0, \bar{z}, \bar{t}) = \rho C^2 (2\mu - A_0 + A_5) f_{x_0 x_0}[\bar{a}\bar{t}, \bar{z}], \tag{3.16}$$

and (3.14) becomes

$$\bar{p}_{\bar{y}\bar{x}}(0^+, 0, \bar{z}, \bar{t}) = \rho C^2 \bar{a}[4M(A_0 - \mu) + A_5\bar{\lambda}_5 + A_0\bar{\lambda}_0] f_{x_0x_0x_0}[\bar{a}\bar{t}, \bar{z}]. \tag{3.17}$$

The differential operator $\bar{D}_{\bar{x}\bar{t}}$ which is the same as that in the two-dimensional problem (Ting & Ludloff 1956) is hyperbolic and can be written as

$$(\partial/\partial\bar{x} + \bar{\lambda}_1\partial/\partial\bar{t})\,(\partial/\partial\bar{x} + \bar{\lambda}_2\partial/\partial\bar{t}).$$

The unknown $\bar{p}_{\bar{y}}(\bar{x} > 0, 0, \bar{t})$, which satisfies the differential equation (3.13) and the boundary conditions (3.16) and (3.17), is obtained in the same manner as the two-dimensional problem (Ting & Ludloff 1952). It takes the form,

$$\bar{p}_{\bar{y}}(\bar{x} > 0, 0, \bar{z}, \bar{t}) = \rho C^2 \sum_{j=1,2,3,4} A_j f_{x_0x_0}[\bar{a}(\bar{t} - \bar{\lambda}_j\bar{x}), \bar{z}]. \tag{3.18}$$

The constants $A_j$ and $\bar{\lambda}_j$ are defined in § 4.

## 4. The final solution and definitions of symbols

The disturbance pressure behind the shock is given by

$$\begin{aligned} p'(\bar{x}, \bar{y}, \bar{z}, \bar{t}) = \bar{p} + p^* = &-\frac{\rho C^2}{2\pi}\int_{-\infty}^{\infty} d\zeta \int_{-\infty}^{0} d\xi \{A_0 f_{\xi_0\xi_0}(\xi_0, \zeta)/\bar{r} + A_5 f_{\xi_5\xi_5}(\xi_5, \zeta)/\bar{r}\} \\ &-\frac{\rho C^2}{2\pi}\int_{-\infty}^{\infty} d\zeta \int_{0}^{\infty} d\xi \sum_{j=1,2,3,4} A_j f_{\xi_j\xi_j}(\xi_j, \zeta)/\bar{r} \\ &-\frac{\rho C^2 A^*}{2\pi}\int_{-\infty}^{\infty} d\zeta \int_{-\infty}^{\infty} d\xi f_{\xi^*\xi^*}(\xi^*, \zeta)/\bar{r}, \end{aligned} \tag{4.1}$$

where $\bar{r} = [(\bar{x} - \xi)^2 + \bar{y}^2 + (\bar{z} - \zeta)^2]^{\frac{1}{2}}$,

$\xi_i = \bar{a}(\bar{\lambda}_i\xi + \bar{t} - \bar{r})$ $(i = 1 \text{ or } 5)$,

$\xi_j = \bar{a}(-\bar{\lambda}_j\xi + \bar{t} - \bar{r})$ $(j = 1, 2, 3, 4)$,

$A_0 = -(\bar{M}_1 - \bar{M}_0 - M)^2$, $M = U/C$, $\bar{M}_0 = U_0/C$, $\bar{M}_1 = U_1/C$,

$\bar{a} = (\bar{M}_1 + \bar{M}_0)/(1 - M^2)^{\frac{1}{2}}$, $\bar{\lambda}_0 = M + (1 - M^2)/(\bar{M}_0 + \bar{M}_1)$,

$A_1 = -A_0 H(-\bar{\lambda}_0)/H(\bar{\lambda}_0)$, $\bar{\lambda}_1 = \bar{\lambda}_0$.

$\bar{\lambda}_2$, $\bar{\lambda}_3$ are two roots of the quadratic equation,

$$H(\bar{\lambda}) = \bar{\lambda}^2 - 2M\bar{\lambda} + M_0^{-2} = 0, \quad M_0 = U_0/C_0,$$

$$-A_5 = A^* = \bar{K}(M/\bar{M}_0)\,\bar{M}_1^2(1 - M^2)/[(\bar{M}_1 + \bar{M}_0)^2 H(-\bar{\lambda}_5)],$$

$$\lambda_5 = \{1 - (M_1^2 - 1)(1 - M^2)/(\bar{M}_0 + \bar{M}_1)^2\}^{\frac{1}{2}},$$

$$\lambda_4 = \lambda_5, \quad A_4 = -A_5 H(-\bar{\lambda}_5)/H(\bar{\lambda}_5),$$

$$\xi^* = \bar{a}(\bar{\lambda}^*\xi + \bar{t} - \bar{r}), \quad M_1 = U_1/C_0,$$

and $A_2$ and $A_3$ are the solution of the two linear simultaneous equations,

$$A_2 + A_3 = 2\mu - A_0 - A_1 - A_4 + A_5,$$

$$\bar{\lambda}_2 A_2 + \bar{\lambda}_3 A_3 = 4M(\mu - A_0) - A_0\bar{\lambda}_0 - A_1\bar{\lambda}_1 - A_4\bar{\lambda}_4 - A_5\bar{\lambda}_5.$$

$\bar{K}$ and $\mu$ are defined by the equations following (2.26).

In (4.1), the last integral with coefficient $A^*$ is the disturbance pressure $p^*$, induced by the equivalent wing to remove the inhomogeneous term in the shock equation induced by the disturbances ahead of the shock. The first integral with coefficient $A_0$ represents the disturbance pressure induced by the position of the wing behind the shock and the induced inhomogeneous terms on the shock condition are removed by its mirror image in the region ahead of the shock, i.e. the integral with the coefficient $A_1$ and $\bar{\lambda}_1 = \bar{\lambda}_0$. The integral with the coefficient $A_5$ $(= -A^*)$ and $\bar{\lambda}_5 = \bar{\lambda}^*$ cancels the normal velocity on the $x$–$z$ plane induced by the presence of the equivalent wing behind the shock and similarly its induced inhomogeneous term is removed by its mirror image, the integral with coefficient $A_4$ and $\bar{\lambda}_4 = -\bar{\lambda}_5$. The remaining two integrals with coefficients $A_2$ and $A_3$ are induced by the image source distribution ahead of the shock. With $\bar{\lambda}_2$ and $\bar{\lambda}_3$ as the two roots of the characteristic equation, the two integrals fulfil the homogeneous shock condition and the coefficients $A_2$ and $A_3$ are chosen so that the final solution fulfils the condition of discontinuity at the intersection of the shock with the wing surface. By the inverse Lorentz transformation, the pressure distribution in physical variables $x, y, z, t$ is obtained.

The density variation is obtained from the differential equation (2.5) and the boundary condition (2.14$a$),

$$\rho'(x,y,z,t) = (1/C^2)\{p'(x,y,z,t) + \Omega_0 p'(x,y,z,t = x/U) + \Omega_3 p_0'[x_0 = (U_1 + U_0)\,x/U, y, z]\}.$$

The shock shape is obtained from (2.14$c$)

$$\psi(y,z,t) = [\rho(U-U_0)]^{-1}\,\Omega_2 \int_0^t p'(x = U\tau, y, z, \tau)\,d\tau + \frac{[1 - \Omega_5(M/\bar{M}_0)\,U_1/(U_0 - U)]}{(U_1 + U_0)}\,\phi_0[x_0 = (U_0 + U_1)\,t, y, z],$$

where $\phi$ is the disturbance velocity potential ahead of the shock with $u_0' = \phi_{0,x_0}$.

## 5. Reduction to quasi-steady integrals

In the seven integrals in (4.1) the integration variables $\xi$ and $\zeta$ are involved implicitly in the first argument of the steady source distribution function. In order to expedite the integration, the variable $\xi$ will be replaced by the first argument of the source distribution function. After this transformation of variables, the last integral becomes a steady three-dimensional solution of an equivalent wing as shown in the appendix. The other six integrals will be reduced to quasi-steady integrals, i.e. the variable $\bar{t}$ appears explicitly in the limit of integration only. From the domains of integration for these new integrals, the boundaries of the disturbed regions behind the shock can be defined directly from the planform of the wing. The limits of integration for $\xi$ for the first two integrals in (4.1) are $-\infty$ and 0 and for the next four integrals are 0 and $\infty$. For these two groups of integrals the transformation of variables will be discussed separately.

With $\xi = \bar{a}(\bar{\lambda}_i \xi + \bar{t} - \bar{r}), i = 0$ or 5, the first group of integrals becomes

$$-\frac{\rho C^2 A_i}{2\pi}\left\{\int_{-\infty}^{\infty} d\zeta \int_{-\infty}^{\tilde{\xi}} F(x_i, \tilde{M}_i, \xi_i, \zeta, \bar{y}, \bar{z})\, d\xi_i + \sigma_i \int_{z-\hat{\xi}_i}^{z+\hat{\xi}_i} d\zeta \int_{\tilde{\xi}}^{\xi_{i,m}} F(x_i, \tilde{M}_i, \xi_i, \zeta, \bar{y}, \bar{z})\, d\xi_i\right\}, \tag{5.1}$$

where

$$x_i = \bar{a}(\bar{\lambda}_i \bar{x} + \bar{t}),$$

$$\tilde{M}_i^2 = 1 + \bar{a}^2(1 - \bar{\lambda}_i^2), \quad \tilde{M}_i \gtrless 1, \quad \text{for} \quad \bar{\lambda}_i \lesseqgtr 1, \tag{5.2}$$

$$F(x_i, \tilde{M}_i, \xi_i, \zeta, \bar{y}, \bar{z}) = f_{\xi_i \xi_i}(\xi_i, \zeta)\{(x_i - \xi_i)^2 - (\tilde{M}_i^2 - 1)[\bar{y}^2 + (\bar{z} - \zeta)^2]\}^{-\frac{1}{2}}, \tag{5.3}$$

$$\tilde{\xi} = \xi_i(\text{at } \xi = 0) = \bar{a}\{\bar{t} - [\bar{x}^2 + \bar{y}^2 + (\bar{z} - \zeta)^2]^{\frac{1}{2}}\}, \tag{5.4}$$

$$\sigma_i = 0, \quad \text{for} \quad \tilde{M}_i < 1, \tag{5.5a}$$

$$\sigma_i = 0, \quad \text{for} \quad \tilde{M}_i > 1 \quad \text{and} \quad \partial\xi_i/\partial\xi \geqslant 0 \quad \text{at} \quad \xi = 0, \tag{5.5b}$$

$$\sigma_i = 2, \quad \text{for} \quad \tilde{M}_i > 1 \quad \text{and} \quad \partial\xi_i/\partial\xi < 0 \quad \text{at} \quad \xi = 0, \tag{5.5c}$$

$$\xi_{i,m} = x_i - \{(M_i^2 - 1)[\bar{y}^2 + (\bar{z} - \zeta)^2]\}^{\frac{1}{2}}, \tag{5.6}$$

$$\tilde{\zeta}_i = \{(1 - \bar{\lambda}_i^2)\bar{x}^2 - \bar{\lambda}_i^2 \bar{y}^2\}^{\frac{1}{2}}/\bar{\lambda}_i. \tag{5.7}$$

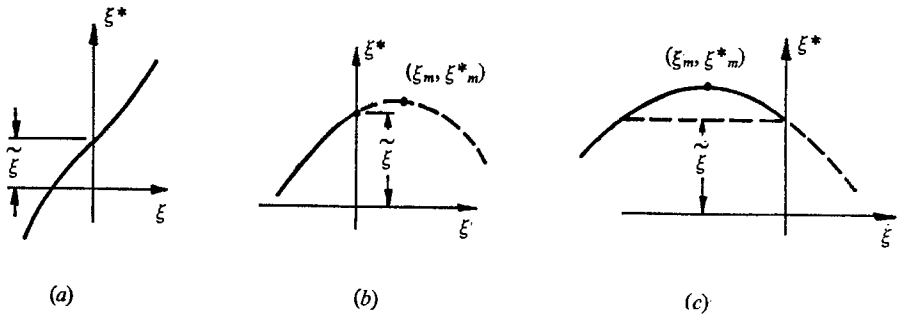


FIGURE 2. Transformation from $\xi$ to $\xi^*$ or $\xi_j$: (a) $1/\bar{\lambda} < 1$, (b) $1/\bar{\lambda} > 1$, $\xi_m > 0$, (c) $1/\bar{\lambda} > 1$, $\xi_m < 0$.

Intermediate steps in the transformation are supplied in the first part of the appendix with the aid of figure 2. The second integral appears only when conditions in (5.5c) are fulfilled. The condition $\partial\xi_i/\partial\xi < 0$ at $\xi = 0$ implies

$$\bar{\lambda}_i + \bar{x}/[\bar{x}^2 + \bar{y}^2 + (\bar{z} - \zeta)^2]^{\frac{1}{2}} < 0. \tag{5.8}$$

This is impossible if $\bar{\lambda}_i < 1$, i.e. $\tilde{M}_i > 1$ and

$$0 < -\bar{\lambda}_i[\bar{y}^2 + (\bar{z} - \zeta)^2]^{\frac{1}{2}}/(1 - \bar{\lambda}_i)^{\frac{1}{2}} < \bar{x}. \tag{5.9}$$

Condition (5.9) in turn defines the limits $\bar{z} \pm \hat{\zeta}_i$ for $\zeta$ in the second integral.

For the second group of integrals, the variable $\xi$ is replaced by $\xi_j$ with

$$\xi_j = \bar{a}[\bar{t} - \bar{r} - \bar{\lambda}_j \xi] \quad (j = 1, 2, 3, 4),$$

the second group becomes

$$-\frac{\rho C^2 A_j}{2\pi}\int_{-\infty}^{\infty} d\zeta \int_{-\infty}^{\tilde{\xi}} F(x_j, \tilde{M}_j, \xi_j, \zeta, \bar{y}, \bar{z})\, d\xi_j,$$

where
$$x_j = \bar{a}(\bar{t} - \bar{\lambda}_j \bar{x}), \tag{5.10}$$
and
$$\tilde{M}_j^2 = 1 + \bar{a}^2(1 - \bar{\lambda}_j^2). \tag{5.11}$$

$F$ and $\tilde{\xi}$ are defined by (5.3) and (5.4). The integrals are evaluated for $\bar{x} < 0$; it is clear that $\partial \xi_j / \partial \xi = \bar{a}[(\bar{x} - \xi)/\bar{r} - \bar{\lambda}_j] < 0$ for $0 \leqslant \xi < \infty$. The negative sign assigned to the square root of the integrand is then cancelled by interchanging the limits. After the transformation of variables, (4.1) becomes

$$\left.\begin{aligned} p'(\bar{x}, \bar{y}, \bar{z}, \bar{t}) &= \bar{p}_J + \bar{p}_0 + \bar{p}_5 + p^*, \\ \bar{p}_J &= -\frac{\rho C^2}{2\pi} \iint_{\tilde{\Gamma}} d\zeta\, d\xi \sum_{j=0}^{5} A_j F(x_j, \tilde{M}_j, \xi, \zeta, \bar{y}, \bar{z}), \\ \bar{p}_0 + \bar{p}_5 &= -\frac{\rho C^2}{2\pi} \sum_{i=0,5} \sigma_i \iint_{\Gamma_i} d\zeta\, d\xi\, A_i F(x_i, \tilde{M}_i, \xi, \zeta, \bar{y}, \bar{z}), \\ p^* &= -\frac{\rho C^2}{\nu\pi} \iint_{\Gamma^*} A_* F(x^*, M_1, \xi, \zeta, \bar{y}, \bar{z})\, d\zeta\, d\xi. \end{aligned}\right\} \tag{5.12}$$

Again $F$ is defined by (5.3). The domain of integration for the first group of integrals is the domain $\tilde{\Gamma}$ inside the hyperbola (figure 3),

$$\tilde{H} : \xi = \bar{a}\{\bar{t} - [\bar{x}^2 + \bar{y}^2 + (\bar{z} - \zeta)^2]^{\frac{1}{2}}\}. \tag{5.13}$$

The domain of integration for the second group, which is real under condition (5.5$c$), is the domain $\Gamma_i$ bounded by the hyperbola $\tilde{H}$ and the hyperbola,

$$H_i : \xi = x_i - \{(\tilde{M}_i^2 - 1)[\bar{y}^2 + (\bar{z} - \zeta)^2]\}^{\frac{1}{2}}, \quad \text{for} \quad i = 0, 5. \tag{5.14}$$

$H_i$ and $\tilde{H}$ are tangential to each other at $\zeta_i = \bar{z} \pm \tilde{\zeta}_i$. For the last integral, the domain of integration, $\Gamma^*$, is the entire $\xi$–$\zeta$ plane for $M_1 < 1$ and for $M_1 > 1$ is the domain inside the hyperbola,

$$H^* : \xi = x^* - \{(M_1^2 - 1)[\bar{y}^2 + (\bar{z} - \zeta)^2]\}^{\frac{1}{2}}. \tag{5.15}$$

From the definitions of $\tilde{M}_j$, $x_j$ and $\bar{\lambda}_j$, the following relevant results are obtained:

(i) $\tilde{M}_0 = \tilde{M}_1 = (U_0 + U_1 - U)/C$ = Mach number of wing relative to the undisturbed stream behind the shock.

(ii) $\tilde{M}_2 > 1$, $\tilde{M}_3 > 1$, since $\bar{\lambda}_2 < 1$, $\bar{\lambda}_3 < 1$ and they depend only on the strength of the shock, $M_0$.

(iii) $M_1 = \tilde{M}_4 = \tilde{M}_5$ = Mach number of the wing relative to the undisturbed stream ahead of the shock.

(iv) $x_0$ is a co-ordinate fixed on the wing and $x_5$ and $x^*$ are the same co-ordinates fixed on the fictitious wing.

(v) For $M_1 > 1$, the hyperbolas $H_5$ and $H^*$ are the same but the domain $\Gamma_5$ is contained inside $\Gamma^*$.

The domains of integrations in (5.12) and the constant $\sigma_i$ and $\nu$ depend on whether the Mach numbers $\tilde{M}_0$ and $M_1$ are greater or less than unity, i.e. they depend on the Mach number of the wing relative to the flow behind and to the flow ahead of the shock, respectively. The following are the three possible combinations for $\tilde{M}_0$ and $M_1$:

(i) $M_1 < 1$, $\tilde{M}_0 < 1$; (ii) $M_1 < 1$, $\tilde{M}_0 > 1$ and (iii) $M_1 > 1$, $\tilde{M}_0 > 1$.

The fourth combination, $M_1 > 1$ and $\tilde{M}_0 < 1$, as shown by the following inequalities and identities, does not exist:

$$[(C_0+U_0-U)^2-C^2]/C_0^2 = 2[(2-\gamma)M_0^2+2M_0-1][M_0^2-1]/[(\gamma+1)M_0^2] > 0, \quad (5.16)$$

and
$$\tilde{M}_0-1 = (M_1C_0+U_0-U-C)/C > (C_0+U_0-U-C)/C > 0. \quad (5.17)$$

For a given wing, the strength of the source distribution vanishes outside the planform $S$ of the wing. The domains of integration for the integrals in (5.12) can therefore be reduced from the appropriate $\Gamma$'s to their intersection with $S$ (figure 3).

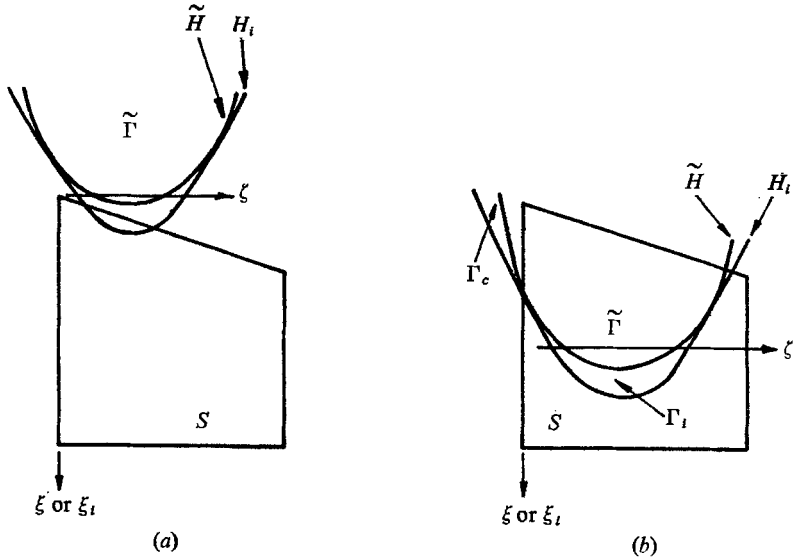


FIGURE 3. Hyperbolas $\tilde{H}$ and $H_t$ (*a*) for a point in $G_2$, i.e. outside the domain of influence of the shock, (*b*) for a point in $G_1$, i.e. in the domain of influence of the shock.

Let $G_1(\bar{t})$ designate the region in the half space $\bar{x} \leqslant 0$, such that for any point $\bar{x}$, $\bar{y}$, $\bar{z}$ in $G_1(\bar{t})$ the domain of integration for the first group of integrals at the instant $\bar{t}$ is not zero, i.e. $S \cap \tilde{\Gamma} \neq 0$. $S \cap \tilde{\Gamma}$ denotes the intersection of the planform $S$ with the domain $\tilde{\Gamma}$ inside the hyperbola $\tilde{H}$. For points in $G_1(\bar{t})$, the first group of integral $p'_J$ which involves $\bar{t}$ explicitly will not vanish. Furthermore, the image of source distributions due to the shock condition are contained only in the first group of integrals, therefore, domain $G_1(\bar{t})$ will be called the domain of influence of the shock.

Let $G_2(\bar{t})$ designate the complement of $G_1(\bar{t})$ in the half space $x \leqslant 0$, i.e. for any point $\bar{x}, \bar{y}, \bar{z}$ in $G_2$, $S \cap \tilde{\Gamma} = 0$ and the first group of integrals vanishes, $\bar{p}_J = 0$. The remaining integrals depend on the combinations of $M_1$ and $\tilde{M}_0$.

(i) For $\tilde{M}_0 < 1$ and $\tilde{M}_5 = M_1 < 1$, $\sigma_0 = \sigma_5 = 0$, the group of integrals $\bar{p}_0$ and $\bar{p}_5$ vanishes. The disturbance pressure $p'$ is given by the steady subsonic solution $p^*$ of the fictitious equivalent wing, i.e.

$$p'(\bar{x},\bar{y},\bar{z},\bar{t}) = p^*(x^*,\bar{y},\bar{z}), \quad \text{for} \quad \bar{x},\bar{y},\bar{z} \quad \text{in} \quad G_2(\bar{t}). \quad (5.18)$$

(ii) For $\tilde{M}_0 > 1$ and $\tilde{M}_5 = M_1 < 1$, $\sigma_0 = 2$ and $\sigma_5 = 0$, the first integral of the second group, $\bar{p}_0$, does not vanish. Since $S \cap \tilde{\Gamma} = 0$, the boundary of the domain

of integration $\Gamma_0 \cap S$ will be composed of the boundary of the planform $S$ and the hyperbola $H_0$. Neither of them depends on $t$ explicitly. The integral $\overline{p}_0$ will therefore be a steady solution in $x_0, y, z$ variables.

(iii) For $\tilde{M}_0 > 1$ and $M_1 > 1$, $\sigma_0 = \sigma_5 = 2$, both integrals $\overline{p}_0$ and $\overline{p}_5$ in the second group do not vanish. The integral $\overline{p}_0$ will have the same properties as that in the proceeding case. Similarly, $\overline{p}_5$ will be a steady solution in $x_5, y, z$ variables.

The domain $G_2$ can be further subdivided with regions where $\overline{p}_0$ vanishes or $\overline{p}_5$ cancels $p^*$. The subdivisions for a general planform are presented in Gunzburger (1969). The basic principle for the subdivisions is illustrated in § 6 for a simple planform with straight edges.

## 6. Examples

The theoretical results will be applied to a wing with a basic planform and thickness distribution as shown in figure 4. The leading edge is $x_0 = kz$ and the two sides are $z = 0$ and $z = B$. The inclination of the upper surface is $\epsilon$, i.e.

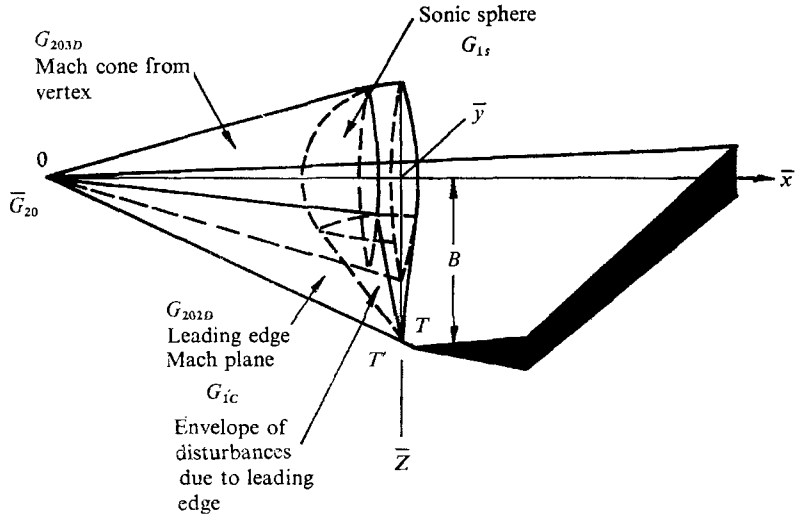


FIGURE 4. Illustration of different regions for wing which is subsonic ahead of shock and supersonic with supersonic edges behind shock.

$f_{x_0}(x_0, z) = 1$. The given planform has two corners, the vertex 0 at the origin of $x_0$–$z$ axes and the wing tip, $T$ at $(kB, B)$. By superposition of the analytical solutions for this basic wing, numerical results for the pressure distributions and aerodynamic forces for more complicated wings are obtained and presented in § 6 (iii). In order to simplify the description for the various regions of § 5 for the basic planform, it is assumed that at the instant under investigation, the wing tip is still ahead of the shock, i.e. $kB > (U_0 + U_1)\,t$. The span $B$ will not appear in the solution except in $p^*(x^*, y, z)$ when $M_1 < 1$. With the planform of the wing behind the shock having only one corner at 0, the boundaries of various regions will depend on the swept back $k$ and the Mach numbers $M_1$ and $\tilde{M}_0$.

(i) *Definition of the regions*

The definition of various regions depend on the combinations of supersonic or subsonic Mach numbers $M_1$ and $\tilde{M}_0$ relative to the stream ahead and behind the shock and the swept back slope $k$ of the leading edge with respect to the Mach cone and the sonic sphere. A special combination is described in detail in this section. Descriptions for all the other possible combinations can be found in Chow & Gunzburger (1969) and Gunzburger (1969).

For the wing moving with subsonic speed relative to the stream ahead of and supersonic to that behind the shock ($M_1 < 1$, $\tilde{M}_0 > 1$) and with a supersonic leading edge $k < \bar{a}(1-\bar{\lambda}_0^2)^{\frac{1}{2}}$, the region of influence of the shock $G_1$ is composed of the hemi-sonic sphere $G_{1s}$ and the half cone, $G_{1c}$ with vertex at the intersection of the leading edge with the shock $T'(0, 0, \bar{a}\bar{t}/k)$ and tangential to the sphere. The cone is the envelope of the sonic spheres created by the passing of the leading edge through the shock. The region $G_2$, which is outside $G_1$ and behind the shock, can be subdivided to $G_{20}$ and its complement $G_{2c}$. In $G_{2c}$ the disturbance pressure is $p^*$ alone, induced by the subsonic disturbance created ahead of the shock. In $G_{20}$, it is the sum of $p^*$ and $\bar{p}_0$, the steady solution for the wing alone.

The boundary between $G_{20}$ and $G_{2c}$ is the Mach cone from the vertex of the wing and the Mach plane from the leading edge. The region $G_{20}$ is composed of two subregions $G_{20,3D}$ and $G_{20,2D}$. $G_{20,3D}$ is bounded by the Mach cone from the vertex 0, the sonic sphere and the half cone containing $G_{1c}$. For the wing with a constant inclined surface, $\bar{p}_0$ in $G_{20,3D}$ is the same as the steady conical solution and $\bar{p}_0$ in $G_{20,2D}$ is given by the constant value on a wedge with supersonic swept back.

(ii) *Evaluation of integrals and numerical results*

With $f_{x_0 x_0}(x_0, z) = 0$ inside the planform, $f_{x_0 x_0}$ becomes a $\delta$-function and the double integrals in (5.12) can be carried out immediately and the line integrals with respect to $\zeta$ can be written as

$$E(X, \tilde{M}, y, z, \zeta) = \int^{\zeta} d\zeta\{(X-k\zeta)^2 - (\tilde{M}^2-1)[y^2+(z-\zeta)^2]\}^{-\frac{1}{2}},$$

$$E = \frac{1}{(\tilde{k})^{\frac{1}{2}}} \sinh^{-1} \frac{\zeta\tilde{k} - Z}{[(1-\tilde{M}^2)I]^{\frac{1}{2}}}, \quad \text{for} \quad \tilde{M} < 1,$$

$$= \frac{-1}{\tilde{k}} \log(X - k\zeta), \quad \text{for} \quad \tilde{M} = 1,$$

$$= \frac{1}{(\tilde{k})^{\frac{1}{2}}} \cosh^{-1} \frac{Z - \zeta\tilde{k}}{[(\tilde{M}^2-1)I]^{\frac{1}{2}}}, \quad \text{for} \quad \tilde{M} > 1, \quad \tilde{k} > 0,$$

$$= -[k^2(y^2+z^2) + X^2 - 2\zeta Z]^{\frac{1}{2}}/Z, \quad \tilde{M} > 1, \quad \tilde{k} = 0,$$

$$= \frac{1}{(-\tilde{k})^{\frac{1}{2}}} \sin^{-1} \frac{Z - \zeta\tilde{k}}{[(\tilde{M}^2-1)I]^{\frac{1}{2}}}, \quad \tilde{M} > 1, \quad \tilde{k} < 0,$$

where

$$\tilde{k} = k^2 + 1 - \tilde{M}^2, \quad Z = kX + (1+\tilde{M}^2)z \quad \text{and} \quad I = [(X-kz)^2 + \tilde{k}y^2]^{\frac{1}{2}}.$$

For the last integral in (5.10) for $p'$, $p^*(x^*, y, z)$ becomes

$$p^* = -A^*[E(x^*, y, z, M_1, S) - E(x^*, y, z, M_1, 0)]/(2\pi), \quad \text{for} \quad M_1 < 1,$$
$$= -A^*[E(x^*, y, z, M_1, \zeta^+) - E(x^*, y, z, M_1, \zeta^-)]/\pi, \quad \text{for} \quad M_1 > 1.$$

$\zeta^+$ and $\zeta^-$ are the two roots of the equation, $(x^* - k\zeta)^2 - (M_1^2 - 1)[y^2 + (z-\zeta)^2] = 0$ with $\zeta^+ \geqslant \bar{\zeta}$. If $\zeta^- < 0$, $\zeta^-$ is set equal to zero, and if $\zeta^+ < 0$, $p^*$ is set equal to zero.

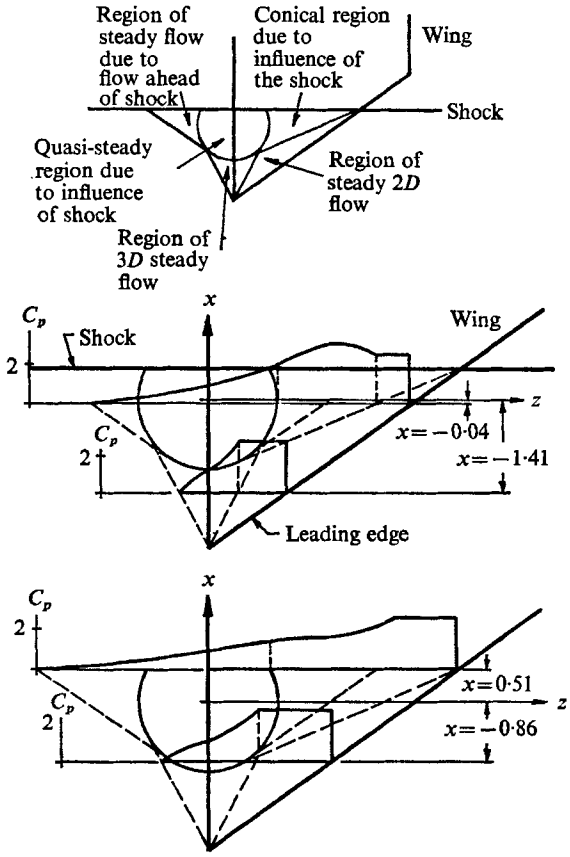


FIGURE 5. Pressure coefficient for supersonic wing with supersonic edges ($M = 0{\cdot}51$, $M_1 = 1{\cdot}5$, $k = 0{\cdot}75$, $y = 0$, $ct = 1$).

For the first group of integrals, $\bar{p}_J$ is equal to zero in region $G_2$; inside region $G_1$,

$$\bar{p}_J = -\frac{1}{2\pi} \sum_{j=1,2,3,4,5} A_j[E(x_j, y, z, \tilde{M}_j, \tilde{\zeta}^+) - E(x_j, y, z, \tilde{M}_j, \tilde{\zeta})],$$

where $\tilde{\zeta}^+$ and $\tilde{\zeta}^-$ with $\tilde{\zeta}^+ \geqslant \tilde{\zeta}^-$ are the $\zeta$ co-ordinates of the points where the leading edge $\xi = k\zeta$ intersect the hyperbola $\tilde{H}$. If $\tilde{\zeta}^- < 0$, it is replaced by zero.

The second group of integrals $\bar{p}_0$ and $\bar{p}_5$ are non-zero only when the conditions stated in (5.4*c*) are fulfilled and then they are defined as follows:

$$\bar{p}_i = -A_i[E(x_i, y, z, \tilde{M}_i, \zeta_i^+) - E(x_i, y, z, \tilde{M}_1, \zeta_i^-)]/\pi \quad \text{in} \quad G_2,$$

and

$$\bar{p}_i = -A_i[E(x_i, y, z, \tilde{M}_i, \zeta_i^+) - E(x_i, y, z, \tilde{M}_i, \tilde{\zeta}^+) + E(x_i, y, z, \tilde{M}_i, \tilde{\zeta}^-) - E(x_i, y, z, \tilde{M}_i, \zeta_i^-)]/\pi \quad \text{in} \quad G_1,$$

where $i = 0$ or 5, $\zeta_i^+$, $\zeta_i^-$ are the two roots of

$$(x_i - k\zeta)^2 - (\tilde{M}_i^2 - 1) - [y^2 + (z-\zeta)^2] = 0$$

with $\zeta_i^+ \geqslant \zeta_i^-$. If $\zeta_i^- < 0$, it is replaced by zero.

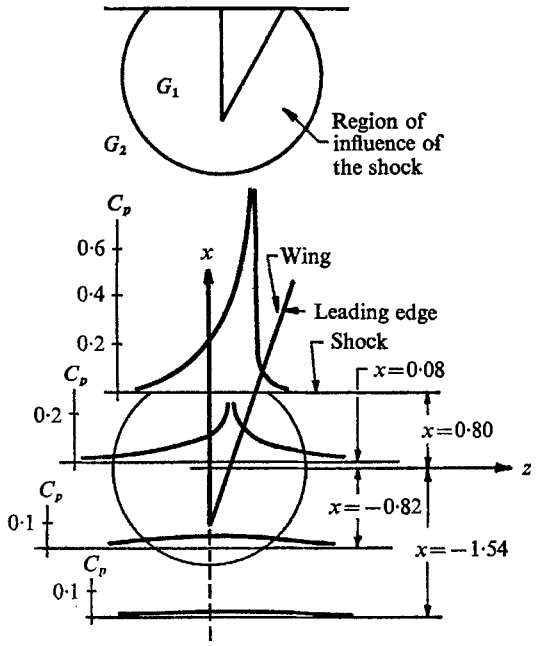


FIGURE 6. Pressure coefficient for a subsonic wing ($M = 0{\cdot}8$, $M_1 = 0{\cdot}25$, $k = 3$, $y = 0$, $ct = 1$).

A numerical program is written to distinguish various regions and to compute from the sum of these explicit expressions for $p^*$, $\bar{p}_J$, $\bar{p}_0$ and $\bar{p}_5$, the disturbance pressure $p'$ behind the shock. The program yields result for all $t$, i.e. it works also when the wing tip passes behind the shock. The program can also superpose several basic planforms. Numerical examples for all possible combinations of Mach numbers $M_1$ and $\tilde{M}_0$ and the swept back $k$ and also for several composite planforms are given in Chow & Gunzburger (1969).

Figures 5 and 6 show two of the numerical examples for the wings with a straight leading edge. The pressure distribution on the wing at various stations of $x$ are shown together with the various domains in $x$, $y$, $z$ space. In figure 5 the Mach numbers of the wing with respect to the stream ahead and behind the shock are both supersonic ($M_1 > 1$, $\tilde{M}_0 > 1$).

The characteristics of the pressure distribution in various regions are quite obvious. The discontinuities in the slope of the pressure curve as it crosses the boundaries of various domains, e.g. the sonic sphere, the Mach cone, are quite obvious. In particular, along the intersection of the wing with the shock, $x = MCt$,

the disturbance pressure is constant outside the Mach cone of the equivalent wing and is the value along a ray from the vertex $T'$ of the conical solution. At $T'$ the pressure is not single valued. It ranges from the two-dimensional value behind the oblique shock attached to the leading edge and the conical values along the rays from the vertex $T'$ to zero ahead of the leading edge. In figure 6, the wing is moving at subsonic speed ($M_1 < 1$, $\bar{M}_0 < 1$). Outside the region $G_1$ the disturbance pressure is the subsonic steady solution $p^*(x^*, y, z)$ corresponding to a wing moving at velocity $(1-\bar{\lambda}^* M)\,C/(\bar{\lambda}^* - M) = U^*$ in $x$–$t$ variables. The pressure distribution behind the shock for $t < 0$ can be obtained from the present result by a translation of $x$ co-ordinate, e.g. the pressure distribution at the instant $t_0 > 0$ at $x = -2Ct_0$ is the same as that at $x = -(2C - U^*)\,t_0$ at the instant $t = 0$.

(iii) *Applications*

For a thin symmetric wing with an arbitrary planform and thickness distribution, the pressure disturbance behind the shock wave can be obtained directly from (4.1) or (5.12) by numerical evaluation of the double integrals. For wings designed for high-speed flight, the planform can be decomposed to several triangles and the inclination of the surface in each triangle is a constant. The pressure distribution for such wings can be obtained by superposition of the explicit solutions given in § 6(i) and § 6(ii) for wings with the basic planform in the same manner as in the steady three-dimensional problems (Donovan & Lawrence 1957).

For a wing at an angle of attack moving at supersonic speed and with supersonic edges relative to the stream behind the shock, the flow fields above and below the wing are not influenced by each other and by the flow field behind the trailing edge. The pressure distribution on the top and the bottom surfaces can therefore be computed by the analysis of this paper for wings with equivalent symmetric thickness distributions.

Figure 7 shows the results of the calculations for a triangular plate at an angle of attack and moving at supersonic speed ($M_1 > 1$, $\bar{M}_1 + \bar{M}_0 - M > 1$) and with supersonic edges. Before the impinging of the shock by the wing ($t < 0$), the lift and drag on the plate are given by the steady flow solution in the stream behind the shock with Mach number $M_1$, i.e. (Liepman & Roshko 1957)

$$L_0 = D/\alpha = \rho_0 U_1^2 \bar{C}_{p_0}(X^2/k), \quad \bar{C}_{p_0} = 2\alpha/(M_1^2 - 1)^{\frac{1}{2}},$$

where $L$ and $D$ are the lift and drag, $X$ is the mid-chord length and $2X/k$ is the span. $\bar{C}_{p_0}$ is the spanwise mean of pressure coefficient, and is equal to the two-dimensional value (Donovan & Lawrence 1957).

When the shock wave intercepts the wing, $X/(U_1 + U_0) > t > 0$, the pressure distribution on the wing ahead of shock remains unchanged and that behind the shock is conical, i.e. $p'$ is a function of $x_0/(Ct)$, $y/(Ct)$ and $z/(Ct)$. The lift variation on the wing is

$$L(t) = \rho_0 U_1^2 \bar{C}_{p_0}\{X^2 - [(U_1 + U_0)\,t]^2\}/k + \rho C^4 \alpha \bar{J}(\bar{M}_1 + \bar{M}_0)\,t^2,$$

where

$$J(\tau) = -4\int_0^\tau d\left(\frac{x_0}{ct}\right)\int_0^{x_0/(kCt)} p'\left(\frac{x_0}{Ct}, 0^+, \frac{z}{Ct}\right) d\left(\frac{z}{Ct}\right),$$

$$\bar{M}_1 = U_1/C, \quad \bar{M}_0 = U/C, \quad x_0 = x + (U_0 + U_1 - U)\,t,$$

and $p'$ is obtained from the explicit solution in § 6 (ii) with a superposition of the latter's mirror image with respect to the $x$–$y$ plane. The lift curve during this period is therefore a parabola as shown in figure 7.

When the trailing edge has passed through the shock and intercepts the sonic sphere, $X/(U_1+U_0-U-C) > t > X/(U_1+U_0)$, the lift is given by the expression $L(t) = \rho C^4 \alpha J(X/Ct)\, t^2$. The lift curve in this interval is not a parabola as shown in figure 7.

When the trailing edge passes through the sonic sphere, $t > X/(U_1+U_0-U-C)$, the wing is outside the domain of influence of the shock. The lift on the wing is

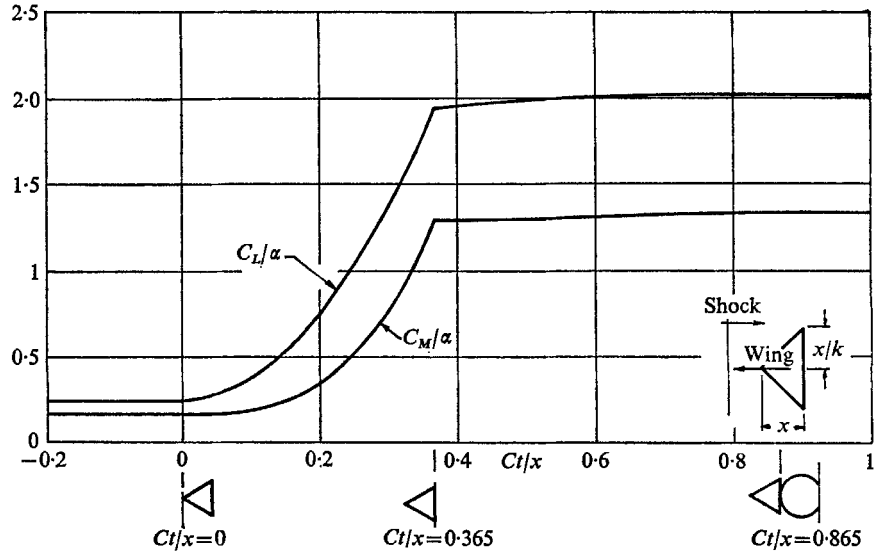


FIGURE 7. Lift and moment coefficients *vs.* non-dimensionalized time for wing and supersonic leading edges ($M = 0{\cdot}51$, $M_1 = 1{\cdot}5$, $k = 0{\cdot}75$). Wing Mach number = 1·5. Pressure ratio across shock = 7·3. $C_L = \mathscr{L}k/\frac{1}{2}\rho\tilde{U}_0^2x^2$; $C_M = \mathscr{M}k/\frac{1}{2}\rho\tilde{U}_0^2x^3$; $\alpha$ = angle of attack.

therefore a constant (figure 7) and is given by the steady supersonic solution with respect to the stream behind the shock with Mach number, $\bar{M}_1+\bar{M}_0-M$. Also shown is the variation of moment about the leading edge.

Figure 8 shows the variation of centre of pressure. It moves forward from the 2/3 chord position in steady flow to about 0·46 and then finally returns to the 2/3 chord position after the trailing edge has passed over the sonic sphere. Figure 9 shows the pressure variation on a flat terrain in the shape of a pyramid when the shock wave has passed over it. The pressure distribution is obtained by superposition of the explicit solution in § 6 (ii) three times corresponding to the three swept back edges with $M_1 = 0$ and their images with respect to the $x$–$y$ plane. Due to the symmetry with respect to the $x$–$y$ plane the pressure distribution is shown for half of the pyramid ($z > 0$). The locations of the discontinuities in the slope of the pressure curves which are pre-determined from the boundaries for various regions described before, are quite essential in drawing the pressure curves for computed data points.

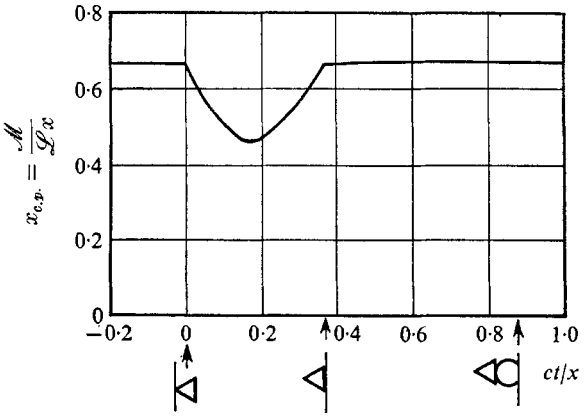


FIGURE 8. Variation of centre of pressure *vs.* non-dimensionalized time for wing in figure 7. Wing Mach number = 1·5. Pressure ratio across shock = 7·3.

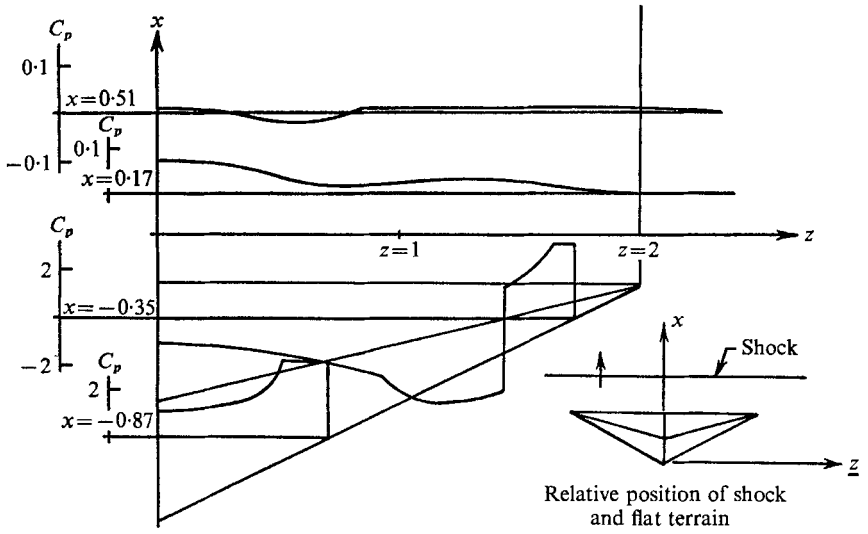


FIGURE 9. Pressure coefficient on thin pyramid like obstacle on the ground after the shock wave has passed over it. ($M$ = 0·51, $M_1$ = 0, $k_1$ = 0·5, $k_2$ = 2·5, $k_3$ = 0.)

This research was supported by the Office of Scientific Research, U.S. Air Force, under Contract no. AF-AFOSR-1062-67.

## Appendix. Reduction of an unsteady solution to a steady solution

An unsteady solution of the wave equation (2.6) in the physical variables $x, y, z, t$ with the speed of sound $C$ is also a solution of the wave equation (2.20) in the Lorentz variables $\bar{x}, \bar{y}, \bar{z}, \bar{t}$ with the speed of sound equal to unity. For a planar source distribution moving with uniform speed $1/\bar{\lambda}$, the solution of (2.20) can be written as

$$\bar{\phi}(\bar{x}, \bar{y}, \bar{z}, \bar{t}) = -\iint_{-\infty}^{\infty} g[a(\bar{\lambda}\xi + \bar{t} - \bar{r}), \zeta]\, d\xi\, d\zeta/(2\pi\bar{r}) \qquad \text{(A 1)}$$

$\bar{\lambda}^{-1}$ is of course also the Mach number of the moving source distribution. In the physical variables, it is moving with Mach number $M_\infty = (1-\bar{\lambda}M)/(\bar{\lambda}-M)$ and velocity $M_\infty C$. Note that $M_\infty - 1$ and $(1/\bar{\lambda})-1$ have the same sign. With $x^*$ as co-ordinate fixed on the source distribution, i.e. $x^* = x + M_\infty Ct$, it is quite obvious that the unsteady solution $\phi$ with respect to the stream behind the shock should be equivalent to a supersonic or subsonic steady solution $\phi(x^*, y, z)$ with the speed of sound $C$. A brief derivation of their equivalence will be given in § (i) of the appendix. In § (ii), a steady solution with respect to the stream ahead of the shock which cannot be equivalent to an unsteady solution behind the shock in the whole space, is made equivalent on a special plane, say the plane of shock.

(i) *Equivalence of an unsteady solution to a steady solution*

By replacing the variable $\xi$ by $\xi^* = a(\bar{\lambda}\xi + \bar{t} - \bar{r})$, (A 1) becomes

$$\bar{\phi} = \frac{-1}{2\pi}\int_{-\infty}^{\infty} d\zeta \int \frac{g(\xi^*, \zeta)\, d\xi^*}{[\bar{r}(\partial\xi^*/\partial\xi)]}. \tag{A 2}$$

After expressing $\bar{r}$ in terms of $\xi^*$, the denominator in the integrand becomes

$$\bar{r}\{\partial\xi^*/\partial\xi\} = \bar{r}\{a[\bar{\lambda} + (\bar{x}-\xi)/\bar{r}]\} = \pm\{(x^*-\xi^*)^2 - (M_\infty^2 - 1)\,[\bar{y}^2 + (\bar{z}-\zeta)^2]\}^{\frac{1}{2}}, \tag{A 3}$$

with
$$M_\infty^2 - 1 = a^2(1-\bar{\lambda}^2) \quad \text{and} \quad x^* = a(\bar{t} + \bar{\lambda}\bar{x}). \tag{A 4}$$

Both $x^*$ and $M_\infty$ will agree with their physical definitions given before when

$$a = M_\infty/(1-M^2)^{\frac{1}{2}}. \tag{A 5}$$

The choice of the appropriate sign for the denominator and that of the limits of integration in (A 2) should be decided by the sign of $\partial\xi^*/\partial\xi$. $\partial\xi^*/\partial\xi > 0$ for all $\xi$ if $1/\bar{\lambda} < 1$, i.e. the motion of the source distribution is subsonic. $\xi^*$ increases monotonically from $-\infty$ to $\infty$ as $\xi$ does and (A 2) becomes

$$\bar{\phi} = \phi(x^*, y, z) = \frac{-1}{\pi\nu}\iint_{\Gamma^*} \frac{g(\xi^*, \zeta)\, d\xi^*\, d\zeta}{\{(x^*-\xi^*)^2 + (1-M_\infty^2)\,[y^2 + (z-\zeta)^2]\}^{\frac{1}{2}}}. \tag{A 6}$$

For $\bar{\lambda}^{-1} < 1$, $\nu = 2$ and $\Gamma^*$ is the entire $\xi^*$–$\zeta$ plane and $\phi(x^*, y, z)$ represents a steady subsonic solution ($M_\infty < 1$).

For the supersonic case, $1/\bar{\lambda} > 1$, $\partial\xi^*/\partial\xi$ has the same sign as $\bar{x} - \xi - \bar{\lambda}\bar{r}$. They vanish at $\xi = \xi_m$ and $\xi^* = \xi_m^*$, with

$$\xi_m = \bar{x} - \bar{\lambda}\{[\bar{y}^2 + (\bar{z}-\zeta)^2]/(1-\bar{\lambda}^2)\}^{\frac{1}{2}}, \quad \xi_m^* = x^* - \{(M_\infty^2 - 1)\,[\bar{y}^2 + (\bar{z}-\zeta)^2]\}^{\frac{1}{2}}.$$

As $\xi$ increases from $-\infty$ to $\xi_m$, $\xi^*$ increases from $-\infty$ to $\xi_m^*$ and the positive sign in (A 3) should be used. As $\xi$ increases from $\xi_m$ to $\infty$, $\xi^*$ decreases from $\xi_m^*$ to $-\infty$ and the negative sign in (A 3) should be used. For the supersonic case, $\bar{\lambda} < 1$, (A 2) again becomes (A 6) with $\nu = 1$ and $\Gamma^*$ being the domain inside the hyperbola $x^* - \xi^* = \{(M_\infty^2 - 1)\,[y^2 + (z-\zeta)^2]\}^{\frac{1}{2}}$ and $\phi(x^*, y, z)$ represents a steady supersonic solution ($M_\infty > 1$). Thus concludes the proof of the equivalence.

(ii) *Matching of a steady solution ahead of the shock on the plane of the shock with an unsteady solution behind the shock*

The inhomogeneous term $\bar{K}p'_{0,x_0x_0}[x_0 = \bar{a}\bar{t}, \bar{y} > 0, \bar{z}]$ in the shock condition (2.24) is associated with a steady solution ahead of the shock defined by (2.4) with the speed of sound $C_0$. The inhomogeneous term will remain unchanged if the variable $x_0$ which is fixed on the wing is replaced by a new variable $x^*$ which is related to $\bar{x}, \bar{t}$ by a linear transformation $x^* = \bar{a}(\bar{t}+\bar{\lambda}^*\bar{x})$ so that $x^* = x_0 = \bar{a}\bar{t}$ on the plane of the shock $\bar{x} = 0$. Elsewhere $x^*$ and $x_0$ are not the same. The constant $\lambda^*$ is free to be defined. The condition of (3.5) that $D_{\bar{x}\bar{t}}p^*$ at $\bar{x} = 0$ matches with the inhomogeneous term $\bar{K}p'_{0,x_0,x_0}(x_0 = \bar{a}\bar{t}, \bar{y}, \bar{z})$ will be fulfilled if $D_{\bar{x}\bar{t}}p^*(\bar{x}, \bar{y}, \bar{z}, \bar{t})$ is identified with $\bar{K}p'_{0,x^*x^*}(x^*, \bar{y}, \bar{z})$, i.e.

$$-\frac{\rho C^2}{2\pi}\bar{a}^2A^*H(\bar{\lambda}^*)\iint_{-\infty}^{\infty}\frac{d\xi\,d\zeta}{\bar{r}}f^{(\mathrm{IV})}[\bar{a}(\bar{\lambda}^*\xi+\bar{t}-\bar{r}),\zeta]$$
$$=\frac{\rho_0U_1^2\bar{K}}{\pi\nu}\iint_{\Gamma^*}\frac{f^{(\mathrm{IV})}(\xi^*,\zeta)\,d\xi^*\,d\zeta}{\{(x^*-\xi^*)^2-(M_1^2-1)[(\bar{z}-\zeta)^2+\bar{y}^2]\}^{\frac{1}{2}}}, \quad (\mathrm{A}\,7)$$

where $f^{(\mathrm{IV})}$ means the fourth derivative with respect to the first argument. By comparison with (A 1) and (A 6), the constants $A^*$ and $\bar{\lambda}^*$ are defined,

$$\bar{\lambda}^* = \{1-(M_1^2-1)(1-M^2)/(\bar{M}_1+\bar{M}_0)^2\}^{\frac{1}{2}}$$

and
$$A^* = -(M/\bar{M}_0)\bar{M}_1^2\bar{K}(1-M^2)/[(\bar{M}_1+\bar{M}_0)^2H(-\bar{\lambda}^*)]. \quad (\mathrm{A}\,8)$$

When $x^*$ is related to $\bar{x}, \bar{t}$ and in turn to the physical variables $x, t$, $A^*f(x^*, z)$ can be considered as a fictitious source distribution for an equivalent wing. From (A 8), it is clear that the equivalent wing moves with supersonic speed, $1/\bar{\lambda}^* > 1$ (or at subsonic speed, $1/\bar{\lambda}^* < 1$) with respect to the stream behind the shock when the original wing is moving with respect to the stream ahead of the shock at supersonic speed, $M_1 > 1$ (or subsonic speed $M_1 < 1$).

For the subsonic case $\bar{\lambda}^*$ given by (A 8) is always real. For the supersonic case, $M_1 > 1$, $\bar{\lambda}^*$ given by (A 8) can be imaginary or zero for certain combinations of $M_1$ and $M_0$. This possibility will be investigated.

For a supersonic flow ahead of the shock, the radius of intersection of the shock and the Mach cone is $R_0 = (\bar{M}_1+\bar{M}_0)\bar{t}/[(M_1^2-1)(1-M^2)]^{\frac{1}{2}}$. The radius of the intersection of the shock and the Mach cone of the equivalent wing moving with Mach number $1/\bar{\lambda}^*$ in $\bar{x}, \bar{t}$ variables is $R^* = \bar{t}/(1-\bar{\lambda}^{*2})$. A necessary condition for the equivalence of those two solutions in the plane of the shock is that $R_0 = R^*$. $R^*$ has a lower bound $\bar{t}$ which is the radius of the sonic circle. When the radius $R_0$ is less than $\bar{t}$, $\bar{\lambda}^*$ is imaginary. This means only that the solution cannot be represented by the type of (3.1). It does not mean that the mathematical problem stated at the end of § 2 has no solution.

The condition for $\bar{\lambda}^*$ real is $R_0 > \bar{t}$ which is equivalent to the condition,

$$[(\gamma-1)(M_0^2-1)^2-(3-\gamma)]M_1 < (\gamma+1)M_0^3$$
$$+\{[2(\gamma-1)M_0^2+4](M_0^2-1)[M_0^4+(\gamma-1)M_0^2+1]\}^{\frac{1}{2}}. \quad (\mathrm{A}\,9)$$

The inequality holds for all values of $M_1$ if $M_0^2 < 1+[(3-\gamma)/(\gamma-1)]^{\frac{1}{2}}$, i.e. $M_0 < 3$ for $\gamma = 1{\cdot}4$ or the shock strength $p/p_0 < 3{\cdot}7$. For stronger shock the inequality

defines an upper bound for $M_1$, e.g. with $p/p_0 = 20$, $M_0 = 4{\cdot}16$, $M_1 < 4{\cdot}50$. It is clear that so long as the shock strength is less than 20, the proposed procedure for the removal of the inhomogeneous term works for wings moving at super- or subsonic speeds. Indeed, in the solution by transform method of the problem for a supersonic moving wing the same restriction was imposed by a statement in Arora (1968) which amounts to assuming $(\bar{\lambda}^*)^2 > 0$.

## REFERENCES


Arora, N. L. 1968 An integral-transform method for shock–shock interaction studies. *J. Fluid Mech.* **34**, 209.

Arora, N. L. 1969 Integral transforms for shock–shock interaction—three dimensional planar wings. *J. Appl. Math. Phys.* **20**, 244.

Baker, E. B. & Copson, E. T. 1950 *The Mathematical Theory of Huygen's Principle.* Oxford University Press.

Blankenship, V. D. 1965 Shock–shock interaction on a slender supersonic cone. *J. Fluid Mech.* **22**, 599.

Chester, W. 1954 The diffraction and reflection of shock waves. *Quart. J. Mech. Appl. Math.* **7**, 57.

Chow, F. & Gunzburger, M. 1969 Numerical program and examples for diffraction of shock by wings. *New York University Report* NYU-AA-69-8.

Donovan, A. F. & Lawrence, H. R. 1957 *Aerodynamic Components of Aircraft at High Speeds.* Section A. Princeton, N.J.: Princeton University Press.

Gunzburger, M. 1969 Diffraction of shock wave by a thin wing-symmetric and anti-symmetric problem. Ph.D. Thesis, School of Engineering and Science, New York University.

Liepman, H. W. & Roshko, A. 1957 *Elements of Gasdynamics.* New York: John Wiley.

Lighthill, M. J. 1949 The diffraction of blast I. *Proc. Roy. Soc.* A **198**, 454.

Ludloff, H. F. & Friedman, M. B. 1952 Diffraction of blasts by axisymmetric bodies. *J. Aero. Sci.* **19**, 425.

Smyrl, J. F. 1963 The impact of a shock wave on a thin two-dimensional aerofoil moving at supersonic speed. *J. Fluid Mech.* **15**, 223.

Ter-Minassiants, S. M. 1969 The diffraction accompanying the regular reflexion of a plane obliquely impinging shock wave from the walls of an obtuse wedge. *J. Fluid Mech.* **35**, 391.

Ting, L. & Ludloff, H. F. 1952 Aerodynamics of blasts. *J. Aero. Sci.* **19**. 317.

*J. Fluid Mech.* (1970), *vol.* 42, *part* 3, *pp.* 609–625
*Printed in Great Britain*



# The flow of a tubular film Part 2. Interpretation of the model and discussion of solutions

By J. R. A. PEARSON AND C. J. S. PETRIE†
Department of Chemical Engineering, University of Cambridge

(Received 3 September 1969)

The equations governing the free-surface flow of a tubular film of liquid are derived from physical arguments, which throw some light on the formal process described in part 1. The solutions of the equations are discussed, in particular with reference to the film-blowing process for the manufacture of thin sheets of thermoplastic material. The qualitative adequacy of a model based on the dominance of viscous forces is demonstrated, and the effect of surface tension, air drag and non-isothermal flow is discussed briefly.

## 1. Introduction

The work described below can be thought of either as an application of the formal results of part 1 (Pearson & Petrie 1970*a*), providing in addition a physical description of the approximations made there, or as a physically based approximate solution of a practical problem, whose formal justification can be found in part 1. The authors hope that they have succeeded in separating the two parts of the work sufficiently for either to be intelligible on its own.

The process studied here is one for the manufacture of a thin sheet or film of a thermoplastic, such as polyethylene, from molten material supplied under pressure by a screw extruder. Figure 1 illustrates the process schematically. The liquid is forced through an annular die and the tubular film produced is thinned by both an internal pressure and an axial tension. Thus, any element of the film is being drawn down in two directions as it flows from the die to the take-up rolls (which are usually vertically above the die). These are arranged to guide the film once it has solidified (and cooled sufficiently to prevent the film sticking to itself) from its cylindrical shape to a plane ('layflat') form as it passes through the nip rolls. The nip rolls form an airtight seal, so that between them and the die the film forms a tubular bubble containg air at a pressure slightly above atmospheric. The air supply led in through the centre of the die is used only to adjust this pressure.

The rate of cooling, and thus the distance to the freeze-line (the region where the molten polymer solidifies) is controlled by jets of cooling air from a ring sur-

† Present address: Department of Engineering Mathematics, University of Newcastle upon Tyne.

rounding the bubble. The nip rolls are driven to provide the axial tension needed to take up the film, and might be driven at either constant speed or constant torque, usually the former. (The implications of this choice for the problem of the control of product dimensions are discussed elsewhere—Pearson & Petrie 1970*b*.)

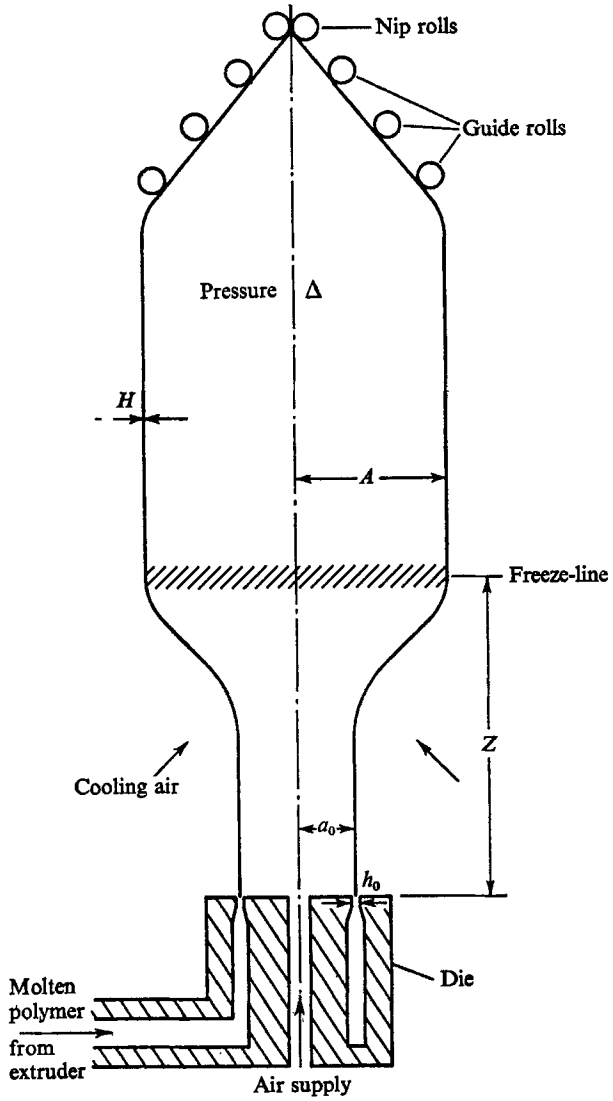


FIGURE 1. Diagram of the film-blowing process; section in a vertical plane.

As far as the steady-state problem is concerned we can take either the speed or the torque as prescribed, and the choice which is most convenient for our analysis of the flow of the liquid polymer is of a given axial tension applied to the film at the freeze-line.

What we seek to do here is to set up and use a mathematical model of the flow in the region between the die and the freeze-line, where we have the free-surface

flow of a highly viscous liquid. We need to prescribe at least seven parameters in order to get a determinate problem, and these are taken to be the bubble radius and the film thickness at the die, the freeze-line distance, the pressure difference across the bubble, the axial tension at the freeze-line, the volumetric flow rate, and the viscosity of the liquid. If we wish to take account of any but the essential factors controlling the flow, more parameters will be required. We can then predict the bubble shape, its thickness and velocity, and the forces acting in it. In particular, the dimensionless ratios of bubble radius, film thickness and velocity at the freeze-line to the corresponding quantities at the die can be predicted in terms of three numbers, which are essentially dimensionless values of the freeze-line distance, the excess pressure inside the bubble, and the axial tension at the freeze-line. (The velocity ratio and the axial tension can be transposed between the lists of dependent and independent quantities, if the velocity, rather than the tension, is prescribed at the freeze-line.)

## 2. The mathematical model

The basic assumptions made are that the forces controlling the flow are the viscous forces arising in the steady axisymmetric isothermal flow of a homogeneous Newtonian liquid, and that the film is thin enough for variations in the flow field across it to be ignored, and for the velocity gradients to be approximated locally by those of a plane film being extended bi-axially. These assumptions, and the neglect of the effects of gravity, surface tension, air drag and the inertia of the liquid, are justified formally to some extent in part 1. They are justified practically, in part at least, by the fact that reasonable predictions are obtained.

Further experimental verification is required before the range of applicability of the simple viscous model can be inferred. Certainly cases are known where other factors cannot be neglected, in particular gravity. The present model can be extended to cover most of these cases.

Equations governing the flow have already been derived in part 1 (equations (16) and (17)) by means of a formal perturbation expansion. Here an alternative, less formal, approach is shown to lead to the same results, and at the same time to help in the understanding of the essential physics of the situation. The two relevant equations are based on a simple balance of forces, one in the axial direction and the other in the direction normal to the film surface.

We take cylindrical polar co-ordinates $(\rho, \phi, z)$ as shown in figures 1 and 2, and define the following symbols:

$a$ is the bubble radius (measured normal to the $z$-axis) which takes values $a_0$ at $z = 0$ (at the die) and $A$ at $z = Z$ (at the freeze-line); corresponding dimensionless quantities are $r = a/a_0$ and $R = A/a_0$. ($r$ corresponds to $h_{03}$ in part 1.)

$h$ is the film thickness (measured normal to the film surface), which takes the values $h_0$ at $z = 0$ and $H$ at $z = Z$; since $h$ only appears as a ratio, it is not necessary to define a dimensionless thickness. ($h/a_0$ corresponds to $\epsilon h_{12}$ in part 1.)

$x = z/a_0$ and $X = Z/a_0$ are dimensionless values of the axial co-ordinate and of the freeze-line distance respectively.

$\theta$ is the angle between the bubble profile and the $z$-axis, so that $\tan\theta = da/dz$.

$\mu$ is the liquid viscosity and $Q$ the total volumetric flow rate.

$\Delta$ is the pressure difference across the bubble, $p$ (inside) $-p$ (outside), and $F_Z$ is the axial force applied at the freeze-line.

In order to obtain the velocity gradients, we define local Cartesian co-ordinates $(\xi_1, \xi_2, \xi_3)$ at a point $P$ in the film, with $\xi_1$ in the direction of flow, $\xi_2$ normal to the film and $\xi_3$ in the transverse (circumferential) direction (see figure 2). For definiteness we take the origin $P$ to be on the inner surface; then the $\xi_2$-axis

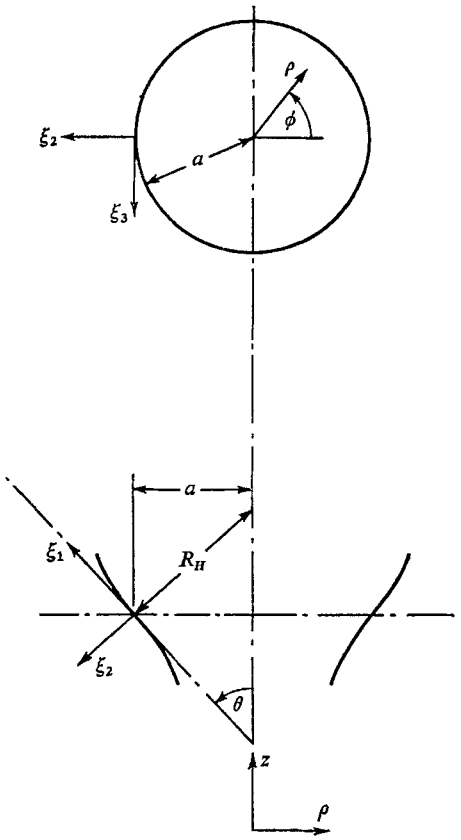


FIGURE 2. Co-ordinate systems; sectioned plan and elevation of a portion of the film.

meets the outer surface at $\xi_2 = h$. (At $P$, the $\xi_i$ directions coincide with the $x_i$ directions of the 'intrinsic' co-ordinates used in part 1.) In this co-ordinate system, we take velocity components $(v_1, v_2, v_3)$, and proceed to obtain approximations to the velocity gradients $\partial v_i/\partial \xi_j$.

On the inner surface $\xi_2 = 0$, $v_2$ is zero, and on the outer surface $v_2 = Dh/Dt$, so that, neglecting the variation of $\partial v_2/\partial \xi_2$ with $\xi_2$, we obtain

$$\partial v_2/\partial \xi_2 = h^{-1} Dh/Dt.$$

Similarly, using the axisymmetry condition and the relation $\xi_3 = a \tan \phi$, we obtain

$$\partial v_3/\partial \xi_3 = a^{-1} Da/Dt;$$

and continuity gives

$$\partial v_1/\partial \xi_1 = -(h^{-1}Dh/Dt + a^{-1}Da/Dt).$$

These quantities are all $O(1)$; the other velocity gradients are $O(h/a)$; they are ignored in this analysis. Treating $a$ and $h$ as functions of $z$, and using $dz/d\xi_1 = \cos\theta$ and $D\xi_1/Dt = v_1$, we obtain

$$\partial v_1/\partial \xi_1 = -v_1 \cos\theta (a^{-1}da/dz + h^{-1}dh/dz).$$

$$\partial v_2/\partial \xi_2 = v_1 \cos\theta\, h^{-1}dh/dz,$$

and

$$\partial v_3/\partial \xi_3 = v_1 \cos\theta\, a^{-1}da/dz.$$

(It may readily be shown that these correspond to the first-order terms obtainable from equation (3), part 1.)

The principal stresses are given by

$$p_{ii} = -p + 2\mu\, \partial v_i/\partial \xi_i, \quad \text{for} \quad i = 1, 2, \text{ and } 3,$$

and the condition that $p_{22}$ is zero (relative to atmospheric pressure) at the free surfaces gives, for the hydrostatic pressure $p$,

$$p = 2\mu v_1 \cos\theta\, h^{-1}dh/dz \tag{1}$$

(cf. equation (15), part 1). This imposes the condition that $\Delta \ll p$; i.e. $\Delta$ is $O(h/a)$ multiplied by a typical viscous stress. (There is no inconsistency in ignoring $\Delta$ here while using it below, since in the equations below it balances terms of order $h$ multiplied by a typical viscous stress.) The stresses are functions of $\xi_1$ only; and they can be integrated across the film to give the longitudinal and transverse (hoop) forces per unit length, $P_L$ ($= hp_{11}$) and $P_H$ ($= hp_{33}$), respectively. Using the overall equation of continuity, $Q = 2\pi a h v_1$, to eliminate $v_1$ gives finally

$$P_L = -\frac{\mu Q \cos\theta}{\pi a}\left\{\frac{1}{a}\frac{da}{dz} + \frac{2}{h}\frac{dh}{dz}\right\}, \tag{2}$$

and

$$P_H = \frac{\mu Q \cos\theta}{\pi a}\left\{\frac{1}{a}\frac{da}{dz} - \frac{1}{h}\frac{dh}{dz}\right\}. \tag{3}$$

The balance of the total axial force between cross-sections at $z$ and at $Z$ (the freeze-line) gives, neglecting inertial forces,

$$2\pi a P_L \cos\theta - \pi a^2 \Delta = F_Z - \pi A^2 \Delta; \tag{4}$$

that of the normal forces on the film gives

$$\Delta = P_L/R_L + P_H/R_H, \tag{5}$$

where $R_L$ and $R_H$ are the principal radii of curvature,

$$R_H = a\sec\theta \quad \text{and} \quad R_L = -\sec^3\theta/(d^2a/dz^2).$$

(See e.g. Novozhilov 1959, p. 96.)

Introducing the dimensionless variables defined above and the dimensionless parameters,

$B = \pi a_0^3 \Delta/\mu Q$ (a dimensionless pressure difference),

$T_Z = a_0 F_Z/\mu Q$ (a dimensionless axial force),

and $T = T_Z - R^2 B$ (the total dimensionless axial force at any cross-section),

and writing $'$ for $d/dx$ give, after some rearrangement,

$$h'/h = -\tfrac{1}{2}r'/r - \tfrac{1}{4}\sec^2\theta(T + r^2 B) = -\tfrac{1}{2}r'/r - \tfrac{1}{4}(1+r'^2)(T + r^2 B), \tag{6}$$

and

$$2r^2(T + r^2 B)\, r'' = 6r' + r\sec^2\theta(T - 3r^2 B) = 6r' + r(1+r'^2)(T - 3r^2 B). \tag{7}$$

(In order to show the equivalence of these equations to (16) and (17), part 1, set $B = P_1/2\phi_0$, $dx/dx^1 = \cos\theta$, and eliminate $T$ by differentiation.) Thus, we have found one integral of the equations derived in part 1, and have separated the problem of finding the shape of the bubble from that of finding the film thickness, (7) being an equation in $r$ alone.

Two boundary conditions for (6) and (7) can be stated immediately. They are

$$h = h_0, \quad r = 1 \quad \text{at} \quad x = 0. \tag{8}$$

A second boundary condition for (7) could be prescribed arbitrarily as

$$r' = b \quad \text{at} \quad x = 0,$$

but physical considerations suggest that it is conditions at the freeze-line end of the bubble that will control the process. If the material freezes (i.e. $\mu \to \infty$), then $r'$ must become zero beyond that line, no further deformation being possible. It is intuitively obvious that the relation,

$$r' = 0, \quad x = X, \tag{9}$$

can be applied to the molten region also, provided $P_L$ and $P_H$ remain bounded. To show this in the case of rapid freezing, we suppose that the viscosity changes from its constant finite value $\mu_0$ to an infinite value within a region of length $e$ (measured in the $x$-direction) where $\epsilon$ can later $\to 0$. If this is the case, then $r$ can be taken as constant in (7) and we get a relation of the form,

$$r'' = A\mu r' + B(1 + r'^2).$$

Here $A$ and $B$ are constants, fixed by the parameters defining the problem, $r' = 0$ at $x = X$ and $\mu$ varies from $\mu_0$ to infinity in the range $[X - \epsilon, X]$. Elementary argument shows that for suitable $\mu$, say

$$\mu = \mu_0(\epsilon/(X - x))^{\frac{1}{2}},$$

the term $r''$ is always $O(1)$ and so $r'$ is always $O(\epsilon)$. Hence, by letting $\epsilon \to 0$, we recover (9) as the suitable boundary condition we sought. It is worth noting that the same argument does not imply $h' = 0$ at $x = X$, which would otherwise overdetermine the problem.

The consequence of these boundary conditions is that the solution of (6), (7) will not in general yield $r' = 0$ at $x = 0$, although for large enough $X$ this is very

nearly true. This is not incompatible with the equations governing flow at a die exit; though at the level of approximation we are concerned with, we cannot investigate this matter further.

## 3. Discussion

### 3.1. *The phase-plane*

We now have a non-linear two-point boundary-value problem; both for the qualitative discussion, and for the numerical solution of (7), it is convenient to take initial conditions $r = R$, $r' = 0$ at $x = X$, then modify the choice of $R$ until we get $r = 1$ at $x = 0$. From this point of view, the parameters $B$ (pressure), $T_Z$ (axial tension), $X$ (freeze-line distance) and the initial value $R$ completely specify the bubble shape ($T = T_Z - R^2B$), and we avoid the problem that, if we start from $x = 0$, $R$ and hence the parameter $T$, which appears in the equation, are not known in advance. (It would be necessary to guess values for $r'$ at $x = 0$ and for $T$, two guesses instead of one.)

We rewrite (7) as

$$\left.\begin{aligned} dr/dx &= s, \\ ds/dx &= \{6s + r(1+s^2)\,(T - 3r^2B)\}/\{2r^2(T + r^2B)\}, \end{aligned}\right\} \tag{10}$$

and study the trajectories (solution curves) of system (10) in the phase plane with co-ordinates $(r, s)$. The system

$$\left.\begin{aligned} dr/d\xi &= -2r^2s(T + r^2B), \\ ds/d\xi &= -6s - r(1+s^2)\,(T - 3r^2B), \end{aligned}\right\} \tag{11}$$

where $dx/d\xi = -2r^2(T + r^2B)$, has the same trajectories as system (10), with $x$ decreasing in the direction of $\xi$ increasing for $r^2(T + r^2B) > 0$. Problems of interpretation on $r = 0$ and on $T + r^2B = 0$ will be postponed.

Since the equations are unaltered if the signs of $r$ and $s$ are both changed, and since the half-lines $r = 0, s > 0$ and $r = 0, s < 0$ are solutions of system (11), and so may not be crossed by any other trajectories, we confine our attention to the half-plane $r \geqslant 0$. In order to keep the discussion manageable, we restrict attention to $B > 0$ and $T_Z > 0$, the ranges relevant to the problem which motivates this study, and consider the three cases $T > 0$, $T = 0$ and $T < 0$. These are further subdivided, according to the number and type of the singular points, into:

$$\begin{aligned} &1(a), \quad T^3 > 81B/16 > 0, \\ &1(b), \quad T^3 = 81B/16 > 0, \\ &1(c), \quad 81B/16 > T^3 > 0, \\ &2, \quad T = 0, \\ &3(a), \quad 0 > T^3 > -9B/16, \\ &3(b), \quad 0 > T^3 = -9B/16, \\ &3(c), \quad 0 > -9B/16 > T^3. \end{aligned}$$

The results are summarized here and illustrated in figures 3–5. The appendix gives more details and outlines proofs of some of the statements made here.

*Case* 1. There are two singular points in $r \geqslant 0$, namely $(0, 0)$, which is a saddle-

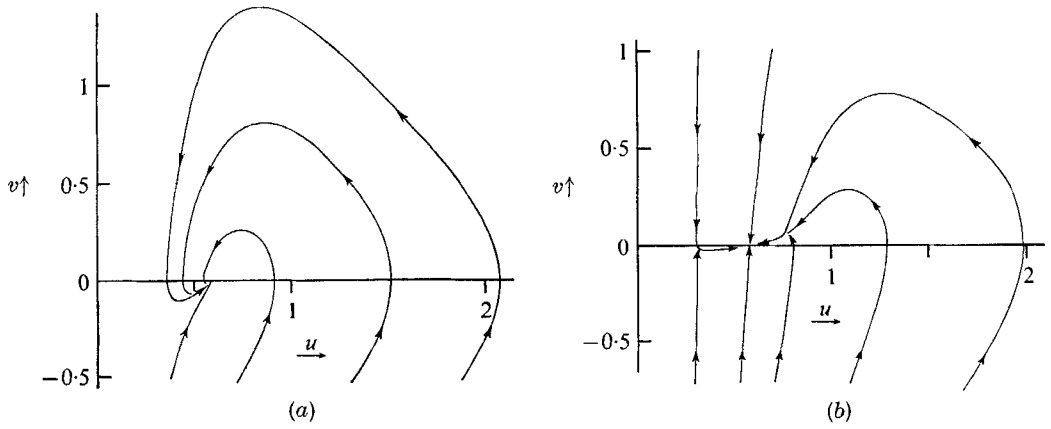


FIGURE 3. Phase plane for case 1, $T > 0$. Sketches of typical trajectories, arrows in the direction of $x$ decreasing: ($a$) case 1($a$), $(B/T^3)^{\frac{1}{2}} = \frac{1}{3}$; ($b$) case 1($c$), $(B/T^3)^{\frac{1}{2}} = \frac{5}{3}$. $v = s$, $u = r(B/T)^{\frac{1}{2}}$.

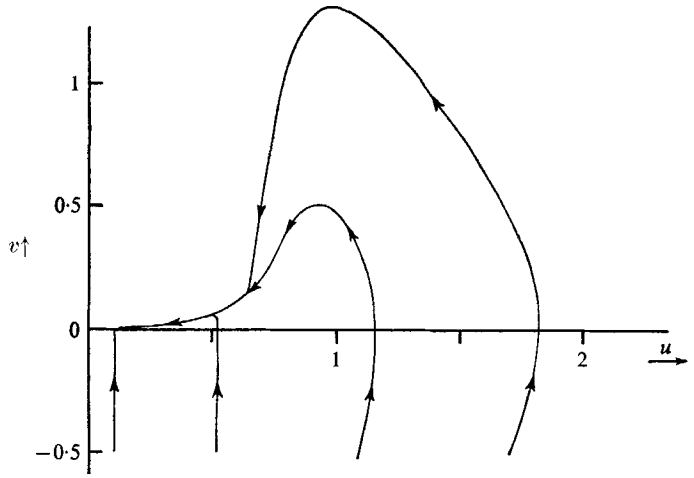


FIGURE 4. Phase plane for case 2, $T = 0$. Sketches of typical trajectories, arrows in the direction of $x$ decreasing. $v = s$, $u = rB^{\frac{1}{3}}$.

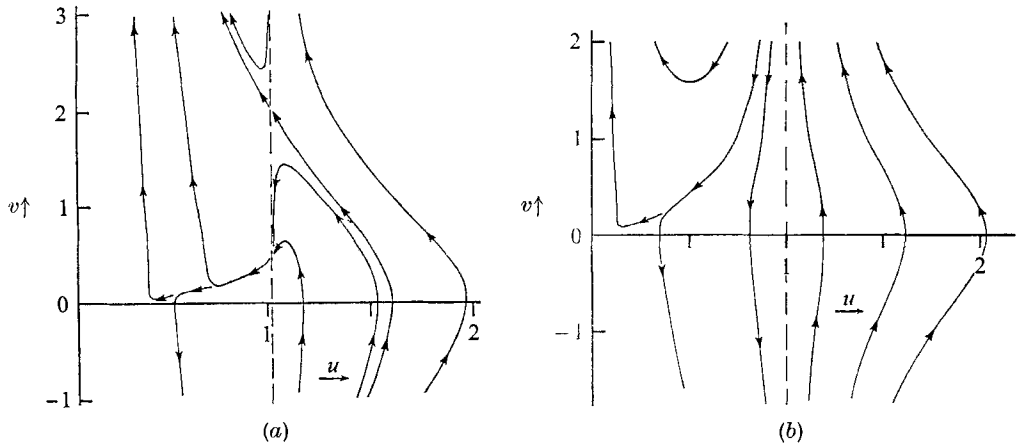


FIGURE 5. Phase plane for case 3, $T < 0$. Sketches of typical trajectories, arrows in the direction of $x$ decreasing. ($a$) Case 3($a$), $(-B/T^3)^{\frac{1}{2}} = \frac{5}{3}$; ($b$) case 3($c$), $(-B/T^3)^{\frac{1}{2}} = \frac{1}{3}$. $v = s$, $u = r(-B/T)^{\frac{1}{2}}$.

point, and $((T/3B)^{\frac{1}{2}}, 0)$, which is a focus in case 1(*a*) and a node in cases 1(*b*) and 1(*c*). This latter singular point is stable as $\xi$ increases ($x$ decreases, from the freeze-line towards the die). It can further be shown that there are no closed trajectories; hence, that every trajectory starting in $r > 0$ tends to $((T/3B)^{\frac{1}{2}}, 0)$ as $x \to -\infty$.

*Case* 2. The only singular point is the origin, which is a node, stable as $\xi$ increases.

*Case* 3. The origin is a saddle-point; in case 3(*c*), this is the only singular point. In case 3(*b*), there is a saddle-node at $((-T/B)^{\frac{1}{2}}, 1)$. In case 3(*a*), the point $((-T/B)^{\frac{1}{2}}, q)$ is a node (stable as $\xi$ increases); the point $((-T/B)^{\frac{1}{2}}, 1/q)$ is a saddle-point, where $q$ is the smaller root of $4q^2 - 6(-B/T^3)^{\frac{1}{2}} q + 4 = 0$.

In case 3, $r < (-T/B)^{\frac{1}{2}}$ corresponds to $T + r^2 B < 0$; so in figure 5 the arrows on the trajectories (in the direction of $x$ decreasing) show $\xi$ decreasing for $r < (-T/B)^{\frac{1}{2}}$ and increasing for $r > (-T/B)^{\frac{1}{2}}$. For system (10), moreover, the points $((-T/B)^{\frac{1}{2}}, q)$ and $((-T/B)^{\frac{1}{2}}, 1/q)$ are not strictly speaking singular points, since they are not themselves solutions of the equations, and solutions tending to these points do in fact reach them in a finite distance ($x$). They are rather points of bifurcation of these solutions, where $ds/dx$ ($= d^2r/dx^2$) is indeterminate. The physical interpretation of this non-uniqueness is discussed below. (See also appendix.)

### 3.2. *Results of the qualitative analysis*

First we discuss case 3, where $T_Z$ is so small that there is a real, positive value of $r$, $r = (R^2 - T_Z/B)^{\frac{1}{2}}$, for which $T + r^2 B$ vanishes, and (7) becomes singular. From (6) (which is (4) in dimensionless form), we see that this means that the longitudinal tension in the bubble $P_L$ vanishes at this value of $r$, so that the radius of curvature $R_L$ in (5) is indeterminate. With this interpretation (that the film becomes slack), it is not surprising that our model fails to predict a unique shape for the bubble; to keep in touch with the practical process, we insist that the axial tension applied is sufficient to keep the film taut between the die and the freeze-line. It is sufficient for this to require that $T_Z > B(R^2 - 1)$.

Numerical solution of the equations (see below) shows that cases 2 and 3 give rise to large blow ratios $R$ and very small freeze-line distances $X$ and thickness reductions $h_0/H$ compared with the values observed in practice, so subsequent discussion is based on case 1. As was mentioned above the qualitative analysis provides additional reasons for the choice of boundary condition that was made ($r' = 0$ at $x = X$). As $x$ decreases (proceeding towards the die), the trajectories approach the singular point and, for large enough freeze-line heights, $r'$ must be small at the die. (Computation suggests that $r'$ will fall below 0·1, in a distance of about 3 die diameters, measured from the freeze-line.) Thus, the observed behaviour of the solutions is predicted without the necessity of imposing any condition at $x = 0$. A similar argument does not apply for $x$ increasing, as we approach the freeze-line; moreover, $d^2r/dx^2$ is large far from the singular point, so that a small change in $X$ would cause a large change in $dr/dx$ at $x = X$ (i.e. the bubble shape would be critically dependent on $X$, and similarly on the other parameters, unless the condition on $dr/dx$ is imposed at the freeze-line).

We can also make some numerical predictions for long bubbles, since all trajectories tend to the singular point $r = (T/3B)^{\frac{1}{2}}$, $r' = 0$, as $x \to -\infty$. Hence, as $X \to \infty$, the die radius tends to $(T/3B)^{\frac{1}{2}}$; since $r(0) = 1$, we have in the limit $T = 3B$, so that the blow ratio $R$ tends to the value $(T_Z/B - 3)^{\frac{1}{2}}$. In case 1(*c*), provided $R$ is not too large, $r$ decreases monotonically from $R$ to $(T/3B)^{\frac{1}{2}}$; so the die radius 1 must be greater than the latter value. Hence,

$$R^2 > T_Z/B - 3,$$

and we have a minimum blow ratio attained for large freeze-line distances. The numerical work confirms that this behaviour is relevant for values of the parameters in the practical range of interest; it also shows that the limiting value is nearly attained in many cases for freeze-line distances of about 10 times the die radius ($X \approx 10$).

Again, this limiting value is independent of liquid flow rate and viscosity, since $T_Z/B = F_Z/\pi a_0^2 \Delta$; it depends only on the applied forces and the die radius. For a long bubble, the blow ratio increases with increased axial tension, and with decreased die radius and internal pressure. This last result is less surprising when one recalls the behaviour of a spherical bubble acted on by an internal pressure and surface tension forces. (The excess pressure required to sustain the bubble is inversely proportional to its radius.)

We can use the foregoing to estimate the effect of increasing the freeze-line distance on the thickness reduction $h_0/H$. Once the bubble is long enough for the limiting value of $R$ to be substantially attained, any increase in $X$ corresponds to a lengthening of the neck of the bubble, where $r$ is close to 1, and $r'$ is close to 0. We consider freeze-line distances $X_1$ and $X_2$, with corresponding film thicknesses $H_1$ and $H_2$; if $R$ is the same in both cases, we have

$$(h_0/H_1)/(h_0/H_2) = \exp \int_{X_2}^{X_1} \tfrac{1}{4}(1 + r'^2)\,(T + r^2 B)\,dx.$$

Between $X_1$ and $X_2$ (measuring from the freeze-line), $r \approx 1$ and $r' \approx 0$, so that

$$(h_0/H_1)/(h_0/H_2) \approx \exp\{B(X_1 - X_2)\}$$

(using $T/3B \approx 1$). Estimates obtained in this way are compared with computed values of the ratio $H_2/H_1$ in table 1.

| | | | | | | |
|---|---|---|---|---|---|---|
| Pressure difference ($B$) | 0·1 | 0·1 | 0·1 | 0·2 | 0·2 | 0·3 |
| Axial tension ($T_Z$) | 0·5 | 0·5 | 2·0 | 1·0 | 2·5 | 2·0 |
| Limiting blow ratio ($R = (T_Z/B - 3)^{\frac{1}{2}}$) | 1·41 | 1·41 | 4·12 | 1·41 | 3·08 | 1·91 |
| Lower freeze-line distance ($X_2$) | 20 | 15 | 10 | 10 | 4 | 6 |
| Upper freeze-line distance ($X_1$) | 30 | 20 | 15 | 15 | 10 | 10 |
| Estimate of $H_2/H_1$, $\exp(B(X_1 - X_2))$ | 2·72 | 1·65 | 1·65 | 2·72 | 3·32 | 3·32 |
| Computed value of $H_2/H_1$ | 2·84 | 1·74 | 1·86 | 2·89 | 3·61 | 3·46 |

TABLE 1. Comparison of estimated and computed values of the change in thickness reduction due to a change in freeze-line distance

### 3.3. *Numerical results*

Numerical estimates of the bubble shape and thickness were obtained by a Runge–Kutta integration procedure, no special precautions being necessary. Values of $B$, $T_Z$, and $X$ were fixed, $R$ was guessed, and (7) was integrated from $x = X$ (with $r = R$ and $dr/dx = 0$) to $x = 0$. This process was repeated with improved guesses for $R$, until the condition $r = 1$ at $x = 0$ was satisfied.† Then (6) was integrated to give $h_0/H$ (and $h_0/h(x)$ if desired). Some typical bubble shapes are shown in figure 6 for values of the parameters corresponding to cases 1 (*a*), 1 (*c*), 2 and 3 (*a*). The shape for case 1 (*c*) is similar to those observed in practice.

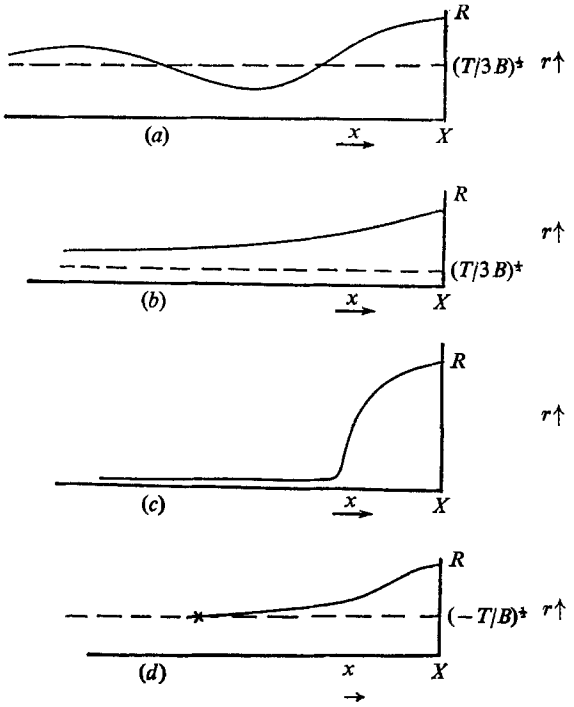


FIGURE 6. Sketches of typical bubble shapes: (*a*) case 1 (*a*), (*b*) case 1 (*c*), (*c*) case 2, (*d*) case 3 (*a*).

For the film-blowing process two of the important parameters are the product dimensions, which are determined by $A$ and $H$, so the dimensionless ratios $R$ ($= A/a_0$) and $h_0/H$ are the quantities we wish to predict as functions of the dimensionless parameters $B$, $T_Z$ and $X$ (i.e. of the physical variables $\Delta$, $F_Z$, $Z$, $a_0$, $\mu$ and $Q$). For results of practical interest, we may restrict attention to the ranges

† If no other information was available (e.g. from calculations with similar values of the parameters), $R$ was chosen by linear interpolation. The first two values used in that case were $((T_Z/B) - 3)^{\frac{1}{2}}$, the limiting value of $R$ as $X \to \infty$, and $(T_Z/B)^{\frac{1}{2}}$, the limiting value of $R$ as the film tension was allowed to fall to zero at some point in a long film. In practice, the final value was often quite near the first of these values, as can be seen in figure 7.

$1{\cdot}5 \leqslant R \leqslant 3$, $10 \leqslant h_0/H \leqslant 30$ and $8 \leqslant X \leqslant 20$; hence, we have the restrictions $0{\cdot}075 \leqslant B \leqslant 0{\cdot}4$ and $0{\cdot}5 \leqslant T_Z \leqslant 2{\cdot}5$. It is not easy to estimate $\mu$ (since in practice it could vary from $10^4$ to $10^6$ poise along the film, on account of the variations of temperature, and, to a lesser extent, of shear rate); there are no data from which $F_Z$ can be obtained (so far as we know). Thus, the above is probably the most reliable way of estimating the relevant values of the parameters. If we take the values (appropriate to a small-scale experimental arrangement) $a_0 = 3{\cdot}75$ cm, $Q = 4\,\mathrm{cm}^3/\mathrm{sec}$, $\Delta = 70\,\mathrm{N/m}^2$ ($\approx 7 \times 10^{-4}$ atmospheres), $\mu = 3 \times 10^5$ poise, and $F_Z = 5\,\mathrm{N}$ ($\approx 1\,\mathrm{lb.\ wt.}$), we obtain $B = 0{\cdot}097$ and $T_Z = 1{\cdot}56$.

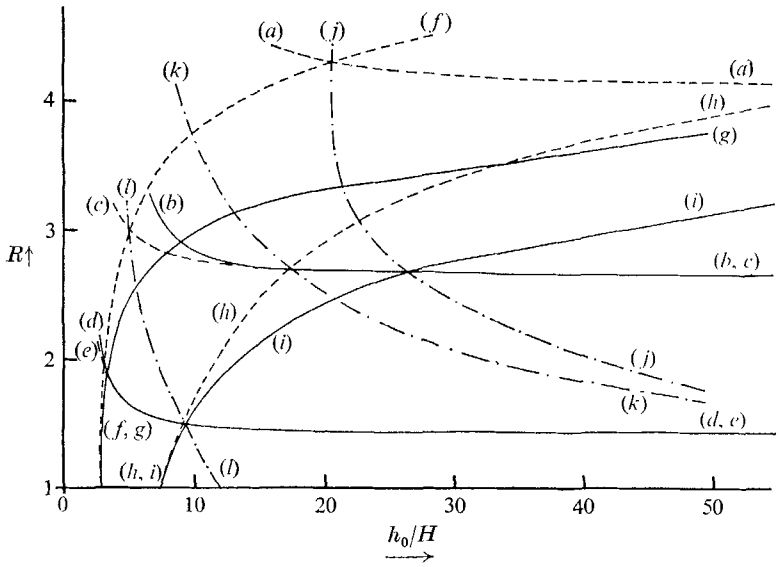


FIGURE 7. Typical results: Blow ratio $R$ against thickness reduction $h_0/H$. Curves of constant $B$ and $T_Z$, $B$ and $X$, and $T_Z$ and $X$. (*a*) $B = 0{\cdot}1$, $T_Z = 2$; (*b*) $B = 0{\cdot}2$, $T_Z = 2$; (*c*) $B = 0{\cdot}1$, $T_Z = 1$; (*d*) $B = 0{\cdot}2$, $T_Z = 1$; (*e*) $B = 0{\cdot}1$, $T_Z = 0{\cdot}5$; (*f*) $B = 0{\cdot}1$, $X = 10$; (*g*) $B = 0{\cdot}2$, $X = 5$; (*h*) $B = 0{\cdot}1$, $X = 20$; (*i*) $B = 0{\cdot}2$, $X = 10$; (*j*) $T_Z = 2$, $X = 10$; (*k*) $T_Z = 1$, $X = 20$; (*l*) $T_Z = 1$, $X = 10$.

| | | | | | |
|---|---|---|---|---|---|
| Pressure difference ($B$) | 0·2 | 0·175 | 0·165 | 0·1 | 0·09 |
| Axial tension ($T_Z$) | 2·3 | 2·0 | 1·85 | 1·15 | 1·0 |
| Freeze-line distance ($X$) | 8 | 9 | 10 | 20 | 23 |

TABLE 2. Typical values of the dimensionless parameters for blow ratio ($R$) = 3 and thickness reduction ($h_0/H$) = 20

The effect of the parameters $B$, $T_Z$ and $X$ on the product dimensions is shown in figure 7, where $R$ is plotted against $h_0/H$ for fixed values of pairs of these parameters. Table 2 shows how these parameters are interrelated by giving typical values of the three of them for $R = 3$ and $h_0/H = 20$. (One of $B$, $T_Z$ and $X$ can be chosen arbitrarily.)

As mentioned in § 1, the take-up of the film, which has here been assumed to imply a prescribed axial tension $T_Z$ at the freeze-line, could be at constant velocity,

equivalent to fixing the axial velocity at the freeze-line. From continuity ($Q = 2\pi a h v_1$), we deduce that $R = v_1(0)\, h_0/v_1(X)\, H$, giving a straight line of slope $v_1(0)/v_1(X)$ on figure 7. Thus, fixing values of $B$ and $X$ (giving another line on figure 7), as well as this ratio, suffices to determine the solution of the problem. To compute a solution from these conditions, a value of $T_Z$ would be guessed, and the value of $T_Z$ needed to give the prescribed value of the ratio $v_1(0)/v_1(X)$ would be found by iteration.

### 3.4. *Neglected factors*

The effect on the feasibility of this approach to the analysis of the film-blowing process of some of the many neglected factors has been discussed from the point of view of the asymptotic analysis in part 1 (Pearson & Petrie 1970*a*). Here remarks will be confined to four topics where the less formal approach can be expected to be helpful. In particular, no mention is made here of gravity, inertia or effects due to a thick film. (In practice the ratio of film thickness to bubble radius will lie between 0·05 and 0·005 at the die, and will be smaller downstream.)

The details of the flow at the die exit, where the flow changes from a constrained to a free-surface flow, have been ignored, despite the quite large 'die-swell' effects observed in the flow of molten polymers. (See e.g. Pearson 1966, p. 48.) The assumption, that the effects of this transition are confined to a region near the die exit, allows the crude approach of 'correcting' the initial values $a_0$ and $h_0$ from the die dimensions to the values the die dimensions would have to take in the absence of any such effects, so as to give the same downstream flow. With the present state of knowledge of the transition flow, this is an empirical correction.

Air drag can perhaps be dealt with (iteratively if necessary), by taking the results of the above analysis in its absence, and calculating the air drag on a bubble of that fixed shape and velocity. Taylor (1959) leads one to hope that the effect will be small. (Taylor estimates a 7 % velocity reduction due to air drag on a water bell.)

The effect of surface tension can easily be allowed for in this approach, with the proviso that, if the surface tension forces are very much greater than the viscous forces, the film thickness is not found in the first approximation, since the equations replacing (6) and (7) become equivalent. We write $P_L + 2\Gamma$ and $P_H + 2\Gamma$ for $P_L$ and $P_H$ in (4) and (5), where $\Gamma$ is the surface tension at the liquid–air interface, and then terms $\frac{1}{2}Gr\sec\theta$ and $2Gr^2\sec\theta$ are added to the right-hand sides of (6) and (7), respectively, where $G = 2\pi a_0^2\Gamma/\mu Q$, the ratio of surface tension to viscous forces. The modified equations have not been studied in detail, but the limiting value of $R$ as $X \to \infty$ is readily obtained from

$$1 = \left(\frac{T}{3B}\right)^{\frac{1}{2}}\left\{\left[1+\frac{G^2}{3BT}\right]^{\frac{1}{2}}+\left[\frac{G^2}{3BT}\right]^{\frac{1}{2}}\right\}, \quad \text{where} \quad R^2 = (T_Z - T)/B,$$

and the phase plane is not altered in any major way for $T > 0$ and $G$ not too large. The non-uniqueness in case 3 is not avoided by taking surface tension into consideration.

Temperature affects the mechanics of the flow through the dependence of viscosity on temperature; an attempt was made to estimate this effect by allowing $\mu$ to vary with position along the film. The viscosity was taken to be $\mu_0$ at the

freeze-line, where it changes discontinuously as in all the models considered, and to decrease towards the die (with increasing temperature) in a predetermined way. Functions $\mu/\mu_0 = 1-0{\cdot}05(X-x)$, $\exp\{-0{\cdot}05(X-x)\}$ and $\exp\{-0{\cdot}5(X-x)\}$ were used for $X$ up to 8, 8 and 10 respectively, giving viscosity reductions of 40 %, 33 % and 99 % over the length of the bubble. The bubble shape was not significantly altered in any of these cases, the major effect being a considerable increase in the thickness reduction $h_0/H$ over the value it took in the constant viscosity case. This is in the main due to more rapid thinning of the film in the long neck of the bubble, where the liquid is hottest and least viscous. Obviously, this will have an important effect on the quantitative predictions, but it leaves the qualitative results substantially unaffected. A similar conclusion probably holds for the effect of the variation of viscosity with rate of shear.

## 4. Conclusions

We can, with reasonable confidence, deduce from the results of this work that the dominant factor controlling the flow is the balance between the viscous forces and the externally applied forces. The major shortcoming of the quantitative predictions (for the practical process of making thermoplastic film) is likely to arise from the neglect of the temperature variation and its effect on the liquid viscosity. The effects of surface tension and air drag are certainly worth investigating, but seem unlikely to affect the main features of the flow. In large bubbles of thick film being slowly drawn, gravity becomes a limiting factor.

Part of the work reported here was carried out while one of us (C. J. S. P.) held a Science Research Council Fellowship in the Department of Chemical Engineering at Cambridge. We are grateful to the Science Research Council, and to the Head of the Department, for enabling us to carry out this work. Some of the computational work was done in the computing laboratories of Cambridge and of Newcastle upon Tyne Universities; we are also grateful to the directors of these laboratories for the use of their facilities.

## Appendix. The phase plane for system (11)

$$\left.\begin{aligned} dr/d\xi &= -2r^2s(T+r^2B), \\ ds/d\xi &= -6s-r(1+s^2)(T-3r^2B). \end{aligned}\right\} \tag{11}$$

(i) The origin is a non-elementary singular point to which the theorems of Keil (Sansone & Conti 1964, pp. 256–267) may be applied. For $T \neq 0$ (cases 1 and 3), we write $u = Tr$, $v = 6s+Tr$, $t = 6\xi$, and $A = B/T^3$, to obtain

$$\left.\begin{aligned} du/dt &= g(u,v), \\ dv/dt &= v+f(u,v), \end{aligned}\right\} \tag{A 1}$$

where $$f(u,v) = \tfrac{1}{36}u(v^2-u^2(1+108A))-\tfrac{1}{36}Au^3(v-u)(3v-5u),$$

and $$g(u,v) = \tfrac{1}{18}u^2(v-u)(1+Au^2).$$

We identify $(v, u)$ with $(x, y)$ of Keil's theorems, and see that system (A 1) satisfies the hypotheses of the theorems; namely, that $f$ and $g$ are dominated by linear terms near $(0, 0)$, and that in a neighbourhood of $(0, 0)$, excluding $(0, 0)$ itself, $du/dt$ and $dv/dt$ do not both vanish.

From the first theorem, there are two and only two trajectories tangent to the $v$-axis at the origin, and for system (A 1) these are clearly the half-lines $u = 0$, $v > 0$ and $u = 0$, $v < 0$. The two regions, into which this pair of trajectories divides the plane, are considered separately; from the second theorem, the trajectories in each region fall into one of two classes: either (1) all trajectories are parabolic (i.e. they tend to the origin) and tangent to the $u$-axis at the origin, or (2) one trajectory is parabolic and tangent to the $u$-axis at the origin, while all the other trajectories are hyperbolic (as are the trajectories near a saddle-point). Thus, the origin is either a node ((1) in both regions), a saddle-point ((2) in both regions), or a saddle-node ((1) in one region and (2) in the other region).

We distinguish between these alternatives by means of the third theorem, by studying the slope $dv/du$ of trajectories on either side of the isocline $J_0$ (where $dv/du = 0$). We consider first the half-plane $u > 0$, where, if $dv/du$ increases with $v$ increasing across $J_0$, we have (1), and, if $dv/du$ decreases, we have (2). The converse is true in the half-plane $u < 0$.

Here we approximate $J_0$ near the origin by

$$v = \tfrac{1}{36}(1 + 108A)\,u^3 + \tfrac{5}{36}Au^5,$$

so that for $A > -1/108$ $J_0$ lies in the first and third quadrants ($uv > 0$). On $v = 0$, $dv/du$ is given by

$$dv/du = (-u^3(1 + 108A) - 5Au^5)/\{-2u^3(1 + Au^2)\},$$

which is positive near the origin for $A > -1/108$, so that, from continuity arguments, $dv/du$ in this case decreases as $J_0$ is crossed in the direction of $v$ increasing. (And, in $u < 0$, it increases.) For $A \leqslant -1/108$, $J_0$ lies in the second and fourth quadrants, and $dv/du$ is negative near the origin, leading to the same conclusion. Thus, for all values of $A$, the origin is a saddle-point with separatrices tangent to the $u$- and $v$-axes (i.e. the separatrices are the lines $r = 0$ and $6s + Tr = 0$ in the $(r, s)$-plane). (See figures 3 and 5.)

For $T = 0$, we set $u = rB^{\frac{1}{4}}$, $v = s$ and $t = -6\xi$ to obtain

$$\left.\begin{aligned} du/dt &= \tfrac{1}{3}u^4v, \\ dv/dt &= v - \tfrac{1}{2}u^3(1 + v^2), \end{aligned}\right\} \tag{A 2}$$

and apply the same methods. (See figure 4.)

(ii) At the singular point $((T/3B)^{\frac{1}{2}}, 0)$ of case 1 the equations are, writing $w = r - (T/3B)^{\frac{1}{2}}$,

$$dw/d\xi = (8T^2/9B)\,s + O(w^2 + s^2),$$

$$ds/d\xi = -2Tw + 6s + O(w^2 + s^2).$$

The standard methods (see e.g. Sansone & Conti 1964, pp. 44–47) lead to the results that the point $((T/3B)^{\frac{1}{2}}, 0)$ is a stable focus for $16T^3/9B > 9$, and a stable node for $16T^3/9B \leqslant 9$. In the latter case, the critical directions are given by $s/w = \frac{27}{8}(B/T^3)^{\frac{1}{2}}[1 \pm (1 - 16T^3/81B)^{\frac{1}{2}}]$.

(iii) Similarly, the results stated in the main text for the singular points of case 3(*a*) can be obtained from

$$d(r-(-T/B)^{\frac{1}{2}})/d\xi = -4q(-T^3/B)^{\frac{1}{2}}(r-(-T/B)^{\frac{1}{2}}) + O((r-(-T/B)^{\frac{1}{2}})^2+(s-q)^2),$$
$$d(s-q)/d\xi = -10(q^2+1)T(r-(-T/B)^{\frac{1}{2}}) + (8q(-T^3/B)^{\frac{1}{2}}-6)(s-q) + O((r-(-T/B)^{\frac{1}{2}})^2+(s-q)^2),$$

for the point $(1, q)$, and

$$d(r-(-T/B)^{\frac{1}{2}})/d\xi = -(4/q)(-T^3/B)^{\frac{1}{2}}(r-(-T/B)^{\frac{1}{2}}) + O((r-(-T/B)^{\frac{1}{2}})^2+(s-1/q)^2),$$
$$d(s-1/q)/d\xi = -(10T(q^2+1)/q^2)(r-(-T/B)^{\frac{1}{2}}) + (8(-T^3/B)^{\frac{1}{2}}/q-6)(s-1/q) + O((r-(-T/B)^{\frac{1}{2}})^2+(s-1/q)^2)$$

where $q = \frac{3}{4}(-B/T^3)^{\frac{1}{2}} - ((-9B/16T^3)-1)^{\frac{1}{2}}$, and $0 > T^3 > -9B/16$.

(iv) In case 3(*b*), we write $u = r-(-T/B)^{\frac{1}{2}}$, $v = s-1$ to obtain

$$du/d\xi = -3u + O(u^2+v^2),$$
$$dv/d\xi = 15(-B/T)^{\frac{1}{2}}u + O(u^2+v^2),$$

so that $u = v = 0$ is a non-elementary singular point, which may be shown to be a saddle-node. (Sansone & Conti 1964, pp. 256–267.)

(v) In case 3, solutions with $dr/dx$ tending to $\infty$ are possible and we can get more information by considering the $(r, \theta)$-plane, where $\tan\theta = dr/dx$; i.e. we have as phase space the surface of a cylinder rather than a plane. System (11) becomes

$$\left.\begin{aligned} du/dt &= -2u^2(u^2-1)\sin\theta, \\ d\theta/dt &= \cos\theta(u(1+3u^2) - m\sin 2\theta), \end{aligned}\right\} \tag{A 3}$$

where $u = r(-B/T)^{\frac{1}{2}}, \quad m = 6(-B/T^3)^{\frac{1}{2}}$

and $dt/dx = -(-T^3/B)^{\frac{1}{2}}/2r^2(T+r^2B)\cos\theta.$

In case 3(*a*), system (A 3) has six singularities on $u = 1$ and a further four on $u = 0$ in $-\pi < \theta \leqslant \pi$. Writing $\alpha$ for the smallest positive root of

$$\sin 2\theta = 4/m \quad (0 < \alpha < \tfrac{1}{4}\pi),$$

these are $(1, \alpha)$, $(1, \frac{1}{2}\pi-\alpha)$, $(1, \frac{1}{2}\pi)$, $(1, -\pi+\alpha)$, $(1, -\frac{1}{2}\pi-\alpha)$, $(1, -\frac{1}{2}\pi)$ and $(0, 0)$, $(0, \frac{1}{2}\pi)$, $(0, \pi)$, $(0, -\frac{1}{2}\pi)$. Solutions relevant to the physical problem start on $\theta = 0$ with $u > 1$ (at the freeze-line) and such solutions, and in fact any solutions starting in $u > 1$, reach either the singularity $(1, \alpha)$ or $(1, \frac{1}{2}\pi)$, apart from the separatrices approaching $(1, \frac{1}{2}\pi-\alpha)$ and leaving $(1, -\frac{1}{2}\pi)$. At these singularities, the solution of system (10) is indeterminate, but there are only certain possibilities open to it. For example, solutions leaving $(1, \alpha)$, apart from the ingoing separatrix to the origin, must approach either $(1, -\frac{1}{2}\pi)$ or $(0, \frac{1}{2}\pi)$, and, by such arguments, certain types of solution can be predicted. The investigation of the solutions of the equations in this case are not discussed in more detail here, because they are not relevant to the particular physical problem motivating the analysis.

(vi) The proof that in case 1 all trajectories in $r > 0$ tend to the singular point $((T/3B)^{\frac{1}{2}}, 0)$ depends on showing that there is a family of closed curves in this half-

plane, which are always crossed from their exterior to their interior by trajectories as $x$ decreases. System (11) may be written

$$\frac{dv}{du} = \frac{mv + u(1-3u^2)(1+v^2)}{2u^2(1+u^2)v}$$

(where $u = r(T/B)^{\frac{1}{2}}$, $t = \xi(T^3/B)^{\frac{1}{2}}$, $m = 6(B/T^3)^{\frac{1}{2}}$ and $v = s$), which can be integrated to give

$$v^2 = Au/(1+u^2)^2 - 1 + E(u),$$

where $A = (1+U)^2(1+V^2)/U$ for the trajectory passing through the point $(U, V)$, and

$$E(u) = \frac{u}{(1+u^2)^2}\int_U^u mv\frac{(1+y^2)}{y^3}dy.$$

Writing $v_1^2 = Au/(1+u^2)^2 - 1$, we see that the curves $v^2 = v_1^2$ are closed, symmetrical about $v = 0$, and cut $v = 0$ once between $u = 0$ and $u = 1/\sqrt{3}$, and once for $u > 1/\sqrt{3}$. ($A$ as defined above is never less than $\frac{16}{9}\sqrt{3}$, that minimum value giving a real value (0) for $v$ only at $u = 1/\sqrt{3}$.)

We treat $v_1$ as an approximation to $v$ with error $E$, and show that $E$ is always such that $|v| < |v_1|$ as we proceed in the direction of $x$ decreasing. Now $m > 0$, $u > 0$, and for $v > 0$ $u$ decreases with $x$ decreasing along a trajectory, so we take $u < U$, and see immediately that $E < 0$. Similarly, for $v < 0$, we take $u > U$, and again $E < 0$, so that $v^2 < v_1^2$, which is the desired result. Since the family of curves $v^2 = v_1^2$ fills the half-plane $u > 0$, this completes the proof.

## REFERENCES


Novozhilov, V. V. 1959 *The Theory of Thin Shells.* Groningen: Noordhoff.

Pearson, J. R. A. 1966 *Mechanical Principles of Polymer Melt Processing.* Oxford: Pergamon.

Pearson, J. R. A. & Petrie, C. J. S. 1970*a* *J. Fluid Mech.* **40**, 1.

Pearson, J. R. A. & Petrie, C. J. S. 1970*b* *Plastics & Polymers*, **38**, 85.

Sansone, G. & Conti, R. 1964 *Non-linear Differential Equations.* Oxford: Pergamon.

Taylor, G. I. 1959 *Proc. Roy. Soc.* A **253**, 289–295.

*J. Fluid Mech.* (1970), *vol.* 42, *part* 3, *pp.* 627–638
*Printed in Great Britain*



# On the development of the wake behind the trailing edge of a flat plate

By S. H. SMITH

Department of Mathematics University of Toronto, Toronto 5, Canada.

(Received 8 February 1969 and in revised form 6 February 1970)

A stream with constant velocity $U$ is impulsively started at time $t = 0$ past the trailing edge of a semi-infinite flat plate. According to boundary-layer theory, it is found that the flow at a distance $x$ downstream from the trailing edge is unaware of the presence of the plate when $x > Ut$; at time $t = x/U$ there is then a discontinuity in the velocity normal to the plate. It is the neglect of diffusion parallel to the axis of the plate that introduces the discontinuity, and when the complete Navier–Stokes equations are considered for $t \simeq x/U$, a solution is found that can be matched with that gained from boundary-layer arguments.

## 1. Introduction

Some time ago Stewartson (1951) considered the following problem: a semi-infinite flat plate is at rest in a slightly viscous liquid when, at time $t = 0$, a uniform stream of constant velocity $U$ is impulsively set up past the leading edge of the plate. This was tackled as a boundary-layer problem, so that for times $t$ less than $x/U$, at points a distance $x$ downstream from the leading edge, the Rayleigh solution for the flow past an infinite plate represents the motion. At later times, however, the steady Blasius solution for the semi-infinite plate eventually dominates. The manner in which the motion passes from one limiting case to the other has been the cause of certain controversy recently. Stewartson himself indicated that the effect of the leading edge is passed by convection with velocity $U$ along the edge of the boundary layer, arriving a distance $x$ downstream when $\tau = Ut/x = 1$; diffusion then transmits this effect through the boundary layer to the plate. Mathematically, an essential singularity is expected at $\tau = 1$. No formal proof could be given, but a solution of the equations was found that did possess such a singularity. The analysis in this paper was generalized by Smith (1967) for the equivalent flow past a wedge, and a similar, tentative conclusion followed.

In a recent paper by Tokuda (1968), the results of Stewartson were disputed, though Stewartson & Brown (see corrigendum to Tokuda 1968) rightly observe that his conclusions were based on inaccurate numerical data, and that his proof of the existence of a series solution for the velocity is false.

To the present author at least, the search for a solution with an essential singularity at $\tau = 1$ seems the only one likely to succeed *when the equations considered are the boundary-layer equations.* The boundary-layer equations for

unsteady flows neglect the diffusion of vorticity parallel to the stream; they include only diffusion perpendicular, and convection parallel to the mainstream flow. Convection is governed by hyperbolic partial differential equations which preserve discontinuities, and diffusion by parabolic partial differential equations which 'smooth out' discontinuities immediately—mathematically by the presence of essential singularities. The author is aware of the numerical solution by Hall (1968) of the boundary-layer equations for the Stewartson problem; a smooth joining of the two limiting cases is exhibited. Mathematically, the discontinuity is a consequence of solving the linearized boundary-layer equations; it is then found that the introduction of the non-linear terms ensures the existence of a smooth solution with the essential singularity.

A factor neglected by Stewartson is the influence of diffusion acting parallel to the stream. The full Navier–Stokes equations would have to be considered if this effect were included, but the mathematics involved is very difficult and has not been attempted here. However, any solution would show that the knowledge of the leading edge is transmitted immediately throughout the flow field; here the only discontinuity would be at the initial moment of time.

In the present work, therefore, we consider the same physical situation except that the uniform stream flows in the opposite direction; that is, we take the edge of the semi-infinite plate to be a trailing edge. With this change the mathematics becomes more amenable to solution and the main features of the flow are displayed. After stating the problem in §2, we first consider the solution of the boundary-layer equations when the variation from a uniform stream is small; this enables us to linearize the equations. For points in the wake region, when $0 < \tau = Ut/x < 1$, the flow has a constant velocity $U$ parallel to the plate. When $\tau = 1$, the influence of the trailing edge is first noticed with a discontinuity in the velocity normal to the axis of the plate.

A discussion follows of the nature of the flow as $\tau \to \infty$. and it is found that the approach to the limiting solution is by means of an exponential decay. When a precise asymptotic analysis is carried through, it is interesting to observe that it is the process of convection acting within the boundary layer that transmits the effect of the trailing edge through the wake.

In an attempt to eliminate the singularity at $\tau = 1$, the Navier–Stokes equations, linearized in the same manner as the boundary-layer equations, are investigated in the region $\tau \simeq 1$ as a singular perturbation problem. A solution is found which matches with the behaviour in the boundary-layer solution for both $0 < 1-\tau \ll 1$ and $0 < \tau-1 \ll 1$. The smooth joining that was anticipated on physical grounds is therefore proved. When the complete (non-linear) Navier–Stokes equations are investigated, it is found that the linearization procedure is certainly valid for regions at the edge of the boundary layer. As points closer to the axis within the boundary layer are considered, the non-linear terms become more important. However, it is unusual to note that when linear and non-linear terms are of equal importance, the leading term in the solution of the differential equation is just that found from the linear Navier–Stokes equations; the higher terms do differ though. This fact considerably extends the validity of the linear solution.

It is of some interest to consider the effect of the non-linear terms in the boundary-layer equations. In the work of Stewartson (1951) it was the influence of these terms that allowed the discontinuity from the linearized equations to be smoothed out by the essential singularity. In §6, a summary is given of arguments which indicate that in the trailing edge situation the discontinuity is not removed by the non-linear terms. There is no essential singularity at $\tau = 1$; in fact the dominant term of the solution of the linear boundary-layer equations near $\tau = 1$ is also the dominant term from the non-linear equations. The physical explanation offered is as follows: in the flow past the leading edge the effect of the edge is convected downstream at a velocity less than that of the uniform stream. At the edge of the boundary layer this difference is certainly very small, but it is non-zero. The presence of the plate instantaneously retards the flow at all points downstream of the leading edge at the initial time. In contrast, the vorticity downstream from the trailing edge is zero at the initial time, and the effect of the edge is convected at exactly the free-stream velocity. Initially the vorticity is discontinuous along the line $x = 0$, and so this line of discontinuity moves downstream with the constant velocity $U$ when the effect of diffusion parallel to the plate is neglected. That is, the discontinuity is preserved at the value $\tau = 1$, and it can only be removed through considering the Navier–Stokes equations.

Finally, we consider the limitations of the model of a semi-infinite flat plate to describe realistic flows.

## 2. Statement of the problem

We consider the problem as one with a constant velocity $U$ impulsively set up in the main stream at time $t = 0$, while the plate remains at rest. The motion is two dimensional, so we take the origin of the co-ordinate system as the trailing edge of the flat plate which otherwise occupies the negative part of the $x$ axis. If $u$ and $v$ are the components of velocity parallel to the $x$ and $y$ axes respectively, then the Navier–Stokes equations are

$$u_x + v_y = 0, \tag{2.1}$$

$$u_t + uu_x + vu_y = -\rho^{-1}p_x + \nu\nabla^2 u, \tag{2.2}$$

$$v_t + uv_x + vv_y = -\rho^{-1}p_y + \nu\nabla^2 v; \tag{2.3}$$

$p(x, y, t)$ is the pressure and $\rho, \nu$ are the constants representing the density and kinematic viscosity of the fluid.

When a stream function $\psi(x, y, t)$ is defined by $u = \psi_y, v = -\psi_x$ the equation of continuity (2.1) is immediately satisfied. The pressure $p$ can then be eliminated from the momentum equations (2.2), (2.3) for

$$\omega_t - \frac{\partial(\psi, \omega)}{\partial(x, y)} = \nu\nabla^2\omega, \tag{2.4}$$

when $\omega = \nabla^2\psi$; this is the Helmholtz equation for the vorticity $\omega(x, y, t)$. Because of a symmetry about the $x$ axis, the solution of these equations is considered for $y \geqslant 0$ only.

The boundary and initial conditions can be stated as follows:

$$u = v = 0 \quad \text{when} \quad y = 0, \quad x < 0, \quad t \geqslant 0; \tag{2.5a}$$

$$u_y = v = 0 \quad \text{when} \quad y = 0, \quad x > 0, \quad t \geqslant 0; \tag{2.5b}$$

$$u = U, \quad v = 0 \quad \text{when} \quad y > 0, \quad x > 0, \quad t = 0; \tag{2.5c}$$

$$u \simeq U, \quad v \simeq 0 \quad \text{when} \quad y \to \infty, \quad t \geqslant 0; \tag{2.5d}$$

$$u \simeq U, \quad v \simeq 0 \quad \text{when} \quad x \to +\infty, \quad t \geqslant 0. \tag{2.5e}$$

The final condition to be stated is that for $x \to -\infty$. Here there is no knowledge of the trailing edge so that the velocities are those for the flow past an infinite plate. That is,

$$u \simeq U \operatorname{erf}\left(\frac{y}{2(\nu t)^{\frac{1}{2}}}\right), \quad v \simeq 0 \quad \text{as} \quad x \to -\infty, \quad t \geqslant 0, \tag{2.5f}$$

where

$$\operatorname{erf} z = 2\pi^{-\frac{1}{2}} \int_0^z e^{-u^2} du;$$

this was given by Rayleigh (1911). The only other point noted here is that, eventually, the velocities tend to zero throughout the flow field. However, the manner of this decay does not interest us; it is the somewhat artificial result of taking a semi-infinite plate rather than one of finite length.

The conditions to be satisfied have been stated for the set of equations (2.1)–(2.3); it is a straightforward matter to adjust these for the equation (2.4).

## 3. A boundary-layer solution

It is the assumption of the Prandtl boundary-layer theory for the unsteady flow past a flat plate that the motion is represented by a balance between convection parallel to, and diffusion normal to, the axis of the plate; the pressure gradient is zero. This leads to the equations (cf. Rosenhead 1963),

$$u_x + v_y = 0, \tag{3.1}$$

$$u_t + uu_x + vu_y = \nu u_{yy}, \tag{3.2}$$

from (2.1), (2.2). In this approximation we neglect the action of diffusion parallel to the plate; convection alone acts in the positive $x$ direction, so that (2.5$f$) must represent the velocities for all $x < 0$. In the remainder of this section we consider $x \geqslant 0$ alone, and set the condition

$$u = U \operatorname{erf}\left(\frac{y}{2(\nu t)^{\frac{1}{2}}}\right), \quad v = 0 \quad \text{when} \quad x = 0, \quad t \geqslant 0, \quad y > 0 \tag{3.3}$$

to replace (2.5$a, f$); (2.5$b$–$e$) remain. These non-linear boundary-layer equations cannot, of course, be solved completely; further assumptions need now be made to gain the information required.

Here our interest centres on the development of the wake downstream from the trailing edge. To begin, therefore, we consider the situation when the motion differs only slightly from the basic flow of a uniform stream; that is, we neglect the products of $v$ and $u$-$U$ in the boundary-layer equation (3.2) to give the linear differential equation

$$u_t + Uu_x = \nu u_{yy} \quad (x, y, t \geqslant 0). \tag{3.4}$$

The solution of this equation, together with the conditions (2.5*b*–*e*), (3.3), is considered in an attempt to describe the flow at a time soon after the disturbance due to the plate reaches the point $P(x, y)$ in the wake region, particularly for $P$ at the edge of the boundary layer. The neglect of the non-linear terms certainly does raise important points; however, we delay a full discussion until a later section. The equation (3.4) is equivalent to that derived by Stewartson (1951); a similar method of solution to the one he used is adopted here.

We define

$$\tau = Ut/x, \quad \zeta = y/(\nu t)^{\frac{1}{2}}, \tag{3.5}$$

and from dimensional arguments it is clear that $u$ is a function of $\zeta$ and $\tau$ only. Consequently, $u(\zeta, \tau)$ satisfies

$$u_{\zeta\zeta} + \tfrac{1}{2}\zeta u_\zeta + \tau(\tau - 1)\, u_\tau = 0 \tag{3.6}$$

subject to the conditions $u_\zeta = 0$ on $\zeta = 0$; $u \to U$ as both $\zeta \to \infty$ and $\tau \to 0$; $u \simeq U \operatorname{erf} \frac{1}{2}\zeta$ as $\tau \to \infty$, $\zeta \neq 0$. A solution is sought in the form of a Fourier cosine transform, defining

$$\bar{u}(\alpha, \tau) = \int_0^\infty u(\zeta, \tau) \cos \alpha\zeta \, d\zeta.$$

With $(u_\zeta)_{\zeta=0} = 0$, the transform of (3.6) becomes the first-order partial differential equation

$$\tfrac{1}{2}\alpha\bar{u}_\alpha - \tau(\tau - 1)\bar{u}_\tau + (\alpha^2 + \tfrac{1}{2})\bar{u} = 0,$$

which has the solution

$$\bar{u} = \alpha^{-1} e^{-\alpha^2} G\{\alpha^2 \tau^{-1}(\tau - 1)\},$$

where $G$ is an arbitrary function. That is,

$$u(\zeta, \tau) = \int_0^\infty \frac{e^{-\alpha^2}}{\alpha} G\left\{\frac{\alpha^2}{\tau}(\tau - 1)\right\} \cos \zeta\alpha \, d\alpha, \tag{3.7}$$

when the constant for the inverse transform is absorbed into $G$. From the condition $\tau \to \infty$ we find

$$\int_0^\infty \alpha^{-1} e^{-\alpha^2} G(\alpha^2) \cos \zeta\alpha \, d\alpha = U \operatorname{erf} \tfrac{1}{2}\zeta.$$

Taking the inverse transform (Erdelyi *et al.* 1954, p. 73),

$$\alpha^{-1} e^{-\alpha^2} G(+\alpha^2) = U\delta(\alpha) - 4\pi^{-\frac{3}{2}} U e^{-\alpha^2} \Phi(\tfrac{1}{2}; \tfrac{3}{2}; \alpha^2),$$

where $\Phi(a; c; z)$ is the Humbert notation for the confluent hypergeometric function (Erdelyi *et al.* 1953, p. 248) and $\delta(\alpha)$ is the Dirac delta function. The other conditions are already satisfied unless $\tau \to 0$ and $\zeta \to \infty$ simultaneously such that $\tau\zeta^2$ is constant. In this case we require

$$\alpha^{-1} G(-\alpha^2) = U\delta(\alpha).$$

Therefore, if $\tau < 1$, the solution is $u = U$, though for $\tau \geqslant 1$ we have, after some simplification,

$$u = U - \frac{4U}{\pi^{\frac{3}{2}}} \left(\frac{\tau - 1}{\tau}\right)^{\frac{1}{2}} \int_0^\infty e^{-\alpha^2} \cos \zeta\alpha \, \Phi\left\{\tfrac{1}{2}; \tfrac{3}{2}; \frac{\alpha^2}{\tau}(\tau - 1)\right\} d\alpha. \tag{3.8}$$

When $0 \leqslant \tau - 1 \ll 1$.

$$u - U \simeq -2\pi^{-1} U (\tau - 1)^{\frac{1}{2}} e^{-\frac{1}{4}\zeta^2}; \tag{3.9}$$

more generally, we can expand the integral of (3.7) into the infinite series

$$u = U - \frac{2U}{\pi}\left(\frac{\tau-1}{\tau}\right)^{\frac{1}{2}} \sum_{n=0}^{\infty} \frac{(-1)^n}{n!\,(2n+1)} \left(\frac{\tau-1}{\tau}\right)^n (e^{-\frac{1}{4}\zeta^2})^{(2n)}, \tag{3.10}$$

when the $(2n)$ superscript represents the $2n$th derivative.

These results can be interpreted immediately: the velocity $u(x, y, t)$ is constant at the point $P(x, y)$ until a time $t = x/U$ has elapsed. Accordingly, there is a finite time within which the flow in the wake is unaware of the presence of the plate because the disturbance due to the trailing edge is transmitted through the liquid by convection at the mainstream velocity. At $\tau = 1$, the velocity $u$, and all its derivatives with respect to $y$ are continuous. However, $u_x$ is discontinuous and so, from the equation of continuity, $v$ is also discontinuous. This conclusion is physically unrealistic, and can be taken to be a natural consequence of neglecting the derivatives with respect to $x$ in the boundary-layer approximation. Alternatively, it can be argued that the discontinuity present in the solution of the linear equation is removed when the non-linear terms are included, and that the real flow is more accurately described in this way. Stewartson (1951) followed the second line of reasoning when he considered the flow past the leading edge. These two possibilities are closely investigated in the following sections.

According to the linear boundary-layer approximation, the vorticity $\omega$ is given by $u_y$. From (3.9) this then indicates $\omega = 0$ for $\tau < 1$, and

$$\omega = \frac{U}{\pi(\nu t)^{\frac{1}{2}}}\left(\frac{\tau-1}{\tau}\right)^{\frac{1}{2}} \sum_{n=0}^{\infty} \frac{(-1)^n}{n!\,(2n+1)} \left(\frac{\tau-1}{\tau}\right)^n (\zeta e^{-\frac{1}{4}\zeta^2})^{(2n)} \tag{3.11}$$

for $\tau \geqslant 1$.

After the work described in this paper had been completed, it was found possible to sum this series. The terms in (3.11) can be rearranged to give an infinite series with terms in $(\tau - 1)$ rather than $(\tau - 1)/\tau$. The resulting expression is just

$$\omega = \frac{U}{\pi(\nu t)^{\frac{1}{2}}} e^{-\frac{1}{4}\zeta^2} \sum_{n=0}^{\infty} \frac{(-1)^n \zeta^{2n+1}}{2^{2n} n!(2n+1)} (\tau-1)^{n+\frac{1}{2}} \quad (\tau \geqslant 1),$$

which is the series expansion for the function

$$\omega = \frac{U}{(\pi\nu t)^{\frac{1}{2}}} e^{-\frac{1}{4}\zeta^2} \operatorname{erf}\left(\frac{\zeta(\tau-1)^{\frac{1}{2}}}{2}\right) \quad (\tau \geqslant 1). \tag{3.12}$$

This rearrangement is a purely formal procedure; however, it is now easily seen that (3.12) does in fact satisfy both the differential equation and boundary conditions required, and so represents the solution for the problem. Corresponding to (3.12) we can gain

$$u = U - \frac{U}{\pi^{\frac{1}{2}}} \int_{\zeta}^{\infty} e^{-\frac{1}{4}\rho^2} \operatorname{erf}\left(\frac{\rho(\tau-1)^{\frac{1}{2}}}{2}\right) d\rho \quad (\tau \geqslant 1),$$

from (3.10).

When the asymptotic expansion is taken for (3.12), we have

$$\omega \simeq U(\pi\nu t)^{-\frac{1}{2}}\{e^{-\frac{1}{4}\zeta^2} - 2(\pi\zeta^2\tau)^{-\frac{1}{2}} e^{-\frac{1}{4}\zeta^2\tau}\} \quad \text{for} \quad \tau \to \infty, \quad \zeta = O(1).$$

The second term is essentially the correction due to the disturbance of the trailing edge at the edge of the boundary layer for large times $t$; the variable

$\zeta^2\tau = Uy^2/\nu x$ is time independent. It is seen, therefore, that the disturbance is carried away by convection, and particularly that it is concentrated near $\zeta$ small, i.e. closer to the axis. It is indeed interesting to observe the role of convection here in transmitting the effect of the trailing edge within the boundary layer itself, and the author is grateful to a referee for bringing this point to his attention.

## 4. A solution in the neighbourhood of $\tau = 1$

It is convenient to consider the Navier–Stokes equations in the form (2.4). Again we begin by considering the flow when it differs slightly from that of a uniform stream, so that it is possible to write $\psi = Uy$ in the Jacobian of (2.4) to give

$$\omega_t + U\omega_x = \nu\nabla^2\omega. \tag{4.1}$$

These circumstances are the same as those under which (3.4) was considered in the previous section; now, however, the $\omega_{xx}$ term is included to represent diffusion parallel to the $x$ axis.

Together with the non-dimensional variables $\zeta$ and $\tau$ (given in (3.5)), we further define

$$\eta = \frac{x}{(\nu t)^{\frac{1}{2}}}.$$

When the function $H(\zeta, \eta, \tau)$ is introduced by $\omega = U(\nu t)^{-\frac{1}{2}}H$, it is seen that $H$ satisfies the linear partial differential equation

$$H_{\zeta\zeta} + \tfrac{1}{2}\zeta H_\zeta + \tfrac{1}{2}H + \tau(\tau-1)H_\tau = \tau\eta H_\eta - \tfrac{1}{2}\eta H_\eta - H_{\eta\eta} - 2\tau\eta^{-2}H_\tau - \tau^2\eta^{-2}H_{\tau\tau} \tag{4.2}$$

from (4.1). When $\eta \to \infty$, and $\partial/\partial\eta = 0$, the right-hand side of (4.2) is zero, so that the resultant equation for the vorticity in terms of $H$ as a function of $\zeta$ and $\tau$ is equivalent to the boundary-layer equation (3.6) for the velocity $u(\zeta, \tau)$. After setting appropriate conditions the solution would then be given by (3.11).

Generally, it is known that the singular points of a differential equation occur where the coefficient of a highest order derivative is equal to zero. Now when $\eta$ is infinite and $\tau = 1$, the coefficients of both the $H_{\tau\tau}$ and $H_\tau$ terms in (4.2) are zero. In the region under consideration it is necessary that the coefficients of these terms are of finite order, together with the coefficients of the other highest derivatives. Physically, this ensures that the processes of diffusion (in both directions) and convection are in balance.

We therefore introduce the transformation

$$\sigma = (\tau-1)\eta \tag{4.3}$$

to replace $\tau$; (4.2) then becomes

$$H_{\zeta\zeta} + \tfrac{1}{2}\zeta H_\zeta + \tfrac{1}{2}H - (\sigma+\eta)H_\eta + \tfrac{1}{2}\sigma H_\sigma + 2\eta^{-2}(\sigma+\eta)H_\sigma + \tfrac{1}{2}\eta H_\eta + 2\sigma\eta^{-1}H_{\sigma\eta} + H_{\eta\eta} + \eta^{-2}\{(\sigma+\eta)^2 + \sigma^2\}H_{\sigma\sigma} = 0. \tag{4.4}$$

When $\eta \gg 1$ and $|\tau - 1| \ll 1$ such that $\sigma = O(1)$, the coefficients of $H_{\sigma\sigma}$ and $H_\sigma$ are both $O(1)$. The transformation (4.3) is a stretching transformation in the terminology of singular perturbation problems.

The boundary conditions are now set in terms of $\zeta$ and $\sigma$ because a solution is sought for (4.4) for large $\eta$. At $\zeta = 0$ we require $H = 0$, since the vorticity is zero on $y = 0$, $x > 0$, cf. (2.5$b$). Further, $H \to 0$ as $\zeta \to \infty$ and also as $\sigma \to -\infty$. Finally we match $H$ onto the dominant term

$$\pi^{-1}(\tau - 1)^{\frac{1}{2}} \zeta e^{-\frac{1}{4}\zeta^2} \tag{4.5}$$

of (3.10) as $\sigma \to +\infty$.

For the first step in the solution it is possible for us to write

$$H = \zeta e^{-\frac{1}{4}\zeta^2} M(\sigma, \eta) \tag{4.6}$$

for some function $M$; in this way the conditions for $\zeta$ can be satisfied as well as (4.5). The corresponding differential equation for $M$ becomes

$$(1 + 2\sigma\eta^{-1} + 2\sigma^2\eta^{-2}) M_{\sigma\sigma} + M_{\eta\eta} + 2\sigma\eta^{-1} M_{\sigma\eta} + (\tfrac{1}{2}\sigma + 2\eta^{-1} + 2\sigma\eta^{-2}) M_\sigma - (\sigma + \tfrac{1}{2}\eta) M_\eta + \tfrac{1}{2} M = 0,$$

the solution of which must match with $\pi^{-1}\sigma^{\frac{1}{2}}\eta^{-\frac{1}{2}}$ from (4.5). Therefore we write $M = \eta^{-\frac{1}{2}} m(\sigma)$, and then note, on retaining only the dominant terms for large $\eta$, that

$$m'' + \tfrac{1}{2}\sigma m' - \tfrac{1}{4} m = 0, \tag{4.7}$$

where dashes denote differentiation with respect to $\sigma$. The general solution of this ordinary differential equation is

$$m(\sigma) = A\Phi(-\tfrac{1}{4}; \tfrac{1}{2}; -\tfrac{1}{4}\sigma^2) + B(-\tfrac{1}{4}\sigma^2)^{\frac{1}{2}} \Phi(\tfrac{1}{4}; \tfrac{3}{2}; -\tfrac{1}{4}\sigma^2), \tag{4.8}$$

where $A$ and $B$ are constants (possibly complex). As a function of the complex variable $z$, $\Phi(a; c; z)$ is defined in the $z$ plane cut along the negative real axis; hence $m(\sigma)$ has different representations for $\sigma > 0$ and $\sigma < 0$ while still retaining continuous derivatives of all orders at $\sigma = 0$. We require $m$ to have an exponential decay as $\sigma \to -\infty$, and $m \sim \pi^{-1}\sigma^{\frac{1}{2}}$ as $\sigma \to +\infty$; the asymptotic expansions for $\Phi$ (Erdelyi *et al.* 1953, p. 278) show

$$A = 2^{-\frac{1}{2}}\pi^{-\frac{3}{2}}\Gamma(\tfrac{3}{4}) \quad \text{and} \quad B = -i(2\pi)^{-\frac{3}{2}}\Gamma(\tfrac{1}{4}). \tag{4.9}$$

We note, in particular, that the values (4.9) imply

$$m \sim 2^{-\frac{1}{2}}\pi^{-1}(-\sigma)^{-\frac{3}{2}} e^{-\frac{1}{4}\sigma^2} \quad \text{as} \quad \sigma \to -\infty. \tag{4.10}$$

Collecting these results together, we can finally write

$$\omega \sim \frac{U}{(\nu t)^{\frac{3}{2}}} \frac{\zeta e^{-\frac{1}{4}(\zeta^2+\sigma^2)}}{(2\pi)^{\frac{3}{2}}\eta^{\frac{1}{2}}} \{2\Gamma(\tfrac{3}{4})\Phi(\tfrac{3}{4}; \tfrac{1}{2}; \tfrac{1}{4}\sigma^2) \pm \tfrac{1}{2}\Gamma(\tfrac{1}{4})\sigma\Phi(\tfrac{5}{4}; \tfrac{3}{2}; \tfrac{1}{4}\sigma^2)\} \tag{4.11}$$

for $\sigma \gtrless 0$ as the vorticity when $\eta \gg 1$, $|\tau - 1| \ll 1$.

The result (4.11) clearly indicates a process whereby the effect of the plate is initially, though only slightly noticed at a point in the wake through the process of diffusion; its effect is then rapidly increased when $\tau \sim 1$ as convection comes to dominate the motion. As $\tau$ increases in value, the boundary-layer solution (3.11) will give an accurate representation for the velocity with an error of the order of $e^{-\frac{1}{4}\eta^2}$ as long as the assumptions $u - U$, $v \ll U$ are valid. This will certainly be true at the edge of the boundary layer, though at points well within this layer the full non-linearity of the differential equations will have to be faced.

We just note here that the matching can be continued for higher terms. When we write $H = (\zeta e^{-\frac{1}{4}\zeta^2})^{(2n)}\, \eta^{-(n+\frac{1}{2})} m_n(\sigma)$, and substitute into (4.4), the dominant terms for $\eta \gg 1$ lead to an ordinary differential equation for $m_n(\sigma)$ with solution

$$m_n = A_n \Phi(-\tfrac{1}{4} - \tfrac{1}{2}n;\ \tfrac{1}{2};\ -\tfrac{1}{4}\sigma^2) + B_n(-\tfrac{1}{4}\sigma^2)^{\frac{1}{2}}\, \Phi(\tfrac{1}{4} - \tfrac{1}{2}n;\ \tfrac{3}{2};\ -\tfrac{1}{4}\sigma^2)$$

for constants $A_n$ and $B_n$; this generalizes (4.8). The constants are calculated on satisfying the conditions $m_n \to 0$ when $\sigma \to -\infty$; $m_n$ is proportional to $\sigma^{n+\frac{1}{2}}$ when $\sigma \to +\infty$. The details are not completed here.

The main question to consider at this juncture in the work is the validity of the linearization procedure that resulted in (4.1). With this end in view, the complete Navier–Stokes equations are considered in terms of the independent variables $\zeta$, $\eta, \sigma$. The function $F(\zeta, \eta, \sigma)$ is defined from the stream function $\psi$ by

$$\psi = U(\nu t)^{\frac{1}{2}}\, (\zeta + F);$$

this isolates the part due to the uniform stream. The vorticity equation (2.4) is then

$$H_{\zeta\zeta} + \tfrac{1}{2}\zeta H_\zeta + \tfrac{1}{2}H + H_{\eta\eta} - \tfrac{1}{2}\eta H_\eta - \sigma H_\eta + 2\sigma\eta^{-1}H_{\sigma\eta} + (1 + 2\sigma\eta^{-1} + 2\sigma^2\eta^{-2})H_{\sigma\sigma} + \tfrac{1}{2}\sigma H_\sigma + 2(\eta^{-1} + \sigma\eta^{-2})H_\sigma = (\sigma + \eta)\{(F_\sigma H_\zeta - F_\zeta H_\sigma) + (F_\zeta H_\eta - F_\eta H_\zeta)\}, \quad (4.12)$$

where

$$H = F_{\zeta\zeta} + F_{\eta\eta} + 2\sigma\eta^{-1}F_{\sigma\eta} + 2(\eta^{-1} + \sigma\eta^{-2})F_\sigma + (1 + 2\sigma\eta^{-1} + 2\sigma^2\eta^{-2})F_{\sigma\sigma}. \quad (4.13)$$

From the linear analysis we have found that

$$H \sim \eta^{-\frac{1}{2}}\zeta e^{-\frac{1}{4}\zeta^2} m(\sigma) \quad \text{for} \quad \zeta \gg 1, \quad \eta \gg 1, \quad \sigma = O(1); \quad (4.14)$$

consequently,

$$F \sim 4\eta^{-\frac{1}{2}}\zeta^{-1}e^{-\frac{1}{4}\zeta^2} m(\sigma) \quad \text{for} \quad \zeta \gg 1, \quad \eta \gg 1, \quad \sigma = O(1). \quad (4.15)$$

When these asymptotic representations are substituted into (4.12), it is observed that the linear terms are of the order $\eta^{-\frac{1}{2}}\zeta^3 e^{-\frac{1}{4}\zeta^2}$, whereas the non-linear terms are of the order $\zeta e^{-\frac{1}{2}\zeta^2}$. Therefore the neglect of the non-linear terms on the right-hand side is justified when

$$\zeta^2 e^{\frac{1}{4}\zeta^2} \gg \eta^{\frac{1}{2}}. \quad (4.16)$$

The variable $\sigma = (\tau - 1)\eta$ is finite, so that $\eta \to \infty$ as $\tau \to 1$; (4.16) shows that $\zeta$ need tend to infinity no quicker than $(2\log\eta)^{\frac{1}{2}}$ as $\tau \to 1$. This indicates that there does exist a region downstream from the origin at the edge of the boundary layer where the linearized Navier–Stokes equations are sufficient to describe the real flow as $\tau \to 1$. At points further into the boundary layer the non-linear terms must be taken into account.

We now introduce new independent variables

$$\phi = \eta^{-1}\zeta^4 e^{\frac{1}{2}\zeta^2} \quad \text{and} \quad \chi = \eta^{-1}\zeta$$

to replace $\zeta$ and $\eta$. The variable $\phi$ is taken to be $O(1)$, which requires $\chi \ll 1$ when $\zeta$ is large; we maintain $\sigma = O(1)$ as before. The asymptotic condition (4.15) becomes $F \sim 4\chi\phi^{-\frac{1}{2}} m(\sigma)$ as $\phi \to \infty$; this enables us to write

$$F = \chi f(\phi, \sigma), \quad (4.17)$$

which is substituted into the equations (4.12), (4.13). It is expected that (4.17) represents the leading term for $\chi$ small in the expression for the stream function within the required region. When the dominant terms only are retained, the resultant partial differential equation for $f$ is

$$\phi^2 f_{\phi\phi\phi} + \tfrac{7}{2}\phi f_{\phi\phi} + \tfrac{3}{2} f_\phi + \phi f_\phi f_{\phi\sigma} - \phi f_\sigma f_{\phi\phi} - f_\sigma f_\phi = 0; \tag{4.18}$$

the ratio of terms neglected to those retained is $O(\zeta^{-2})$. The boundary conditions to be posed are $f \sim 4\phi^{-\frac{1}{2}} m(\sigma)$ as $\phi \to \infty$, $f \sim 4\pi^{-1}\phi^{-\frac{1}{2}}\sigma^{\frac{1}{2}}$ as $\sigma \to \infty$ and

$$f \sim 2^{\frac{3}{2}}\pi^{-1}\phi^{-\frac{1}{2}}(-\sigma)^{-\frac{3}{2}} e^{-\frac{1}{4}\sigma^2} \quad \text{as} \quad \sigma \to -\infty.$$

A solution that satisfies (4.18) and all these conditions is in fact

$$f = 4\phi^{-\frac{1}{2}} m(\sigma). \tag{4.19}$$

That is, the solution of the linear part of the differential equation also satisfies the non-linear part when equated to zero. This could, of course, have been noted immediately from observing that the dominant terms gained from substituting (4.15) into (4.12) do cancel. Nevertheless, the formal analysis pursued above is necessary for later observations.

The function (4.19) is a solution of (4.18), but because insufficient boundary conditions have been imposed we cannot be certain yet that it is the unique solution. No condition has been stated at $\phi = 0$ on the boundary of the domain $-\infty < \sigma < \infty$, $\sigma \geqslant 0$. Uniqueness can be investigated by taking (4.19) to be the first term in an asymptotic series for $\phi$ large of the exact solution of (4.18). We write $f = 4\phi^{-\frac{1}{2}} m(\sigma) + f_1(\phi, \sigma)$, where $|f_1| \ll \phi^{-\frac{1}{2}}$ for $\phi \gg 1$, and $f_1$ does not upset the conditions as $\sigma \to \pm\infty$. When the quadratic terms in $f_1$ are rejected, the resultant linear differential equation is seen to be

$$\begin{aligned}(\phi^2 f_{1\phi\phi\phi} + \tfrac{7}{2}\phi f_{1\phi\phi} + \tfrac{3}{2} f_{1\phi}) \\ - (4\phi^{\frac{1}{2}} m' f_{1\phi\phi} + 2\phi^{-\frac{1}{2}} m f_{1\phi\sigma} + 6\phi^{-\frac{1}{2}} m' f_{1\phi} + \phi^{-\frac{3}{2}} m f_{1\sigma}) = 0.\end{aligned} \tag{4.20}$$

The terms in the first bracket dominate for $\phi \gg 1$, and when the other terms are neglected the differential equation can be formally integrated for

$$f_1 = A(\sigma)\phi^{-\frac{1}{2}} + B(\sigma)\log\phi + C(\sigma),$$

where $A, B, C$ are arbitrary functions. To satisfy the condition $|f_1| \ll \phi^{-\frac{1}{2}}$ for $\phi \gg 1$ it is clear that the functions $A, B$ and $C$ are all identically zero.

The only other way in which a solution with continuous derivatives of all orders can arise from a linear equation such as (4.20) is through the presence of an essential singularity at some value $\phi = \phi_0 > 0$. Now essential singularities are only anticipated for values $\phi_0$ which give a zero coefficient for the highest order derivative with respect to $\phi$; it is immediately observed that there are no positive values $\phi_0$ with this property in the present case. These arguments show that (4.19) is, in fact, the unique solution for all $\phi, \sigma$ in the given domain. The range of validity of the solutions (4.14), (4.15) is thereby increased; nevertheless the formulation of (4.18) involved neglecting terms that were $O(\zeta^{-2})$, so it is still not possible to take $\zeta = O(1)$.

We now consider the higher order terms. The approximation (4.17) is known to incur an error that is $O(\zeta^{-2})$. Now $\zeta^3 e^{\frac{1}{4}\zeta^2} = \phi\chi^{-1}$ and so for small $\chi$ we can write $\zeta^{-2} = -(2\log\chi)^{-1}$; the first two terms in the expansion for $F$ are then given by

$$F = 4\chi\phi^{-\frac{1}{2}}m(\sigma) + \chi(\log\chi)^{-1}f^*(\phi,\sigma)$$

for some function $f^*$. The dominant terms gained when this is substituted into (4.12), (4.13) provide the linear differential equation

$$\phi^4 f^*_{\phi\phi\phi\phi} + \tfrac{13}{2}\phi^3 f^*_{\phi\phi\phi} + \tfrac{17}{2}\phi^2 f^*_{\phi\phi} + \tfrac{3}{2}\phi f^*_{\phi} - \phi^{-\frac{1}{2}}m'(4\phi^2 f^*_{\phi\phi\phi} + 12\phi f^*_{\phi\phi} + 3f^*_{\phi})$$
$$- \tfrac{1}{2}\phi^{-\frac{3}{2}}m(4\phi^2 f^*_{\phi\phi\sigma} + 4\phi f^*_{\phi\sigma} - f^*_{\sigma}) = 4\phi^{-1}(m'm'' - mm'''). \quad (4.21)$$

No general solution of (4.21) seems to be possible, though we can note that there exists the solution $f^* = A(\sigma)\phi^{-\frac{1}{2}}$, for all functions $A$, of the homogeneous differential equation. Particular solutions of the inhomogeneous equation for $\phi$ large and $\phi$ small are respectively

$$f^* = 8\phi^{-1}(m'm'' - mm''') \quad \text{and} \quad f^* = 2\phi^{\frac{1}{2}}\log\phi m^{-1}(mm'' - m'^2);$$

both are small in comparison with $\phi^{-\frac{1}{2}}$ in their separate domains. Consequently, the corrective effects for the dominant term (4.19) from the non-linear part of the differential equation do not enter the resultant expression for $F$ until higher orders than the second. The details are not considered any further here.

## 5. Discussion

In § 3 the boundary-layer equations are linearized to give an understanding of the flow at the edge of the boundary layer; we now briefly consider the role of the non-linear terms in these equations in the neighbourhood of $\tau = 1$. Because the analysis is very long, in some places following closely that already given in § 4, the conclusions are just summarized here.

When the stream function $\psi(x,y,t)$ is written as $\psi = U(\nu t)^{\frac{1}{2}}\{\zeta + F(\zeta,\tau)\}$, $F$ satisfies the differential equation

$$F_{\zeta\zeta\zeta} + \tfrac{1}{2}\zeta F_{\zeta\zeta} + \tau(\tau-1)F_{\zeta\tau} + \tau^2(F_\zeta F_{\zeta\tau} - F_\tau F_{\zeta\zeta}) = 0. \quad (5.1)$$

It is already known that $F \equiv 0$ for $0 < \tau < 1$, while linear theory states that

$$F \sim 4\pi^{-1}(\tau-1)^{\frac{1}{2}}\zeta^{-1}e^{-\frac{1}{4}\zeta^2} \quad \text{for} \quad 0 < \tau - 1 \ll 1, \quad \zeta \to \infty. \quad (5.2)$$

Now the linearization of (5.1) is invalid when $\xi \equiv (\tau-1)\zeta^4 e^{\frac{1}{2}\zeta^2}$ is positive and $O(1)$, which gives a non-uniform region as $\tau \to 1+$ when $\zeta \gg 1$; however, when (5.2) is substituted into (5.1), it is seen that the dominant terms cancel. This leads us to conjecture that (5.2) represents the leading term in the solution to the non-linear boundary-layer equations as $\xi \to 0+$. The conjecture is justified when it is proved (i) that (5.2) is the unique solution to (5.1) for $\xi = O(1)$ with the correct behaviour as $\xi \to \infty$, and (ii) that there is no further region of non-uniformity within which $\xi = O(1)$. (An infinite number of solutions to (5.1) with an essential singularity at $\tau = 1$ do exist, but all have a rapidly oscillating part that is physically unrealistic and must be rejected.) These conclusions imply that the

discontinuity in the velocity perpendicular to the axis of the plate is a natural consequence of the boundary-layer assumption.

To conclude, we can state the error involved in the calculations of the preceeding sections when the plate is real with a finite length $l$.

The point $P(x, y)$ is taken to be in the wake with $x > 0$; the origin represents the trailing edge and the point $(-l, 0)$ the leading edge. Any influence of the leading edge will be transported by convection to the point $P$ after the time $(l+x)/U$; at this time the solution will completely break down. However, there is the physical effect of diffusion parallel to the plate; this transmits the effect of the leading edge to $P$ instantaneously. From (4.10) we can see that, for times less than $(l+x)/U$, the error involved in ignoring the existence of the leading edge is exponentially small as

$$\exp\left\{-\frac{(l+x-Ut)^2}{4\nu t}\right\},$$

which it is reasonable to neglect.

The author wishes to thank the National Research Council of Canada for an operating grant during the time this work was completed.

## REFERENCES

CARSLAW, H. S. & JAEGER, J. C. 1948 *Operational Methods in Applied Mathematics.* Oxford University Press.

ERDELYI, A., MAGNUS, W., OBERHETTINGER, F. & TRICOMI, F. G. 1953 *Higher Transcendental Functions*, vol. I. Bateman Manuscript Project. New York: McGraw-Hill.

ERDELYI, A., MAGNUS, W., OBERHETTINGER, F. & TRICOMI, F. G. 1954 *Tables of Integral Transforms*, vol. I. Bateman Manuscript Project. New York: McGraw-Hill.

HALL, M. G. 1968 *XII Int. Cong. Appl. Mech., Stanford.*

RAYLEIGH, LORD, 1911 *Phil. Mag.* (6), **21**, 697–711.

ROSENHEAD, L. 1963 *Laminar Boundary Layers.* Oxford University Press.

SMITH, S. H. 1967 *Z. angew. Math. Phys.* **18**, 508–522.

STEWARTSON, K. 1951 *Quart. J. Mech. Appl. Math.* **4**, 182–198.

TOKUDA, N. 1968 *J. Fluid Mech.* **33**, 657–672. Corrigendum: **35**, 828.

*J. Fluid Mech.* (1970), *vol.* 42, *part* 3, *pp.* 639–656
*Printed in Great Britain*



# The solitary wave in water of variable depth

By R. GRIMSHAW
University of Melbourne

(Received 17 December 1969)

Equations are derived for two-dimensional long waves of small, but finite, amplitude in water of variable depth, analogous to those derived by Boussinesq for water of constant depth. When the depth is slowly varying compared to the length of the wave, an asymptotic solution of these equations is obtained which describes a slowly varying solitary wave; also differential equations for the slow variations of the parameters describing the solitary wave are derived, and solved in the case when the solitary wave evolves from a region of uniform depth. For small amplitudes it is found that the wave amplitude varies inversely as the depth.

## 1. Introduction

The behaviour of surface gravity waves on a beach has been a subject of considerable theoretical and experimental research. In the simplest situation the flow is two-dimensional and irrotational, and the fluid is inviscid, incompressible and of constant density. Then, for a train of infinitesimally small amplitude oscillatory waves of frequency $\omega$ and wave-number $\kappa$, the change in amplitude $\alpha$ due to a gradual slope may be determined by the assumption that the rate of energy propagation remains constant (Rayleigh 1911). Thus

$$c_g \alpha^2 = \text{constant}, \tag{1.1}$$

where $c_g$ is the group velocity,

$$c_g = \frac{d\omega}{d\kappa}, \quad \omega^2 = g\kappa \tanh \kappa h \tag{1.2}$$

is the dispersion relation, and $h$ is the undisturbed depth. Since $\omega$ remains constant, the elimination of $\kappa$ between (1.1) and (1.2) determines $\alpha$ as a function of $h$. For infinitely long waves, $\kappa h \to 0$, and this procedure leads to Green's law (Green 1837)

$$\alpha h^{\frac{1}{4}} = \text{constant}. \tag{1.3}$$

These results may also be derived by constructing an asymptotic expansion based on the assumption that if reflexion processes are ignored and the variation of $h$ with the horizontal co-ordinate $x$ is very small over a typical wavelength then the wave form is locally sinusoidal (Keller 1958). In addition conservation of mass requires the set up of a mean reverse flow and conservation of momentum requires a decrease in the mean depth as $h$ decreases, both $O(\alpha^2)$ (Longuet-Higgins & Stewart 1964).

For infinitely long waves of finite amplitude, the governing equations are

analogous to those of gas dynamics, and it is well known that no permanent progressing wave form is possible. However, it may be shown that a discontinuity in wave slope for a wave of elevation will cause the wave to break (i.e. the wave slope becomes infinite) before the shoreline is reached (Greenspan 1958). On the other hand if a bore reaches the shoreline in finite time, it does so with a finite speed and zero amplitude (Keller, Levine & Whitham 1960).

In this paper we shall consider the modulations formed on the Boussinesq solitary wave by a slow variation in the depth. This solitary wave is a permanent progressing wave form consisting of a simple elevation above the undisturbed surface whose amplitude $\alpha$ and length $\lambda$ (usually defined as the width when the free surface is one-tenth of its maximum height) are such that $\alpha/h$ and $h^2/\lambda^2$ are comparable small quantities. It was first observed by Russell (1837), and established theoretically, to the lowest order in $\alpha/h$, by Boussinesq (1871, 1872). Ippen & Kulin (1955) have performed experiments in which a solitary wave is incident on a beach of constant slope. They found that the amplitude increased with decreasing depth approximately according to the law $h^{-k}$ where $k$ depends on the beach slope and decreased as the slope was increased (e.g. $k = 0{\cdot}47$ for a beach slope of 0·023). In addition the wave crest became more pronounced, and there was increasing asymmetry due to steepening on the front face, as the wave climbed the beach; eventually wave breaking was observed, either due to 'peaking' at the wave crest and subsequent spilling, or due to an infinite slope on the front face and subsequent plunging.

To discuss the behaviour of a solitary wave on a beach, we first derive, in §2, equations analogous to those used by Boussinesq for the case of constant undisturbed depth. In §3 we derive various properties of the solitary wave. In §4 we consider the case when the still water depth $h$ is a slowly varying function of the horizontal co-ordinate $x$ and so varies little over a distance comparable with $\lambda$, the length of the wave. An asymptotic expansion is introduced, analogous to those used by Whitham (1965*a*, *b*) to discuss modulations on cnoidal waves on a constant depth, and in other situations also (we note that the solitary wave may be regarded as a limiting case of a cnoidal wave as the wave period becomes infinite). Then transport equations for the amplitude and for the other parameters determining the solitary wave are derived, either by imposing conditions which ensure that the asymptotic expansion is uniformly valid in $x$, or by using conservation laws. In §5 these transport equations are solved; the principal conclusion is that when the wave develops from a region where $h$ is constant then the variation of the amplitude $e_m$ is determined by conservation of the energy in the wave and this causes $e_m$, for small $e_m/h$, to vary as $h^{-1}$. Finally, in §6 the relationship of the asymptotic expansion to a certain exact solution of the governing equations is considered.

## 2. Equations of motion

It will be assumed that the flow is two-dimensional and irrotational, and that the fluid is inviscid, incompressible and of constant density. We shall be concerned with long waves so that if $\lambda$ is a horizontal length scale for the waves, and

$h_0$ is a length scale for the undisturbed depth, then the parameter $\epsilon = h_0^2/\lambda^2$ is small compared to one. Since it can be anticipated that for long waves the Froude number will be close to critical we choose $(gh_0)^{\frac{1}{2}}$ as a typical velocity scale. Then introducing dimensionless co-ordinates based on $\lambda$, $h_0$, $(gh_0)^{\frac{1}{2}}$ we find that the equations of motion for the velocity potential $\phi(x, y, t)$ are

$$\epsilon\phi_{xx} + \phi_{yy} = 0 \quad \text{for} \quad -h < y < \eta, \tag{2.1}$$

$$\epsilon h_x\phi_x + \phi_y = 0 \quad \text{for} \quad y = -h, \tag{2.2}$$

$$\epsilon(\eta_t + \eta_x\phi_x) - \phi_y = 0 \quad \text{for} \quad y = \eta, \tag{2.3}$$

$$\epsilon(\eta + \phi_t + \tfrac{1}{2}\phi_x^2) + \tfrac{1}{2}\phi_y^2 = 0 \quad \text{for} \quad y = \eta, \tag{2.4}$$

where $y = \eta(x, t)$ is the free surface, and $y = -h(x)$ is the undisturbed depth, (q.v. figure 1). Equations (2.2), (2.3) are kinematic boundary conditions and (2.4) is the condition that the pressure be constant on the free surface.

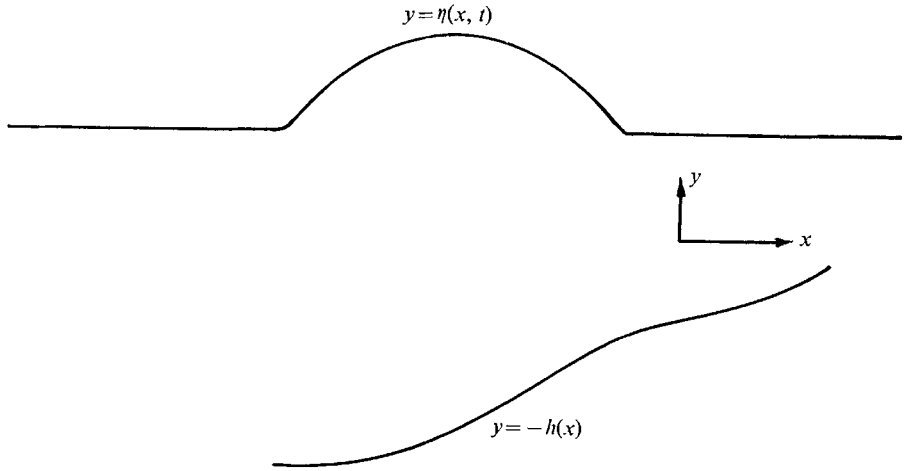


FIGURE 1. Co-ordinate system.

For small $\epsilon$ we seek a solution of (2.1) and (2.2) in the form $\phi = \alpha(\phi_0 + \epsilon\phi_1 + \ldots)$, where $\alpha$ is a measure of the wave amplitude. We find that, to $O(\epsilon)$, $\phi$ may be expressed in terms of a new unknown function $F(x, t)$ as follows

$$\phi = \alpha(F + \epsilon(-y(hF_x)_x - \tfrac{1}{2}y^2F_{xx}) + O(\epsilon^2)). \tag{2.5}$$

Substitution into (2.3) and (2.4) then gives a pair of coupled equations for $\eta$ and $F$, both functions of $x$ and $t$ only. However, these will be further simplified as it is well known that the Boussinesq solitary wave may be characterized by requiring $\alpha$ and $\epsilon$ to be comparable small quantities (Ursell 1953). Thus we put

$$\eta = \alpha(E + O(\epsilon^2)), \tag{2.6}$$

where $E(x, t)$ is another unknown function, substitute into (2.3) and (2.4) and retain all terms up to $O(\epsilon^3)$ or $O(\alpha\epsilon^2)$, etc. This procedure leads to the Boussinesq equations

$$E + F_t + \tfrac{1}{2}\alpha F_x^2 = 0, \tag{2.7}$$

$$E_t + (hF_x)_x + \alpha(EF_x)_x + \epsilon(\tfrac{1}{3}h^3F_{xx})_{xx} + \epsilon(\tfrac{1}{2}h^2h_{xx}F_x)_x = 0. \tag{2.8}$$

These equations are analogous to those used by Boussinesq (1872) when $h$ is constant, and equivalent versions have been given by Mei & Le Méhauté (1966), and Peregrine (1967). When the terms of $O(\epsilon)$ are omitted they reduce to the non-linear shallow water equations, and when the terms of $O(\alpha)$ are also omitted they reduce to the linearized shallow water equations. Thus they contain the first-order effects of non-linearity, represented by $\alpha$, and of frequency dispersion represented by $\epsilon$.

It will be useful in the sequel to identify (2.7) and (2.8) as the Euler equations of a certain Lagrangian. Indeed, Whitham (1967) has shown that the Boussinesq equations for constant $h$ may be derived by suitably approximating a certain Lagrangian for the system (2.1) to (2.4), and we shall follow a similar procedure here. Luke (1966*b*) has shown that the system (2.1) and (2.4) can be derived from the variational principle

$$\delta \iint \left\{ \int_{-h}^{\eta} (\phi_t + y + \tfrac{1}{2}\phi_x^2 + \epsilon^{-1} \tfrac{1}{2}\phi_y^2)\, dy \right\} dx\, dt = 0, \tag{2.9}$$

where the infinitesimal variations $\delta\phi$, $\delta\eta$ are sufficiently differentiable and vanish as $x, t$ approach the boundary of the region of integration. If the expansions (2.5) and (2.6) are now substituted into (2.9) the integrand, to $O(\epsilon^3)$ with the omission of certain divergence terms which do not contribute to the Euler equations, is $\alpha^2 L$ where

$$L(E, F_x, F_{xx}, F_t; x) = EF_t + \tfrac{1}{2}E^2 + \tfrac{1}{2}(h + \alpha E)\, F_x^2 - \epsilon \tfrac{1}{6} h^3 F_{xx}^2 + \epsilon \tfrac{1}{4} h^2 h_{xx} F_x^2, \tag{2.10}$$

and $L$ may now be identified as an appropriate Lagrangian for (2.7) and (2.8). Indeed the variation of $L$ with respect to $E$ gives (2.7), and the variation with respect to $F$ gives

$$\frac{\partial}{\partial t}\left(\frac{\partial L}{\partial F_t}\right) + \frac{\partial}{\partial x}\left(\frac{\partial L}{\partial F_x}\right) - \frac{\partial^2}{\partial x^2}\left(\frac{\partial L}{\partial F_{xx}}\right) = 0, \tag{2.11}$$

which is just (2.8). The form of (2.11) will be useful in the sequel as it is in conservation form, and corresponds to the explicit absence of $F$ in $L$. It represents for small $\epsilon$, conservation of mass. Another conservation law may be found from the explicit absence of $t$ in $L$, and is

$$\frac{\partial}{\partial t}\left(F_t \frac{\partial L}{\partial F_t} - L\right) + \frac{\partial}{\partial x}\left(F_t \frac{\partial L}{\partial F_x} + 2F_{tx} \frac{\partial L}{\partial F_{xx}}\right) - \frac{\partial^2}{\partial x^2}\left(F_t \frac{\partial L}{\partial F_{xx}}\right) = 0. \tag{2.12}$$

This equation represents conservation of energy, and $-\{F_t(\partial L/\partial F_t) - L\}$ may be regarded as an energy density, although it differs from the exact energy density, even for small $\epsilon$, by the previous omission of divergence terms from $L$. Nevertheless, it may be shown that certain average energy densities can be computed from $F_t(\partial L/\partial F_t) - L$. An equation, which corresponds to (2.11) and (2.12), but represents momentum, is

$$\frac{\partial}{\partial t}\left(F_x \frac{\partial L}{\partial F_t}\right) + \frac{\partial}{\partial x}\left(F_x \frac{\partial L}{\partial F_x} - L + 2F_{xx} \frac{\partial L}{\partial F_{xx}}\right) - \frac{\partial^2}{\partial x^2}\left(F_x \frac{\partial L}{\partial F_{xx}}\right) + \frac{\partial L}{\partial x} = 0, \tag{2.13}$$

where the last term is the explicit derivative of $L$ with respect to $x$ through the dependence of $L$ on $h$. This is not a true conservation law as it contains the

inhomogeneous term $\partial L/\partial x$ which represents the horizontal pressure thrust due to the bottom slope. A further conservation law is

$$\frac{\partial}{\partial t}(F_x)+\frac{\partial}{\partial x}(-F_t)=0. \tag{2.14}$$

Now that the ordering parameters $\alpha, \epsilon$ have served their purpose, we shall, in the following sections, revert to dimensionless co-ordinates based on a length scale $h_0$ and a velocity scale $(gh_0)^{\frac{1}{2}}$. Thus we shall use (2.7), (2.8) and the subsequent equations, but with $\alpha=\epsilon=1$, so that e.g. $y=E$ is the equation of the free surface to the approximation considered. We shall also, without any ambiguity, call $F$ the velocity potential and

$$U=F_x \tag{2.15}$$

the velocity.

## 3. The solitary wave

In this section it will be assumed that $h$ is constant. We shall seek a solution of the Boussinesq equations (2.7) and (2.8) for which $E$ and $U$ are functions only of the phase

$$\theta=\kappa(x-ct), \tag{3.1}$$

where $\kappa$ (wave-number) and $c$ (wave speed) are constants. Thus we seek a solution of the form

$$E=B+e(\theta), \tag{3.2}$$

$$U=A+u(\theta), \tag{3.3}$$

where $A$, $B$ are constants, representing the mean velocity and mean height respectively and defined so that $e$, $u$ and all their derivatives vanish as $|\theta|\to\infty$ (we are anticipating from the form of (2.7) and (2.8) that any such solution will be even in $\theta$). The corresponding form for the potential, $F$, which must satisfy $U=F_x$ and be consistent with (2.7) is

$$F=Ax-Ct+f(\theta), \tag{3.4}$$

where

$$f(\theta)=\int_0^\theta \kappa^{-1}u(\theta')\,d\theta'$$

and $C$ is a constant, related to the Bernoulli constant.

Substitution of (3.2) and (3.4) into (2.7), and application of the limiting behaviour as $|\theta|\to\infty$ implies that

$$e=c^*u-\tfrac{1}{2}u^2, \tag{3.5}$$

$$C=B+\tfrac{1}{2}A^2, \tag{3.6}$$

where $c^*$ is defined below (3.7). Then substitution of (3.2) and (3.3) into (2.8), elimination of $e$ by (3.5), and two integrations with respect to $\theta$, imply that

$$\tfrac{1}{3}h^3\kappa^2u_\theta^2=w(u)\equiv(c^{*2}-h^*)\,u^2-c^*u^3+\tfrac{1}{4}u^4, \tag{3.7}$$

where

$$c^*=c-A, \quad h^*=h+B.$$

This has the solution
$$u = \frac{u_m \operatorname{sech}^2 p\theta}{1 - d\tanh^2 p\theta}, \tag{3.8}$$

where
$$u_m = 2(c^* - \sqrt{h^*}), \tag{3.9}$$

$$d = \frac{c^* - \sqrt{h^*}}{c^* + \sqrt{h^*}}, \tag{3.10}$$

$$\kappa p = \sqrt{\tfrac{3}{4}}(c^{*2} - h^*)^{\frac{1}{2}} h^{-\frac{3}{2}}, \tag{3.11}$$

and we have selected the origin of $\theta$ to be the wave crest, where both $e$ and $u$ achieve their maximum values $e_m$ and $u_m$ respectively. Indeed we find that

$$e_m = \sqrt{(h^*)}\, u_m. \tag{3.12}$$

Thus the solitary wave profile, the wave amplitude $e_m$ and the 'wavelength' $(\kappa p)^{-1}$ are determined completely by the constants $A$, $B$ and $c$; the constant $\kappa$ plays the subsidiary role of relating the $x$ scale to the $\theta$ scale. For small values of $e_m$ ($h$ and $h^*$ being $O(1)$), $d$ is $O(e_m)$ and may be neglected, and then (3.8) reduces to the solitary wave profile found by Boussinesq (1871); also the wave speed formula (3.9) is then equivalent to the more commonly quoted formula

$$c^{*2} = h^* + e_m.$$

Although our derivation of the Boussinesq equations was such that, for consistency, all formulae such as (3.8) should be reduced to their lowest order in $e_m$, we shall continue to work with the 'exact' formulae above ('exact' in the sense that they are exact solutions of the Boussinesq equations (2.7) and (2.8)); indeed it causes no extra algebraic inconvenience to ignore the smallness of $e_m$, and the retention of the higher order terms in $e_m$ may give some indication of the effects of increasing non-linearity. It may be shown that the profile given by (3.8) is a close approximation to the Boussinesq profile (e.g. the maximum difference is approximately 2% for $e_m h^{-1} = 0{\cdot}1$, and approximately $7\frac{1}{2}$% for $e_m h^{-1} = 0{\cdot}4$) and the latter was shown by Daily & Stephan (1952) to be in good agreement with experimentally observed profiles for values of $e_m h^{-1}$ as large as 0·6 (for the larger values of $e_m h^{-1}$ the experimentally observed profile is thinner near the crest than the Boussinesq profile); similarly the observations of Daily & Stephan show that the wave speed given by (3.9) is approximately 6% too high for $e_m h^{-1} = 0{\cdot}6$, with a decreasing error for decreasing $e_m h^{-1}$.

We shall conclude this section with the calculation of various quantities of interest associated with the solitary wave. First, we give the following definitions. If $P(\theta)$ is the relevant quantity, then its mean is

$$\bar{P} = \lim_{|\theta| \to \infty} \bar{P}(\theta); \tag{3.13}$$

the reduced (or wave) quantity is

$$p(\theta) = P(\theta) - \bar{P}; \tag{3.14}$$

and its wave average (or mean) is

$$\hat{p} = \int_{-\infty}^{\infty} p(\theta)\, d\theta, \tag{3.15}$$

so that $\kappa^{-1}\hat{p}$ is the wave average with respect to the $x$ scale. Clearly $\bar{P}$ is a function of $A$, $B$ and $\kappa^{-1}\hat{p}$ is a function of $A$, $B$ and $c$. Thus we find that

$$\hat{e} = \sqrt{\tfrac{16}{3}}\kappa h^{\frac{3}{2}}(c^{*2}-h^*)^{\frac{1}{2}}, \tag{3.16}$$

$$\hat{u} = \sqrt{\tfrac{16}{3}}\kappa h^{\frac{3}{2}}\cosh^{-1}(c^*/\sqrt{h^*}); \tag{3.17}$$

also the mean Lagrangian, and the wave average Lagrangian are

$$\bar{L} = -BC + \tfrac{1}{2}B^2 + \tfrac{1}{2}(h+B)A^2, \tag{3.18}$$

$$\hat{l} = \hat{u}(h^*A - cB) - \hat{w}, \tag{3.19}$$

where $\hat{w}$ is the wave average of the polynomial $w(u)$ defined in (3.7), and is given by

$$\hat{w} = \kappa W, \tag{3.20}$$

where

$$W = W(A,B;c,h) = \sqrt{\tfrac{4}{3}}h^{\frac{3}{2}}\int_0^{u_m}\sqrt{(w(u))}\,du. \tag{3.21}$$

It may be noted that $\hat{e}$ is the wave average of the mass density (apart from the constant proportionality factor $\rho h_0$, where $\rho$ is the density of the fluid), so that $\kappa^{-1}\hat{e}$ is the mass carried forward by the wave. Also the wave average of the momentum density (apart from the factor $\rho h_0\sqrt{(gh_0)}$) is

$$h^*\hat{u} + A\hat{e} + \partial\hat{w}/\partial c. \tag{3.22}$$

Finally, the wave average of the energy density (apart from the factor $\rho g h_0^2$) is

$$C\hat{e} + Ah^*\hat{u} + \left(c\frac{\partial\hat{w}}{\partial c} - \hat{w}\right), \tag{3.23}$$

and further

$$c(\partial\hat{w}/\partial c) - \hat{w} = (\tfrac{4}{3})^{\frac{3}{2}}\kappa h^{\frac{3}{2}}(c^{*2}-h^*)^{\frac{3}{2}} + A(\partial\hat{w}/\partial c). \tag{3.24}$$

## 4. Modulations caused by slowly varying depth

It will now be supposed that $h$ is a function of $x$ but is *slowly varying* in the sense that $h$ varies little over a distance comparable with the length of the wave. Thus we shall assume that $h = h(X)$ where

$$X = \beta x, \quad T = \beta t, \tag{4.1}$$

and $\beta$ is a small parameter such that $\beta \ll \kappa p$. In this section we shall find equations which govern the modulations to the solitary wave of §3 caused by this slow variation of the depth. This will be achieved by finding an asymptotic solution of the Boussinesq equations which represents a slowly varying solitary wave i.e. locally this asymptotic solution may be represented by the uniform solution of §3, but the parameters $A$, $B$, $C$, $c$ and $\kappa$ which determine that solution are now slowly varying and so functions of $X, T$. Our principal aim is the determination of transport equations for these parameters. Whitham (1965*a*, *b*) has considered problems of this type for periodic slowly varying wave trains governed by non-linear, dispersive equations. The procedures described in this section are closely related to the procedures developed by Whitham and other workers in this field.

Thus we are motivated to seek an asymptotic solution of the Boussinesq equations (2.7) and (2.8) of the form

$$\left.\begin{aligned} E &= B(X,T)+e(\theta;X,T)+\beta E_1(\theta;X,T)+O(\beta^2),\\ U &= A(X,T)+u(\theta;X,T)+\beta U_1(\theta;X,T)+O(\beta^2).\end{aligned}\right\} \tag{4.2}$$

$A$, $B$ are determined so that $e$, $u$ and all their derivatives with respect to $\theta$ vanish as $|\theta| \to \infty$, and the phase $\theta$ is such that

$$\theta_x = \kappa, \quad \theta_t = -\kappa c, \tag{4.3}$$

and so
$$\theta = \beta^{-1}\Theta(X,T), \quad \text{where} \quad \kappa = \Theta_X, \; -\kappa c = \Theta_T. \tag{4.4}$$

$\theta$ is a *fast* variable, which has yet to be determined, and $X$, $T$ are *slow* variables; (4.2) is a two-scale asymptotic expansion of a type familiar in the context of ordinary differential equations. Since derivatives with respect to $\theta$ are $O(1)$, while derivatives with respect to $X$ and $T$ are $O(\beta)$, it is clear that when (4.2) is substituted into (2.7) and (2.8), the terms of $O(1)$ are just those which describe the solitary wave of § 3 and so $e$, $u$ are determined as functions of $\theta$ by (3.5) to (3.11), except that the parameters $A$, $B$, $C$, $c$ and $\kappa$ are now functions of $X$, $T$. The transport equations which determine these parameters are found by applying the principle that the asymptotic expansion (4.2) is to be uniformly valid i.e. $\beta E_1$ and $\beta U_1$ are $O(\beta)$ with respect to $B+e$ and $A+u$ respectively for all $\theta$. Thus we shall assume that $E_1$ and $U_1$ can be constructed so that

$$A_1^{\pm} = \lim_{\theta \to \pm\infty} U_1, \quad B_1^{\pm} = \lim_{\theta \to \pm\infty} E_1 \tag{4.5}$$

exist, and all derivatives of $U_1$ and $E_1$ with respect to $\theta$ vanish as $|\theta| \to \infty$. It will be shown in subsection ($a$) below that such a construction is indeed possible. From (4.5) we define

$$A_1 = \tfrac{1}{2}(A_1^+ + A_1^-), \quad [U_1] = (A_1^+ - A_1^-), \quad u_1 = U_1 - A_1, \tag{4.6}$$

with similar definitions for $B_1$, $[E_1]$ and $e_1$.

Next we seek an asymptotic expansion for the potential $F$ such that $U = F_x$ where $U$ is given by (4.2). Thus

$$F = \beta^{-1}\psi(X,T)+f(\theta;X,T)+\psi_1(X,T)+\beta f_1(\theta;X,T)+\ldots, \tag{4.7}$$

where the remaining terms are $O(\beta^2)$ if they involve $\theta$ and $O(\beta)$ otherwise, and

$$\psi_X = A, \quad \psi_T = -C, \tag{4.8}$$

$$f = \int_0^\theta \kappa^{-1} u(\theta';X,T)\,d\theta', \tag{4.9}$$

$$\psi_{1X} = A_1, \quad \psi_{1T} = -C_1, \tag{4.10}$$

$$\kappa f_{1\theta} = u_1 - f_X. \tag{4.11}$$

It follows that

$$F_t = -C - cu + \beta(-C_1 - cu_1 + f_T + cf_X) + O(\beta^2). \tag{4.12}$$

Then substitution of (4.2) and (4.12) into (2.7) gives, for the terms of $O(1)$, (3.5) and (3.6), while the term of $O(\beta)$ is

$$B_1 + e_1 - C_1 - cu_1 + f_T + cf_X + (A+u)(A_1+u_1) = 0. \tag{4.13}$$

Letting $\theta \to \pm\infty$ we find that

$$C_1 = B_1 + AA_1, \tag{4.14}$$

$$[E_1] = c^*[U_1] - (\kappa^{-1}\hat{u})_T - c(\kappa^{-1}\hat{u})_X. \tag{4.15}$$

Next, substitution of (4.2) and (4.12) into the consistency relation (2.14) yields, for the term of $O(\beta)$,

$$A_T + C_X + \{\kappa_T + (\kappa c)_X\}u = 0; \tag{4.16}$$

and letting $|\theta| \to \infty$ we have

$$A_T + C_X = 0, \tag{4.17}$$

whence

$$\kappa_T + (\kappa c)_X = 0. \tag{4.18}$$

These two equations are just the consistency relation for $\psi$ and $\theta$ respectively and provide two transport equations. A third is (3.6); two more are needed and may now be determined in each of three ways.

### (*a*) *Direct method*

In this subsection the transport equations will be found by first finding $U_1$ (and hence $E_1$) explicitly. The methods used here are similar to those used for slowly varying periodic wave trains by Luke (1966*a*) for a Klein–Gordan equation, and Hoogstraten (1968) for the Korteweg–de Vries equation, and for the Boussinesq equations of constant depth, and are analogous to the Poincaré technique for ordinary differential equations (e.g. in particular to the work of Kuzmak 1959).

If (4.2) is substituted into (2.8), then the term of $O(1)$ defines the solitary wave of § 3, while the term of $O(\beta)$ gives

$$\kappa\{-cE_1 + (h^* + e)U_1 + (h + E_1)(A + u) + \tfrac{1}{3}\kappa^2 h^3 U_{1\theta\theta} + h^3\kappa_X u_\theta + h^3\kappa u_{\theta X} + 2h^2 h_X \kappa u_\theta\}_\theta + \{B + e\}_T + \{(h^* + e)(A + u)\}_X = 0. \tag{4.19}$$

Letting $|\theta| \to \infty$ we see that

$$B_T + (h^* A)_X = 0, \tag{4.20}$$

which is the fourth transport equation. Then (4.19) is integrated with respect to $\theta$, and after elimination of $e$ and $e_1$ by (3.5) and (4.13) respectively, we find that

$$\tfrac{1}{3}h^3\kappa^2 u_{1\theta\theta} - (c^{*2} - h^*)u_1 + 3c^* u u_1 - \tfrac{3}{2}u^2 u_1 = G, \tag{4.21}$$

where

$$G = D_1 - \kappa^{-1}\int_0^\theta \{e_T + (h^* u)_X + (Ae)_X + (eu)_X\}d\theta' - h^3\kappa_X u_\theta - h^3\kappa u_{\theta X} - 2h^2 h_X \kappa u_\theta - (c^* - u)(f_T + cf_X) - uB_1 - 2uc^* A_1 + \tfrac{3}{2}u^2 A_1, \tag{4.22}$$

where $D_1(X, T)$ is a 'constant' of integration. It may now be observed, by differentiating (3.7) twice with respect to $\theta$, that the homogenous part of (4.21) (i.e. when $G$ is replaced by zero) has the solution $u_1 = u_\theta$. Thus (4.21) may be integrated again with respect to $\theta$ after first multiplying by $u_\theta$, and we find that

$$\tfrac{1}{3}h^3\kappa^2(u_{1\theta}u_\theta - u_1 u_{\theta\theta}) = \int_{-\infty}^{\theta} u_\theta G d\theta' + D_2, \tag{4.23}$$

where $D_2(X,T)$ is another 'constant' of integration. Letting $\theta \to \pm\infty$ we see that the left-hand side then vanishes, and so therefore must the right-hand side. Thus $D_2 = 0$ and

$$\int_{-\infty}^{\infty} u_\theta G\, d\theta = 0. \tag{4.24}$$

Since $u$ is an even function of $\theta$, (4.24) involves only $A$, $B$, $c$ and $\kappa$ and is the fifth transport equation. The complete set of transport equations is thus (3.6), (4.17), (4.18), (4.20) and (4.24). One further integration of (4.23) yields

$$\tfrac{1}{3}h^3\kappa^2 u_1 = \left(D_3 + \int_0^\theta H(u_\theta)^{-2}\, d\theta'\right) u_\theta, \tag{4.25}$$

where

$$H = \int_{-\infty}^{\theta} u_\theta G\, d\theta',$$

and $D_3(X,T)$ is another 'constant' of integration. It may now be shown that $Hu^{-1}$ remains finite as $\theta \to \pm\infty$ (in spite of the fact that e.g. $u_X$ contains terms of the type $\theta u_\theta$), and so $u_1$ remains bounded as $\theta \to \pm\infty$, and all its derivatives vanish as $\theta \to \pm\infty$. Of course, $u_1$ is determined by (4.25) as a function of $\theta$ only, and still depends on the 'unknown' constants $A$, $B_1$, $D_1$ and $D_3$; these may presumably be determined in a similar way to the above by continuing the asymptotic expansion (4.2) to a higher order in $\beta$.

### (*b*) *Averaged conservation laws*

In this subsection the transport equations will be derived by applying suitable averaging procedures to the conservation laws (2.11), (2.12), (2.13) and (2.14). These procedures are analogous to those used by Whitham (1965*a*) for slowly varying periodic wave trains, and are related to the Krylov–Boguliobov technique familiar in the context of ordinary differential equations.

The typical conservation law has the form

$$\partial P/\partial t + \partial Q/\partial x + \beta R = 0, \tag{4.26}$$

where $R$ is proportional to $h_X$ and its presence is due to the inhomogeneity of the medium. Since $E$, $U$ have asymptotic expansions of the form (4.2), it follows that $P$, $Q$, $R$ have similar expansions e.g.

$$P = P_0(\theta; X, T) + \beta P_1(\theta; X, T) + O(\beta^2). \tag{4.27}$$

Then our hypotheses on $E$, $U$ are such that

$$P_i^{\pm} = \lim_{\theta \to \pm\infty} P_i \quad (i = 0, 1) \tag{4.28}$$

certainly exist, and we define

$$\overline{P}_i = \tfrac{1}{2}(P_i^+ + P_i^-), \quad [P_i] = (P_i^+ - P_i^-) \quad (i = 0, 1). \tag{4.29}$$

Since $P_0$, etc., are even in $\theta$, $[P_0]$, etc., vanish but as we shall see, $[P_1]$, etc., in general are not zero. Also we observe that

$$\overline{P}_i = \lim_{\gamma \to \infty} \frac{1}{2\gamma} \int_{-\gamma}^{\gamma} P_i\, d\theta. \tag{4.30}$$

Next we define the reduced (or wave) quantity by

$$p = P_0 - \bar{P}_0 \tag{4.31}$$

and its wave average (or mean) by

$$\hat{p} = \lim_{\gamma\to\infty} \int_{-\gamma}^{\gamma} p\, d\theta. \tag{4.32}$$

We now substitute the expansions such as (4.27) into (4.26) and equate to zero the term of $O(1)$, and the term with coefficient $\beta$; the former gives a relation satisfied identically by the solitary wave of § 3, and the latter gives

$$\bar{P}_{0T} + \bar{Q}_{0X} + \bar{R}_0 + p_T + q_X + r - \kappa c P_{1\theta} + \kappa Q_{1\theta} = 0. \tag{4.33}$$

First we take the mean of (4.33), i.e. the averaging procedure defined by (4.30). This yields the equation

$$\bar{P}_{0T} + \bar{Q}_{0X} + \bar{R}_0 = 0. \tag{4.34}$$

Next we substract (4.34) from (4.33), and take the wave average, i.e. the averaging procedure defined by (4.32). This yields the equation

$$(\hat{p})_T + (\hat{q})_X + \hat{r} - \kappa c[P_1] + \kappa[Q_1] = 0. \tag{4.35}$$

Equations (4.34) and (4.35) are transport equations for $A$, $B$, $C$, $c$ and $\kappa$, and also for $[E_1]$ and $[U_1]$.

It is convenient when applying the averaged conservation laws (4.34) and (4.35) to do so in conjunction with the formulae (3.5), (3.6) and (4.15), all of which are derived from (2.7) (which is not in conservation form). If (4.34) is applied to (2.14) and (2.11), then we obtain (4.17) and (4.20) respectively; further applications to (2.12) and (2.13) yield two transport equations for $A$, $B$, $C$ which are equivalent to (4.17) and (4.20). Application of (4.35) to (2.14) yields the transport equation (4.18); application of (4.35) to (2.11) yields

$$(\hat{e})_T + \left(h^*\hat{u} + A\hat{e} + \frac{\partial \hat{w}}{\partial c}\right)_X + \kappa(-c^*[E_1] + h^*[U_1]) = 0, \tag{4.36}$$

where $\hat{w}$ is defined by (3.20), (3.21). $[E_1]$ and $[U_1]$ may now be found in terms of $A$, $B$, $C$, $c$ and $\kappa$ by solving (4.15) and (4.36) simultaneously. Next application of (4.35) to (2.12) and subsequent elimination of $[E_1]$ and $[U_1]$ yields

$$\left(c\frac{\partial \hat{w}}{\partial c} - \hat{w}\right)_T + \left(c\left(c\frac{\partial \hat{w}}{\partial c} + \hat{w}\right)\right)_X - \frac{\partial \hat{w}}{\partial T} = 0; \tag{4.37}$$

similarly application of (4.35) to (2.13) and subsequent elimination of $[E_1]$ and $[U_1]$ yields

$$\left(\frac{\partial \hat{w}}{\partial c}\right)_T + \left(c\frac{\partial \hat{w}}{\partial c}\right)_X - \frac{\partial \hat{w}}{\partial X} = 0, \tag{4.38}$$

which is easily seen to be equivalent to (4.37). In both of these equations $\hat{w} = \kappa W(c; X, T)$ so that e.g. $\partial\hat{w}/\partial T$ means differentiation with respect to $T$ while $c$ and $\kappa$ are kept constant; $\hat{w}$ depends on $X$, $T$ through its dependence on $A$, $B$ and $h$. Finally, it may be shown that (4.24) can be reduced to either of (4.37) or (4.38).

### (c) *Averaged variational principle*

Whitham (1965*a*, 1967) (see also Bretherton 1968) has developed an heuristic procedure for finding the transport equations for slowly varying periodic wave trains, when the governing equations are the variational equations of a Lagrangian density. Briefly this procedure consists of calculating the average value over one period of this Lagrangian density for the uniform wave train, which itself depends on a set of parameters such as frequency, wave-number, etc.; this averaged Lagrangian is then subjected to the variation of these parameters.

The Boussinesq equations (2.7) and (2.8) for constant $h$ possess a solution of the form (3.2), (3.3) and (3.4) which has a period $\gamma$, where now $u$ has zero mean so that

$$A = \frac{1}{2\gamma}\int_{-\gamma}^{\gamma} U\,d\theta, \tag{4.39}$$

with a similar equation for $B$, and

$$\tfrac{1}{3}h^3\kappa^2 u_\theta^2 = K_1 + K_2 u + (B + \tfrac{1}{2}A^2 - C)\,u^2 + w(u) \equiv v(u); \tag{4.40}$$

$w(u)$ is defined by (3.7), and $K_1$, $K_2$ are constants of integration. If the polynomial $v(u)$ has the four real zeros $d^{-1}u_m > u_m > u_1 > u_2$, we select that solution of (4.40) for which $u$ lies between $u_1$ and $u_m$. Then if $K_1$, $K_2 \to 0$ simultaneously, so that the period $\gamma \to \infty$, the solution of (4.40) becomes the solitary wave (3.8). The averaged Lagrangian is defined to be

$$\mathscr{L} = \frac{1}{2\gamma}\int_{-\gamma}^{\gamma} L\,d\theta \tag{4.41}$$

and is given by

$$\mathscr{L} = \bar{L}(A, C; B) + \tfrac{1}{2}K_1 - \gamma^{-1}\sqrt{\tfrac{4}{3}}\kappa h^{\frac{3}{2}}\int_{u_1}^{u_m}\sqrt{(v(u))}\,du, \tag{4.42}$$

where $\bar{L}$ is defined by (3.18). $\mathscr{L}$ is thus a function of the parameters $A$, $B$, $C$; $K_1$, $K_2$, $\omega$ ($= \kappa c$ the frequency) and $\kappa$. For a slowly varying wave train these parameters are functions of $X$, $T$, and Whitham's procedure is to subject $\mathscr{L}$ to variations of $\psi$ (where $\psi_X = A$, $\psi_T = -C$), $\Theta$ (where $\Theta_X = \kappa$, $\Theta_T = -\omega$), $B$, $K_1$ and $K_2$. Thus the transport equations are

$$\left(\frac{\partial\mathscr{L}}{\partial C}\right)_T - \left(\frac{\partial\mathscr{L}}{\partial A}\right)_X = 0, \tag{4.43}$$

$$\left(\frac{\partial\mathscr{L}}{\partial \omega}\right)_T - \left(\frac{\partial\mathscr{L}}{\partial \kappa}\right)_X = 0, \tag{4.44}$$

$$\frac{\partial\mathscr{L}}{\partial B} = 0, \tag{4.45}$$

$$\frac{\partial\mathscr{L}}{\partial K_1} = 0, \tag{4.46}$$

$$\frac{\partial\mathscr{L}}{\partial K_2} = 0, \tag{4.47}$$

Equation (4.46) is the dispersion relation which determines $\gamma$ as a function of the parameters, and (4.47) is the condition that $u$ have zero mean. Two more

transport equations are obtained by applying the consistency relations (4.17) and (4.18). Altogether there are seven transport equations for the seven parameters. Now we can let $K_1, K_2 \to 0$, so that $\gamma \to \infty$ and $\mathscr{L} \to \bar{L}$; (4.43) and (4.45) become

$$\left.\begin{aligned}\left(\frac{\partial \bar{L}}{\partial C}\right)_T - \left(\frac{\partial \bar{L}}{\partial A}\right)_X &= 0,\\ \frac{\partial \bar{L}}{\partial B} &= 0,\end{aligned}\right\} \tag{4.48}$$

which are just (4.20) and (3.6) respectively. Equation (4.44) becomes

$$\left(\frac{\partial \hat{w}}{\partial \omega}\right)_T - \left(\frac{\partial \hat{w}}{\partial \kappa}\right)_X = 0, \tag{4.49}$$

where $\hat{w}$ is regarded as a function of $\omega, \kappa$ and $X, T$; if instead $\hat{w}$ is regarded as a function of $c, \kappa$ and $X, T$ then (4.49) is just (4.37), or (4.38). Equations (4.46) and (4.47) do not retain any significance as $\gamma \to \infty$. The form of (4.48) and (4.49) shows that our transport equations can be derived from two variational principles; first by subjecting $\bar{L}$, a function of $A, B, C$, to variations of $\psi$ and $B$; and secondly by subjecting $\hat{w}$, a function of $\omega(=\kappa c)$, $\kappa$ and $X, T$ (through $A, B$ and $h$), to variations of $\Theta$.

## 5. Solution of the transport equations

The transport equations are (3.6), (4.17), (4.20), (4.18) and (4.37), and are displayed here again for convenience:

$$C = B + \tfrac{1}{2}A^2, \tag{5.1}$$

$$A_T + C_X = 0, \tag{5.2}$$

$$B_T + (A(h+B))_X = 0, \tag{5.3}$$

$$K_T + (\kappa c)_X = 0, \tag{5.4}$$

$$\left(c\frac{\partial \hat{w}}{\partial c} - \hat{w}\right)_T + \left(c\left(c\frac{\partial \hat{w}}{\partial c} - \hat{w}\right)\right)_X + \frac{\partial \hat{w}}{\partial T} = 0. \tag{5.5}$$

The first three equations involve only $A$, $B$ and $C$; they are, perhaps not unexpectedly, just the shallow-water equations (i.e. (2.7) and (2.8) with the dispersive terms absent), and can, in principle, be solved. In particular if $A$ and $B$ vanish at $T = 0$ for all $X$, then they vanish for all $T$. In any event, $A$ and $B$ can be regarded as known when considering (5.4) and (5.5). Since $\hat{w} = \kappa W$, and $W$ is a function only of $c$ and $X, T$ (through $A$, $B$ and $h$), it is convenient to eliminate $\kappa$ from (5.5):

$$\left(c\frac{\partial W}{\partial c} - W\right)_T + c\left(c\frac{\partial W}{\partial c} - W\right)_X + \frac{\partial W}{\partial T} = 0. \tag{5.6}$$

This is a single equation for $c$, or better, for

$$V = c\frac{\partial W}{\partial c} - W \tag{5.7}$$

and its general solution can, in principle, be obtained.

We shall now consider a special case when (5.6) may be integrated explicitly. It will be supposed that $h = 1$ for all $X \leqslant 0$, and so the wave evolves from a region where it is uniform. Thus the transport equations are to be solved subject to the initial values, $A = B = 0$ and $\kappa, c$ constant. (This cannot be exactly true as the solitary wave is infinite in extent, and even when its crest is over a large negative value of $X$, part of the wave is interacting with the varying $h$ in $X > 0$; however, it is reasonable to suppose that this interaction can be made as small as we please by taking the initial values to be those at an indefinitely large negative value of $X$.) Thus $A \equiv B \equiv 0$, and since $W$ then depends only on $c$ and $h$, $\partial W/\partial T \equiv 0$ and (5.6) becomes

$$V_T + cV_X = 0 \tag{5.8}$$

where from (5.7) $c = c(V, X)$. The general solution of (5.8) is

$$V = M(T_0),$$

where

$$T_0 = T - \int_0^X ds\{c(M(T_0), s)\}^{-1}. \tag{5.9}$$

$V$ is therefore an 'adiabatic invariant', i.e. it is constant on the wavelet which passed $X = 0$ at a time $T_0$ and is travelling with speed $c(M(T_0), X)$. In general (5.9) contains the possibility of shock formation at those places where $T_0$ cannot be found as a function of $X$, $T$. However, since $\kappa$, $c$ are initially constant, so is $V$ and the solution of (5.8) required is just $V$ equals a constant (i.e. $M$ is a constant). We note that since $A$ and $B$ are zero, it follows from (3.23) that $V$ is the wave-average of the energy density with respect to the $x$ scale, and so the solution we have obtained is just that which preserves the energy of the wave. This of course, might have been expected, as our asymptotic expansion is one which ignores reflexions and there is no other outlet for the loss of energy. Further, it follows from (3.24) that

$$c^2 = h + Nh^{-1}, \tag{5.10}$$

where $N$ is a constant (in general $N$ is a function of $T_0$). The wave amplitude is found from (3.9) and (3.12), and is

$$e_m = 2((h^2 + N)^{\frac{1}{2}} - h). \tag{5.11}$$

Figure 2 shows a plot of $e_m/(e_m)_0$ against $h$ where $(e_m)_0$ is the value of $e_m$ at $h = 1$ (i.e. $X = 0$); it exhibits the fact that $e_m/(e_m)_0$ for each $N$, increases as $h$ decreases, but, for each $h$, decreases as $N$ (and hence $(e_m)_0$) increases. Also shown is the graph of $h^{-0{\cdot}47}$ which represents the results of Ippen & Kulin's (1955) experiments on the behaviour of a solitary wave on a beach of constant slope 0·023; they observed a fairly wide scatter, and the curve shown is a best fit for several observations with values of $(e_m)_0$ ranging from 0·2 to 0·7 (and also with varying values for the initial depth of fluid). They also observed a small decrease in amplitude at the foot of the beach, where, in the experimental set up, there was an abrupt change in beach slope from zero to 0·023; this was presumably due to a reflexion. We have ignored this initial energy loss in displaying their results on figure 2 by allowing the graph of the experimental points (viz. $h^{-0{\cdot}47}$) to pass

through $h = 1$ when $e_m = (e_m)_0$ whereas the true curve would be similar in shape but displaced downwards by a small amount. For small values of $(e_m)_0$ we have

$$e_m/(e_m)_0 \approx h^{-1}, \tag{5.12}$$

an approximation which is accurate to within 5 % for $(e_m)_0 = 0{\cdot}01$, $0{\cdot}3 \leqslant h \leqslant 1$ and also for $(e_m)_0 = 0{\cdot}1$, $0{\cdot}6 \leqslant h \leqslant 1$ but becomes increasingly inaccurate for larger values of $(e_m)_0$.

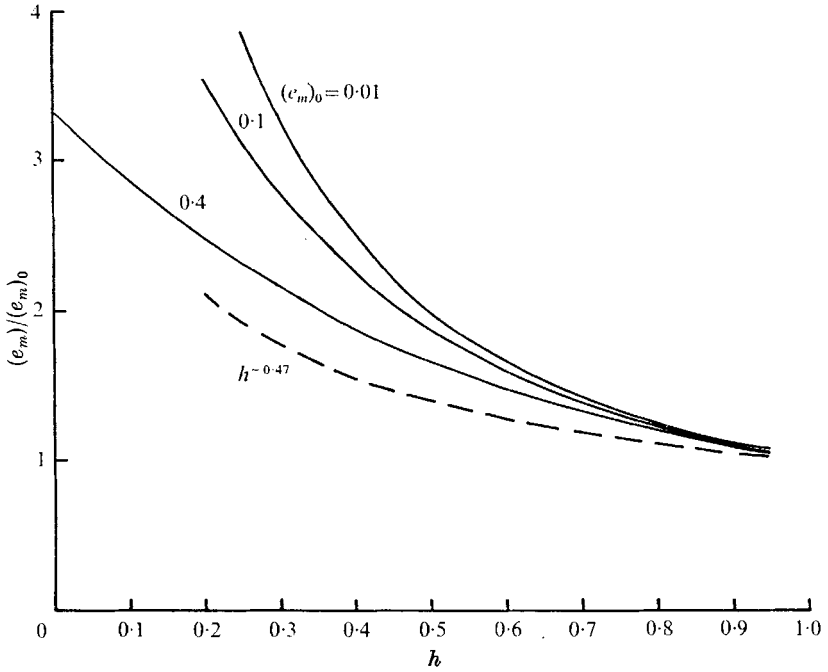


FIGURE 2. Graph of $(e_m)/(e_m)_0$ against $h$.

Other properties of the wave can also be determined from (5.10). Thus we find that

$$\kappa p = \sqrt{\left(\frac{3N}{4}\right)} h^{-2}, \tag{5.13}$$

$$\kappa^{-1}\hat{e} = \sqrt{\left(\frac{16N}{3}\right)} h, \tag{5.14}$$

$$\kappa^{-1}\hat{u} = \sqrt{(\tfrac{16}{3})}\, h^{\frac{3}{2}} \cosh^{-1}(1 + Nh^{-2})^{\frac{1}{2}}, \tag{5.15}$$

$$N[E_1] = \tfrac{3}{2} h^{\frac{1}{2}} h_X (h^2 + N)^{\frac{1}{2}} (\kappa^{-1}\hat{u}) + \sqrt{\left(\frac{16N}{3}\right)} N h_X, \tag{5.16}$$

$$N[U_1] = \tfrac{3}{2} h_X (h + Nh^{-1}) (\kappa^{-1}\hat{u}). \tag{5.17}$$

Equation (5.13) shows that the length of the wave, $(\kappa p)^{-1}$ decreases as $h$ decreases; (5.14) to (5.17) show that the mass contained in the wave is not conserved, and is fed into a mean flow, and a change in the mean depth, both proportional to $\beta h_X$. Further the equations (5.16) and (5.17) indicate that the effect of the terms of $O(\beta)$ in the asymptotic expansion (4.2) is to cause increasing asymmetry

due to steepening on the front face, and flattening on the rear face. If we adopt the criterion that the wave will break when $u_m = c$ (i.e. the velocity at the crest equals the wave velocity) then (5.10) implies that the wave will break when $h = \sqrt{(\frac{1}{3}N)}$; at this value of $h$, $e_m h^{-1} = 2$ which is much greater than the most commonly accepted theoretical value of 0·78 for the highest wave on a constant depth (McCowan 1894), although Ippen & Kulin's experiments showed that $e_m h^{-1} \approx 1{\cdot}2$ at the breaking depth for a beach slope of 0·023. Of course the value $u_m = c$ is almost certainly outside the range of validity of the Boussinesq equations. Finally, from (5.4) we see that $\kappa c$ is constant, and this determines $\kappa$.

## 6. Error estimate

The procedures outlined in §4 have enabled us to construct functions

$$\tilde{E} = B + e + \beta E_1, \quad \tilde{F} = \beta^{-1}\psi + f + \psi_1 + \beta f_1, \quad \tilde{U} = \tilde{F}_x, \tag{6.1}$$

which satisfy the Boussinesq equations (2.7) and (2.8) approximately, with an error of $O(\beta^2)$. That is if

$$D_1(E, F) \equiv \partial L/\partial E, \tag{6.2}$$

$$D_2(E, F) \equiv \frac{\partial}{\partial t}\left(\frac{\partial L}{\partial F_t}\right) + \frac{\partial}{\partial x}\left(\frac{\partial L}{\partial F_x}\right) - \frac{\partial^2}{\partial x^2}\left(\frac{\partial L}{\partial F_{xx}}\right), \tag{6.3}$$

where $L(E, F_x, F_{xx}, F_t; X)$ is defined by (2.10) (with $\alpha = \epsilon = 1$) then

$$D_1(\tilde{E}, \tilde{F}) = O(\beta^2), \quad D_2(\tilde{E}, \tilde{F}) = O(\beta^2). \tag{6.4}$$

We now pose the problem: does there exist an exact solution $E, F, U = F_x$ of the Boussinesq equations for which $\tilde{E} - E$ and $\tilde{U} - U$ are $O(\beta^2)$? The following analysis provides a partial answer to this problem.

For simplicity, it will be supposed that $h = 1$ for $X \leqslant 0$ and $h$ takes another constant value for $X$ large and positive and that $h$ is as smooth as desired. Then we may assume that $B$ and $\psi$ vanish for all $x$ and $t$, and that, from (5.16) and (5.17), $[E_1]$ and $[U_1]$ vanish for sufficiently large $|X|$. Also we can assume that $B_1$ and $\psi_1$ vanish for all $x$ and $t$ as their values were not relevant in the construction of $E_1$ and $f_1$. Thus the functions defined by (6.1) have been constructed so that $\tilde{E}$, $\tilde{U}$ with all their derivatives, vanish as $|x| \to \infty$, for some time interval $0 \leqslant t \leqslant t_0$. Let $E$, $F$ be that exact solution of the Boussinesq equations which agrees with $\tilde{E}$, $\tilde{F}$ at $t = 0$, so that

$$E - \tilde{E}|_{t=0} = 0, \quad F - \tilde{F}|_{t=0} = 0. \tag{6.5}$$

We shall now assume that for the initial values (6.5) there exists an exact solution of the Boussinesq equations over the time interval $0 \leqslant t \leqslant t_0$, such that $E$, $U$ with all their derivatives, vanish as $|x| \to \infty$. Given this, we shall now show that $\tilde{E}$, $\tilde{U}$ differ from $E$, $U$ by terms of $O(\beta^2)$. Let

$$E' = E - \tilde{E}, \quad F' = F - \tilde{F}, \quad U' = F_x - \tilde{F}_x; \tag{6.6}$$

then

$$D_1(E', F') = -U'\tilde{U} + O(\beta^2), \tag{6.7}$$

$$D_2(E', F') = -(E'\tilde{U} + U'\tilde{E})_x + O(\beta^2), \tag{6.8}$$

where the terms $O(\beta^2)$ are uniform for all $x$, and $0 \leqslant t \leqslant t_0$. Now if

$$D_3(E,F) \equiv \left(F_t \frac{\partial L}{\partial F_t} - L\right)_t + \left(F_t \frac{\partial L}{\partial F_x} + 2F_{tx}\frac{\partial L}{\partial F_{xx}}\right)_x - \left(F_t \frac{\partial L}{\partial F_{xx}}\right)_{xx} \tag{6.9}$$

then
$$D_3(E,F) \equiv -E_t D_1(E,F) + F_t D_2(E,F). \tag{6.10}$$

It was remarked in §2 that $D_3 = 0$ is the equation for conservation of energy, and that

$$\mathscr{E}(E,F) \equiv L - F_t \partial L/\partial F_t \equiv \tfrac{1}{2}E^2 + \tfrac{1}{2}(h+E)\,U^2 - \tfrac{1}{6}h^3U_x^2 + \tfrac{1}{4}h^2h_{xx}U^2 \tag{6.11}$$

may be regarded as an energy density; although it is not positive definite, it may be assumed that it takes only positive values in the long wave approximation being used here (e.g. $|hU_x| \ll |U|$), and that its vanishing implies that $E$ and $U$ vanish. Then, using (6.7), (6.8) and (6.10), it follows that

$$D_3(E',F') = I + O(\beta^2), \tag{6.12}$$

where
$$I = (E' + \tfrac{1}{2}U'^2)\,(E'\tilde{U} + U'\tilde{E})_x - U'\tilde{U}(hU' + E'U' + (\tfrac{1}{3}h^3U'_x)_x)_x. \tag{6.13}$$

On integrating (6.12) with respect to $x$, we find that

$$\frac{\partial}{\partial t}\int_{-\infty}^{\infty} \mathscr{E}(E',F')\,dx = \int_{-\infty}^{\infty} I\,dx + O(\beta^2). \tag{6.14}$$

Clearly, using integration by parts where necessary and the long wave approximation, the integral of $I$ can be estimated in terms of the integral of $\mathscr{E}$, so that

$$\frac{\partial}{\partial t}\int_{-\infty}^{\infty} \mathscr{E}(E',F')\,dx \leqslant K\int_{-\infty}^{\infty} \mathscr{E}(E',F')\,dx + Q\beta^2, \tag{6.15}$$

where $K$, $Q$ are constants. Since $\mathscr{E}(E',F')$ vanishes when $t = 0$ it follows that

$$\int_{-\infty}^{\infty} \mathscr{E}(E',F')\,dx \leqslant \beta^2 Q K^{-1}(e^{Kt_0} - 1), \tag{6.16}$$

from which we may deduce that

$$E - \tilde{E} = O(\beta^2), \quad U - \tilde{U} = O(\beta^2). \tag{6.17}$$

Since $\tilde{E}$, $\tilde{F}$ contain no reflected terms, (6.17) shows that any reflected energy is $O(\beta^2)$. Indeed this same argument could be used to show that if $\tilde{E}$, $\tilde{F}$ were such that the error in (6.4) was $O(\beta^N)$ for arbitrarily large $N$, then the reflected energy is also $O(\beta^N)$.

This work was completed while the author was visiting the Department of Applied Mathematics and Theoretical Physics, University of Cambridge, during the tenure of a Royal Society and Nuffield Foundation Commonwealth Bursary.

## REFERENCES


BOUSSINESQ, J. 1871 *Comptes Rendus*, **72**, 755–759.

BOUSSINESQ, J. 1872 *Journal of Mathematics, Liouville*, **17**, 55–108.

BRETHERTON, F. P. 1968 *Proc. Roy. Soc.* A **302**, 555–576.

DAILY, J. W. & STEPHAN, S. C. 1952 *M.I.T. Hydrodynamics Laboratory Staff Publication*, S-17.

GREEN, G. 1837 *Trans. Camb. Phil. Soc.* (Republished in 1871 *Math. Papers*, pp. 225–230.)

GREENSPAN, H. 1958 *J. Fluid Mech.* **4**, 330–334.

HOOGSTRATEN, H. W. 1968 *J. Eng. Math.* **2**, 249–274.

IPPEN, A. T. & KULIN, G. 1955 *M.I.T. Hydrodynamics Laboratory Tech. Report*, no. 15.

KELLER, H. B., LEVINE, D. A. & WHITHAM, G. B. 1960 *J. Fluid Mech.* **7**, 302–316.

KELLER, J. B. 1958 *J. Fluid Mech.* **4**, 607–612.

KUZMAK, G. E. 1959 *P.M.M.* **23**, 515–526. (Translated in 1959 *Appl. Math. Mech.* **23**, 730–744.)

LONGUET-HIGGINS, M. H. & STEWART, R. W. 1964 *Deep Sea Res.* **11**, 529–562.

LUKE, J. C. 1966*a* *Proc. Roy. Soc.* A **292**, 403–412.

LUKE, J. C. 1966*b* *J. Fluid Mech.* **27**, 395–398.

MCCOWAN, J. 1894 *Phil. Mag.* **38**, 351–358.

MEI, C. C. & LE MÉHAUTÉ 1966 *J. Geophysical Research*, **71**, 393–400.

PEREGRINE, D. H. 1967 *J. Fluid Mech.* **27**, 815–827.

RAYLEIGH, LORD 1911 *Phil. Mag.* **21**, 177–195.

RUSSELL, J. SCOTT 1837 Report on Waves. *Meeting of the British Association for the Advancement of Science*, Liverpool, 417–496.

URSELL, F. 1953 *Proc. Camb. Phil. Soc.* **49**, 685–694.

WHITHAM, G. B. 1965*a* *Proc. Roy. Soc.* A **283**, 238–261.

WHITHAM, G. B. 1965*b* *J. Fluid Mech.* **22**, 273–283.

WHITHAM, G. B. 1967 *Proc. Roy. Soc.* A **299**, 6–25.